In vitro dopaminergic neurotoxicity of pesticides; a link with neurodegeneration?

Hendrik Johan Heusinkveld

ISBN: 978-90-393-6081-1

Printed in The Netherlands by Drukkerij Modern BV, Bennekom

Layout by: HJ Heusinkveld
Cover design by: Bart Pausma

The research described in this thesis was performed at the
Institute for Risk Assessment Sciences, (IRAS)
Faculty of Veterinary medicine, Utrecht University.

In vitro dopaminergic neurotoxicity of pesticides;
a link with neurodegeneration?

In vitro dopaminerge neurotoxiciteit door pesticiden;
een link met neurodegeneratie?

(met een samenvatting in het Nederlands)

Proefschrift

ter verkrijging van de graad van doctor aan de Universiteit Utrecht
op gezag van de rector magnificus prof. dr. G.J. van der Zwaan, ingevolge
het besluit van het college voor promoties
in het openbaar te verdedigen op dinsdag 4 februari 2014
des middags te 2.30 uur

door

Hendrik Johan Heusinkveld

geboren op 19 februari 1982 te Arnhem

Promotor: Prof. dr. M. van den Berg

Co-promotor: Dr. R.H.S. Westerink

Contents

List of abbreviations

ACh	acetylcholine
ADME	absorption, distribution, metabolism, excretion
AMPA-R	ionotropic glutamate receptor
B35	Rat neuroblastoma cell line
BBB	blood-brain barrier
CA	Canada
Ca^{2+}	calcium
$[Ca^{2+}]_i$	intracellular calcium concentration
CAMK-II	Ca^{2+}-calmodulin-dependent protein kinase II
cAMP	cyclic adenosine monophosphate
Cav1/Cav1.3	L-type voltage-gated calcium channel
cDNA	complementary DNA
CNS	central nervous system
COMT	Catechol-*O*-methyltransferase
CYP	cytochrome P450 superfamily
DA	dopamine
DAT	dopamine membrane transporter
DNOC	4,6-dinitro-ortho-cresol
DNP	2,4-dinitrophenol
EC_{10}	effective concentration that evokes 10% of the max. response
EC_{20}	effective concentration that evokes 20% of the max. response
EC_{50}	effective concentration that evokes 50% of the max. response
EC_{100}	effective concentration that evokes 100% of the max. response
ER	endoplasmic reticulum
ES	Spain
GABA	gamma-aminobutyric acid
$GABA_A$-R	ionotropic GABA receptor type A
GB	United Kingdom
$hGABA_A$-R	human ionotropic GABA receptor type A
GPCR	G-protein coupled receptor
HED	human equivalent dose
HVA	high-voltage activated
IC_{10}	effective concentration that inhibits 10% of the max. response
IC_{20}	effective concentration that inhibits 20% of the max. response
IC_{50}	effective concentration that inhibits 50% of the max. response
IN	India
IP_3	inositol 1,4,5-triphosphate
$InsP_3R$	IP3 receptor
L-DOPA	L-3,4-dihydroxydopamine

LOEC	lowest observed effect concentration
log K_{ow}	octanol-water partinioning coeficient
MAO	monoamine oxidase
MES23.5	rat-mouse hybrid mesencephalic cell line
mGlu-R	metabotropic glutamate receptor
MNCX	mitochondrial Na^+/Ca^{2+} exchanger
MPTP	1-methyl-4-phenyl-1,2,3,6-tetrahydropyridine
MPP^+	1-methyl-4-phenylpyridinium
MTT	3-(4,5-dimethylthiazol-2-yl)-2,5-diphenyltetrazolium bromide
N27	rat mesencephalic cell line
NA	nucleus accumbens
nACh	nicotinic acetylcholine receptor
NCX	Na^+/Ca^{2+} exchanger
ng/g l.w.	nanogram per gram on lipid-weight basis
ng/ml	nanogram per milliliter
NL	The Netherlands
NOAEL	no observed adverse effect level
PBPK	physiologically-based pharmacokinetic
PC12	pheochromocytoma cell line
PD	Parkinson's disease
PFC	prefrontal cortex
PMCA	plasma membrane calcium ATPase
RyR	ryanodine receptor
RfD	reference dose
SERCA	sarco/endoplasmic reticulum Ca^{2+}-ATPase
SH-SY5Y	human neuroblastoma cell line
SN	substantia nigra
SN_{pc}	substantia nigra pars compacta
SN_{pr}	substantia nigra pars reticulata
STN	sub-thalamic nucleus
$T_{1/2}$	half-life
US	United States of America
VGCC	voltage-gated calcium channel
VMAT	vesicular monoamine transporter
VTA	ventral tegmental area

To accomplish great things,
we must not only act, but also dream;
not only plan, but also believe.

Anatole France

Chapter 1

General Introduction

1.1 Pesticides

Ever since people culture crops for food and feed production, people have been struggling with plagues and pests. In an attempt to assure a stable production of food and feed, humans used and designed numerous pesticides to treat animals and crops and destroy specific plagues. The first recorded use of (natural) compounds as pesticides dates back more than 3 millennia, to the use of sulphur as fumigant in the time of Homer around 1000 B.C. (Whitacre and Ware 2004). Still, sulphur is among the most widely used fungicides in vineyards around the world.

Systematized development of synthetic chemicals for crop protection started in the 1930s and resulted in the development of a number of still well-known chemicals, such as dichlorodiphenyltrichloroethane (DDT) and 2,4-dichlorophenoxyaceticacid (2,4-D). After the Second World War, the field of agrochemicals developed quickly and a wide array of compounds has been introduced for pesticidal use.

Primary classification of pesticides is based on and named after the pesticidal target such as herbicides, insecticides, fungicides and rodenticides. Within these classes, further classification is based on similarities in chemical structure. Well known sub-classes include organochlorine insecticides, phenoxyacetic herbicides and azole fungicides. Insecticides and fungicides can have an agricultural and/or pharmaceutical application. Examples of compounds with a double use are the organochlorine insecticide lindane (Nolan, *et al*. 2012) and the azole fungicides (Stevens 2012), which are used as pharmaceutical in both humans and animals but are also applied in agriculture as pesticide.

Toxicity of pesticides in humans

Although it seems self-explanatory, it is important to note that all pesticides possess an inherent degree of toxicity to some living organism; otherwise they would be of no practical use. In general, the target-species and the main pathway of toxicity are believed to determine the risk to humans. In other words, a herbicide targeting a plant-specific process that is absent in animals, is perceived more safe than an insecticide targeting the nervous system of insects. From many insecticides it is known that they are indeed also neurotoxic in mammals, for example organochlorine insecticides (Hatcher, *et al*. 2008, Raymond-Delpech, *et al*. 2005).

However, for many pesticides that presumably target species-specific pathways that seem not relevant to humans, such as herbicides and fungicides, this is less obvious. From epidemiological studies it is now known that a relationship exists between exposure to certain classes of pesticides and the occurrence of Parkinson's disease (Elbaz and Tranchant 2007, Freire and Koifman 2012, Mostafalou and Abdollahi 2013, Rajput and Birdi 1997), though the underlying mechanism is often unknown.

1.2 Neurotransmission

Communication in the (human) central nervous system is based on the transmission of a (chemical) signal from one cell to another (Fig. 1). A neuron contains many dendrites to receive input from neighbouring cells. Upon activation of its dendrites, a neuron generates an action potential (AP) via opening of voltage-gated sodium and potassium channels. This AP will travel along the axon to reach the synapse (1). In the synapse, the electrical signal is translated to a chemical signal via opening of voltage-gated calcium channels (VGCC) and release of neurotransmitter from the presynaptic cell (2). These neurotransmitters are chemical signalling molecules that, following release into the synaptic cleft, bind to receptors on the membrane of the postsynaptic cell (3). In the postsynaptic cell, the chemical signal is then either translated again to an AP that will travel to the cell body of the postsynaptic cell or it translates to activation of intracellular signalling pathways (4). Signal transduction in the synaptic cleft is terminated by either degradation or reuptake with transporters (5) of the neurotransmitter (for review see: Westerink 2006).

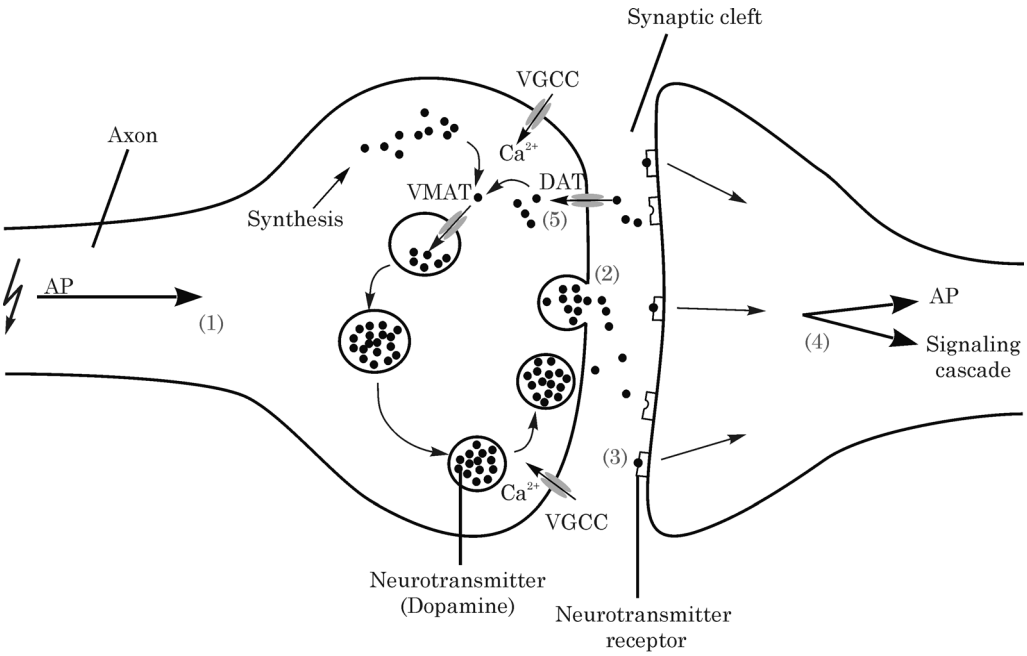

Fig. 1 Schematic view of a presynaptic (left) and postsynaptic (right) cell. AP: action potential, VMAT: vesicular monoamine transporter, VGCC: voltage-gated calcium channel, DAT: (membrane) dopamine transporter.

Dopaminergic neurotransmission

Within the brain, several subtypes of cells are available in different regions. These different cell types can utilize different neurotransmitters, such as acetylcholine (ACh), glutamate, GABA and dopamine (DA). DA is synthesized intracellularly by tyrosine hydroxylase-mediated conversion of tyrosine to the DA-precursor L-3,4-dihydroxyphenylalanine (L-DOPA) and subsequent conversion to DA by aromatic amino acid decarboxylase (for review see: Westerink 2006). Upon synthesis, DA is stored in vesicles by active transport through the vesicular monoamine transporter (VMAT). Dopaminergic neurotransmission is achieved through fusion of a DA-filled vesicle with the plasma membrane, releasing its contents in the synaptic cleft. This process of neurotransmitter release is called exocytosis. Once released in the synaptic cleft, DA binds to DA receptors present on both the pre- and postsynaptic membrane. Two families of G-protein-coupled DA receptors can be distinguished; D1- and D2-like receptors (for review see: Neve, *et al.* 2004). Activation of D1 receptors is linked to regulation of VGCCs and potassium channels, an increase in phosphorylation and activation of calcium-binding proteins. Activation of D1 receptors thereby increases the vesicular release of DA. Activation of D2 receptors, also known as auto-receptors, results in less phosphorylation and an inhibitory effect on dopaminergic neurotransmission (Neve, *et al.* 2004). DA is broken down extracellularly by Catechol-*O*-methyltransferase (COMT) to terminate neurotransmission. Alternatively, DA is recycled from the synaptic cleft by transport through the dopamine transporter (DAT) making DA available for either storage in vesicles or enzymatic degradation by monoamine oxidase (MAO).

Dopaminergic neurotransmission is involved in a large variety of human behaviours, including (psycho)motor function, memory, motivation, reward and addiction. Areas containing most dopaminergic neurons can be found in a small number of nuclei, mainly located in the forebrain and the basal ganglia. Among the nuclei in the basal ganglia, the substantia nigra (SN), the ventral tegmental area (VTA) and the striatum (ST) contain the most dopaminergic neurons (Obeso, *et al.* 2008). The basal ganglia and forebrain are innervated by three distinct major dopaminergic pathways; the nigrostriatal, mesocortical and mesolimbic pathway (Fig. 2). The nigrostriatal pathway arises in the SN pars compacta (SNpc) and projects to the striatum. Spontaneous and continuing rhythmic activity (i.e. pacemaking) of this dopaminergic innervation of the striatum tightly regulates DA levels in the ST (Guzman, *et al.* 2009). This pathway is involved in facilitation of voluntary movement as well as inhibition of unwanted movement (Obeso, *et al.* 2008).

The mesocortical pathway arises from the VTA, projects to the prefrontal cortex (PFC) and is critically involved in normal cognitive function. The mesolimbic pathway also arises from the VTA, but innervates the nucleus accumbens, hippocampus,

amygdala and PFC. This pathway is involved in e.g. the reward circuitry and is therefore important in conditions such as addiction.

In general, dopaminergic neurotransmission in the SN and ST is regulated by excitatory input from glutamatergic neurons, whereas inhibitory input is generated by GABA-ergic neurons. Depending on the type of input, dopaminergic neurotransmission increases (excitatory input) or decreases (inhibitory input). Excitatory input generally results in a depolarization of the membrane evoking Ca^{2+}-influx and exocytosis. Contary, inhibitory GABA-ergic input results in hyperpolarization of the membrane reducing the chance of generation of an AP and consequently reducing the chance of VGCC opening and Ca^{2+}-influx, thus reducing the chance of exocytosis.

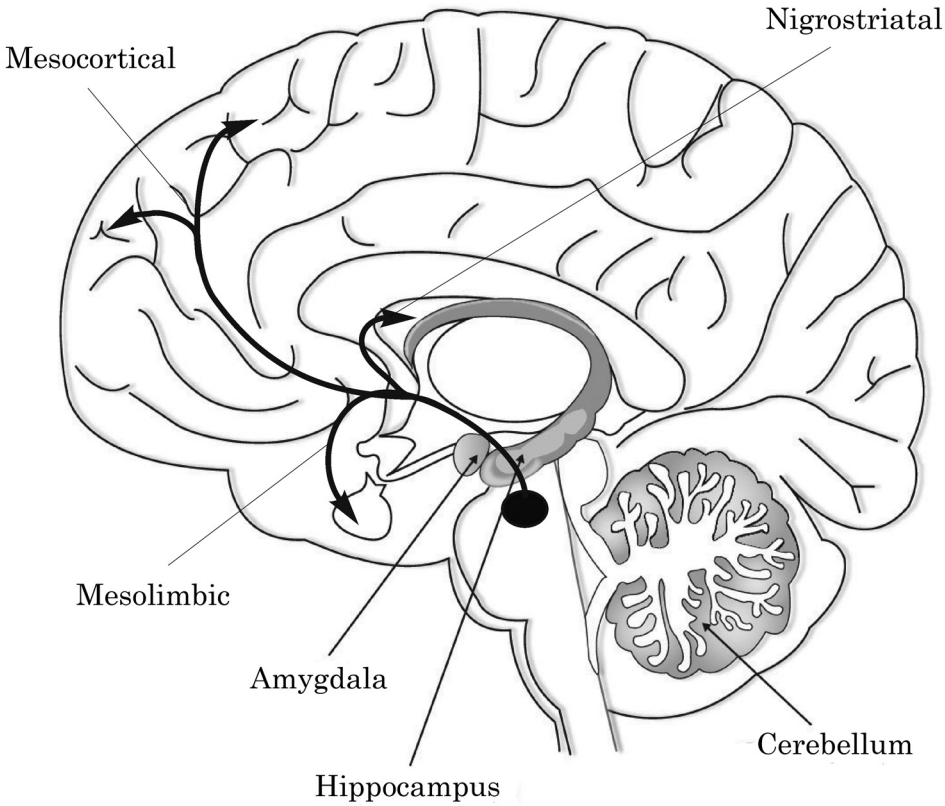

Fig. 2 Schematic view of the mesocortical, mesolibic and nigrostriatal dopaminergic pathways in the human brain (modified from http://www.peoi.org chapter 8, section B)

Intracellular Ca^{2+} homeostasis

Dopaminergic neurotransmission relies heavily on calcium signalling (for review see: Barclay, *et al.* 2005, Garcia, *et al.* 2006, Westerink 2006). However, Ca^{2+} plays pivotal roles in many additional inter- and intraneuronal processes, including neurodevelopment (Pravettoni, *et al.* 2000) and neurodegeneration (Mattson 2012). Therefore, the intracellular Ca^{2+} concentration ($[Ca^{2+}]_i$; typically 10^{-7} M) is tightly regulated by a system of VGCCs, sensors and pumps located in the plasma membrane and in the membrane of intracellular stores, in particular mitochondria (MNCX, uniporter) and the endoplasmic reticulum (ER: $InsP_3R$, SERCA, RyR) (Fig. 3). As a roughly 10.000x Ca^{2+} gradient exists between the intra- and extracellular space (Fig. 3), maintenance of the intracellular $[Ca^{2+}]_i$ is an essential but energy consuming process.

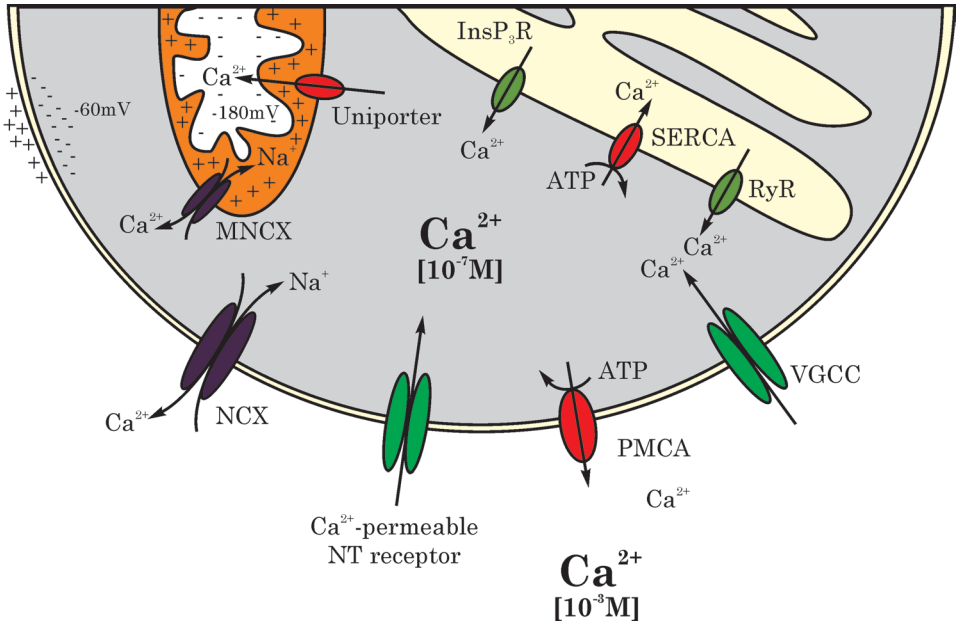

Fig. 3 Schematic representation of channels and receptors in the cell membrane and the membrane of intracellular stores implicated in maintenance of the intracellular calcium homeostasis. NCX: Na^+/Ca^{2+} exchanger, PMCA: plasma membrane Ca^{2+}-ATPase, VGCC: voltage-gated calcium channel, RyR: ryanodine receptor, SERCA: sarco/endoplasmic reticulum Ca^{2+}-ATPase, $InsP_3R$: inositol triphosphate receptor, MNCX: mitochondrial Na^+/Ca^{2+} exchanger

1.3 Neurodegeneration and PD

Loss of neurons in the CNS is an inevitable process that every individual experiences with ageing. Whenever this decline in neurons leads to functional impairment of e.g. cognition or motor control, the diagnosis neurodegeneration is evident. Parkinson's disease (PD), one of the best known neurodegenerative disorders, is named after James Parkinson who first described the symptoms of so-called shaking palsy in "modern" medical literature back in 1817 (republication: Parkinson 2002). In developed countries, PD is the second most common neurodegenerative disorder after Alzheimer's disease and affects more than 1% of the population over the age of 60 (de Lau and Breteler 2006). The large majority (90-95%) of PD cases is not related to inheritable genetic mutations and is therefore considered idiopathic PD (Bartels and Leenders 2009, Lees, *et al.* 2009). Idiopathic PD is characterized by bradykinesia, muscle rigidity and resting tremor (Brooks 2012, Hughes, *et al.* 1992, Lees, *et al.* 2009). Parkinsonian neurodegeneration is characterized by selective degeneration of dopaminergic cells in the basal ganglia leading to reduced feedback in the neuronal circuitry involved in voluntary movement. According to a long established scientific view, PD becomes clinically manifest when at least 70% of the striatal dopamine levels and 50% of the dopaminergic neurons in the nigrostriatal pathway (Fig 2) is lost (Braak, *et al.* 2003, Lees, *et al.* 2009). Although more brain areas are affected, degeneration of the nigrostriatal pathway reduces the amount of dopaminergic input in the ST, resulting in decreased DA levels and loss-of-function (Blandini, *et al.* 2000, Rice, *et al.* 2011). This is held responsible for the clinical observation of loss of (voluntary) movement control.

Although first described in 1817, PD and parkinsonism are far from modern-age diseases. Already the traditional Indian medicine (Ayurveda; 1000 B.C.) as well as China's first medical texts (Nei Jing; 500 B.C.) and the Old Testament (Ecclesiastes) describe a disability with symptoms and signs known today as PD (Parkinson 2002, Sladek 2012). Peculiarly, the Indian traditional medicine Ayurveda described already millennia ago a treatment for the disorder using a herbal product containing mucuna pruriens (velvet bean). This particular plant is now known to contain a bioavailable and well-tolerated natural source of L-DOPA which is still today's primary PD treatment for restoration of DA levels (Katzenschlager, *et al.* 2004). The dopamine precursor L-DOPA crosses the blood-brain-barrier easily and is converted to DA in dopaminergic neurons (Lees, *et al.* 2009). Although this treatment can relieve symptoms effectively in some cases, it is not a curative therapy.

Aetiology of PD and related disorders

Idiopathic PD and parkinsonisms are considered as multifactorial and complex disorders with limited involvement of (inheritable) genetic defects (Bartels and Leenders 2009).intrinsic production of oxidative molecules (H_2O_2, quinones etc) as a consequence of dopamine turnover and accelerated ageing of mitochondria in dopaminergic cells due to the reliance on energy-consuming mechanisms for neurotransmission (Schapira and Jenner 2011, Surmeier, *et al.* 2011).

Cell-autonomous hypotheses generally focus on characteristics of dopaminergic neurons or dysfunction of DA-related intracellular processes that can lead to degeneration. This includes excess oxidative stress due to high trinsic production of oxidative molecules (H_2O_2, quinones etc) as a consequence of dopamine turnover and accelerated ageing of mitochondria in dopaminergic cells due to the reliance on energy-consuming mechanisms for neurotransmission (Schapira and Jenner 2011, Surmeier, *et al.* 2011). In addition, changes in intracellular Ca^{2+}-homeostasis leading to impaired dopamine handling, hampered neurotransmission and dysfunction of ER and mitochondria are implicated (Bezprozvanny 2009, Mattson 2012, Surmeier, *et al.* 2010).

Alternatively, non-cell autonomous hypotheses comprise activation of glial cells and astrocytes by both exogenous (e.g. environmental factors) and endogenous (e.g. systemic inflammation, brain trauma) factors inducing and propagating inflammatory processes leading to damage to the surrounding cells (McGeer and McGeer 2004, Taylor, *et al.* 2013).

Furthermore, neurodegenerative disorders including PD and parkinsonisms are often referred to as proteinopathy as degeneration is accompanied with intracellular protein deposition and formation of Lewy bodies. Lewy bodies are cytoplasmic protein aggregates consisting mainly of α-synuclein (Agorogiannis, *et al.* 2004, Marques and Outeiro 2012). α-Synuclein is an intracellular protein that, under physiological circumstances, is involved in various processes including vesicular dopamine release (Marques and Outeiro 2012, Venda, *et al.* 2010). The presence of misfolded α-synuclein and/or an inhibition of protein degradation via ubiquitination can lead to the development of PD via aggregation to protofibrils and fibrilisation of α-synuclein (Breydo, *et al.* 2012, Witt 2012). The involvement of α-synuclein is underlined by the observation that mutations leading to overexpression or hampered intracellular handling of α-synuclein is linked to parkinsonism (Bezard and Przedborski 2011, Venda, *et al.* 2010).

1.4 The role of pesticides in PD

In the early 1980's it was observed that accidental exposure of intravenous drug abusers to synthetic drugs contaminated with 1-methyl-4-phenyl-1,2,3,6-tetrahydropyridine (MPTP) caused acute parkinsonism (Langston, *et al.* 1983, Langston 1996). Soon thereafter, the close chemical resemblance between the

active metabolite of MPTP, the cation 1-methyl-4-phenylpyridinium (MPP^+), and the well-known and widely used herbicide paraquat, raised the question about the role of pesticides and other environmental factors in the pathophysiology of PD (Barbeau 1984). By now, epidemiological studies have demonstrated an increased risk for the development of PD related to pesticide exposure (Ascherio, *et al.* 2006, Brown, *et al.* 2006, Mostafalou and Abdollahi 2013, Pezzoli and Cereda 2013, van der Mark, *et al.* 2011). However, considerable heterogeneity in the available studies precludes conclusiveness as to which class of pesticides is involved (van der Mark, *et al.* 2011). Available epidemiological studies point towards an increased risk associated with insecticides (in particular organochlorine insecticides; Elbaz, *et al.* 2009, Freire and Koifman 2012) and herbicides (Pezzoli and Cereda 2013). Interestingly, the epidemiological evidence for the involvement of organochlorine insecticides is underlined by biomarkers of exposure in serum (Weisskopf, *et al.* 2010) and post mortem detection of elevated levels of organochlorines in brains of PD patients (Corrigan, *et al.* 1996, Corrigan, *et al.* 2000).

The human brain is sealed from the rest of the body by the blood-brain barrier (BBB). Although the BBB protects the brain against a plethora of potential noxious insults such as proteins and infectious agents, animal models revealed that many chemicals including MPTP and pesticides simply diffuse through the BBB because of their lipophilicity (Cicchetti, *et al.* 2009). Also, some pesticides (e.g. paraquat) are actively transported over the BBB by means of for instance the neutral amino acid transporter (Shimizu, *et al.* 2001). Therefore, whether or not the brain is exposed to a pesticide depends largely on the physicochemical properties of the compound or whether the compound is a suitable ligand for a transporter.

1.5 Proposed mechanisms of pesticide-induced PD

The first mechanisms by which pesticides can induce dopaminergic neurodegeneration were revealed in research on the toxicity of MPP^+ and paraquat. Paraquat was reported to cause oxidative stress, mitochondrial dysfunction and ER stress in dopaminergic cells from the SN_{pc}, ultimately resulting in misfolded proteins and degeneration (Chinta, *et al.* 2008). Therefore, paraquat is considered as a model compound for pesticide-induced PD.

Another model compound for PD is the insecticide rotenone, naturally occurring in several plant species (Betarbet, *et al.* 2000). Rotenone administration in rodents results in degeneration of the nigral dopaminergic pathway, characterized by α-synuclein aggregation and reactive astrogliosis (Betarbet, *et al.* 2000, Sherer, *et al.* 2003a, Sherer, *et al.* 2003b). Also in case of rotenone, the mechanism of toxicity is pinpointed to uncoupling of complex I of the mitochondrial phosphorylation (Radad, *et al.* 2006).

In addition to uncoupling of mitochondrial oxidative phosphorylation by inhibition of mitochondrial complexes I or III (Bywood and Johnson 2003), changes in

Ca^{2+} homeostasis leading to altered DA handling as well as ER stress leading to protein (e.g. α-synuclein) related stress have been implicated as underlying mechanisms (Jiang, *et al.* 2010, Silva, *et al.* 2013, Surmeier, *et al.* 2011, Venda, *et al.* 2010). However, exactly which compounds are related to the development of dopaminergic neurodegeneration in addition to MPTP, paraquat and rotenone is still under debate. Importantly, mechanisms underlying pesticide-related dopaminergic neurodegeneration are also still largely unclear.

Chapter 2

Thesis Outline

Chapter 1 clearly indicates that considerable knowledge on how pesticide exposure can be related to degenerative processes is already available. A number of key processes has been identified in *in vitro* and *in vivo* research that reportedly play a role in pesticide-induced PD. However, a lot is known about only a few compounds, whereas the large majority of compounds is still under-studied. In line with this, there are only a few compounds that are clearly linked to the human diseased state. Therefore, it remains to be determined which pesticides, or classes of pesticides, and which cellular processes are truly determining the risk of PD.

The research presented in this thesis focused on several overt and more subtle adverse effects of well-known as well as unknown pesticides. The adverse effects of these pesticides have been studied with various techniques in dopaminergic cells (**chapter 3**) in an attempt to shed some light on common pathways of toxicity that are potentially involved in dopaminergic neurodegeneration.

Considering the lack of neurotoxicological data for many classes of chemical compounds, including pesticides, there is an increasing demand for high throughput techniques for neurotoxicological hazard identification. The available high throughput methodologies usually assess rather basic endpoints (e.g. cell viability, oxidative stress, apoptosis) rather than more subtle endpoints, such as functional properties (e.g. membrane channel function, neurotransmitter release). Functional properties are usually still assessed using fluorescence microscopy and electrophysiological techniques, which are sensitive and accurate though rather laborious. As intracellular calcium is a vital parameter in many processes including inter- and intracellular communication, the first aim of this research was to explore the potential of a high-throughput multiwell system to screen for effects on intracellular Ca^{2+} homeostasis (**chapter 4**). We performed a study comparing a multiwell plate reader system with single-cell fluorescence microscopy. It turned out that the high-throughput approach was far from flawless; therefore, we still rely on single-cell fluorescence microscopy for the assessment of intracellular Ca^{2+} homeostasis to determine effects of pesticide exposure.

Organochlorine insecticides are persistent chemicals that are linked to parkinsonian neurodegeneration in epidemiological studies as well as *in vitro* mechanistic studies. To investigate whether changes in intracellular Ca^{2+} homeostasis of dopaminergic cells could play a role, we studied the effects of the organochlorine insecticide lindane on Ca^{2+} homeostasis and other neurophysiological measures of functionality, such as dopamine release and membrane potential (**chapter 5.1**). In biological samples lindane is found often concurrent with another organochlorine insecticide, dieldrin. Notably, in a study on chemical exposure in post-mortem human brains, lindane and dieldrin were detected more frequently and in higher concentrations in the basal ganglia of brains of PD patients. Therefore, we studied the effects of dieldrin and mixtures of dieldrin and lindane on Ca^{2+} homeostasis and parameters of cell viability (**chapter 5.2**). These studies provide data on the

differential effects of lindane and dieldrin on measures of functionality in dopaminergic neurotransmission.

Despite the fact that one of the most well-known PD-linked pesticides is an herbicide (i.e., paraquat), herbicides are clearly an under-studied type of pesticides in neurotoxicology. Derivatives of 2,4-dinitrophenol comprise a widely used class of herbicides, notorious for their acute toxicity. It has been shown that agricultural workers have experienced high levels of exposure to these compounds during the spraying season. However, data on long-term effects of exposure to sub-toxic levels of dinitrophenolic herbicides is lacking. Therefore, we studied the effects of dinitrophenolic herbicides on parameters of dopaminergic neuro-degeneration as observed in PD (**chapter 6.1**) as well as acute neurotoxicity on neurotransmitter (GABA) receptor function (**chapter 6.2**).

Besides exposure to persistent (often phased-out) compounds, such as organochlorine insecticides, humans are also exposed to a range of pesticides that are currently in use or abundantly present in the environment. Azole fungicides comprise a substantial fraction of current human food-borne pesticide exposure. They are applied in considerable quantities, both pre- and post-harvest to prevent fungal infections in food and feed. Despite the fact that they are widely used and abundantly present in the food chain, fungicides represent a relatively under-studied group of compounds with respect to neurotoxicology. Therefore, we investigated the neurotoxic potential of six different azole fungicides with respect to Ca^{2+} homeostasis, oxidative stress and cell viability, both as single compounds and in mixtures (**chapter 7**).

The abovementioned research resulted in a set of five reference pesticides that target different aspects of dopaminergic neurotoxicity. Though the well-characterized PC12 cell model proved suitable to study *in vitro* neurotoxicity, it has often been criticized as it is a non-human, non-neuronal, tumour-derived model. We therefore characterized a number of novel as well as widely used cell lines with regards to the presence of neurotransmitter receptors. In addition, we compared the response of these different models in oxidative stress and cell viability studies using exposure to our five reference pesticides (**chapter 8**).

In the general discussion (**chapter 9.1**) the observed effects (**chapters 4-8**) will be placed in the context of available literature, proposed mechanisms of action and relevant human exposure. A risk assessment of possible human neurotoxicity upon exposure to pesticides in general and the discussed pesticides in particular is included in **chapter 9.2**. Data gaps and future directions are discussed, and conclusions are summarized in **chapter 9.3**.

Chapter 3

Endpoints and Applied Methodologies

3.1 Cell lines

There are many cell models available for the study of compound-induced neurotoxicity. However, intrinsic properties of the available cell lines differ considerably, rendering some cell lines more suitable for specific techniques than others.

Rat pheochromocytoma PC12 cells

PC12 cells are well-characterized dopaminergic cells derived from a rat adrenal tumor (pheochromocytoma) (Greene and Tischler 1976). PC12 excrete considerable amounts of catecholamines, including DA, in particular upon differentiation with dexamethasone. As a result, the PC12 cell is a suitable model for electrophysiological techniques, such as amperometry (Westerink 2006, Westerink and Ewing 2008). PC12 cells contain several functional VGCCs, including dihydropyridine-sensitive Cav1.3 (L-type), ω-conotoxin-sensitive Cav2.2 (N-type) and ω-agatoxin-sensitive Cav2.1 (P/Q-type) channels (Dingemans, *et al.* 2009, Greene and Tischler 1976, Shafer and Atchison 1991). Therefore, PC12 cells provide a good model to study the influence of environmental contaminants on exocytosis and properties of Ca2+-homeostasis.

Rat neuroblastoma B35 cells

The B35 rat neuroblastoma cell line provides a non-dopaminergic cell model that has proven useful for the study of endocytosis and intra- and intercellular signalling pathways (Otey, *et al.* 2003). As a consequence of their high expression of calcium-permeable nACh channels, they display a robust Ca^{2+}-influx upon stimulation with acetylcholine (Heusinkveld and Westerink 2011; see also chapter 4) providing a useful model to study the influence of toxic compounds on ACh-mediated signalling (see e.g. Hendriks, *et al.* 2012).

Hybrid mesencephalic MES23.5 cells

The MES23.5 cell line is derived from a somatic fusion of rat embryonic mesencephalon cells and the murine N18TG2 neuroblastoma-glioma cell line (Crawford 1992). These hybrid cells contain ω-conotoxin-sensitive calcium channels (N-type, Cav2.2), express tyrosine hydroxylase (TH) and synthesize DA (Crawford 1992, Schneider, *et al.* 1995). Differentiation of MES23.5 with cAMP results in a more pronounced dopaminergic phenotype characterized by elevated expression of VGCCs as well as elevated TH activity and DA synthesis (Crawford 1992). The MES23.5 cells reportedly resemble mesencephalic dopaminergic neurons from the substantia nigra, thus rendering these cells of interest for the study of (parkinsonian) dopaminergic neurodegeneration.

Rat mesencephalic N27 cells

The N27 cell line is an immortalized rat mesencephalic dopaminergic cell line. N27 cells reportedly express TH and are used to study biochemical aspects of *in vitro* (parkinsonian) dopaminergic neurodegeneration (see e.g. Kanthasamy, *et al.* 2006, Latchoumycandane, *et al.* 2005).

Human neuroblastoma SH-SY5Y cells

The human SH-SY5Y cell is a neuroblastoma clone, derived from a sympathetic ganglion (Ross and Biedler 1985). SH-SY5Y cells express functional Cav1.3 (L-type) and Cav2.2 (N-type) VGCCs as well as muscarinic (M1-3) and bradykinin (B2) receptors and synthesize DA as well as noradrenaline. Although the cell line is often referred to as dopaminergic, the cells contain more noradrenaline than dopamine, rendering SH-SY5Y cells above all a suitable model to study compound-induced effects in sympathetic neurons.

The cell lines described here, have been exposed to a selection of pesticides (see table 1), where after a wide array of endpoints is measured as described in chapter 3.2 and 3.3.

3.2 Measurements of cell damage and death

Alamar Blue / CFDA-AM (for more details see chapter 6.1, 7 & 8)

There are many assays available to measure toxicity of pesticides via changes in cell viability. A combined alamar Blue / CFDA assay was used to assess two different readouts of cell viability in one assay using a protocol adapted from a publication by Bopp and Lettieri (Bopp and Lettieri 2007).

The alamar Blue (aB) assay is based on the reduction of the non-toxic and non-fluorescent resazurin to the bright fluorescent resorufin by mitochondrial oxidoreductases (including complex 1) in viable cells. Resorufin is excreted from the cell and thus requires no cell lysis prior to measurement. As such, the readout represents mitochondrial activity that can be used as a measure for viability of the cells. Since cell lysis is not required for measurement, the aB assay can be combined with the CFDA-AM assay.

aB is added to the cells together with the non-fluorescent dye CFDA-AM. With its acetoxymethyl (AM) ester bound, this dye is a non-fluorescent cell permeable dye. Once diffused into the cell the dye is de-esterified by non-specific intracellular esterases. De-esterification results in a fluorescent CFDA molecule, which is trapped inside the cell. Viable cells with an intact plasma membrane will readily take up and de-esterify the dye, whereas this process is hampered in damaged-cells.

Therefore, CFDA serves as a measure for membrane integrity and as such as a second measure of cell viability.

The technical advantages of this combined assay over widely established methods such as the MTT-reduction assay is that this assay is non-invasive and simultaneously provide two measures of cell viability. In addition, under most circumstances the assay does not require washing steps, thus reducing the risk of cell loss and related artefacts.

Neutral Red (for more details see chapter 5.1)

The Neutral Red (NR) uptake assay is a widely used assay, based on the ability of viable cells for uptake of the dye in the lysosomes because of the steep pH gradient between the cytosol and the interior of the lysosome (Repetto, *et al.* 2008). Uptake of NR in viable cells is a passive process and as integrity of the lysosomal pH correlates to cell viability, the amount of dye incorporated in the lysosomes provides a measure of cell viability. Measurement of NR fluorescence is an invasive process, requiring wash- and extraction steps. Therefore, the assay is less suitable for cells with a weak attachment to culture material, such as PC12 cells. When using well-attached cells, the NR assay can be performed subsequent to the non-invasive combined aB/CFDA assay.

Oxidative stress (for more details see chapter 4 – 6.1, 7 & 8)

Oxidative stress is implicated in a wide variety of pathological processes, including dopaminergic neurodegeneration. ROS generation upon exposure to pesticides was assessed using the cumulative fluorescent dye H_2-DCFDA. The fact that H_2-DCFDA is a cumulative dye is an advantage for its use in high-throughput techniques as kinetic measurements are not needed for detection of oxidative stress. 2,7-DCF (2,7-dichlorofluorescin) based ROS assays such as the H_2-DCFDA assay detect a number of different radicals (Jakubowski and Bartosz 2000) and provide thus a broad indication of oxidative stress. Therefore, these assays are not suitable to identify the specific reactive (oxygen) species produced.

Caspase (for more details see chapter 6.1)

Activation of caspase-mediated apoptosis is one of the possible scenarios upon cell damage and involves a cascade of processes ultimately leading to death of the cell. Relatively independent of the upstream processes and the organelles involved, the cascade of caspase-mediated apoptosis ends with the activation of one of the effector caspases (caspase-3, -6 or -7; for review see: Orrenius, *et al.* 2011). Therefore, measurement of caspase-3 activity is an appropriate readout for caspase-mediated apoptosis.

Immunostaining of α-synuclein (for more details see chapter 6.1)

α-Synuclein is an intracellular protein that is implicated in the pathophysiology of, among others, PD. Under physiological conditions, cytosolic (soluble) α-synuclein is involved in regulation of the vesicle cycle and thus in the release of neurotransmitters, including DA. Under pathological conditions, α-synuclein monomers aggregate to protofibrils that can result in insoluble α-synuclein fibrils and the formation of intracellular inclusions called Lewy-bodies (for review see: Venda, *et al*. 2010). It is known that exposure to compounds implicated in PD, such as rotenone, results in the formation of pathological α-synuclein aggregates (Betarbet, *et al*. 2000, Sherer, *et al*. 2003b).

To assess intracellular α-synuclein levels, α-synuclein was stained using specific antibodies and analysed using confocal microscopy. Cells were permeabilized and α-synuclein was labelled with a primary antibody, which was subsequently labelled using a secondary antibody with a fluorophore attached. A-specific binding was checked using samples labelled with either primary or secondary antibody and a-specific binding was not detectable. Considering the sensitivity and spatial resolution of confocal microscopy this was considered the most appropriate method.

Other methods of detection for α-synuclein include flow cytometry analysis (FACS) and western blotting. Although FACS detects fluorescence on single-cell basis, the method proved not suitable to detect the changes in intracellular α-synuclein upon exposure to DNOC and dinoseb (chapter 6.1) in a reproducible way. Also, aggregation of α-synuclein without an increased total α-synuclein protein level will most likely stay unnoticed using FACS.

Alternatively, Western blotting can be used to identify different aggregated forms of α-synuclein, but Western blotting relies strongly on the availability of specific antibodies and provides information in cell population level. With regards to quantification, Western blotting has no added value compared to confocal microscopy as quantification in western blotting relies on fluorescence-intensity measurements as well.

3.3 Measurements of cell function

Intracellular calcium homeostasis (for more detail see chapters 4 - 6.1 & 7-8)

Calcium is a highly versatile signalling molecule used by neuronal cell types for a wide variety of functions from inter- and intracellular signalling, development and degeneration. Cells maintain their intracellular Ca^{2+} homeostasis by a tightly controlled system of pumps and channels located either in the cell membrane or in the membrane of the intracellular organelles used for extrusion or compartmentalization of cytosolic Ca^{2+}. Compartmentalization into the ER involves mainly the sarco/endoplasmic reticular Ca^{2+}/ATPase (SERCA), whereas in mitochondria the

mitochondrial uniporter is involved (see Fig 3). Considering the highly dynamic nature of intracellular Ca^{2+} handling, real time kinetic measurements are required with sufficient spatial and temporal resolution. For this reason, single-cell fluorescence microscopy measurements are the method of choice over high-throughput plate reader-based technology. As single-wavelength dyes such as Fluo-4 are unable to discriminate between artefacts, such as quenching or dye leakage, and real changes in intracellular Ca^{2+}, dual-wavelength dyes (e.g. Fura-2) are preferred.

Measurement of DA release by amperometry (for more details see chapter 5.1)

To detect effects on basal and depolarization-evoked DA release in PC12 cells, DA-release was measured using carbon-fiber microelectrode amperometry in dexamethasone-differentiated PC12 cells as described previously (Westerink 2006, Westerink 2004).

Measurement of exocytosis with amperometry relies on the measurement of oxidizable neurotransmitter (in this case DA) with an electrode placed against the cell surface. The electrode is set at a sufficiently high voltage (700 mV) to oxidize released neurotransmitter. Upon exocytosis, DA is released and instantaneously oxidized on the electrode surface. The current measured upon release and oxidation is proportional to the amount of DA released. Vesicular DA content can be calculated from the time integral of the current during the release event.

Advantages of this technique are its high temporal resolution (ms) and high sensitivity (~9000 oxidizable catechol molecules, 15 zeptomole). Disadvantages are mainly related to the limitation to detection of oxidizable neurotransmitters such as DA and serotonin (5-HT), rendering neurotransmitters such as glutamate and GABA undetectable with this technique. In addition, measurements are limited to the area under or near the electrode and hence measurements do not represent full cellular dopamine release.

Two-electrode voltage-clamp (for more details see chapter 6.2)

To investigate pesticide-induced effects on human $GABA_A$ ($hGABA_A$) receptors, Xenopus laevis oocytes injected with cDNA of the different $hGABA_A$ receptor subunits were used. Based on the composition of the cDNA mixture injected, $GABA_A$ receptors with an α1ß2γ2 subunit composition are expected to be expressed. Three to five days after injection, GABA-evoked currents were measured using the two-electrode voltage-clamp technique.

This oocyte model in combination with the voltage-clamp technique allows for the assessment of chemical-induced effects on functional parameters of a single channel (sub)type and is therefore suitable to assess pesticide-induced effects on human $GABA_A$ receptors.

Table 1 Pesticides used in the research included in this thesis

Class	Chemical name	Trade name	CAS #	MW	log K_{ow}
Organochlorine insecticide	γ-hexachlorocyclohexane	Lindane	58-89-9	290,8	3,9
	1,2,3,4,10,10-hexachloro-6,7-epoxy-1,4,4a,5,6,7,8,8a-octahydr-1,4,5,8-dimethano-naphtalene	Dieldrin	60-57-1	380,9	6,2
Triazole fungicide	2-(4-Chlorophenyl)-3-cyclopropyl-1-(1H-1,2,4-triazol-1-yl)-2-butanol	Cyproconazole	94361-06-5	291,8	2,90
	1-(4-Chlorophenyl)-4,4-dimethyl-3-(1H-1,2,4-triazol-1-ylmethyl)-3-pentanol	Tebuconazole	107534-96-3	307,8	3,70
	1-{[Bis(4-fluorophenyl)(methyl)silyl]methyl}-1H-1,2,4-triazole	Flusilazole	85509-19-9	315,4	3,87
	1-(4-Chlorophenoxy)-3,3-dimethyl-1-(1H-1,2,4-triazol-1-yl)-2-butanone	Triadimefon	43121-43-3	293,7	2,77
	2-(2,4-Difluorophenyl)-1,3-di(1H-1,2,4-triazol-1-yl)-2-propanol	Fluconazole	86386-73-4	306,3	0,25
Imidazole fungicide	1-[2-(Allyloxy)-2-(2,4-dichlorophenyl)ethyl]-1H-imidazole	Imazalil	35554-44-0	297,2	3,82
Dinitrophenolic herbicide	2,4-Dinitrophenol	2,4-DNP	51-28-5	184,1	1,67
	3,5-Dinitro-ortho-cresol	DNOC	497-56-3	198,1	2,56
	2-sec-Butyl-4,6-dinitrophenol	Dinoseb	88-85-7	240,2	3,56
	2-(Methyl-2-propanyl)-4,6-dinitrophenol	Dinoterb	1420-07-1	240,2	3,64
Botanical insecticides	(2RS,6aS,12aS)-2-Isopropenyl-8,9-dimethoxy-1,2,12,12a-tetrahydrochromeno[[3,4-b]furo[2,3-h]chromen-6(6aH)-one	Rotenone	83-79-4	394,4	2,54

Do not condemn the judgment of another
because it differs from your own.
You may both be wrong.

Attrib. to Tao Tze

Chapter 4

Caveats and limitations of plate reader-based high-throughput kinetic measurements of intracellular calcium levels

Harm J. Heusinkveld[1], Remco HS Westerink[1]

[1] Neurotoxicology Research Group, Institute for Risk Assessment Sciences (IRAS), Utrecht University, the Netherlands

Toxicology and Applied Pharmacology 255, 1-8

Abstract

Calcium plays a crucial role in virtually all cellular processes, including neurotransmission. The intracellular Ca^{2+} concentration ($[Ca^{2+}]_i$) is therefore an important readout in neurotoxicological and neuropharmacological studies. Consequently, there is an increasing demand for high-throughput measurements of $[Ca^{2+}]_i$, e.g. using multi-well microplate readers, in hazard characterization, human risk assessment and drug development. However, changes in $[Ca^{2+}]_i$ are highly dynamic, thereby creating challenges for high-throughput measurements. Nonetheless, several protocols are now available for real-time kinetic measurement of $[Ca^{2+}]_i$ in plate reader systems, though the results of such plate reader-based measurements have been questioned. In view of the increasing use of plate reader systems for measurements of $[Ca^{2+}]_i$ a careful evaluation of current technologies is warranted. We therefore performed an extensive set of experiments, using two cell lines (PC12 and B35) and two fluorescent calcium-sensitive dyes (Fluo-4 and Fura-2), for comparison of a linear plate reader system with single cell fluorescence microscopy. Our data demonstrate that the use of plate reader systems for high-throughput real-time kinetic measurements of $[Ca^{2+}]_i$ is associated with many pitfalls and limitations, including erroneous sustained increases in fluorescence, limited sensitivity and lack of single cell resolution. Additionally, our data demonstrate that probenecid, which is often used to prevent dye leakage, effectively inhibits the depolarization-evoked increase in $[Ca^{2+}]_i$. Overall, the data indicate that the use of current plate reader-based strategies for high-throughput real-time kinetic measurements of $[Ca^{2+}]_i$ is associated with caveats and limitations that require further investigation.

Keywords: Calcium measurements, high-throughput screening, probenecid, plate reader, Fura-2, Fluo-4

Introduction

There is an increasing demand for high-throughput screening (HTS) in toxicity testing, mainly because of its cost-effectiveness and speed. Until recent years, HTS was largely limited to screening for cytotoxicity, using e.g., the MTT assay (Denizot and Lang 1986). Nowadays, several high-throughput assays are available to assess cell viability, cytotoxicity and apoptosis (see e.g., Lövborg, *et al.* 2005, Schoonen, *et al.* 2009). Though useful as a first step to determine non-cytotoxic concentrations for further testing, several more subtle and organ- and cell type-specific endpoints that do not necessarily lead to acute cytotoxicity (e.g., disruption of intracellular calcium homeostasis, mitochondrial disregulation, or inhibition of transporters or channels) need to be assessed for proper hazard characterization.

This requirement makes the use of HTS challenging, particularly in neuroscience, neuropharmacology and neurotoxicology. Neuron specific endpoints, including calcium homeostasis, electrical activity, neurotransmitter release as well as receptor and channel activation, are highly dynamic. Although static fluorescent or luminescent signals are, due to experimental design of plate reader, the favored endpoints for high-throughput (neurotoxicity) studies, efforts have been made to use HTS for real-time kinetic measurements of neuronal signals, including agonist or chemical-induced dynamic changes in the intracellular Ca^{2+} concentration ($[Ca^{2+}]_i$). Ca^{2+} plays an essential role in a large number of cellular processes, including neurotransmission (for reviews see: Garcia, *et al.* 2006, Westerink 2006), gene expression (for review see: Carrasco and Hidalgo 2006) and programmed (apoptosis) as well as necrotic (e.g., via mitochondrial disruption or release of degradative enzymes) cell death (for review see: Orrenius, *et al.* 2011). Neuronal cells therefore exert strong control over the dynamics of their Ca^{2+} signals, i.e., tightly regulate the balance between Ca^{2+} influx, Ca^{2+} extrusion, Ca^{2+} sequestration and Ca^{2+} buffering by cytosolic Ca^{2+} binding proteins (for reviews see: Berridge, *et al.* 2003, Garcia, *et al.* 2006, Kostyuk and Verkhratsky 1994, Miller 1991, Westerink 2006). As a result, Ca^{2+} signals are highly dynamic with fast, transient increases and oscillations that occur in seconds to minutes (Eilers, *et al.* 1995). Due to the dynamics of Ca^{2+} signals, real-time kinetic measurements of Ca^{2+} are required. Also, Ca^{2+} fluorescent dyes and equipment to measure the Ca^{2+}-derived transient fluorescent signals need to have sufficient sensitivity and temporal resolution. While single cell fluorescent microscopy meets these demands it is also labor intensive and time consuming. Despite the fact that the sensitivity of plate readers is rather low compared to fluorescent microscopy, measurements of $[Ca^{2+}]_i$ kinetics with plate readers would thus be favorable. Consequently, many laboratories now use plate readers and a large amount of HTS data on changes in $[Ca^{2+}]_i$ has become available. However, the accuracy and suitability of plate readers to determine dynamic changes in $[Ca^{2+}]_i$ has recently been questioned as results obtained with plate readers differ between studies and in many cases do not match electro

physiological recordings and fluorescent microscopy data (Westerink and Hondebrink 2010). As there is a clear need for reliable HTS strategies in (neuro) toxicity testing and drug development, the aim of this study is to carefully compare current high-throughput real-time kinetic Ca^{2+} measurement strategies with (single cell) fluorescent microscopy. We therefore used extensively characterized dopaminergic PC12 cells (Westerink and Ewing 2008) as well as non-dopaminergic B35 neuroblastoma cells (Otey, *et al.* 2003) for measurements of $[Ca^{2+}]_i$ using two common fluorescent dyes (Fura-2 and Fluo-4) to compare plate reader and single cell microscopy experiments.

Materials and methods

Chemicals.

NaCl, KCl and HEPES were obtained from Merck (Whitehouse Station, NJ, USA); $MgCl_2$, $CaCl_2$, glucose, sucrose, and NaOH were obtained from BDH Laboratory Supplies (Poole, UK). Fura-2 (pentapotassium salt), Fura-2 AM, and Fluo-4 AM were obtained from Molecular Probes (Invitrogen, Breda, The Netherlands). All other chemicals were obtained from Sigma-Aldrich (St. Louis MO, USA) unless otherwise noted. Saline solutions were prepared with deionized water (Milli-Q®; resistivity >10 MΩ cm). Stock solutions were prepared just prior to the experiments.

Cell culture.

Rat pheochromocytoma (PC12) cells (Greene and Tischler 1976) were cultured in RPMI 1640 (Invitrogen, Breda, The Netherlands) supplemented with 5% fetal calf serum and 10% horse serum (ICN Biomedicals, Zoetermeer, The Netherlands) as described previously (Heusinkveld, *et al.* 2010). Rat neuroblastoma (B35) cells (Otey, *et al.* 2003) were cultured in DMEM (Invitrogen, Breda, The Netherlands) supplemented with 10% fetal calf serum (ICN Biomedicals, Zoetermeer, The Netherlands) and 1% additional amino acids (stock solution containing 40 mM of L-Cys, L-Ala, L-Asp, L-Pro, L-Glu and L-Asx). For fluorescent microscopy Ca^{2+} imaging experiments, undifferentiated PC12 (1.4×10^6 cells/dish; ± 75% confluency) or B35 (1.4×10^6 cells/dish; ± 75% confluency) cells were subcultured in poly-L-lysine (50 µg/ml) coated glass-bottom dishes (MatTek, Ashland, MA) as described previously (Heusinkveld, *et al.* 2010). For fluorescent plate reader Ca^{2+} imaging experiments, undifferentiated PC12 ($1.5\ 10^5$ cells/well; ± 100% confluency) or B35 ($1.2\ 10^5$ cells/well; ± 100% confluency) cells were subcultured in poly-L-lysine (50 µg/ml) coated, black, clear-bottom, 96-well plates (Greiner Bio-one, Solingen, Germany). Cells were grown in a humidified incubator at 37°C and 5% CO_2.

Fluorescent Ca^{2+} imaging.

Changes in $[Ca^{2+}]_i$ were measured using the Ca^{2+}-sensitive fluorescent ratio dye Fura-2 or the Ca^{2+}-sensitive fluorescent single wavelength dye Fluo-4. Briefly, cells were loaded with 5 µM Fura-2 AM or 5 µM Fluo-4 AM (Molecular Probes; Invitrogen, Breda, The Netherlands) in saline (containing in mM: 1.8 $CaCl_2$, 24 glucose, 10 HEPES, 5.5 KCl, 0.8 $MgCl_2$, 125 NaCl, and 36.5 sucrose at pH 7.3, adjusted with NaOH) for 20 min at room temperature (RT), followed by 15 min (Fura-2 AM) or 30 min (Fluo-4 AM) de-esterification in external saline at RT. In specific experiments, probenecid was used to prevent/reduce dye-leakage. Briefly, probenecid was dissolved in external saline and pH was adjusted to 7.3. Unless otherwise noted cells were loaded for 15 min with probenecid (2.5 mM) during de-esterification (protocol adapted from Di Virgilio, *et al.* 1990). Cells were continuously exposed to probenecid during measurements. For microplate reader experiments, cells were placed in an Infinite M200 microplate reader equipped with a Xenon Flash light source (10W; Tecan Trading AG, Männedorf, Switzerland) controlled by iControl software (version 7.1). For fluorescence microscopy, cells were placed on the stage of an Axiovert 35 M inverted microscope (40× oil-immersion objective, NA 1.0; Zeiss, Göttingen, Germany) equipped with a TILL Photonics Polychrome IV (Xenon Short Arc lamp, 150W) and an Image SensiCam digital camera (TILL Photonics GmBH, Gräfelfing, Germany). Camera and polychromator were controlled by imaging software (TILLvisION, version 4.01), which was also used for data collection and processing. Fluorescence was evoked by 340- and 380-nm excitation wavelengths (F340 and F380, Fura-2) or 488-nm excitation wavelength (F488, Fluo-4) and collected at 510 nm (Fura-2) or 520 nm (Fluo-4). Data was collected every 3 s in the plate reader (exposure: 15 flashes at 40 Hz) and every 6 s in fluorescence microscopy (exposure: 2 ms). Significant dye bleaching did neither occur in plate reader nor in microscopy. To assess dynamic ranges for both plate reader and microscopy, maximum and minimum fluorescence values (at 340 and 380 nm excitation wavelength) were determined in separate experiments in which Fura-2 loaded PC12 cells were incubated with ionomycin (5 µM) and ethylenediamine-tetraacetic acid (EDTA; 17 mM). Data on changes in F340/F380 (Fura-2) from fluorescence microscopy were analyzed using a custom-made MS-Excel macro which calculates F340/F380 ratio values from the raw F340 and F380 data reflecting changes in $[Ca^{2+}]_i$ and includes background correction. Data on changes in F488 (Fluo-4) from fluorescence microscopy as well as all data from the plate reader were analyzed manually with correction for background where applicable.

Data analysis and statistics.

All data are presented as mean F340/F380 (± SD; normalized to baseline; Fura-2 AM) or as F488 (± SD; normalized to baseline; Fluo-4 AM) from the number of cells (*n*; fluorescence microscopy) or wells (*n*; plate reader) in 3–5 independent experiments unless otherwise noted. Statistical analyses were performed using GraphPad Prism version 4.00 (GraphPad Software, San Diego, California, USA). Continuous data were compared using the Student's *t*-test, paired or unpaired where applicable. A p-value ≤ 0.05 is considered statistically significant; n.s. indicates the absence of a significant effect.

Results

Initial experiments were performed to check reproducibility of the plate reader and to identify those conditions that yield the best signal and signal-to-noise ratio for measurements of $[Ca^{2+}]_i$. As most plate readers can operate in top-read and in bottom-read mode, experiments were performed with the plate reader either in top or in bottom fluorescence reading mode. The results presented in Fig. 1A demonstrate a sharp but limited increase in F340/F380 in Fura-2-loaded PC12 cells upon injection of 100 µl high-K^+ containing saline into 200 µl starting volume per well (final concentration: 50 mM K^+), both in top- and in bottom-read mode. Although data obtained in bottom read mode reveal a larger change in F340/F380 compared to top-read measurements, suggestive of a higher sensitivity, raw experimental data (not shown) revealed that the fluorescence yield (F340 and F380) in bottom-read experiments is often only 10 – 20% of the yield in top-read experiments in the same well plate. Similarly, a sharp but limited increase in F340/380 is observed upon injection of 100 µl ATP containing saline (final concentration 100 µM ATP; Fig. S1) in both top- and bottom-read mode, with the bottom-read mode yielding a lower total fluorescence yield (raw data; not shown). In summary, the change in F340/F380 is highest in bottom-read experiments but the standard deviation is also high and the total fluorescence yield is low. Hence, subsequent experiments were performed in top-read mode.

To obtain a dynamic range for both plate reader assays and fluorescence microscopy, PC12 cells were loaded with Fura-2 and subsequently incubated with ionomycin (5 µM) to obtain maximum F340/F380 followed by addition of EDTA (17 mM) to obtain minimum F340/F380. The results revealed a dynamic range in fluorescence microscopy ranging from an R_{min} of 0.60 ± 0.37 (n=8) to an R_{max} of 10.94 ± 1.18 (n=8). In the plate reader the dynamic range ranges from an R_{min} of 0.87 ± 0.15 (n=4) to an R_{max} of 3.71 ± 0.10 (n=4) (Fig. S2). The width of these dynamic ranges suggests that the sensitivity of the plate reader to detect changes in fluorescence is lower compared to fluorescence microscopy.

Notably, in plate reader experiments the changes in F340/F380 in Fura-2-loaded PC12 cells appear to be sustained rather than transient, irrespective of the type of stimulation. To investigate whether these sustained increases could be due to changes in the volume of the wells, experiments were performed with injection of different volumes in two different starting volumes. Injection of 50 µl saline to a starting volume of 100 µl saline increases F340/F380 from 1.00 ± 0.01 to 1.05 ± 0.02 (n=7; data not shown). Injection of 50 µl to 200 µl induces a rather comparable change in F340/F380 to 1.04 ± 0.02 (n=10; Fig. 1B). Injection of 100 µl to 100 µl increases F340/F380 to a level of 1.09 ± 0.03 (n=7; data not shown), whereas injection of 100 µl saline to a starting volume of 200 µl saline increases F340/F380 from 1.00 ± 0.01 to 1.11 ± 0.03 (n=10; Fig. 1B). Though this increase to ~1.1 appears modest, it should be noted that 50 mM K^+ or 100 µM ATP increase the ratio only to ~1.3.

These experiments thus demonstrate that the injection volume can be a considerable source of bias in plate reader experiments and should be kept constant. In addition to injection volume, changes in ionic composition or ionic strength of the medium may further affect the fluorescent signal as fluorescent dyes are known to be sensitive to changes in ionic condition (Roe, *et al.* 1990, Westerink and Vijverberg 2002a).

Therefore, experiments were performed with Fura-2-loaded PC12 cells to assess the effects of injection of different concentrations of high-K^+ containing saline in different volumes on the changes in F340/F380 (Fig. 1C). These experiments confirm that the increase in fluorescence ratio upon injection of high-K^+ containing saline (final concentration 10 mM) is affected by the injected volume as injection of 7 µl stock solution induces an average increase in fluorescence to 1.04 ± 0.03 (n=8), whereas injection of 100 µl from a less-concentrated stock solution to obtain the same final-concentration (10 mM) induces a fluorescence increase amounting to 1.10 ± 0.03 (n=17). However, at higher final concentrations of K^+ (≥50mM) differences in injection volume do not account for differences in the increase in F340/F380. This illustrates that a change in ionic composition from high Na^+ to high K^+ contributes to the observed sustained increase in F340/F380. Experiments with membrane-impermeable Fura-2 pentapotassium salt (in the absence of cells) further illustrate this concentration-dependent sustained increase in F340/F380 upon a change in ionic composition (from high-Na^+ to high-K^+; see Fig. S3).

The data above demonstrate that great care should be taken in selecting the appropriate conditions for plate reader measurements to minimize errors due to changes in volume and ionic conditions. Further experiments with different stimuli (including receptor activation and depolarization) in two different cell lines were therefore performed using a fixed starting volume (200 µl) as well as a fixed injection volume (100 µl).

For plate reader measurements, Fura-2-loaded PC12 cells were challenged by application of 100 µl of different stock solutions of high-K^+ containing saline to obtain final concentrations of 10, 50 and 100 mM K^+. The results demonstrate a concentration-dependent increase of F340/F380 (Fig. 2A1). At 10 mM K^+, the increase in F340/ F380 corresponds to the increase induced solely by a change in volume with 100 µl, whereas at 50 mM K^+, the increase merely consists of a sustained phase amounting to 1.26 ± 0.09 (n=25). Upon depolarization of PC12 cells with 100 mM K^+, the increase in F340/ F380 (amounting to 1.42 ± 0.14; n=14) clearly consists of a transient part, which is absent at lower K^+ concentrations, superimposed on a sustained phase.

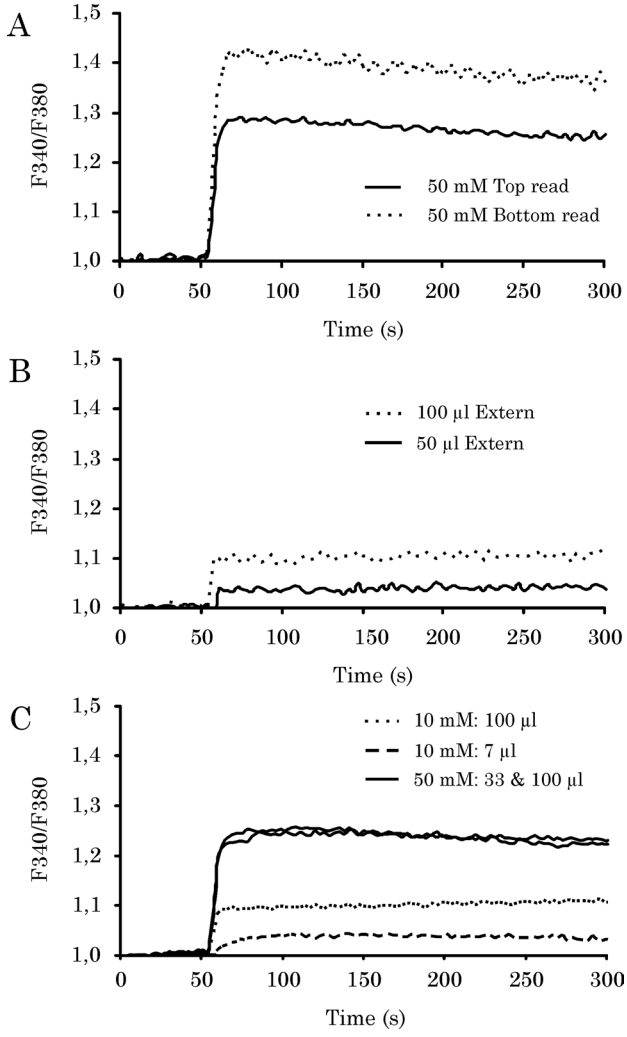

Fig. 1. Plate reader: A) Example traces illustrating the increase in F340/F380 in Fura-2-loaded PC12 cells upon injection of 100 µl high-K^+ saline (final concentration 50 mM K^+) as recorded in either top- (dotted line) or bottom- (solid line) read mode. Bottom read mode results in a larger change in F340/F380 but the noise is also increased. Therefore, all subsequent experiments are performed in top-read mode. B) Example traces illustrating the increase in F340/F380 in Fura-2-loaded PC12 upon injection of different volumes of external saline (50 (solid line) and 100 (dotted line) µl) to a starting volume of 200 µl external saline. C) Example traces illustrating the change in F340/F380 in Fura-2-loaded PC12 upon stimulation with 10 and 50 mM K^+ (final concentration) using different injection volumes (10 mM: 7 (dashed line) or 100 (dotted line) µl; 50 mM: 33 or 100 µl (both solid lines)) to 200 µl saline start volume. The increase in F340/F380 upon injection of 10 mM K^+ depends on the volume injected, whereas the increase upon stimulation with 50 mM K^+ appears less dependent on injection volume.

Depolarization using high-K^+-containing saline has the potential disadvantage of changing the ionic composition and ionic strength of the medium. These disadvantages are virtually absent when increases in $[Ca^{2+}]_i$ are evoked by activation of neurotransmitter receptors, e.g., by application of ATP or acetylcholine (ACh). To investigate whether application of ATP to Fura-2-loaded PC12 cells evoked a change in fluorescence, a fixed volume (100 µl) of ATP-containing saline was injected from different stock solutions to obtain final concentrations of 1, 10 and 100 µM ATP (Fig. 2B1). Stimulation with 1 µM ATP results in a sustained increase amounting to 1.06 ± 0.03 (n=21), whereas stimulation with 10 µM ATP induces a slightly larger and partly transient increase amounting to 1.10 ± 0.04 (n=22; $p \leq 0.05$). The largest increase in F340/F380 was observed upon injection of 100 µM ATP, which induces a transient increase amounting to 1.29 ± 0.15 (n=24; $p \leq 0.001$) that slowly decreases to a sustained level of 1.18 ± 0.08. Notably, the amplitude of the sustained increase is very comparable for 1 and 10 µM ATP but significantly larger for 100 µM ATP ($p \leq 0.001$). To assess the response of PC12 to ACh, Fura-2-loaded PC12 cells were stimulated with 10 and 100 µM ACh (100 µl fixed volume injected from different stock solutions; Fig. 2C1). The results demonstrate that exposure of PC12 cells to 10 µM ACh induces a stepwise sustained increase in fluorescence ratio amounting to 1.11 ± 0.03 (n=28), whereas exposure to 100 µM ACh induces a transient increase amounting 1.16 ± 0.07 (n=33) superimposed on a sustained level. Notably, the amplitude of the sustained increase is very comparable for 10 and 100 µM ACh.

The above-described ATP and ACh plate reader experiments were repeated in B35 cells (Fig. S4A). Compared to PC12 cells, the transient increases evoked by ATP and ACh are higher in B35 cells, amounting to a maximum fluorescence level of respectively 1.82 ± 0.54 (100 µM ATP, n=10) and 2.05 ± 0.24 (100 µM ACh, n=15). In both cases, a sustained increase was observed with ATP displaying a lower sustained increase (amounting to 1.05 ± 0.06) compared to ACh (1.31 ± 0.15). This illustrates that the maximum increase in fluorescence upon stimulation depends on the cell line used and that the occurrence of sustained increases apparently is not uniquely linked to a particular cell line. Using Fluo-4 instead of Fura-2 (see supplemental material: Fig. S4B) yields comparable results, indicating that the observed results are also not uniquely linked to the use of a dual-wavelength dye. The above-described plate reader experiments were replicated using single cell fluorescence microscopy in both PC12 (Fig. 2) and B35 cells (Fig. S5). Superfusion of Fura-2-loaded PC12 cells with different stimuli induces a sharp and fast transient increase in F340/F380 amounting to respectively 4.78 ± 1.94 (100 mM K^+; n=41), 5.80 ± 1.83 (100 µM ATP; n=61) and 2.04 ± 1.25 (100 µM ACh; n=72). Comparable results were obtained with Fluo-4 instead of Fura-2 (see supplemental material, Fig. S6 (PC12) and S7 (B35)).

When comparing the traces in Fig. 2, it is evident that the change in F340/F380 is much larger for single cell fluorescence microscopy than for the plate reader. Consequently, subtle effects may remain unnoticed in the plate reader but not in fluorescence microscopy. For example, two types of response can be observed upon stimulation of PC12 cells with 100 µM ATP (Fig. 3A1 example traces and 3A2 summary bar graph of maximum fluorescence ratio). These two different types of response are indicative of the co-existence of two different cell types with different types of receptors (Fabbro, *et al.* 2004).

The so-called type 1 response (48% of the cells) displays a fast transient increase (maximum F340/F380: 5.44 ± 0.53, n=22) with a slow decreasing tail in ~9 min descending to base-line. On the contrary, so-called type 2 responses (observed in 52% of the cells) display a significantly higher transient compared to type 1 (max. F340/F380: 8.39 ± 1.03, n=24, $p \leq 0.001$), followed by a sustained increase that does not decrease to baseline within 10 min. When stimulated with 10 µM ATP, the fraction of cells that displays a so-called type 2 response is only 11% (not shown).

By definition, plate reader experiments do not allow for single cell resolution so the signal recorded in the plate reader will be an average of type 1 and type 2 responses. As the ratio between type 1 and type 2 responses depends at least partly on the applied ATP concentration, specific effects on one of the types of response may be blurred or unnoticed in HTS experiments using a plate reader. In B35 cells, comparable type 1 and type 2 responses occur. However, compared to PC12 cells, a lower percentage of B35 cells displays a type 2 response (respectively 18% and 23% for 10 and 100 µM ATP; Fig. S8A1 example traces and S8A2 summary bar graph of maximum fluorescence ratio). This implies that the type1/type 2 ratio varies between cell lines and hence, the extent to which results are blurred by different types of response to ATP also varies.

Similarly, the fraction of ACh-responsive PC12 cells increases with the concentration of ACh from 13% at 10 µM to 63% at 100 µM ACh (Fig. 3B1 example traces; Fig. 3B2 summary bar graph). B35 cells show a comparable concentration-dependent increase in the percentage of responsive cells from 19% (1 µM ACh) to 73% (100 µM ACh) (Fig. S8B1 example traces; Fig. S8B2 summary bar graph). Again, the response recorded in a plate reader is composed of responsive and non-responsive cells, which will negatively affect detection of subtle effects

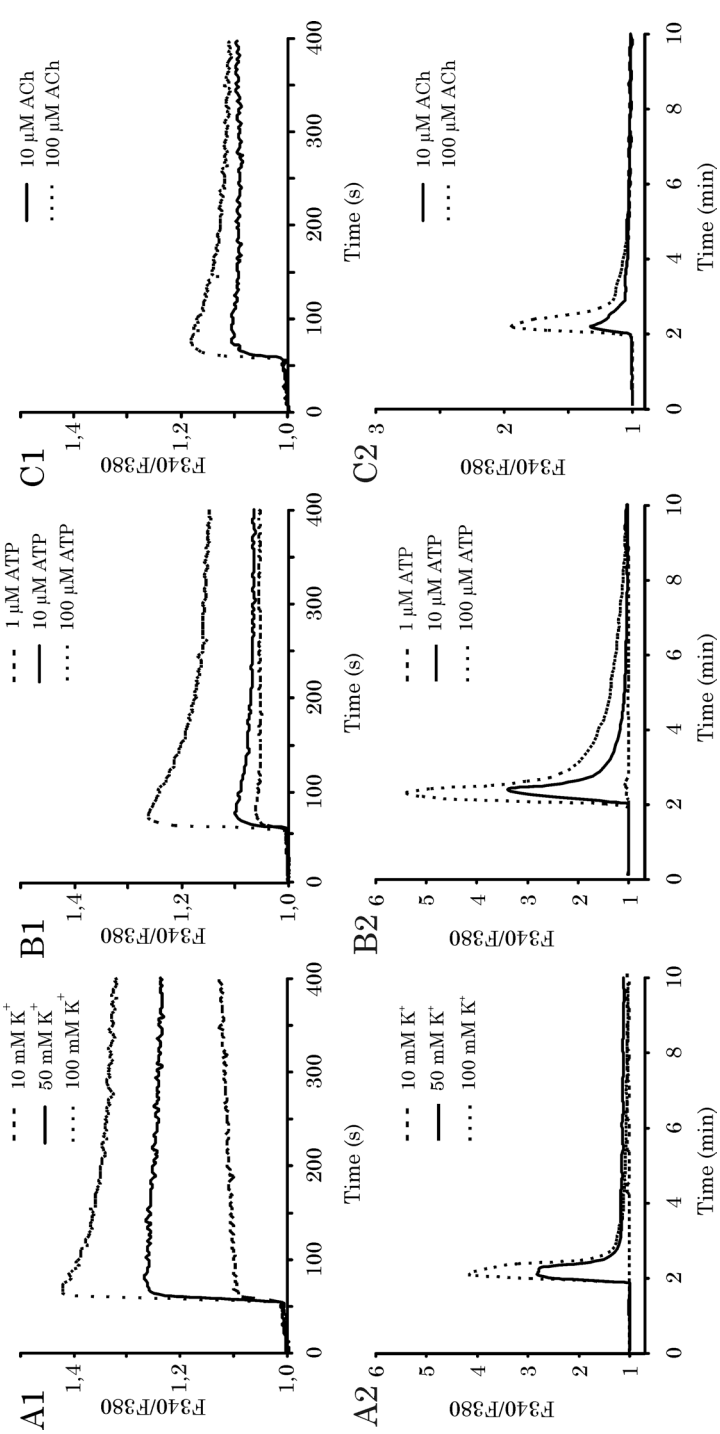

Fig. 2. Plate reader: A1) Example recordings illustrating the concentration-dependent increase in F340/F380 upon stimulation of Fura-2-loaded PC12 cells with a fixed volume of different stock solutions of K^+ to obtain final concentrations of 10 (dashed line), 50 (solid line) and 100 mM (dotted line) K^+. B1) Example recordings illustrating the concentration-dependent increase in F340/F380 upon stimulation (fixed volume) of PC12 cells with 1 (dashed line), 10 (solid line) and 100 µM (dotted line) of ATP. C1) Example recordings illustrating the concentration-dependent increase in F340/F380 upon stimulation (fixed volume) (continuation of caption Fig 2) of PC12 cells with 10 (solid line) and 100 µM(dotted line) of ACh. It should be noted that all observed increases are sustained, except for strong stimulations (i.e., 100 mM K^+, 100 µM ATP and 100 µM ACh), which induce a transient increase on top of the sustained increase. Moreover, the sustained increases can also be observed following

(Fig 2 continued) application of agonist at concentrations below effect level (e.g., 10 mM K^+). Single cell fluorescence microscopy: graph with example traces illustrating the increase in F340/F380 recorded with fluorescence microscopy upon stimulation of Fura-2-loaded PC12 cells with (A2), 10 (dashed line), 50 (solid line) and 100 mM(dotted line) K^+ (B2), 1 (dashed line), 10 (solid line) and 100 µM(dotted line) ATP and (C2), 10 (solid line) and 100 µM(dotted line) ACh. It can be observed that all three stimuli induce a sharp and fast transient increase in F340/F380 upon stimulation, all decreasing to baseline fluorescence.

The occurrence of sustained step-wise increases in F340/F380 in plate reader experiments under conditions that do not evoke any (or otherwise a transient) increase in $[Ca^{2+}]_i$ in single cell fluorescence microscopy is remarkable (see for instance Fig. 2A/B). Possibly, the step-wise increases observed in the plate reader are caused by (abrupt) leakage of dye into the recording medium. Dye leakage will result in an immediate and sustained change of dye fluorescence due to the difference in $[Ca^{2+}]_i$ and in ionic conditions between the intracellular environment and the extracellular medium. Consequently, probenecid or similar compounds are often used in an attempt to prevent dye leakage (Beacham, *et al.* 2010, Di Virgilio, *et al.* 1990, Liu, *et al.* 2010).

To assess the usefulness of probenecid in measurements of $[Ca^{2+}]_i$, plate reader experiments were carried out in Fura-2-loaded PC12 cells either incubated with 2.5 mM probenecid or DMSO vehicle. Subsequently, cells were challenged with 100 µM ATP or 100 mM K^+ to assess the increase in F340/F380. Though the sustained increase is still evident, the results demonstrate that upon loading with probenecid, the response to 100 µM ATP shows a larger transient (Fig. 4A). However, upon depolarization with 100 mM K^+ following incubation with probenecid the expected increase in F340/F380 is completely absent (Fig. 4B). Fluorescence microscopy confirms the absence of the depolarization-evoked increase in F340/F380 in responsive cells following incubation with probenecid while ATP increases F340/F380 as expected (Fig. 4C). The combined results thus demonstrate that although probenecid may reduce dye leakage, it does not prevent the sustained increase and, importantly, it clearly abolishes depolarization-evoked increases in $[Ca^{2+}]_i$.

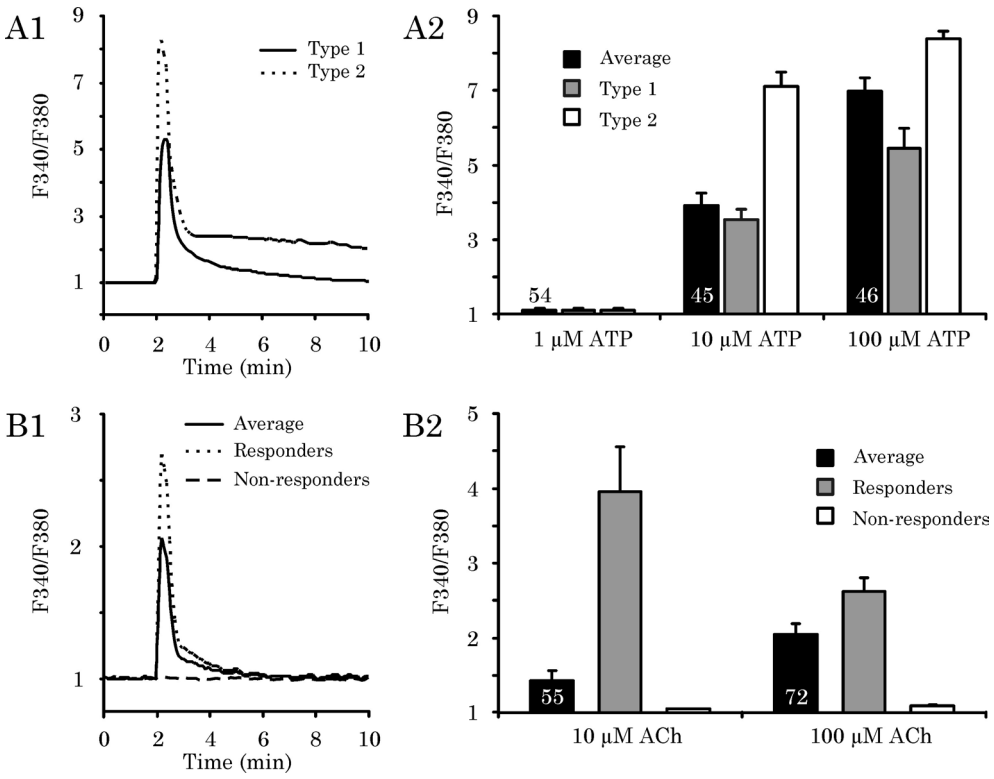

Fig. 3. Single cell fluorescence microscopy: A1) Example traces illustrating the presence of two different types of response, with different amplitudes and kinetics, in Fura-2-loaded PC12 cells stimulated with 100 µM ATP. A2) Summary bar graph displaying average maximum increase in F340/F380 upon stimulation of PC12 cells with 1, 10 or 100 µM ATP. Columns represent responses per type as well as the average overall response. Bars display average data (± SE) from the number of cells (*n*) indicated in the bars (3–5 experiments per concentration). B1) Example traces illustrating the response of Fura-2-loaded PC12 cells to stimulation with 100 µM ACh. Notably, the fraction of non-responsive cells obscures the average response, which is even more marked in experiments with 10 µM ACh (see B2). B2) summary bar graph displaying the average maximum increase in F340/F380 upon stimulation of PC12 cells with 10 or 100 µM ACh. Columns represent responses per type as well as the average overall response. Bars display average data (± SE) from the number of cells (*n*) indicated in the bars (3–5 experiments per concentration).

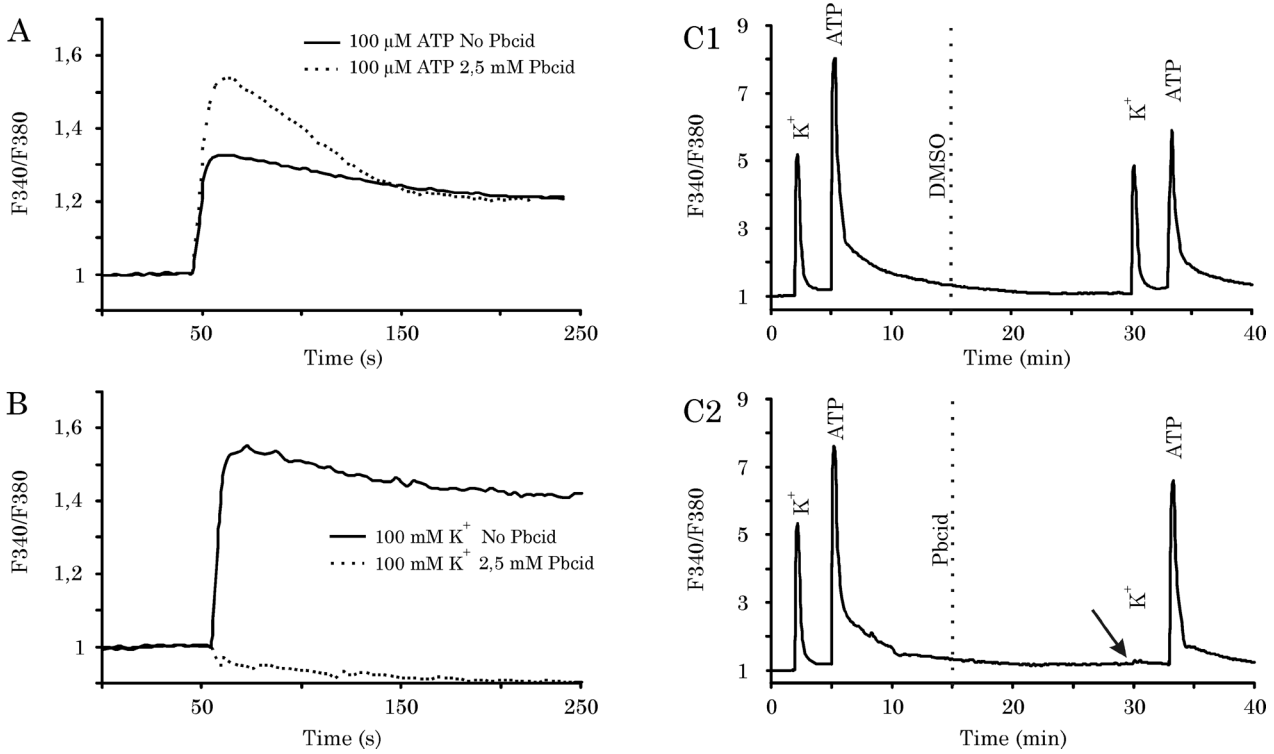

Fig. 4. Plate reader: Example traces of changes in F340/F380 upon exposure of Fura-2-loaded PC12 cells to 100 µM ATP (A) or 100 mM K^+ (B) with or without incubation with probenecid (Pbcid; 2.5 mM). Incubation with probenecid increases the response to 100 µM ATP, but does not prevent the sustained increase (A). Importantly, the response to K+-evoked depolarization is completely absent (B). Single cell fluorescence microscopy: C) example traces of Fura-2-loaded PC12 cells incubated for 15 min. with probenecid (2.5 mM) or DMSO (1 µl/ml) in between stimulations with 100 mM K^+ and 100 µM ATP (start incubation marked with dotted line). Control cells, exposed to DMSO in between stimulations, show sharp and fast transient increases in F340/F380 during both stimulations (C1). In probenecid-exposed cells, the second depolarization-evoked increase in F340/F380 is absent (arrow), while the ATP-evoked increase is still present (C2).

Concluding discussion

Our results demonstrate that plate reader-based measurements of $[Ca^{2+}]_i$ differ considerably from single cell fluorescence microscopy measurements (Fig. 2). Though sensitivity compared to fluorescence microscopy is rather low as also indicated by the width of the dynamic range in plate reader compared to microscopy (Fig. S2), most plate readers have sufficient temporal resolution to measure dynamic changes in Ca^{2+} homeostasis. Two distinct types of multi-well plate reader systems exist, i.e., linear systems measuring one well at a time and the more expensive parallel systems measuring multiple wells at the same time (for review see: Monteith and Bird 2005). Logically, for real-time measurements of several minutes, linear systems introduce a rather long delay between measurement of the first and last well. For instance, kinetic Ca^{2+} measurements of only a few minutes/well already introduce a delay of several hours between the first and the last measurement in a 96-well plate. During this delay, cells are maintained in suboptimal conditions, which may of course affect cell function and viability. Moreover, such long delays could result in dye leakage as well as dye sequestration in intracellular organelles, e.g., mitochondria. Consequently, the number of wells per plate should be restricted (preferably to limit recording time to less than an hour) and this restriction clearly hampers HTS.

Most plate readers allow for so-called top-read and bottom-read measurements. Our data (Fig. 1A) demonstrate that results obtained with different reading modes differ considerably. Although ratio changes are higher in bottom-read mode, we consider top-read mode favorable due to the higher fluorescence yield and lower noise levels. Our results are in line with findings of Kassack and co-workers (Kassack, *et al.* 2002), who also concluded that top-reading yields more stable results with the possibility to correct for artificial sustained increases.

Both single wavelength dyes (e.g., Fluo-4) and ratiometric dual wavelength dyes (e.g., Fura-2) are subject to volume-induced artificial sustained increases and dye leakage. However, in case of a single wavelength dye, the fluorescent signal is also highly dependent on experimental conditions. Variability in factors like cell density, loading efficiency of the dye as well as absolute dye concentration and leakage of dye from the cells will inevitably influence the results. Despite the higher fluorescence yield of Fluo-4, it can thus be concluded that the use of a ratiometric dye (e.g., Fura-2) is advantageous over the use of single wavelength dyes.

Differences in cell-attachment may further contribute to the variability as loosely attached cells may be stressed and/or relocated following injection of saline, potentially affecting fluorescence or its detection. Noteworthy in this respect, any test compound that induces acute cytotoxicity in a fraction of the cells will also show an increased sustained response as these cells will not be able to maintain their low $[Ca^{2+}]_i$.

Even under these optimized conditions (plate reader in top-read mode and using a ratiometric dye in properly attached cells), the increase in F340/F380 is sustained and dependent on the injection volume(Fig. 1B), irrespective of the type of stimulation (Fig. 2). As noted previously (Westerink and Hondebrink 2010), it can be debated whether these sustained increases in F340/F380 represent true increases in $[Ca^{2+}]_i$ as the stringent regulation of intracellular Ca^{2+} levels (for review see e.g., Garcia, *et al.* 2006, Toescu and Verkhratsky 2007, Westerink 2006) dictates transient rather than sustained changes in $[Ca^{2+}]_i$. Transient increases, as observed in single cell fluorescence microscopy (Figs. 2A2–C2 & S5–7), would also be in line with electrophysiological recordings (e.g., Eilers, *et al.* 1995). Notably, the observed sustained increases in plate reader measurements, if true, would indicate a continuous activation of Ca^{2+}-dependent cellular processes, including massive neurotransmission as well as imminent cell death following any kind of stimulation. Moreover, as shown in Fig. 2A1, the increase detected upon injection of a low concentration of K^+ (final concentration 10 mM) is solely due to the change in volume and, as confirmed in fluorescence microscopy, 10 mM K^+ does not induce sufficient depolarization to trigger opening of voltage-gated Ca^{2+} channels (Fig. 2A2).

Interestingly, strong stimuli capable of triggering exocytosis yield large concentration-dependent sustained increases in fluorescence in plate reader measurements. It can therefore be hypothesized that these sustained increases in F340/F380 are due to exocytosis of hydrolyzed dye that was internalized in intracellular structures, such as vesicles and endosomes. During exocytosis, the Ca^{2+}-sensitive dye will be released in the extracellular space, which has a different Ca^{2+} concentration and ionic composition compared to the intracellular environment. Stronger stimuli will induce more exocytosis and thus more release of dye, in turn resulting in a higher sustained fluorescence yield.

In addition to exocytosis, trans-membrane leakage of hydrolyzed dye to the extracellular space could also contribute to the observed sustained increases observed in the plate reader. One widely used strategy to prevent dye leakage relies on the use of probenecid as inhibitor of channel-mediated dye leakage (Di Virgilio, *et al.* 1990). In line with the results of Di Virgillio and co-workers, our data on ATP-stimulated PC12 cells indicate that dye leakage is reduced and the signal and signal-to-noise are apparently improved following incubation with probenecid (Fig. 4A). However, probenecid has additional unwanted effects as cells became unresponsive to depolarization (Fig. 4B). Experiments in single cell fluorescence microscopy confirmed the absence of depolarization-evoked increases in F340/F380 in cells incubated with probenecid, whereas the response to ATP remains intact (Fig. 4C2). These findings thus indicate that probenecid is in fact inhibiting depolarization-evoked Ca^{2+} influx, rendering it unsuitable for measurements of $[Ca^{2+}]_i$.

Several factors thus contribute to the observed sustained increases in fluorescence. Though these sustained increases appear erroneous, the transient fluorescent signal on top of the sustained increase most likely does reflect changes in $[Ca^{2+}]_i$. To isolate the transient phase of the signal, a step-subtraction procedure has previously been suggested by Kassack and colleagues (Kassack, *et al.* 2002). Subtracting the amplitude of the sustained increase observed under control conditions, i.e., following injection of only external saline, could correct for procedure-based sustained increases. However, this requires the use of a fixed injection volume of comparable ionic composition to standardize the sustained increase as much as possible. Alternatively, one could subtract the sustained phase of the individual measurements, thereby isolating the transient phase, leaving a signal that represents the actual increase in $[Ca^{2+}]_i$, independent of changes in injection volume or ionic strength. Nevertheless, this procedure does not consider stable sustained Ca^{2+} signals, which can occur following certain types of stimuli, e.g., type-2 ATP-induced responses (Fig. 3A).

Plate reader-based measurements of $[Ca^{2+}]_i$ have a rather low sensitivity compared to fluorescence microscopy (Fig. 2). Consequently, subtle effects may be overlooked in the plate reader. Additionally, the lack of single cell resolution may blur the interpretation of the obtained results. This is illustrated by the response to stimulation with ATP (PC12: Fig. 3A; B35: Fig. S8A). In the plate reader, the F340/F380 signal is an average of these two types of responses, whereas fluorescence microscopy allows for identification of these two different responses (that are possibly due to expression of ion channel P2X and the G-protein coupled P2Y purinergic receptors (Fabbro, *et al.* 2004)) and hence detection of differential effects on these two types of response.

Comparable difficulties arise in case of stimulation with ACh, where the percentage of cells showing an increase in Ca^{2+} depends on the strength of the stimulus applied (PC12: Fig. 3B). Importantly, a rather high fraction of PC12 cells is not responsive to stimulation with ACh. As with different types of ATP responses, this is not a unique characteristic of PC12 cells, illustrated by the results from B35 cells (Fig. S8B). Consequently, the non-responsive cells may preclude detection of small effects on ACh-mediated changes in $[Ca^{2+}]_i$ in plate reader systems, whereas these effects can be observed in fluorescence microscopy by first selecting for ACh-responsive cells. Naturally, over selection should be prevented and the percentage responsiveness should always be quantified as a change herein may of course result from the treatment.

These specific difficulties, arising from cell and receptor heterogeneity, may however be (partly) circumvented with the use of recombinant cells, expressing only a well-defined single type of receptor. Therewith, artificial changes in fluorescence can be more easily discriminated from the actual change in Ca^{2+}, as characteristics of the particular channel or receptor will be known. However, other limitations will

remain, such as poor sensitivity, dye leakage and limitations in high-throughput because of the delay between wells.

It appears that plate-reader-based measurements of dynamic intracellular calcium levels can under certain conditions be used as a first tier screening method, but only to detect those chemicals that exert strong effects on calcium homeostasis. These high-throughput measurements are undoubtedly less expensive and faster than measurements in a fluorescence microscopy setting. However, the present results suggest that several chemicals that actually affect calcium levels will not show up in the plate-reader screen. This may not be a problem for pharmaceutical research focused on finding only the most potent compounds, but is unwanted in a toxicological screen to identify also chemicals that modestly affect calcium homeostasis. It can therefore be argued that first tier screening using plate reader based measurements should be restricted to static endpoint measurements, such as cytotoxicity, whereas single cell fluorescence microscopy would be the first tier of choice for real-time measurement of $[Ca^{2+}]_i$ dynamics.

Most linear plate readers are equipped with one or two injectors to add compounds (from a stock solution) to the medium in the well. Unfortunately, this can strongly affect the osmotic value of the medium, especially in case of addition of high K^+-containing saline. On the other hand, microscopes can be relatively easy equipped with a superfusion pencil (or bath perfusion) allowing for more experimental freedom and preventing large changes in osmotic value. Consequently, microscopy with a 5–10× objective may be a good alternative for screening compounds as it combines the sensitivity of the microscopy with a large number of cells (n) per experiment thus theoretically reducing the number of experiments (N). Also, limitations caused by different receptor types (e.g. ATP) or heterogeneity in receptor expression (e.g. ACh) are non-existing as this is in essence a single-cell approach. However, care should be taken to obtain these data from multiple experiments (N) to take into account day-to-day variation as well as variation between cell batches. In practice, cell numbers (n) will be sufficiently large (>25) when performing 3 – 5 independent experiments (N) with a 20 – 40× objective. An advantage of using a higher magnification (e.g., 40×) is that it may already provide clues regarding the sub-cellular distribution and/or origin of the calcium signal.

To summarize, current linear plate reader systems could allow for real-time kinetic measurements of $[Ca^{2+}]_i$, though these measurements are hampered by a number of factors, including the choice of cell line, injection volume and type of stimulus. Importantly, the observed sustained increases appear to be experimental artifacts. Furthermore, the lack of single cell resolution and the low sensitivity compared to fluorescence microscopy increase the likelihood of false negative results, i.e., compounds that induce only a modest increase in $[Ca^{2+}]_i$ or in only a fraction of the cells but will escape detection in plate reader experiments.

Moreover, when performing real-time kinetic measurements of $[Ca^{2+}]_i$ of only a few minutes/well, the delay between measurements of different wells in linear multi-well microplate reader systems already considerably limits the use of plate readers for HTS. Importantly, in addition to the described plate reader (Infinite M200 microplate reader, Tecan Trading AG) experiments, pilot experiments (not shown) with two other plate readers (FLUOstar Galaxy V4.30-0, BMG Labtechnologies (linear system) and the FlexStation® 3, Molecular Devices Inc. (parallel system) as well as the results presented in the cited papers by Kassack, *et al.* (2002), Di Virgilio, *et al.* (1990) and Monteith and Bird (2005) illustrate that the observations described in the current paper are not unique for a particular plate reader system. Therefore, the conclusion that current plate reader-based strategies for high throughput real-time kinetic measurements of $[Ca^{2+}]_i$ are associated with serious caveats and limitations appears justified.

Conflict of interest statement

The authors do not have any competing financial interest or any other conflict of interest regarding the submitted article.

Acknowledgments

We thank Dr. Milou Dingemans and Maarke Roelofs, M.Sc. for critically reading the MS and for the helpful suggestions and the members of the neurotoxicology research group for the helpful discussions. This work was supported by the Dutch "Internationaal Parkinson Fonds" (IPF), the European Union-funded project ACROPOLIS (grant agreement KBBE-245163) and the Faculty of Veterinary Sciences of Utrecht University.

SUPPLEMENTAL Results

Fura-2-loaded PC12 cells; plate reader in top- or bottom-read mode (S1)

Experiments were performed to identify those conditions that yield the best signal and signal-to-noise ratio. In addition to the experiments performed in both top- and bottom-read mode with high-K^+ depolarization (Fig. 1A), experiments were performed with injection of 100 µl of ATP containing saline to 200 µl starting volume (final concentration 100 µM ATP). The results presented in Fig. S1 demonstrate a sharp but limited increase in F340/F380. Although data from top- and bottom-read mode appear comparable, the total fluorescence yield in bottom-read mode is often only 10-20% of the yield in top-read experiments (raw data, not shown) and bottom-read signal has a larger noise.

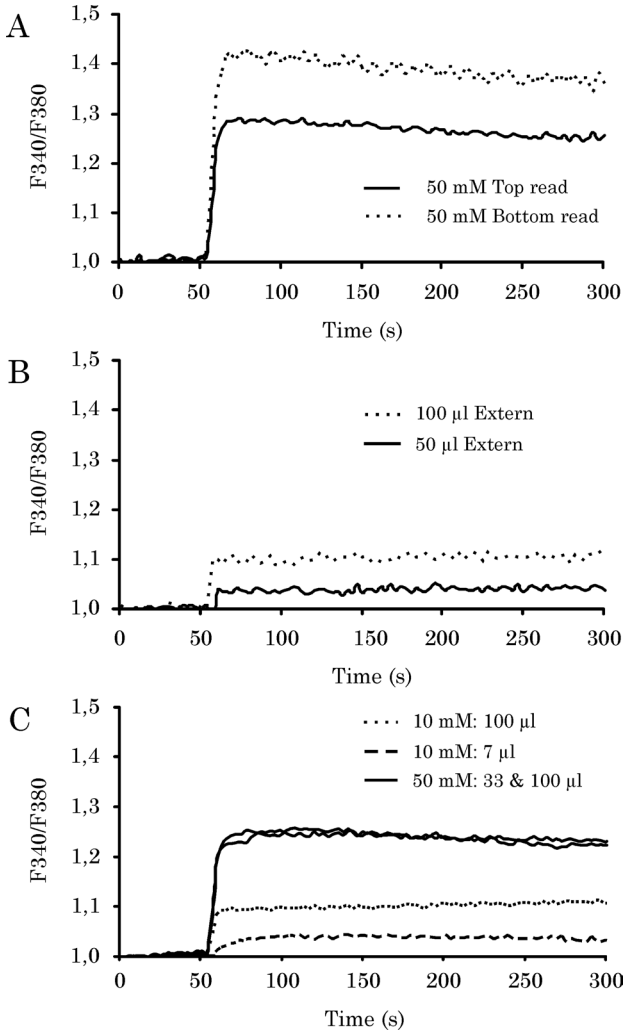

Dynamic range; plate reader and fluorescence microscopy (S2; figure next page)

Experiments were performed in Fura-2 loaded PC12 cells to determine the dynamic range in both plate reader and microscopy. The results presented in Fig. S2 demonstrate that the dynamic range for fluorescence measurements in plate reader-based experiments is smaller compared to fluorescence microscopy indicating a lower sensitivity of the plate reader.

Figure S1. Platereader: Example traces representing the increase in F340/F380 upon stimulation of Fura-2-loaded PC12 cells with 100 µM ATP as recorded in either top- (solid line) or bottom- (dotted line) read mode.

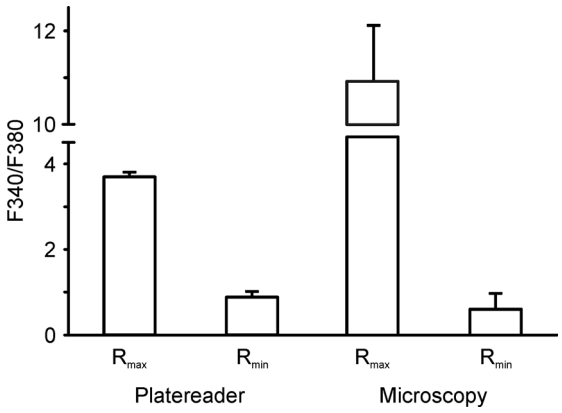

Figure S2. Bargraph representation of R_{max} and R_{min} values in both platereader and microscopy upon incubation of Fura-2 loaded PC12 cells with respectively ionomycin (5 µM) and EDTA (17 mM). These results illustrate the difference in dynamic range between the two strategies. Bars display average data (± SD; *n* = 4 wells or 8 cells).

Fura-2 Pentapotassium salt; plate reader (S3)

To further assess the influence of ionic composition on changes in F340/F380, experiments were performed in the absence of cells, but with membrane-impermeable Fura-2 pentapotassium salt dissolved in nominal Ca2+-free external saline. The results presented in Fig. S3 demonstrate that a change in ionic composition as induced by different concentrations K^+ (10, 50 and 100 mM) induces a Ca^{2+}-independent, sustained step-wise increase in F340/F380 that depends solely on the K^+ concentration.

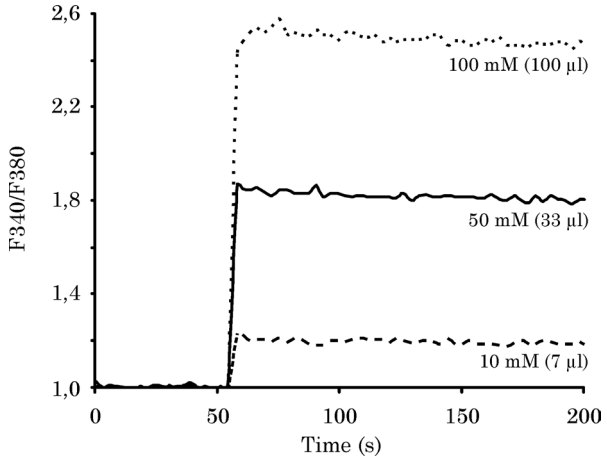

Figure S3. Platereader: Average traces (n = 9) illustrating the increase in F340/F380 upon injection of different volumes of high-K^+ saline to saline containing 1 µM Fura-2 pentapotassium salt. Final concentrations of K^+ amounting to 10, 50 and 100 mM were obtained by injecting respectively 7 (dashed line), 33 (solid line) and 100 (dotted line) µl of stock solution.

Fura-2- and Fluo-4-loaded B35 cells; plate reader (S4)

For reasons of comparison and generalization, plate reader experiments in Fura-2-loaded PC12 were replicated in Fura-2- or Fluo-4-loaded B35 cells. The results presented in Fig. S4A demonstrate a sharp increase in F340/F380 for both exposure to 100 µM ATP and 100 µM ACh. This increase is largely transient upon exposure to 100 µM ATP, whereas the increase in F340/F380 upon exposure to 100 µM ACh reveals a sustained level of fluorescence not returning to baseline within 5 min. The results presented in Fig. S4B illustrate the F488 in Fluo-4-loaded B35 cells exposed to 100 µM ATP or 100 µM ACh. Interestingly, in contrast to the increase observed in Fura-2-loaded B35 cells in plate reader experiments (Fig. S4A), but in line with the data from fluorescence microscopy (Fig. S5), the increase upon exposure to ACh appears smaller than the increase upon exposure to ATP.

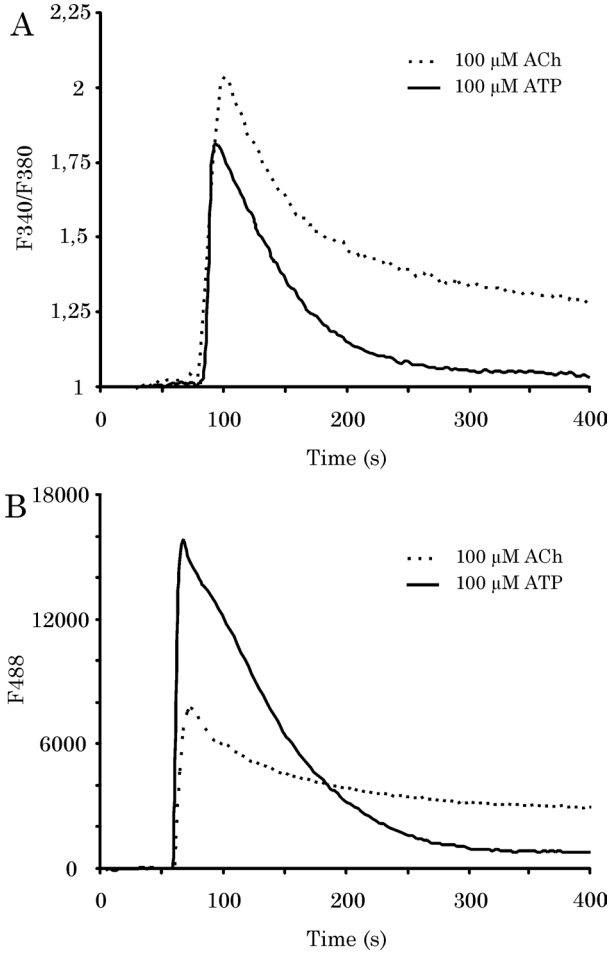

Figure S4 Plate-reader: Example traces illustrating the increase in F340/F380 (A) and F488 (B) recorded in plate reader experiments upon stimulation of B35 cells with 100 µM ATP (solid line) and 100 µM ACh (dotted line).

Fura-2-loaded B35 cells; single cell fluorescence microscopy (S5)

For reasons of generalization experiments in PC12 cells have been replicated in B35 cells. Stimulation of Fura-2-loaded B35 cells with different concentrations ATP resulted in a sharp transient increase in F340/F380 upon exposure to 10 µM ATP to 4.53 ± 2.48 (n = 60, p<0.001; Fig S5A). The highest increase in F340/F380 was observed upon exposure to 100 µM ATP (5.80 ± 1.84, n = 61, p<0.001; Fig. S5A). No increase was observed upon exposure to 1 µM ATP (Fig. S5A). Superfusion of Fura-2-loaded B35 cells with different concentrations ACh induces a sharp transient increase in F340/F380 amounting to respectively 1.42 ± 1.14 (1 µM ACh, n = 89, p<0.001; Fig. S5B) and 3.64 ± 2.94 (10 µM ACh, n = 104, p<0.001; Fig. S5B), whereas the highest increase was observed upon exposure to 100 µM ACh (3.92 ± 2.97 (n = 73, p<0.001; Fig. S5B).

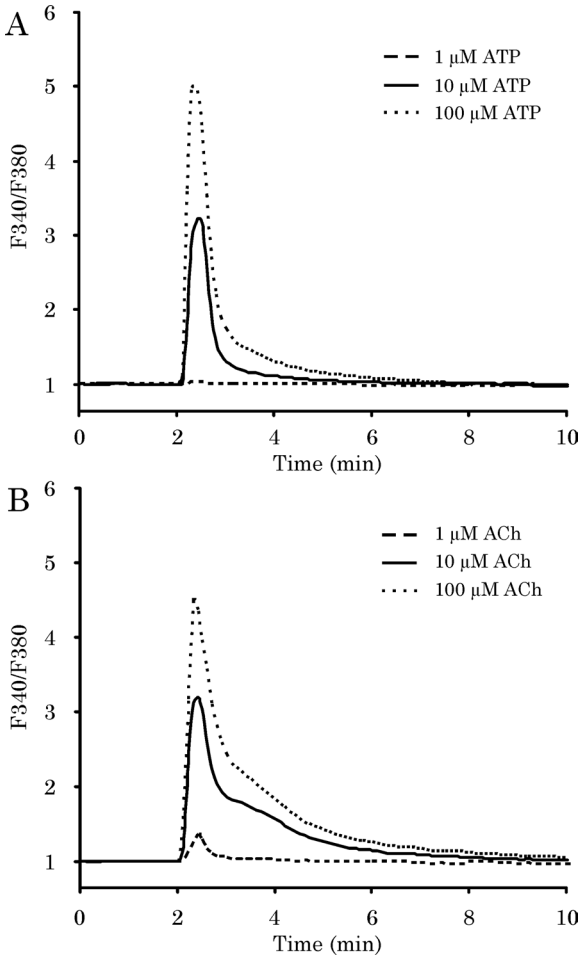

Figure S5. Single cell fluorescence micro-scopy: Example traces illustrating the fast transient increase in F340/F380 recorded with single cell fluorescence microscopy upon stimulation of Fura-2-loaded B35 cells with (A), 1 (dashed line), 10 (solid line) and 100 µM (dotted line) ATP and (B), 1 (dashed line), 10 (solid line) and 100 µM (dotted line) ACh.

Fluo-4-loaded PC12 cells; single cell fluorescence microscopy (S6)

To be able to compare the use of a dual wavelength dye (Fura-2) with a single wavelength dye (Fluo-4) the experiments involving K^+, ATP and ACh (see Fig. 2) have been repeated using Fluo-4-loaded PC12 cells. Stimulation of Fluo-4-loaded PC12 cells with different concentrations K^+ resulted in a sharp and transient increase in fluorescence upon exposure to 50 mM K^+ amounting to 113.4 ± 11.6 RFU (n = 30, p<0.001; Fig. S6A), whereas exposure to 10 mM K^+ did not increase fluorescence (Fig. S6A). The highest increase in fluorescence was observed upon exposure to 100 mM K^+ (135.1 ± 9.6 RFU, n = 52, p<0.001; Fig. S6A). Stimulation of Fluo-4-loaded PC12 cells with different concentrations ATP resulted in a small and transient increase in fluorescence upon exposure to 10 μM ATP amounting to 21.3 ± 4.0 RFU (n = 46, p<0.001; Fig. S6B), whereas exposure to 1 μM ATP did not increase fluorescence (Fig. S6B). The highest increase in fluorescence was observed upon exposure to 100 μM ATP (222.8 ± 19.7 RFU, n = 53, p<0.001; Fig. S6B). Superfusion of Fluo-4-loaded PC12 cells with different concentrations ACh induces a transient, but limited, increase in fluorescence amounting to respectively 31.1 ± 4.0 RFU (10 μM ACh, n = 59, p<0.01; Fig. S6C) and 44.0 ± 6.1 RFU (100 μM ACh, n = 52, p<0.001; Fig. S6C). No significant increase in fluorescence was observed upon exposure to 1 μM ACh (Fig. S6C).

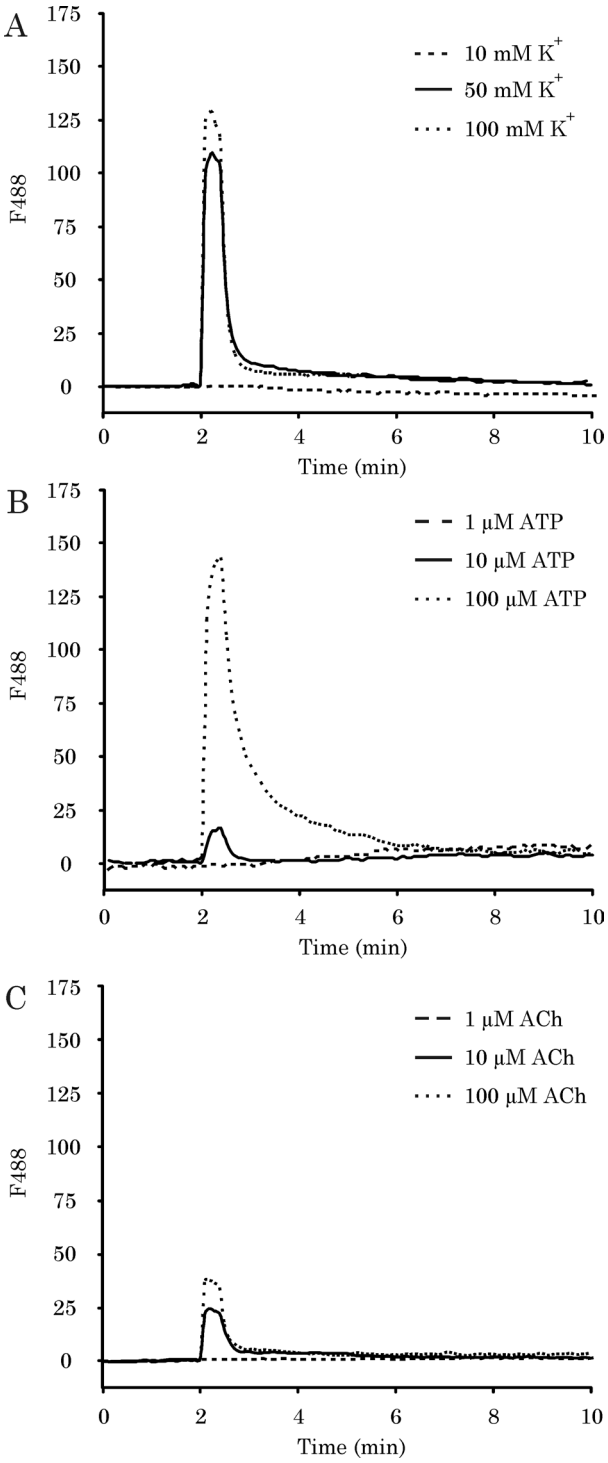

Figure S6. Single cell fluorescence microscopy: Example traces illustrating the fast transient increase in F488 recorded with single cell fluorescence microscopy upon stimulation of Fluo-4-loaded PC12 cells with (A), 10 (dashed line), 50 (solid line) and 100 mM (dotted line) K^+ (B), 1 (dashed line), 10 (solid line) and 100µM (dotted line) ATP and (C), 1 (dashed line), 10 (solid line) and 100 µM (dotted line) ACh.

Fluo-4-loaded B35 cells; single cell fluorescence microscopy (S7)

To be able to compare the use of a dual wavelength dye (Fura-2) with a single wavelength dye (Fluo-4), experiments involving ATP and ACh have been repeated using Fluo-4-loaded B35 cells. Stimulation of Fluo-4-loaded B35 cells with different concentrations ATP resulted in a sharp transient increase in fluorescence upon exposure to 1 µM ATP amounting to 66.6 ± 11.6 RFU (n = 64, p<0.001; Fig. S7A), whereas exposure to 10 µM ATP increased fluorescence to 263.8 ± 17.0 RFU (n = 61, p<0.001; Fig. S7A). The highest increase in fluorescence was observed upon exposure to 100 µM ATP (368.5 ± 12.3 RFU, n = 72, p<0.001; Fig. S7A). Superfusion of Fluo-4-loaded B35 cells with different concentrations ACh induces a sharp transient increase in fluorescence amounting to 128.8 ± 13.8 RFU (10 µM ACh, n = 101, p<0.001; Fig. S7B) and 180.6 ± 15.4 RFU (100 µM ACh, n = 110, p<0.001; Fig. S7B). No significant increase in fluorescence was observed upon exposure to 1 µM ACh (Fig. S7B).

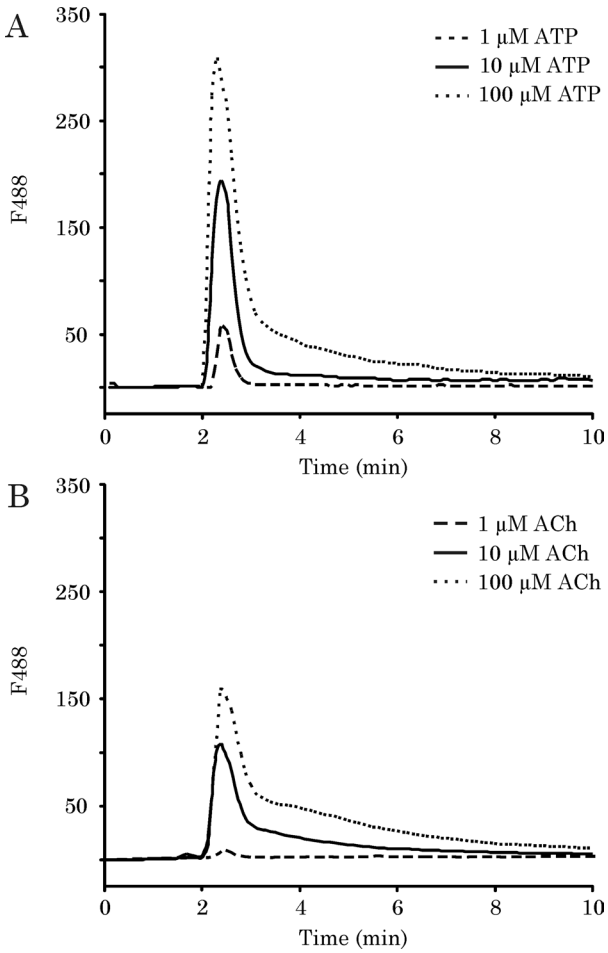

Figure S7. Single cell fluorescence microscopy: Example traces illustrating the fast transient increase in F488 recorded with single cell fluorescence microscopy upon stimulation of Fluo-4-loaded B35 cells with (A), 1 (dashed line), 10 (solid line) and 100 µM (dotted line) ATP and (B), 1 (dashed line), 10 (solid line) and 100 µM (dotted line) ACh.

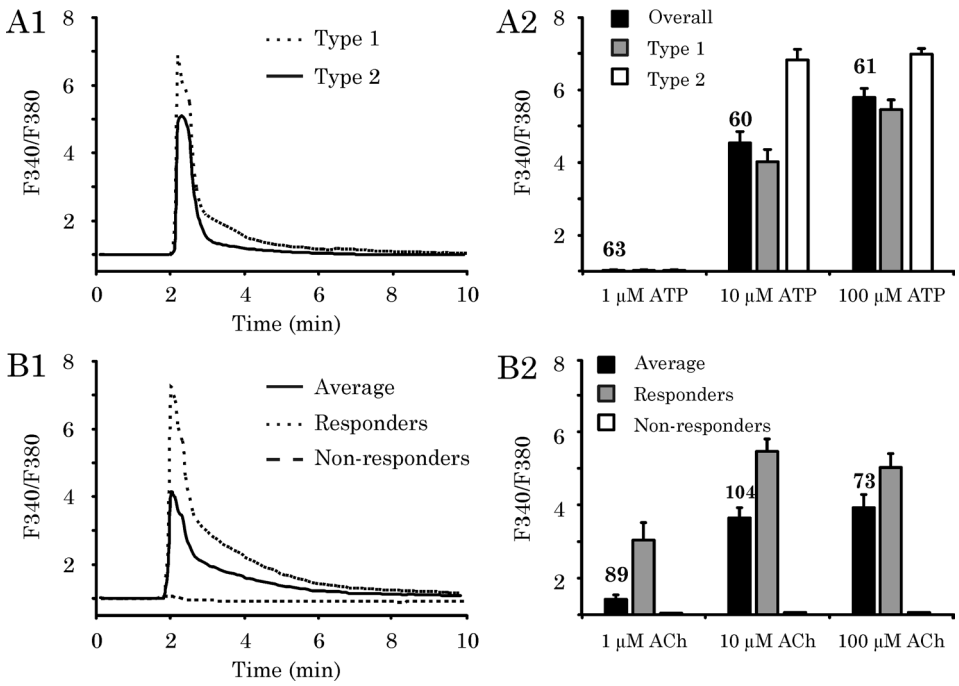

Figure S8. Single cell fluorescence microscopy: A1) Example traces illustrating the presence of two different types of response, with different amplitudes and kinetics, in Fura-2-loaded B35 cells stimulated with 100 µM ATP. A2) Summary bar graph displaying average maximum increase in F340/F380 upon stimulation of B35 cells with 1, 10 or 100 µM ATP. Columns represent responses per type as well as the average overall response. Bars display average data (± SE) from the number of cells (*n*) indicated in the bars (3-5 experiments per concentration). B1) Example traces illustrating the response of Fura-2-loaded B35 cells to stimulation with 100 µM ACh. Notably, the fraction of non-responsive cells obscures the average response. B2) Summary bar graph displaying the average maximum increase in F340/F380 upon stimulation of B35 cells with 1, 10 or 100 µM ACh. Columns represent increases from responsive cells, non-responsive cells as well as the average overall response. Bars display average data (± SE) from the number of cells (*n*) indicated in the bars (3-5 experiments per concentration).

Chapter 5.1

Dual Actions of lindane (gamma-hexachlorocyclohexane) on calcium homeostasis and exocytosis in rat PC12 cells

Harm J. Heusinkveld[1], Gareth O. Thomas[1,2,] Ischa Lamot[1], Martin van den Berg[1], Alfons B.A.Kroese[1,3,] Remco H.S. Westerink[1]

[1] Neurotoxicology Research Group, Institute for Risk Assessment Sciences (IRAS), Utrecht University, the Netherlands
[2] Department of Environmental Science, Lancaster University, United Kingdom
[3] Department of Surgery University Medical Center Utrecht, Utrecht, the Netherlands

Toxicology and Applied Pharmacoloyg **248**, 12-19

Abstract

The persistent organochlorine pesticide lindane is still abundantly found in the environment and in human and animal tissue samples. Lindane induces a wide range of adverse health effects, which are at least partially mediated via the known inhibition of $GABA_A$ and glycine receptors. Additionally, lindane has been reported to increase the basal intracellular Ca^{2+} concentration ($[Ca^{2+}]_i$). As Ca^{2+} triggers many cellular processes, including cell death and vesicular neurotransmitter release (exocytosis), we investigated whether lindane affects exocytosis, Ca^{2+} homeostasis, production of reactive oxygen species (ROS) and cytotoxicity in neuroendocrine PC12 cells. Amperometric recordings and $[Ca^{2+}]_i$ imaging experiments with fura-2 demonstrated that lindane (≥10 µM) rapidly increases basal exocytosis and basal $[Ca^{2+}]_i$. Additional imaging and electrophysiological recordings revealed that this increase was largely due to a lindane-induced membrane depolarization and subsequent opening of N- and P/Q-type voltage-gated Ca^{2+} channels (VGCC). On the other hand, lindane (≥3 µM) induced a concentration-dependent but non-specific inhibition of VGCCs, thereby limiting the lindane-induced increase in basal $[Ca^{2+}]_i$ and exocytosis. Importantly, the nonspecific inhibition of VGCCs also reduced stimulation-evoked exocytosis and Ca^{2+} influx. Though lindane exposure concentration-dependently increased ROS production, cell viability was not affected indicating that the used concentrations were not acute cytotoxic. These combined findings indicate that lindane has two, partly counteracting effects. Lindane causes membrane depolarization, thereby increasing basal $[Ca^{2+}]_i$ and exocytosis. In parallel, lindane inhibits VGCCs, thereby limiting the basal effects and reducing stimulation-evoked $[Ca^{2+}]_i$ and exocytosis. This study further underlines the need to consider presynaptic, non-receptor-mediated effects in human risk assessment.

Keywords

Vesicular catecholamine release; Persistent organochlorine insecticides; Amperometry; Voltage-gated Ca^{2+} channels; Fura-2 Ca^{2+}-imaging; Neurotoxicology

Introduction

Lindane (γ-hexachlorocyclohexane, γ-HCH, γ-benzene hexachloride, γ-BHC) is a persistent, lipophilic and bioaccumulative organochlorine pesticide. Lindane has been used for many years as a broad range insecticide in agriculture and for the treatment of lice and scabies in humans. In some areas lindane is probably still in use, but its use has been banned or severely restricted in most countries for more than 15 years (Li, *et al.* 1996). Lindane is mobile in the environment, accumulates in the food chain and lindane residues are ubiquitous in environmental samples (including biota) globally (Roche, *et al.* 2009). Humans are exposed to lindane predominantly through the diet.

Despite the decline of lindane concentrations in environmental media (for review see: Hoferkamp, *et al.* 2010), lindane levels in Europe reach up to hundreds of ng/g lipid weight (ng/g l.w.) in human tissues (Dirtu, *et al.* 2006, Thomas, *et al.* 2006), including (cord) serum, breast milk and amniotic fluid (Campoy, *et al.* 2001, Jimenez-Torres, *et al.* 2006, Luzardo, *et al.* 2009). Breast milk samples from heavily polluted areas in India were reported to even contain up to 4500 ng/g l.w. (corresponding with approx 650 nM; calculated using average physiological values; Subramanian, *et al.* 2007), whereas blood levels in Mexican school children are reported to reach 8200 ng/g l.w. (corresponding with a blood concentration of approximately 315 nM; calculated using average physiological values; Trejo-Acevedo, *et al.* 2009). As lindane is reported to bioaccumulate, it is not unlikely that brain levels will reach even higher levels. Considering the known adverse effects of lindane on human health, these findings should be of major societal concern. Importantly, lindane exposure and elevated lindane levels in human brain have been associated with the development of neurodegenerative diseases, including idiopathic Parkinson's disease (PD; Corrigan, *et al.* 1996, Corrigan, *et al.* 2000), whereas perinatal exposure to lindane has been associated with the development of PD later in life (Barlow, *et al.* 2007).

The nervous system is among the most vulnerable targets for lindane exposure (Mariussen and Fonnum 2006), which holds in particular for the developing nervous system (Singal and Thami 2006). Already decades ago, it was shown that lindane exposure affects learning behaviour as well as motor activity (for review see: Mariussen and Fonnum 2006). Although the primary working mechanism of lindane was reported to be inhibition of postsynaptic $GABA_A$ and glycine receptors in the nervous system (Anand, *et al.* 1998, Vale, *et al.* 2003), lindane was also reported to exert presynaptic effects. At high concentrations (50 μM), lindane increases the frequency of basal neurotransmitter release at frog neuromuscular junctions (Publicover and Duncan 1979) as well as depolarization-evoked noradrenaline release in the rat hippocampus (Cristofol and Rodriguez-Farre 1994). Noteworthy, effects of lindane on the intracellular calcium concentration ($[Ca^{2+}]_i$) were reported to occur in the low μM range. Lindane (1–50 μM) increases basal

$[Ca^{2+}]_i$ in a range of cell types within seconds or minutes of application (Criswell, *et al.* 1994, Hawkinson, *et al.* 1989, Lu, *et al.* 2000, Rosa, *et al.* 1997). This effect depends, at least partly, on the presence of extracellular Ca^{2+} and appears to be related to different mechanisms in different cell types, including Ca^{2+} release from intracellular ionositol-1,4,5-triphosphate (IP_3)-sensitive Ca^{2+} stores followed by capacitive Ca^{2+} entry (Lu, *et al.* 2000). Also, non-GABA mediated, Ca^{2+}-sensitive effects of lindane on transcriptional parameters of neuronal development *in vitro* have been observed at concentrations as low as 100 nM (Ferguson and Audesirk 1995). Furthermore, it has been suggested from subchronic *in vivo* studies that lindane-induced changes in $[Ca^{2+}]_i$ might be related to increased oxidative stress (for review see: Mariussen and Fonnum 2006).

Exocytosis is driven by an increase in $[Ca^{2+}]_i$ and is regulated by a variety of cytoplasmic, vesicle- and membrane-associated proteins (for review see: Catterall and Few 2008, Garcia, *et al.* 2006, Westerink 2006). Hence, in view of the reported lindane-induced effects on basal $[Ca^{2+}]_i$ and considering the importance of depolarization-evoked Ca^{2+} influx for exocytosis, it is surprising that effects of lindane on depolarization-evoked changes in $[Ca^{2+}]_i$ and exocytosis are thus far not reported. The finding that lindane, while its primary neurotoxic mechanism appears to be inhibition of GABA and glycine receptors, affects $[Ca^{2+}]_i$ and is linked to selective degeneration of dopaminergic brain areas, has led to the hypothesis that lindane affects critical parameters of dopaminergic neurotransmission. Therefore, the aim of the present study was to investigate effects of acute lindane exposure on basal as well as depolarization-evoked dopamine exocytosis, Ca^{2+} homeostasis and cytotoxicity in PC12 cells. Dopaminergic PC12 cells are extensively characterized as an *in vitro* model to study changes in Ca2+ homeostasis and exocytosis (Westerink and Ewing 2008). Additionally, PC12 cells lack functional GABA receptors (Hales and Tyndale 1994), thereby providing an appropriate model for identification of non-GABA receptor-mediated neurotoxicity of lindane. Using these neuroendocrine PC12 cells, it is now demonstrated that lindane differentially affects $[Ca^{2+}]_i$, resulting in disturbed dopamine exocytosis.

Materials and methods

Chemicals

NaCl, KCl and HEPES were obtained from Merck (Whitehouse Station, NJ, USA); $MgCl_2$, $CaCl_2$, glucose, sucrose and NaOH were obtained from BDH Laboratory Supplies (Poole, UK); ω-conotoxin GVIA and ω-conotoxin MVIIC were obtained from Biotrend Chemicals AG (Zürich, Switzerland); Fura-2AM and 2,7-dichlorofluorescein diacetate (H_2-DCFDA) were obtained from Molecular Probes (Invitrogen, Breda, The Netherlands). All other chemicals were obtained from Sigma (St. Louis MO, USA), unless otherwise noted. Saline solutions were prepared with de-ionized water (Milli-Q®; resistivity >10MΩ•cm). Stock solutions of 2 mM ionomycin in DMSO were kept at −20°C. Stock solutions of 1–100 mM lindane (Pestanal® grade, 99.8% pure, Riedel de Haën, Seelze, Germany) and 2 mM nifedipine were prepared in DMSO and diluted in saline solution to obtain the desired concentrations just prior to the experiments (all solutions used in experiments, including control experiments, contained 1 µl DMSO/ml). Stock solutions of 100 µM ω-conotoxin GVIA and MVIIC were prepared in de-ionized water and stored at 4 °C.

Cell culture

Rat pheochromocytoma (PC12) cells (Greene and Tischler 1976) were grown for 10 passages in RPMI 1640 (Invitrogen, Breda, The Netherlands) supplemented with 5% fetal calf serum and 10% horse serum (ICN Biomedicals, Zoetermeer, The Netherlands) as described previously (Dingemans, *et al.* 2009). For Ca^{2+} imaging and electrophysiological experiments, undifferentiated PC12 cells were sub cultured in poly-L-lysine coated glass-bottom dishes (MatTek, Ashland, MA) as described previously (Dingemans, *et al.* 2009). As exocytosis is limited in undifferentiated PC12 cells, cells were differentiated for 3–5 days with 5 µM dexamethasone for amperometric recordings as described previously (Dingemans, *et al.* 2009). Dexamethasone differentiation is known to enhance exocytosis by increasing the number of releasable vesicles as well as the total amount of dopamine per vesicle (Westerink and Vijverberg 2002b). Control experiments (not shown) demonstrated that intracellular calcium homeostasis was not qualitatively affected by differentiation with dexamethasone, neither under basal conditions nor during lindane exposure.

Cell viability assay

To exclude that results are confounded by acute lindane-induced cytotoxicity, effects of lindane on cell viability were determined using a combined alamar Blue (aB) and Neutral Red (NR) assay in undifferentiated PC12 cells. One day before the cell viability test, cells were seeded in (poly-L-lysine coated) 96-wells plates (Greiner Bio-one, Solingen, Germany) at a density of 10^5 cells/well. Cells were

exposed in serum-free medium to concentrations up to 100 µM for 6 h. Mitochondrial activity of the cells was recorded as a measure of cell viability with the aB assay, which is based on the ability of the cells to reduce resazurin to resorufin (protocol adapted from Magnani and Bettini 2000). Membrane integrity and lysosomal activity were subsequently determined as a measure of cell viability using the NR assay (protocol adapted from Repetto, et al. 2008). Briefly, cells were incubated for 30 min with 200 µl resazurin solution (12 µM in phosphate buffered saline; PBS, Invitrogen, Breda, The Netherlands). Resorufin was measured spectrophotometrically at 530/590 nm (FLUOstar Galaxy V4.30-0, BMG Labtechnologies, Offenburg, Germany). After removal of the aB solution, cells were incubated for 1h with 200 µl NR solution (12 µM in PBS). Following the incubation, cells were rinsed with warm (37°C) PBS and 100 µl extraction solution (1% glacial acetic acid, 50% ethanol and 49% H_2O) was added to the wells. After 30 min extraction fluorescence was measured at 430/480 nm.

ROS measurement using H_2-DCFDA

ROS production was assessed using the fluorescent dye H_2-DCFDA (protocol adapted from Lee, et al. 2009). Briefly, undifferentiated PC12 cells were seeded in black, glass-bottom, 96-wells plates (Greiner Bio-one, Solingen, Germany) at a density of 1.5×10^5 cells/well. Cells were loaded with 5 µM H_2-DCFDA for 30 min at 37°C. Subsequently, cells were exposed for up to 6 h to 1, 10 or 100 µM lindane and fluorescence was measured spectrophotometrically at 480/530 nm (FLUOstar Galaxy V4.30-0, BMG Labtechnologies, Offenburg, Germany). As control cells show a basal ROS production over time, data is expressed as average percentage compared to the time-matched control values.

Amperometry

Amperometric recordings of basal and K^+-evoked exocytosis from dexamethasone-differentiated PC12 cells using carbon fibre microelectrodes (Dagan Corp. Minneapolis MN, USA) were made as described previously (Dingemans, *et al.* 2009, Westerink and Vijverberg 2002b). Following 135 s of baseline recording, PC12 cells were superfused for 15 s with high-K^+-containing saline (K^+ increased to125 mM and Na^+ lowered to 5.5 mM) to determine their exocytotic capacity. Cells were allowed to recover for at least 2 min before a subsequent 10 min exposure to lindane to investigate acute effects on exocytosis. Following this 10 min lindane exposure, cells were depolarized again with high-K^+-containing saline to determine effects of lindane on depolarization-evoked exocytosis. Recordings, with millisecond temporal resolution and a detection limit of 20 zmol (10−21 mol),were performed at room temperature. PC12 cells with high basal release (>2.5 events/min), low evoked release (<5 events during first 15 s of depolarization) or slow recovery to basal release (i.e., release still >2.5 ev./min following 2 min recovery after depolarization), were

excluded from data analysis (~5%). Selected cells were used to investigate effects of lindane on the frequency of exocytosis and on vesicular release parameters, i.e., amplitude, $t_{1/2}$ (half-width) and time integral (Q, vesicular content) of the amperometric release events.

Ca^{2+} imaging

Changes in $[Ca^{2+}]_i$ were measured using the Ca^{2+}-sensitive fluorescent ratio dye Fura-2 AM as described previously (Dingemans, *et al.* 2009). Briefly, cells were loaded with 5 µM Fura-2 AM (Molecular Probes; Invitrogen, Breda, The Netherlands) for 20 min at room temperature, followed by 15 min de-esterification. After de-esterification, the cells were placed on the stage of an Axiovert 35 M inverted microscope (Zeiss, Göttingen, Germany) equipped with a TILL Photonics Polychrome IV camera (TILL Photonics GmBH, Gräfelfing, Germany). Fluorescence, evoked by 340 and 380 nm excitation wavelengths (F340 and F380), was collected every 12 s at 510 nm with an Image SensiCam digital camera (TILL Photonics GmBH). Changes in F340/F380 ratio (R), reflecting changes in $[Ca^{2+}]_i$, were further analysed using custom-made MS-Excel macros. After 5 min baseline recording, cells were exposed to saline containing DMSO

(1 µl/ml) or lindane (1–100 µM). Direct membrane depolarization by 100 mM K^+ was used to investigate effects of lindane on the depolarization-evoked increase in $[Ca^{2+}]_i$. Maximum and minimum ratios (R_{max} and R_{min}) were determined at the end of the recording by addition of ionomycin (5 µM) and ethylenediamine tetraacetic acid (EDTA; 17 mM). Free cytosolic $[Ca^{2+}]_i$ was calculated using Grynkiewicz's equation: $[Ca^{2+}]_i = Kd^* \times (R - R_{min})/(R_{max} - R)$ where Kd* is the dissociation constant of Fura-2 determined in the experimental set-up (Deitmer and Schild 2000). The amplitude of the lindane-induced increase in basal $[Ca^{2+}]_i$ was determined to quantify the effects of lindane on basal $[Ca^{2+}]_i$. The maximum amplitude of $[Ca^{2+}]_i$ observed during depolarization was used to investigate possible effects of lindane on the depolarization-evoked increase of $[Ca^{2+}]_i$. The involvement of specific voltage-gated Ca^{2+} channels (VGCCs) was investigated by a selective and complete pharmacological block of the different VGCCs using 2 µM nifedipine (L-type VGCC), 2 µM ω-conotoxin GVIA (N-type VGCC) and 2 µM ω-conotoxin MVIIC (P/Q-type VGCC). Cells were preincubated with the VGCC blockers for 5 min and subsequently co-exposed to lindane and the blocking agent. Maximal block of VGCC subtypes was achieved at 2 µM (data not shown).

Electrophysiological recordings

After 1 or 2 days in culture, PC12 cells were placed in a recording chamber and perfused with modified Kreb's solution (containing in mM: 127 NaCl, 1.9 KCl, 1.2 KH_2PO_4, 1.3 $MgSO_4$, 20 $NaHCO_3$, 2.4 $CaCl_2$, 10 D-glucose; gassed with 95% O_2 – 5% CO_2; pH 7.4) at a rate of 3 ml/min at 34°C. The chamber was placed on the stage of

a Zeiss Axioscope FS microscope equipped with a differential interference contrast system. Cells were visualized using a 40× water-immersion objective (40×/0.80W; Zeiss; working distance 3.6 mm). Intracellular recordings were made using sharp glass microelectrodes, bent about 90° approximately 1 mm from their tips and filled with 3 M KCl (resistance: 60–90 MΩ) (Hudspeth and Corey 1978). Under visual control, cells (Ø ~14 µm) were penetrated perpendicular to their apical surface. Resting membrane potential was recorded with an electrometer (Axoprobe 1-A, Axon Instruments), by which also small rectangular hyperpolarizing (~5 mV) current pulses of 50 ms (0.5 Hz) were injected for measurement of membrane input resistance. After amplification and low-pass filtering (6 kHz), the voltage and current signals were digitized using a 1401plus CED interface (Cambridge Electronic Design, UK) at a sampling rate of 12 kHz and displayed and stored on a PC. Lindane was added to the superfusate to obtain final concentrations of 10 and 30 µM.

Data-analysis and statistics

All data are presented as mean ± standard error of the mean (SEM) from the number of cells (n) indicated, derived from 4 to 11 independent experiments. Statistical analyses were performed using SPSS 12.0.1 (SPSS, Chicago, IL, USA). Continuous data were compared using Student's t-test, paired or unpaired where applicable. Concentration–response curves were calculated using GraphPad Prism version 4.00 (GraphPad Software, San Diego, California, USA). Regression analysis was performed using Origin 7.5 (OriginLab Corporation, Northampton, USA). A p-value ≤ 0.05 is considered statistically significant; n.s. indicates the absence of a statistically significant effect.

Results

Effects of lindane on cell viability and oxidative stress

To investigate the cytotoxic effects following acute lindane exposure, effects of lindane on cell viability and ROS production were determined in PC12 cells exposed to different concentrations (0–100 µM) of lindane for 6 h. Both the NR and aB assay indicated that cell viability was not affected by any of the used concentrations (data not shown). These results thus indicate that lindane for up to 6 h, at concentrations up to 100 µM, does not induce overt cytotoxicity. However, exposure to lindane (10 and 100 µM) induces a modest but concentration-dependent and transient increase in ROS production (Fig. 1), at 1 h amounting to 139 ± 10% (10 µM) and 164 ± 16% (100 µM) compared to time-matched controls. No increase was observed with 1 µM lindane. Further measurements (2, 4 and 6 h exposure) demonstrate that lindane-induced ROS production is decreasing over time (Fig. 1), indicating that lindane-induced ROS production has a transient nature.

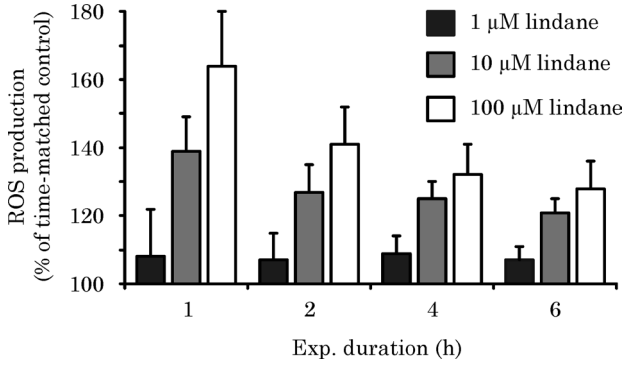

Fig. 1. Exposure to lindane increases ROS production over time in a transient, concentration-dependent manner. Bar graph demonstrating that lindane (10 and 100 µM) increases ROS production (1 µM: no increase compared to control). Bars represent average percentage ROS production at 1, 2, 4 and 6 h exposure duration (± SEM; n=48 wells per concentration) compared to time-matched control.

Effects of lindane on basal cytosolic exocytosis and $[Ca^{2+}]_i$.

To investigate the effects of acute lindane exposure on neurotransmitter release, exocytosis was measured using amperometry. Analysis of the release frequencies shows that the average basal release frequency amounts to 0.4 ± 0.1 events/min in control cells (n=47). Cells exposed to 10 µM lindane (n=12) did not show a detectable increase in the release frequency (0.3 ± 0.2 ev./min) as compared to pre-exposure levels (0.3 ± 0.1 ev./min) or to DMSO-exposed control cells (1 µl/ml final DMSO concentration, 0.4 ± 0.2 ev./min, n=11). However, cells exposed to saline containing

50 µM lindane (n=12) displayed a significant increase in release frequency amounting to 2.5 ± 1.0 ev./min ($p \leq 0.05$; Fig. 2A and B). Higher concentrations of lindane (100 µM) did not result in a further increase in release frequency (1.4 ± 0.5 ev./min, n=12, n.s., data not shown). When PC12 cells were exposed to lindane (50 µM) in the absence of extracellular Ca^{2+} ($CaCl_2$ replaced with 10 µM EDTA), lindane-induced exocytosis was markedly attenuated (0.5 ± 0.2 ev./min, n=12, not shown) compared to lindane-induced exocytosis in the presence of Ca^{2+} (2.5 ± 1.0 ev./min, n=12), indicating that influx from extracellular Ca^{2+} plays a major role in the observed enhancement of exocytosis. These results demonstrate that lindane rapidly induces exocytosis in dexamethasone-differentiated PC12 cells with a threshold for exocytosis between 10 and 50 µM lindane (Fig. 2A and B).

To demonstrate that the observed changes in exocytosis were caused by disruption of Ca^{2+} homeostasis, the effects of lindane on $[Ca^{2+}]_i$ were measured using Fura-2 AM. Cells exposed to DMSO (1 µl/ml), 1 µM lindane or 3 µM lindane, following 5 min of baseline recording, did not show a significant alteration of basal $[Ca^{2+}]_i$ (DMSO: 120 ± 3 nM, n=95; 1 µM lindane: 132 ± 3 nM, n=68 (not shown); 3 µM lindane: 127 ± 5 nM, n=42) (Fig. 3B). However, cells exposed to 10 µM lindane showed a significant increase in $[Ca^{2+}]_i$, with an amplitude amounting to 273 ± 14 nM (n=134, $p \leq 0.001$). The increase in $[Ca^{2+}]_i$ was larger in cells exposed to 30 µM lindane, amounting to 501 ± 45 nM (n=52, $p \leq 0.001$). Exposure to 100 µM lindane did not further increase $[Ca^{2+}]_i$ (amplitude: 509 ± 45 nM, n=63) compared to 30 µM lindane (Fig. 3A and B).

The observed increase of basal $[Ca^{2+}]_i$ after exposure to lindane (lowest observed effect concentration (LOEC): 10 µM; calculated EC_{50}: 11 µM, R^2 >0.95) was strongly attenuated in Ca^{2+}-free medium containing 10 µM EDTA (Fig. 4A and B). This indicates that the increase in $[Ca^{2+}]_i$ is predominantly caused by influx of extracellular Ca^{2+} and that Ca^{2+} release from intracellular stores apparently plays only a very modest or no role in this neuroendocrine cell model.

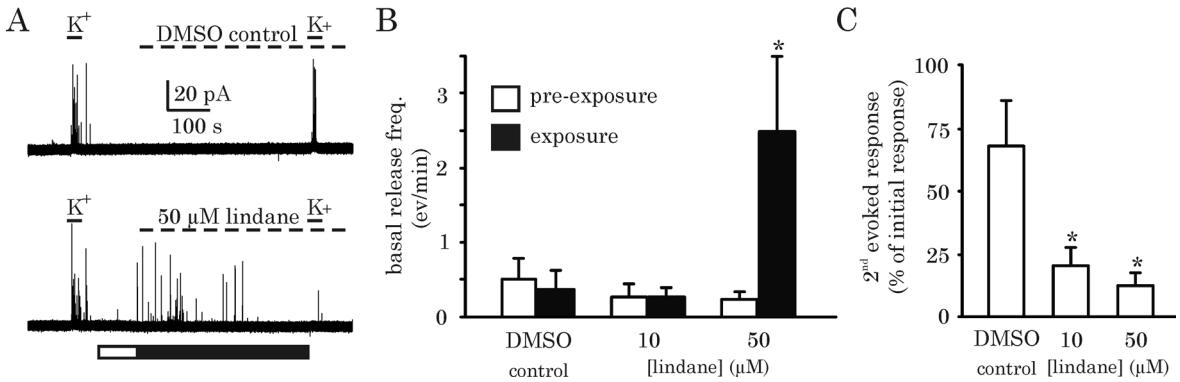

Fig. 2. Acute exposure to lindane increases basal exocytosis, but inhibits depolarization-evoked exocytosis. A) Representative examples of amperometric recordings obtained from single PC12 cells. In control cells (top trace), two successive K^+-induced depolarizations (indicated by the solid lines on top of the recording) evoke robust exocytosis, whereas cells exhibit a very low release frequency during exposure to DMSO-containing saline (indicated by the dashed lines on top of the recording). On the other hand, cells exposed to 50 µM lindane (lower trace) display a marked increase in the release frequency, whereas depolarization-evoked exocytosis is clearly reduced. B) Bar graph displaying the lindane-induced increase in the basal release frequency. The frequency of exocytosis during lindane exposure (closed bars) is compared with the (basal) release frequency before exposure of the same cells to lindane (open bars). Significant enhancement of the release frequency is observed at 50 µM lindane (paired *t*-test; $*p \leq 0.05$; vs. control). C) Bar graph displaying the lindane-induced decrease in depolarization-evoked exocytosis. Following a 10 min exposure to DMSO-containing saline (control) or 10 – 50 µM lindane, the exocytotic response evoked by the depolarization, is expressed as a percentage of the initial response to depolarization. The response to depolarization was inhibited by lindane (unpaired *t*-test; $*p \leq 0.05$; vs. control). No difference between 10 and 50 µM was observed. Bars represent average values (±SEM) of 10 – 12 cells.

Exposure of cells to lindane (100 µM) in presence of the GABA receptor antagonist gabazine (25 µM) or the glycine receptor antagonist strychnine (100 µM) demonstrated that the effects of lindane on basal $[Ca^{2+}]_i$ are neither mediated by effects on the GABA- nor on the glycine receptor (data not shown).

Regression analysis (Origin 7.5) was applied to determine a possible correlation between the observed lindane-induced changes in $[Ca^{2+}]_i$ (Fig. 3) and ROS production at 1 h (Fig. 1). This yielded a positive linear (p=0.001) correlation with a regression coefficient of 0.95.

To determine whether the changes in basal release frequency and $[Ca^{2+}]_i$ can be explained by a lindane-induced membrane depolarization, electrophysiological recordings of the membrane potential of PC12 cells were made. Cells had a membrane potential of -52 ± 3 mV (n=11) and a membrane resistance of 63 ± 7 MΩ. Addition of 10 µM lindane to the superfusion solution rapidly evoked a long-lasting depolarization with an amplitude of 17 ± 2 mV (n=6); a concentration of 30 µM evoked a larger depolarization of 32 ± 7 mV (n=5, $p \leq 0.05$, not shown). This clearly indicates that lindane exposure induces a concentration-dependent membrane depolarization.

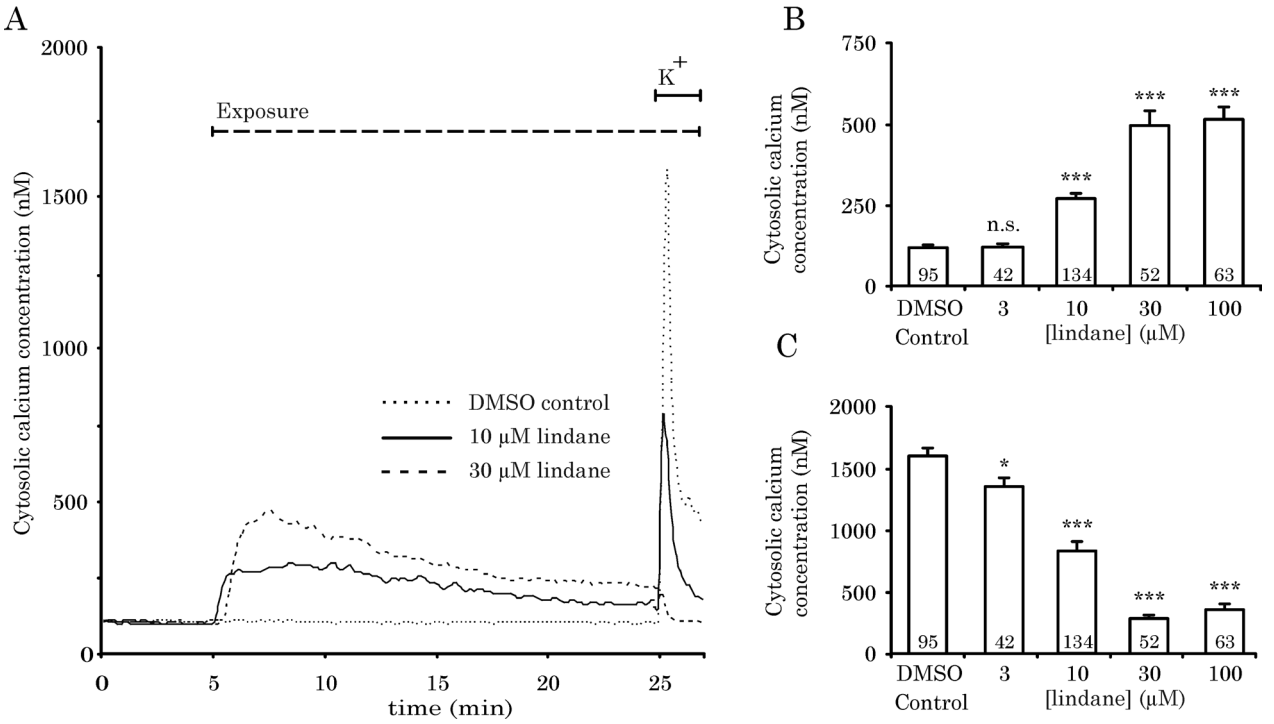

Fig. 3. Exposure of PC12 cells to lindane induces an increase in basal $[Ca^{2+}]_i$ and decreases the depolarization-evoked increase in $[Ca^{2+}]_i$. A) Representative traces of cytosolic $[Ca^{2+}]_i$ measurements of individual PC12 cells are shown, illustrating the increase in basal $[Ca^{2+}]_i$ as well as the reduction of the depolarization-evoked increase in $[Ca^{2+}]_i$ by exposure to DMSO (control, dotted line), 10 µM lindane (solid line) and 30 µM lindane (dashed line).B) Bar graph showing the lindane-induced concentration-dependent increase in basal $[Ca^{2+}]_i$.No difference was observed between 30 and 100 µM. C) Bar graph demonstrating the lindane-induced, concentration-dependent decrease in depolarization-evoked $[Ca^{2+}]_i$. No significant difference was observed between 30 and 100 µM. Bars display average data (±SEM) from the number of cells (n) indicated in the bars (4 – 11 experiments per concentration). Difference from control: *$p \leq 0.05$; ***$p \leq 0.001$.

Effects of lindane on depolarization-evoked exocytosis and cytosolic $[Ca^{2+}]_i$

In addition to the acute effects on basal exocytosis, acute effects of lindane on depolarization-evoked exocytosis were investigated. Upon depolarization, the release frequency increased to 90.3 ± 8.1 ev./min in control cells (n=47) and slowly declined to basal release levels after cessation of depolarization. Following a 10 min period, the release frequency during a subsequent depolarization was, as observed previously (Westerink and Vijverberg 2002b), reduced to 68 ± 17% of the initial release frequency in control cells (paired t-test: $p \leq 0.05$, n=11, Fig. 2A and C). Cells exposed for 10 min to 10 or 50 µM lindane displayed a much stronger reduction in the depolarization-evoked release frequency, amounting to 20 ± 7% (n=10) and 12 ± 5% (n=12), respectively (Fig. 2A and C). Further analysis of the amperometric data revealed that the quantal size, i.e., the amount of neurotransmitter released per vesicle (in zmol), was not affected (control: 380 ± 104 zmol, n=6, 100 µM lindane: 409 ± 71 zmol, n=6, n.s.). The mean event amplitude (in pA), which reflects changes in the concentration of catecholamine reaching its postsynaptic target receptor, was also unaffected following lindane exposure (control: 16.9 ± 4.3 pA, n=6; 100 µM lindane: 14.0 ± 4.6 pA, n=6, n.s.). The amperometry data thus indicate that, although lindane increases basal exocytosis and reduces depolarization-evoked exocytosis, the fundamental processes underlying vesicle fusion are not affected by acute exposure to lindane.

To investigate whether the observed changes in exocytosis were caused by disruption of Ca^{2+} homeostasis, cells were depolarized with high-K^+ saline to evoke Ca^{2+} influx through VGCC following 20 min of exposure to DMSO (control) or lindane. In control cells (n=95), depolarization evoked a strong increase in $[Ca^{2+}]_i$ (amounting to 1,6 µM). Despite the ongoing depolarization, $[Ca^{2+}]_i$ declined within minutes (Fig. 3A).

This decline is probably due to inactivation of VGCCs, resulting in reduced Ca^{2+} influx, and enhanced activity of Ca^{2+} pumps and exchangers. The depolarization-evoked increase in $[Ca^{2+}]_i$ was concentration-dependently reduced by ≥3 µM lindane (Fig. 3A and C). Lindane apparently exerted its maximum reducing effect on depolarization-evoked $[Ca^{2+}]_i$ at 100 µM (346 ± 16 nM, n=63, $p \leq 0.001$). The LOEC for lindane-induced effects on depolarization-evoked $[Ca^{2+}]_i$ was 3 µM (calculated IC_{50}: 8 µM; R^2 >0.95). It should be noted that direct co-application of lindane (10 µM) with the depolarizing medium, i.e., without lindane exposure prior to depolarization, resulted in a similar inhibition of the depolarization-induced increase in $[Ca^{2+}]_i$ (Fig. 5A). These findings indicate that lindane directly and immediately affects the VGCC-mediated Ca^{2+} influx.

Exposure of cells to lindane (100 µM) in presence of the GABA receptor antagonist gabazine (25 µM) or the glycine receptor antagonist strychnine (100 µM) demonstrated that the effect of lindane on depolarization-evoked $[Ca^{2+}]_i$ is neither mediated by effects on the GABA nor the glycine receptor (data not shown).

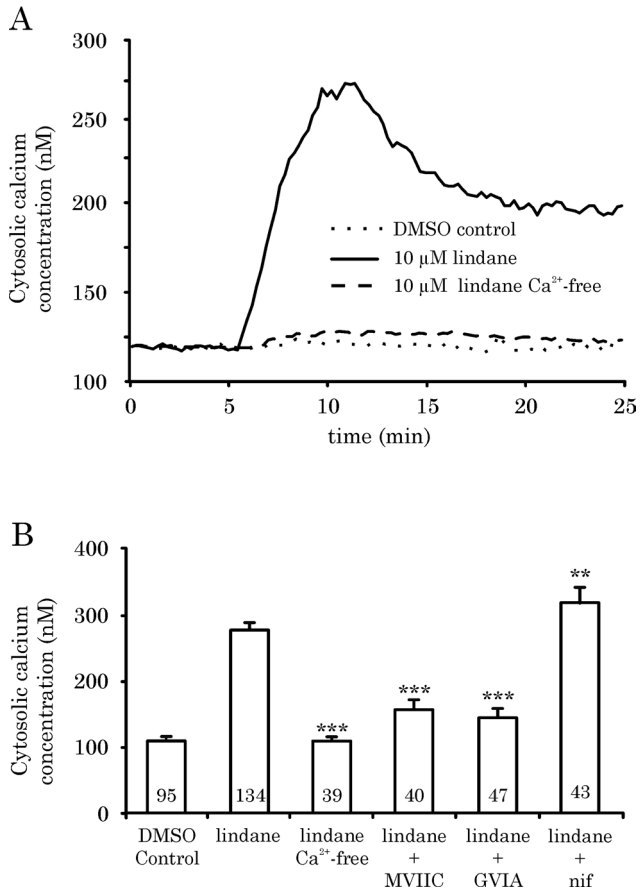

Fig. 4. The lindane-induced increase in basal $[Ca^{2+}]_i$ in PC12 is strongly attenuated in Ca^{2+}-free conditions and by addition of blockers of N- and P/Q-type VGCCs, but not by blockers of L-type VGCCs. A) Representative traces of cytosolic $[Ca^{2+}]_i$ measurements of individual PC12 cells, illustrating the increase in basal $[Ca^{2+}]_i$ by exposure to DMSO (dotted line), 10 µM lindane in normal (solid line) and Ca^{2+}-free saline (dashed line). B) Bar graph representing the effects of lindane (10 µM) on basal $[Ca^{2+}]_i$ and the effects of pharmacological manipulation of VGCCs on the lindane-induced increase of basal $[Ca^{2+}]_i$. Bars display average data (±SEM) from the number of cells (*n*) indicated in the bars (4 – 11 experiments per concentration). Significance compared to lindane-only (10 µM): $^{**}p \leq 0.01$; $^{***}p \leq 0.001$. The difference between lindane (10 µM) and control is significant ($p \leq 0.001$) as indicated in Fig. 3B.

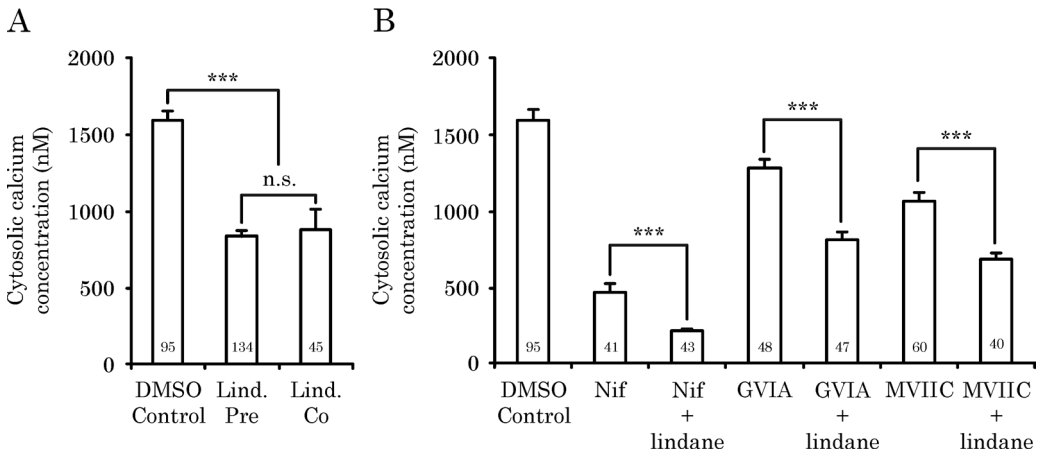

Fig. 5. Exposure to lindane induces an immediate reduction of depolarization-evoked $[Ca^{2+}]_i$ that is not specifically mediated by L-,N-, or P/Q-type VGCCs. A) Bar graph demonstrating that effects of lindane on depolarization-evoked $[Ca^{2+}]_i$ are immediate and not depending on foregoing increases of basal $[Ca^{2+}]_i$, as co-application of 10 µM lindane with high-K^+ medium (Lind. co) induced an identical reduction of depolarization-evoked $[Ca^{2+}]_i$ compared to depolarization following 20 min lindane exposure (Lind. pre). B) Bar graph demonstrating that the lindane-induced reduction of depolarization-evoked $[Ca^{2+}]_i$ has no VGCC-specificity. Selective pharmacological blocking of L- (Nif: Nifedipine),N-(GVIA: ω-conotoxin GVIA) as well as P/Q-type (MVIIC: ω-conotoxin MVIIC) VGCCs is additive to the lindane-induced effects. Bars display average data (±SEM) from the number of cells (*n*) indicated in the bars (4–11 experiments concentration). Significance; ***$p \leq 0.001$. All blocker-induced effects are significant compared to control ($p \leq 0.001$).

In additional experiments, L-, N- and P/Q-type VGCCs were pharmacologically blocked to investigate whether specific VGCCs were involved in the inhibitory effects of lindane on the depolarization-evoked increase in $[Ca^{2+}]_i$ (Fig. 5B). Though all VGCC blockers decreased the depolarization-evoked increase in $[Ca^{2+}]_i$ in control cells, nifedipine had the largest effect, reducing depolarization evoked $[Ca^{2+}]_i$ to 498 ± 63 nM (*n*=41). This indicates that L-type VGCCs account for the largest part of the Ca^{2+} influx upon depolarization in undifferentiated PC12 cells. If lindane specifically blocks one subtype of VGCC, a combined exposure to lindane and the specific VGCC blocker should inhibit the depolarization-evoked increase in $[Ca^{2+}]_i$ to a similar extent as the specific blocker alone, as an additive effect of lindane is not expected. However, exposure to lindane (10 µM) while blocking either the L-, N- or P/Q-type VGCCs, still results in a further decrease of the depolarization-evoked increase in $[Ca^{2+}]_i$ compared to the specific blockers alone (Fig. 5B). It can therefore be concluded from these combined data that the effect of lindane on depolarization-evoked $[Ca^{2+}]_i$ is VGCC non-specific.

Discussion

The present results demonstrate a dual action of lindane on PC12 cells. On the one hand, lindane depolarizes the cell membrane, thereby increasing basal $[Ca^{2+}]_i$ as well as basal exocytosis of dopamine. On the other hand, lindane inhibits VGCCs resulting in a reduction of depolarization-evoked $[Ca^{2+}]_i$ and exocytosis (Fig. 2 and 3). It is likely that the observed difference between the lowest observed effect concentration (LOEC) for the increase in basal $[Ca^{2+}]_i$ (10 µM) and basal exocytosis (50 µM) can be explained by a $[Ca^{2+}]_i$ threshold for exocytosis (Catterall and Few 2008), which is apparently not reached during exposure to 10 µM lindane. The observed effects on $[Ca^{2+}]_i$ and exocytosis cannot be explained by acute cytotoxic effects of lindane as cell viability was not affected by concentrations up to 100 µM for 6 h. Although a concentration-dependent transient increase in ROS production is observed (Fig. 1). Experiments with gabazine and strychnine revealed that the demonstrated effects on $[Ca^{2+}]_i$ and exocytosis are not mediated by a lindane-induced inhibition of GABA or glycine receptors (data not shown). Furthermore, the observed disturbances in exocytosis and $[Ca^{2+}]_i$ are apparently not mediated by effects on intracellular Ca^{2+} stores but by effects on VGCC-mediated influx of Ca^{2+}.

Our finding that lindane increases the basal $[Ca^{2+}]_i$ is in line with a number of studies from decades ago that indicated effects on $[Ca^{2+}]_i$ at varying concentrations lindane, including induction of Ca^{2+} influx into synaptosomes (0.03 – 25 µM), rat cerebellar granule neurons (150 µM) and astrocytes (0.3 µM) (for review see: Mariussen and Fonnum 2006). Consistent with earlier observations (Silvestroni, *et al.* 1997), it is likely that the increase in basal $[Ca^{2+}]_i$ is caused by the observed lindane-induced depolarization of the cell membrane resulting in opening of VGCCs. According to our results, the increase in basal $[Ca^{2+}]_i$ depends, at least in PC12 cells, mainly on opening of N- and P/Q-type VGCCs (Fig. 4).

The observation that lindane induces a membrane depolarization explains the increase in basal $[Ca^{2+}]_i$. However, the apparent saturation of basal $[Ca^{2+}]_i$, suggests that a counteracting mechanism plays a role. This is in agreement with the lindane-induced inhibition of the depolarization-evoked increase in $[Ca^{2+}]_i$ (LOEC: 3 µM), which appears mainly due to a lindane-induced, concentration-dependent, non-specific block of VGCCs (Fig. 5B). Additionally, this is in accordance with findings in neuroblastoma cells, where an undefined lindane-induced VGCC block was reported (EC_{20}: 3 µM; Forsby and Blaauboer 2007).

It is unlikely that the lindane-induced inhibition of depolarization-evoked exocytosis and $[Ca^{2+}]_i$ is caused by e.g., Ca^{2+}-induced inhibition of VGCCs, as the lindane-induced inhibition of depolarization-evoked Ca^{2+} influx occurs immediately and independent of the foregoing increase in basal Ca^{2+} (see Fig. 5A). In addition, it is unlikely that vesicle depletion caused by exocytosis during the foregoing exposure accounts for the observed reduction of depolarization-evoked exocytosis,

as the observed number of lindane-induced fusion events is well below the total release potential of PC12 cells (Westerink and Vijverberg 2002b).

To conclude, we report that lindane exerts two distinct effects. On the one hand, lindane depolarizes the cell membrane, thereby inducing basal Ca^{2+} influx and exocytosis. On the other hand, lindane induces a non-specific block of VGCCs, which inhibits depolarization-evoked Ca^{2+} influx and exocytosis. Accordingly, this block limits the basal effect of lindane-induced membrane depolarization. Although the changes in $[Ca^{2+}]_i$ correlate with an increase in ROS production, none of these effects is due to acute cytotoxicity or inhibition of GABA or glycine receptors.

The question remains how lindane exerts the observed depolarization. Elaborating on the study of Silvestroni et al. (Silvestroni, *et al.* 1997) it can be hypothesized that lindane quickly partitions into the lipid bilayer of the cell membrane and accumulates there. As a result, the membrane dipole potential (ψd) will be changed and Na^+-K^+-ATPase function will be disturbed (Qin, *et al.* 1995, Srivastava and Shivanandappa 2010, Starke-Peterkovic, *et al.* 2005), leading to depolarization the cell membrane. However, it cannot be excluded that lindane induces depolarization via another mechanism, e.g., direct opening or prolonging the open time of Na^+-channels and subsequent opening of VGCCs, analogues to the pyrethroid insecticides (Ray and Fry 2006).

Background exposure levels of lindane measured in adult non-occupationally exposed humans vary from 1.2 to 17.7 ng/ml serum (Botella, *et al.* 2004, Carreno, *et al.* 2007, Jimenez-Torres, *et al.* 2006, corresponding with a blood concentration of 2–33 nM; calculated using average physiologic values). Though maximum concentrations found in non-occupationally exposed adult populations are often around one order of magnitude higher than median values, this is still approximately 2–3 orders of magnitude lower (comparing blood concentration to experimental saline concentration) than the LOECs (3 and 10 µM) in this study. It seems therefore likely that acute effects of lindane on $[Ca^{2+}]_i$ and dopaminergic neurotransmission, as well as effects on GABA and glycine receptors, may occur only in cases of extreme exposure, such as accidental and deliberate ingestion of lindane, or in case of prolonged skin contact. However, it has been observed that lipophilic persistent compounds tend to accumulate in neuronal tissue, *in vitro* as well as *in vivo* (see e.g., Mundy, *et al.* 2004), implicating that blood concentrations may underestimate the actual concentration of lindane in the brain.

Additional concern arises from the detection of lindane in breast milk at concentrations ranging from 0.23 up to 106 ng/g l.w. (corresponding with approx. 0.03 – 15 nM; e.g., Mueller, *et al.* 2008, Prachar, *et al.* 1993), in cord serum at concentrations up to 100 ng/ml (corresponding with approx. 190 nM in whole cord blood; (Jimenez-Torres, *et al.* 2006), and children's blood levels in some communities easily reaching 8200 ng/g l.w. (corresponding with approx. 315 nM) (Trejo-Acevedo,

et al. 2009). Considering the bioaccumulative properties of lindane *in vivo*, it is not unlikely that in extreme cases high nanomolar or even low micromolar brain levels can be reached. This indicates that the developing brain, which is more vulnerable for neurotoxic insults (Singal and Thami 2006), is at risk of being chronically exposed to concentrations of lindane even less than 1 order of magnitude lower than our *in vitro* acute exposure LOECs for disturbance of Ca^{2+} homeostasis and dopamine exocytosis.

In case of *in vivo* exposure to non-lethal concentrations of lindane the acute toxic effect will consist of a combination of the known inhibition of postsynaptic GABA and glycine receptors with (non receptor-mediated) presynaptic disturbance of dopaminergic neurotransmission by membrane depolarization and disturbance of $[Ca^{2+}]_i$. As dopaminergic neurotransmission is under inhibitory control of GABA, it can be expected that the effect of lindane-induced GABA receptor inhibition will add up to the lindane-induced disturbance of dopaminergic neurotransmission. However, sophisticated experiments in neural networks, consisting of dopaminergic neurons and GABA-ergic neurons, are required to resolve this issue.

Although acute dopaminergic cell death following lindane exposure *in vitro* was not observed, it is not unlikely that prolonged exposure *in vivo* results in cell death and neurodegeneration. In particular since disturbance of Ca^{2+} and dopamine homeostasis as well as increased ROS production, appear to play a pivotal role in neurodegeneration of dopaminergic brain areas (for review see: Bartels and Leenders 2009,Mattson 2007). Intracellular accumulation of lindane and an enduring disturbance of GABA/glycine-ergic and dopaminergic neurotransmission might provide an additional basis for cell death and neurodegeneration *in vivo* (for review see: Mariussen and Fonnum 2006). Furthermore, perinatal exposure to organochlorine pesticides has been linked to increased vulnerability to develop PD later in life (Barlow, *et al.* 2007) and even more interesting, significantly elevated levels of lindane (concentrations up to 1.4 µg/g l.w., corresponding with 0.6 µM; calculated using average physiological values) have been detected in the substantia nigra of Parkinson's patients (Corrigan *et al.* 2000). This is only 1 order of magnitude lower than our LOECs for acute disturbance of Ca^{2+} homeostasis, dopamine exocytosis and ROS production obtained *in vitro*, and 1 – 2 orders of magnitude above plasma levels in the general population. This illustrates that, although general population-based plasma levels are apparently well below the reported LOECs, tissue levels can approach *in vitro* effect concentrations, which raises specific concern for highly exposed individuals, especially children (see also above).

The observed effect concentrations for both increased basal $[Ca^{2+}]_i$ (LOEC 10 µM; calculated EC_{50}: 11 µM;) and inhibition of depolarization-evoked increase in $[Ca^{2+}]_i$ (LOEC 3 µM; calculated IC_{50}: 8 µM) are in the same low micromolar range as the effect levels of the presumed primary mode of action, i.e., inhibition of $GABA_A$

(IC_{50}: 6 µM) and glycine (IC_{50}: 5µM; Vale, *et al.* 2003) receptors. It can thus be concluded that modulation of intracellular Ca^{2+} homeostasis as well as (dopaminergic) exocytosis, contribute to the neurotoxic potential of lindane. As the reported effect concentrations for the (postsynaptic) presumed primary mechanism of action are in the same range as reported here for presynaptic effects, the current findings must be taken into account for human risk assessment. In particular since human tissue levels in extreme cases are close to the LOECs reported here for acute effects.

Conflict of interest statement

There are no conflicts of interest.

Acknowledgments

We are grateful to Aart de Groot and Gina van Kleef for expert technical assistance. This work was supported by the Dutch "Internationaal Parkinson Fonds" (IPF) and The UK Joint Environment and Human Health Programme (jointly funded by the Natural Environment Research Council, Defra, the Environment Agency, the MOD and the Medical Research Council) [grant reference NE/E007732/1].

Chapter 5.2

Organochlorine insecticides lindane and dieldrin and their binary mixture disturb calcium homeostasis in dopaminergic PC12 cells

Harm J. Heusinkveld[1], Remco H.S. Westerink[1]

[1] Neurotoxicology Research Group, Institute for Risk Assessment Sciences (IRAS), Utrecht University, the Netherlands

Environmental Science and Technology **46**, 1842-1848 (2012)

Abstract.

Current hypotheses link long-term environmental exposure of humans to persistent organochlorine (OC) insecticides lindane (HCH) and dieldrin (HEOD) to the development of neurodegenerative disorders, such as Parkinson's disease. Primary adverse neurological effects of these insecticides are directed at inhibition of $GABA_A$ and glycine receptors, although GABA-independent effects have also been reported. In this paper we describe the effect of dieldrin and a binary mixture of dieldrin and lindane on a critical parameter of neuronal function and survival, i.e., intracellular calcium homeostasis. The intracellular calcium concentration ($[Ca^{2+}]_i$) has been monitored using real-time single-cell fluorescence microscopy in dopaminergic PC12 cells loaded with the calcium-sensitive dye Fura-2. The results demonstrate that nanomolar concentrations of dieldrin time- and concentration-dependently inhibit depolarization-evoked influx of Ca^{2+}. Co-exposure of PC12 cells to a mixture of dieldrin and lindane revealed an additive inhibition of the depolarization-evoked increase in $[Ca^{2+}]_i$, whereas the lindane-induced increase in basal $[Ca^{2+}]_i$ is inhibited by dieldrin. The combined findings indicate that dieldrin and binary mixtures of organochlorines affect $[Ca^{2+}]_i$ already at concentrations below commonly accepted effect concentrations and close to human internal dose levels. Consequently, current findings illustrate the need to take mixtures of OC insecticides into account in human risk assessment.

Introduction

Organochlorine (OC) compounds have been used for decades as broad-spectrum insecticides in agriculture as well as in human- and veterinary medicine (Kaushik and Kaushik 2007). Many OC insecticides are subject to long-range transport, persist in the environment and food chain, and are therefore classified as persistent organic pollutants (POPs; for review see: Sonne 2010).

Consequently, OC compounds, such as dieldrin (1,2,3,4,10,10-hexachloro-6,7-epoxy-1,4,4a,5,6,7,8,8a-octahydro-1,4,5,8-dimethano-naphthalene, HEOD), are found ubiquitously in the environment and throughout the food chain up to (arctic) top-predators, including humans (Sonne 2010). Human exposure to OC compounds is mainly through the diet, with children being exposed to higher levels than adults because of their relatively high food intake and low body volume (Fromberg, *et al.* 2011). Despite the ban on the use of dieldrin in Europe and the US in the 1980s, dieldrin is detected in up to 90% of human blood samples in the USA (Patterson, *et al.* 2009). Dieldrin adult blood levels in Spain easily reach up to 28 ng/ml serum (Rivas, *et al.* 2007), and comparable (maternal and cord-) blood levels have been detected in blood samples from India (Mustafa, *et al.* 2010), illustrating the world-wide abundance of dieldrin in the environment and food chain.

Dieldrin is often detected together with another persistent OC insecticide, γ-hexachlorocyclohexane (γ-HCH, lindane). Like dieldrin, lindane accumulates in the food chain and is subject to long-range transport, and lindane residues are ubiquitous in environmental samples (including food) globally (Roche, *et al.* 2008). Lindane levels in Europe reach up to hundreds of ng/g lipid weight (ng/g l.w.) in human tissues, including (cord) serum, breast milk, and amniotic fluid (see e.g., Luzardo, *et al.* 2009), and much higher levels have been found in heavily polluted areas (Subramanian, *et al.* 2007, Trejo-Acevedo, *et al.* 2009Subramanian, *et al.* 2007, Trejo-Acevedo, *et al.* 2009, Trejo-Acevedo, *et al.* 2009).

Due to the high lipophilicity of dieldrin (log K_{ow} 6.2) and lindane (log K_{ow} 3.9), concentrations in breast milk are in general considerably higher than blood concentrations (Solomon and Weiss 2002). The detection of equal nanomolar levels of dieldrin in cord- and maternal blood samples indicates that biological membranes such as the placental barrier are easily crossed by these OC insecticides (Luzardo, *et al.* 2009, Mustafa, *et al.* 2010). This is of major concern for the nervous system, which is one of the most vulnerable targets for exposure to environmental toxicants, in particular during development (for review see: Mariussen and Fonnum 2006). For example, developmental exposure to dieldrin has been shown to increase the vulnerability of DA neurons for degeneration later in life (Richardson, *et al.* 2006). Moreover, dieldrin and lindane have been detected at low micromolar levels in brains of Parkinson's disease patients (Corrigan, *et al.* 2000), and serum levels of dieldrin have recently been related to the development of PD (Weisskopf, *et al.* 2010).

Despite the co-occurrence of these two OCs in humans and the food chain, human risk assessment is mainly based on the presumed primary effects of the single compounds, i.e., inhibition of GABA- and glycine-receptors (for review see: Mariussen and Fonnum 2006, Vale, *et al.* 2003). Acute intoxication in mammals results in convulsions, which are frequently lethal and can be explained by the inhibitory action of OCs on the GABA-ergic input of the brain (Bloomquist 1993). However, we recently reported that lindane can also induce GABA- and glycine-independent effects on the intracellular Ca^{2+} concentration ($[Ca^{2+}]_i$), neurotransmitter release, and production of reactive oxygen species (ROS) in dopaminergic PC12 cells (Heusinkveld, *et al.* 2010).

PC12 cells are extensively characterized as an *in vitro* model to study changes in Ca^{2+} homeostasis and exocytosis (Westerink and Ewing 2008). Since these neuroendocrine cells lack functional GABA receptors (Hales and Tyndale 1994), they serve as a functional model for investigations of non-GABA receptor-mediated neurotoxicity of OC compounds.

As Ca^{2+} plays a crucial role in neuronal function and survival, the aim of the present study was to investigate effects of acute dieldrin exposure on basal and depolarization-evoked $[Ca^{2+}]_i$ in PC12 cells. Considering the concurrent exposure to OCs in humans, the effects of combined exposure to lindane and dieldrin on Ca^{2+} homeostasis were also investigated. The combined results demonstrate that nanomolar concentrations of dieldrin disrupt Ca^{2+} homeostasis, whereas the concurrent exposure with lindane revealed both additive as well as antagonistic effects on Ca^{2+} homeostasis.

Materials and methods

Chemicals

NaCl, KCl, and HEPES were obtained from Merck (Whitehouse Station, NJ, USA); $MgCl_2$, $CaCl_2$, glucose, sucrose, and NaOH were obtained from BDH Laboratory Supplies (Poole, UK); Fura-2 AM was obtained from Molecular Probes (Invitrogen, Breda, The Netherlands); all other chemicals were obtained from Sigma (St. Louis MO, USA), unless otherwise noted. Saline solutions, containing (in mM) 125 NaCl, 5.5 KCl, 2 $CaCl_2$, 0.8 $MgCl_2$, 10 HEPES, 24 glucose, and 36.5 sucrose (pH 7.3), were prepared with deionized water (Milli-Q; resistivity >10 MΩ•cm). Stock solutions of 2 mM ionomycin in DMSO were kept at −20°C. Stock solutions of 0.01 − 100 mM lindane and dieldrin (Pestanal grade, 99.8% purity, Riedel de Haën, Seelze, Germany) were prepared in DMSO and diluted in saline to obtain the desired concentrations just prior to the experiments (all solutions used in experiments, including control experiments, contained 1 µl DMSO/ml).

Cell culture

Rat dopaminergic pheochromocytoma (PC12 cells; Greene and Tischler 1976) were grown for 10 passages in RPMI 1640 (Invitrogen, Breda, The Netherlands) supplemented with 5% fetal calf serum and 10% horse serum (ICN Biomedicals, Zoetermeer, The Netherlands) in a humidified incubator at 37°C and 5% CO_2 as described previously (Heusinkveld, *et al.* 2010). For Ca^{2+} imaging experiments, cells were subcultured in poly-L-lysine coated glass-bottom dishes (MatTek, Ashland, MA) as described previously (Dingemans, *et al.* 2009, Heusinkveld, *et al.* 2010).

Cell viability

To exclude that results are confounded by acute cytotoxicity, effects of dieldrin, lindane, and binary mixtures on cell viability were determined using a Neutral Red (NR) assay in undifferentiated PC12 cells (Heusinkveld, *et al.* 2010). Cells were seeded in (poly-L-lysine coated) 96-wells plates (Greiner Bio-one, Solingen, Germany) at a density of 10^5 cells/well, 1 day prior to exposure. Cells were exposed in serum-free medium to concentrations up to 100 µM for 24 h. Membrane integrity and lysosomal activity were determined as a measure of cell viability using the NR assay (protocol adapted from: Repetto, *et al.* 2008). Briefly, following 24 h exposure cells were incubated for 1 h with 200 µL NR solution (175 µM in PBS, Invitrogen, Breda, The Netherlands). Following the incubation, cells were rinsed with warm (37°C) PBS and 100 µL extraction solution (1% glacial acetic acid, 50% ethanol, and 49% H_2O) was added to the wells. After 30 min extraction, fluorescence was measured spectrophotometrically at 430/480 nm (FLUOstar Galaxy V4.30-0, BMG Labtechnologies, Offenburg, Germany).

Ca^{2+} imaging

Changes in $[Ca^{2+}]_i$ were measured using the Ca^{2+}-sensitive fluorescent ratio dye Fura-2 AM as described previously (Heusinkveld, *et al.* 2010, Hondebrink, *et al.* 2011). Briefly, cells were loaded with 5 µM Fura-2 AM (Molecular Probes; Invitrogen, Breda, The Netherlands) for 20 min at room temperature, followed by 15 min de-esterification. After de-esterification, the cells were placed on the stage of an Axiovert 35M inverted microscope (Zeiss, Göttingen, Germany) equipped with a TILL Photonics Polychrome IV (TILL Photonics GmBH, Gräfelfing, Germany). Fluorescence, evoked by 340 and 380 nm excitation wavelengths (F340 and F380), was collected every 6 s at 510 nm with an Image SensiCam digital camera (TILL Photonics GmBH). After 5 min baseline recording, cells were de-polarized by high-K^+ containing saline (100 mM K^+) for 20 s. Following a 5 min recovery period, cells were exposed to DMSO (1 µl/ml), dieldrin (10 nM – 10 µM), or a combination of dieldrin with lindane for 20 min. Subsequently, cells were de-polarized for a second time to evaluate effects of exposure on depolarization-evoked Ca^{2+} influx. In experiments involving time-dependence or reversibility, exposure

duration was extended up to 40 min. Minimum and maximum ratios (R_{min} and R_{max}) were determined at the end of the recording by addition of ionomycin (5 µM) and ethylenediamine tetraacetic acid (EDTA; 17 mM). Changes in the F340/F380 ratio (R), reflecting changes in $[Ca^{2+}]_i$, were further analyzed using custom-made MS-Excel macros.
Free cytosolic $[Ca^{2+}]_i$ was calculated using Grynkiewicz's equation:

$$[Ca^{2+}]_i = Kd^* \times (R - R_{min})/(R_{max} - R)$$

where Kd* is the dissociation constant of Fura-2 determined in the experimental setup (Deitmer and Schild 2000). The maximum amplitude of basal $[Ca^{2+}]_i$ during exposure was determined to quantify effects on basal $[Ca^{2+}]_i$. The maximum amplitude of $[Ca^{2+}]_i$ observed during depolarization was used to investigate possible effects on the depolarization-evoked increase of $[Ca^{2+}]_i$.

Data analysis and statistics.

Cell viability data are presented as % viability ± standard error of the mean (SEM) compared to control from the number of wells indicated in the bars. Data from fluorescence microscopy is presented as mean $[Ca^{2+}]_i$ ± SEM from the number of cells (*n*) indicated, obtained from 4 to 9 independent experiments (N) as the cells (*n*) are the most important source of variation rather than the different dishes (N). Additionally, using N as statistical unit limits the possibility to evaluate single cell calcium dynamics. Treatment ratio (TR) represents the second depolarization-evoked increase in $[Ca^{2+}]_i$ in treated cells as a percentage of the response to the first depolarization, expressed relative to the TR in control cells. Statistical analyses were performed using SigmaPlot 12.0 (Systat Software Inc. San Jose, California USA). Continuous data were compared using One-way ANOVA and posthoc Bonferroni test. In Ca^{2+} imaging experiments, a decrease in TR of 10% is considered a minimal relevant effect size. A p-value <0.05 is considered statistically significant; n.s. indicates the absence of a statistically significant effect.

Results

Effects of OC insecticides on cell viability.

To exclude that the results presented in this study are due to direct cytotoxicity of dieldrin, lindane, or their binary mixtures, effects on cell viability were determined using a NR assay. Exposure of PC12 cells to 10 or 100 µM lindane or dieldrin for 24 h did not affect cell viability. Similarly, 24 h exposure to a binary mixture of 10 µM lindane and 10 µM dieldrin did not reduce cell viability. However, co-exposure of cells to 100 µM lindane and 100 µM dieldrin resulted in a moderate decrease of cell viability to 47 ± 3% (n = 36; $p \leq 0.001$) compared to DMSO control (100 ± 1%, n=72; Fig. 1).

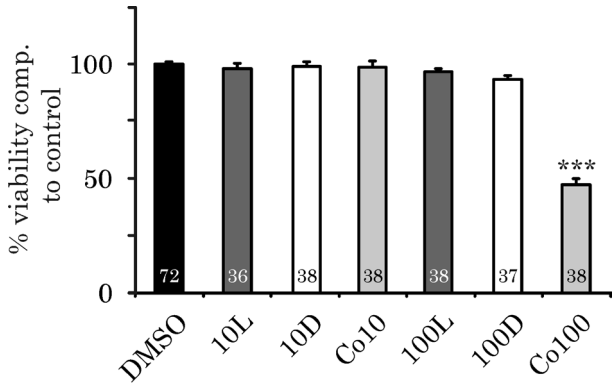

Fig. 1. Organochlorine-induced cytotoxicity in PC12 cells. Bar graph demonstrating that a binary mixture (Co) of lindane (L) and dieldrin (D), both at 100 µM, reduces cell viability in PC12 cells after 24 h of exposure. Lindane (10 and 100 µM), dieldrin (10 and 100 µM), and a binary mixture of lindane and dieldrin (both at 10 µM) do not induce overt cytotoxicity. Bars represent average percentage cell viability (±SEM; n=36 − 72 wells per concentration) compared to control. Difference from control: *** $p \leq 0.001$.

Effects of dieldrin on basal and depolarization-evoked $[Ca^{2+}]_i$.

In control cells (n=119), basal $[Ca^{2+}]_i$ was low (95 ± 2 nM), whereas depolarization evoked a strong, transient increase in $[Ca^{2+}]_i$ up to 2 µM. After the depolarization, superfusion was switched back to saline and $[Ca^{2+}]_i$ recovered to near basal values within minutes. Following a 5 min recovery period, cells were exposed to DMSO (1 µl/ml) and during this 20 min exposure to DMSO containing saline $[Ca^{2+}]_i$ was maintained at low levels (100 ± 2 nM). A second depolarization evoked an increase in $[Ca^{2+}]_i$ up to 1.7 ± 0.1 µM, i.e., up to ~85% of the first depolarization (illustrated by example traces Fig. 2A). To investigate whether exposure to dieldrin affects basal or depolarization-evoked $[Ca^{2+}]_i$, cells were exposed to dieldrin for 20 min following recovery of the first depolarization. In contrast to lindane (see

Supporting Information Fig. 1A,B), dieldrin (10 nM – 10 µM) did not affect basal $[Ca^{2+}]_i$ (Fig. 2A). However, in line with the findings on lindane (see Supporting Information Fig. 1A,C), dieldrin concentration-dependently inhibited the second depolarization-evoked increase in $[Ca^{2+}]_i$ (calculated IC_{50}: 125 nM). Exposure to 10 nM dieldrin resulted in a depolarization-evoked $[Ca^{2+}]_i$ of 1.5 ± 0.1 µM (TR 91 ± 3%; *n*=59; n.s.; Fig. 2B), whereas exposure to 100 nM dieldrin decreased the depolarization-evoked increase in $[Ca^{2+}]_i$ to 1.0 ± 0.1 µM (TR: 60%, n=56, $p \leq 0.001$). Dieldrin apparently exerted its maximum inhibitory effect at 1 µM ($[Ca^{2+}]_i$: 245 ± 17 nM, TR 10 ± 1%; *n*=62, $p \leq 0.001$) as exposure to 10 µM did not induce a further decrease in the depolarization-evoked $[Ca^{2+}]_i$ (276 ± 27 nM, TR 11 ± 1%; *n*=32).

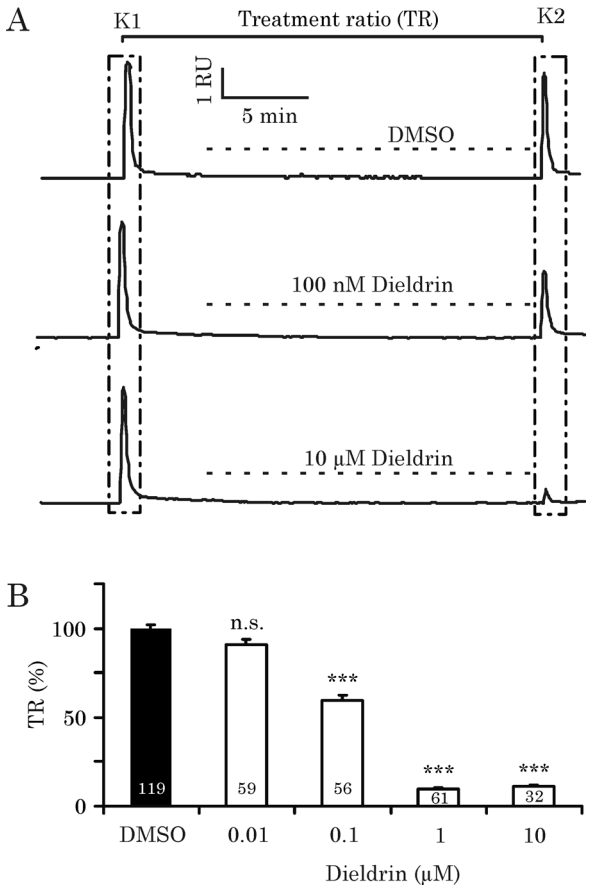

Fig. 2. Dieldrin concentration-dependently inhibits the depolarization-evoked increase in $[Ca^{2+}]_i$ in PC12 cells. A. Example traces of cytosolic $[Ca^{2+}]_i$ of individual PC12 cells, illustrating the inhibition of the second depolarization-evoked increase in $[Ca^{2+}]_i$ (K2) by exposure to DMSO (control, upper trace), 100 nM dieldrin (middle trace) and 10 µM dieldrin (lower trace). B. Bar graph summarizing the dieldrin-induced, concentration-dependent inhibition in depolarization-evoked $[Ca^{2+}]_i$. No significant difference was observed between 1 and 10 µM. Bars display average data (±SEM) from the number of cells (*n*) indicated in the bars (4 − 9 experiments per concentration). Difference from control: *** $p \leq 0.001$.

Time-Dependence and Reversibility of Dieldrin Effects.

In subsequent experiments we assessed the influence of exposure duration on the degree of dieldrin-induced inhibition of the depolarization-evoked increase in $[Ca^{2+}]_i$. When cells were exposed to a maximal inhibiting concentration dieldrin (10 µM) only during the second depolarization, the inhibition of depolarization-evoked $[Ca^{2+}]_i$ was less compared to 20 min exposure (TR 87 ± 3%, n=44, $p \leq 0.001$; Figure 3A), clearly indicating that the observed dieldrin-induced inhibition of depolarization-evoked $[Ca^{2+}]_i$ is time-dependent. Therefore, exposure duration was increased to 40 min in subsequent experiments. The results demonstrate that increasing the exposure duration induces a stronger inhibition of the depolarization-evoked increase in $[Ca^{2+}]_i$ compared to 20 min exposure, suggestive of accumulation of dieldrin in the cell membrane. The TR for 100 nM dieldrin dropped significantly from 60 ± 3% at 20 min (n=56) to 41 ± 3% at 40 min (n=42; $p \leq 0.001$), whereas in case of exposure to 10 nM dieldrin the TR drops from 91 ± 3% at 20 min (n=59) to 72 ± 4% (n=48; $p \leq 0.001$) (Figure 3A). Increasing the exposure duration thus results in a clear left-shift of the concentration-response curve. To investigate reversibility of the dieldrin-induced inhibition of depolarization-evoked increases in $[Ca^{2+}]_i$, cells were exposed to dieldrin for 20 min followed by 20 min superfusion with saline prior to the second depolarization. The TR in these cells (TR 92 ± 5%; n=32; Figure 3B) is not significantly different from control cells exposed only to saline for 40 min. Cells that were first superfused with saline for 20 min and then with dieldrin for 20 min prior to the second depolarization had a TR of 15 ± 2% (n=28), which is comparable to the results obtained with 20 min dieldrin exposure (TR 11 ± 1%, n=32). The results thus demonstrate that the dieldrin-induced inhibition of depolarization-evoked increases in $[Ca^{2+}]_i$ is time-dependent and largely reversible.

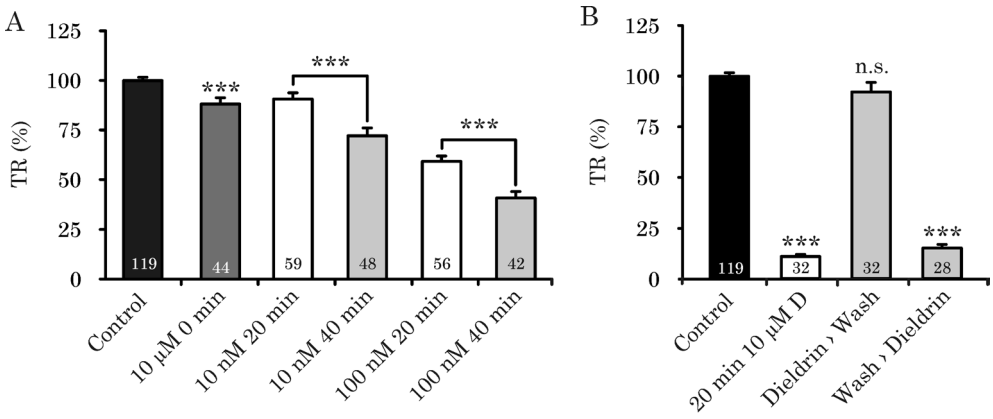

Fig. 3. The dieldrin-induced inhibition of depolarization-evoked $[Ca^{2+}]_i$ is time-dependent and reversible. A. Cells that are depolarized immediately upon exposure to 10 µM dieldrin (10 µM 0 min) do not show any dieldrin-induced inhibition of depolarization-evoked $[Ca^{2+}]_i$. In contrast, prolonged exposure to dieldrin increases the degree of inhibition of depolarization-evoked $[Ca^{2+}]_i$ as cells exposed to 10 or 100 nM dieldrin for 40 min instead of 20 min display a significantly stronger inhibition of depolarization-evoked $[Ca^{2+}]_i$. B. Effects of dieldrin on depolarization-evoked $[Ca^{2+}]_i$ are reversible. Bar graph demonstrates that in PC12 cells a 20 min washout period following 20 min exposure to 10 µM dieldrin (Dieldrin → Wash) abolishes the dieldrin-induced effect on depolarization-evoked $[Ca^{2+}]_i$. In contrast, 20 min exposure to saline followed by 20 min exposure to 10 µM dieldrin (Wash → Dieldrin) induces a comparable inhibition of depolarization-evoked $[Ca^{2+}]_i$ as exposure to only 20 min 10 µM dieldrin. Bars display average data (±SEM) from the number of cells (*n*) indicated in the bars (4 – 9 experiments per concentration). Significance: *** $p \leq 0.001$.

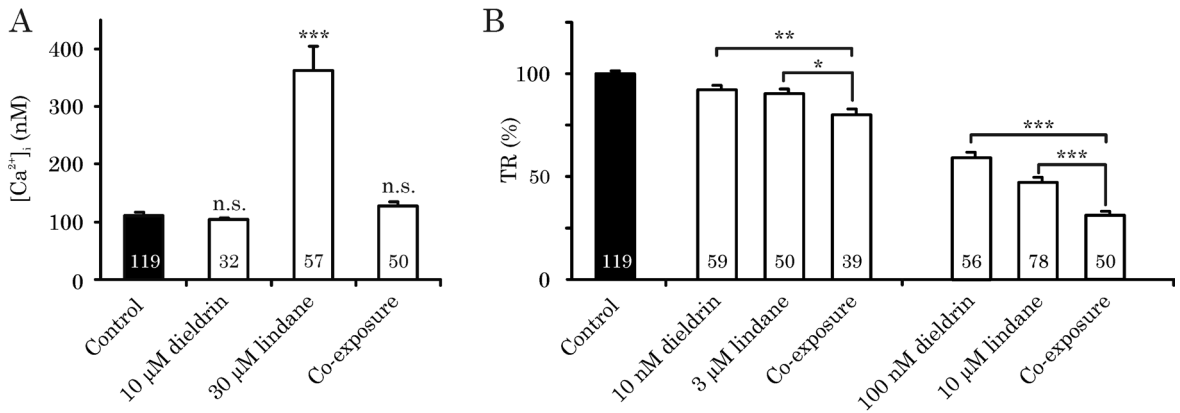

Fig. 4. Effects of exposure of PC12 cells to a binary mixture of dieldrin and lindane on basal and depolarization-evoked $[Ca^{2+}]_i$. A. Bar graph demonstrates that dieldrin (10 µM) does not induce changes in basal $[Ca^{2+}]_i$, whereas lindane (30 µM) induces an increase in basal $[Ca^{2+}]_i$. When cells are 20 min pre-exposed to dieldrin (10 µM) and subsequently co-exposed to a mixture of dieldrin (10 µM) and lindane (30 µM), the lindane-induced increase in basal $[Ca^{2+}]_i$ is abolished. B. Bar graph demonstrating that binary mixtures of dieldrin and lindane at (near) IC_{10} or (near) IC_{50} concentrations exert an additive inhibition of the depolarization-evoked $[Ca^{2+}]_i$. Bars display average data (±SEM) from the number of cells (*n*) indicated in the bars (4–9 experiments per concentration). Difference from control: * $p \leq 0.05$; ** $p \leq 0.01$; *** $p \leq 0.001$

Effects of binary mixtures of dieldrin and lindane on basal and depolarization-evoked $[Ca^{2+}]_i$.

As human exposure is usually not to a single OC compound, a number of mixture experiments were performed. We previously reported that lindane induces an increase in basal $[Ca^{2+}]_i$ (Heusinkveld, *et al.* 2010; Fig. S1), whereas dieldrin did not induce increases in basal $[Ca^{2+}]_i$ (Fig. 2A). To assess the effects of dieldrin exposure on the lindane-induced basal increase in $[Ca^{2+}]_i$, cells were first exposed to dieldrin (10 µM) for 20 min and subsequently co-exposed for 20 min to dieldrin (10 µM) and lindane (30 µM). Results from these co-exposure experiments indicated that the lindane-induced increase in basal $[Ca^{2+}]_i$ is largely abolished by dieldrin (Fig. 4A; example trace lindane in Supporting Information Fig. 1A), i.e., dieldrin antagonizes the lindane-induced increase in basal $[Ca^{2+}]_i$. We demonstrated that dieldrin and lindane both inhibit the depolarization-evoked increase in $[Ca^{2+}]_i$ (Fig. 1B and S1). To assess whether effect additivity applies, cells were exposed for 20 min to combinations of (near) IC_{10} concentrations dieldrin and lindane (respectively 10 nM (TR 92 ± 3%, n=59) and 3 µM (TR 90 ± 2%, n=50)). Upon exposure to this binary mixture of the respective IC_{10} concentrations the TR decreased to 80% (± 2%, n=39, $p \leq 0.01$; Fig. 4B). When cells were exposed for 20 min to combinations of (near) IC_{50} concentrations (respectively 100 nM (TR 59 ± 3%, n=56) and 10 µM (TR 47 ± 3%, n=78)), the TR decreased to 31% (± 2%, n=50, $p \leq 0.001$; Fig. 4B). The combined results thus demonstrate that co-exposure of cells to dieldrin and lindane induces a stronger inhibition of the depolarization-evoked increase in $[Ca^{2+}]_i$ and are suggestive of effect addition.

Discussion

The present results demonstrate that dieldrin, comparable to lindane (Heusinkveld, *et al.* 2010), concentration-dependently inhibits the depolarization-evoked increase in $[Ca^{2+}]_i$ (Fig. 2). Importantly, the lowest observed effect concentration (LOEC) for dieldrin-induced inhibition of the depolarization-evoked increase in $[Ca^{2+}]_i$ depends on exposure duration and amounts to only 10 nM after 40 min exposure (Fig. 3). When cells are exposed to equipotent mixtures of dieldrin and lindane (IC_{10} or IC_{50}), effects on depolarization-evoked $[Ca^{2+}]_i$ appear to be additive (Fig. 4B). In contrast to lindane (Heusinkveld, *et al.* 2010), exposure to dieldrin has no effect on basal $[Ca^{2+}]_i$ (Fig. 2A). In fact, dieldrin antagonized the lindane-induced increase in basal $[Ca^{2+}]_i$ (Figure 4A).

Literature on dopaminergic neurotoxicity of dieldrin reveals that exposure to dieldrin is (indirectly) linked to oxidative stress and activation of apoptotic pathways, both *in vitro* and *in vivo* (for review see: Drechsel and Patel 2008). However, acute cytotoxicity cannot explain the observed effects of dieldrin, lindane, or their binary mixture on calcium homeostasis as cell viability was not affected by concentrations up to 10 µM for 24 h. In addition, the absence of func-

tional GABA- and glycine receptors in our model system (Hales and Tyndale 1994, Heusinkveld, *et al.* 2010) indicates that the observed effects are neither GABA- nor glycine-receptor mediated. Furthermore, the absence of dieldrin-induced changes in basal $[Ca^{2+}]_i$ effectively excludes the involvement of Ca^{2+}-dependent inactivation of voltage-gated calcium channels (VGCCs; Budde, *et al.* 2002) in the dieldrin-induced inhibition of depolarization-evoked Ca^{2+}-influx. The data thus indicate that dieldrin acts as a nonspecific inhibitor of VGCCs, comparable to lindane (Heusinkveld, *et al.* 2010). Considering the dependence on the exposure duration it is not unlikely that the inhibition of depolarization-evoked Ca^{2+}-influx is mediated by effects of dieldrin on a second messenger pathway or by partitioning and accumulation in the cell membrane. The rapid reversibility makes it unlikely that the inhibition is due to adaptive internalization of calcium channels as previously observed for NMDA receptors following prolonged (days) exposure to dieldrin (Briz, *et al.* 2010). As lipophilic compounds tend to bind to proteins and thus form a continued source of exposure, the observed reversibility may not be relevant for the *in vivo* situation. Consequently, the exact mechanism underlying the dieldrin-induced inhibition of depolarization-evoked $[Ca^{2+}]_i$ as well as the effects of long-term exposure remain to be determined.

Additive effects of dieldrin and lindane have until now solely been reported for parameters of oxidative stress and cell death, though only at moderate to high micromolar concentrations (Kanthasamy, *et al.* 2008, Mao and Liu 2008, Sharma, *et al.* 2010). In line with these findings, our data demonstrate that inhibition of depolarization-evoked $[Ca^{2+}]_i$ by exposure to a binary mixture of dieldrin and lindane is additive. When dieldrin and lindane are both applied at IC_{10}, the resulting inhibition amounts to ~20%, whereas the inhibition amounts to ~70% when dieldrin and lindane are both applied at IC_{50} (Figure 4B), suggesting that at increasing concentrations a form of competition at a common target (in this case competitive inhibition of VGCCs) could limit additivity. Importantly, these findings add to the body of evidence that demonstrates that combined exposure is more toxic than exposure to the single compounds, which may have important consequences for human risk assessment.

Despite the fact that (dopaminergic) neurons heavily rely on proper calcium homeostasis for their function and survival, dieldrin-induced effects on calcium homeostasis are hardly investigated. Our results demonstrate that dieldrin can inhibit calcium influx in excitable cells already at nanomolar concentrations. As dopaminergic neurotransmission is under inhibitory control of GABA in adults, it can be argued that the inhibition of VGCCs counteracts the primary effect of dieldrin and lindane, i.e., enhanced excitation via inhibition of GABA receptors. However, sophisticated experiments in neural networks, consisting of dopaminergic neurons and GABA-ergic neurons, are required to resolve this issue.

Both lindane and dieldrin have been classified as persistent organic pollutant (POP) by the Stockholm Convention (http://www.pops.int). Due to the high lipophilicity and resistance to biodegradation, dieldrin and lindane are persistent and bioaccumulating in the food-chain. Human exposure occurs mainly via fat-containing food, such as meat and dairy products (Fromberg, *et al.* 2011). Upon exposure, the nervous system is among the most vulnerable targets for OC insecticides (Mariussen and Fonnum 2006). This holds in particular for the developing nervous system (Singal and Thami 2006), and it is therefore concerning that dieldrin has been detected in almost 99% of all samples of breast milk (for review see: Solomon and Weiss 2002). Moreover, perinatal exposure to OC insecticides is related to persistent changes in the dopaminergic system (Richardson, *et al.* 2006) and the development of PD later in life (Barlow, *et al.* 2007, Cory-Slechta, *et al.* 2005, Richardson, *et al.* 2006, Richardson, *et al.* 2006). In this respect, it is of interest that elevated levels of OC insecticides, including dieldrin and lindane, have been found in the substantia nigra of Parkinson's patients (Corrigan, *et al.* 1996, Corrigan, *et al.* 2000). Despite these findings, the exact mechanisms underlying the role of dieldrin and related compounds in neurodegeneration still remain to be elucidated.

A pharmacokinetic study from the 1970s (Walsh and Fink 1972) indicated that after a single i.v. dose of dieldrin in mice the blood concentration decreased rapidly, whereas the concentration in liver, fat, and brain increased, suggestive of fast disposition in fat-rich tissue. The authors further demonstrated that the kinetics of brain- and fat tissue uptake of dieldrin are comparable, indicating that dieldrin concentrations in fat tissue might be a more reliable representation of actual internal exposure to dieldrin than serum concentrations. Considering the accumulating properties of dieldrin and the Tolerable Daily Intake (TDI) of 50 ng/kg body weight, the 95th percentile intake for children (6.7 ng/kg body weight/day for dieldrin) as calculated by Fromberg and colleagues (Fromberg, *et al.* 2011) indicates that the protection level for dieldrin is fairly low. This is emphasized by the finding of dieldrin in adipose tissue of Spanish children at concentrations up to 130 ng/g l.w. (corresponding with a tissue concentration of ~270 nM, calculated using average physiological values (Lopez-Espinosa, *et al.* 2008), indicative of a potential brain concentration of the same order of magnitude and thus well above the LOEC found in this study.

To conclude, dieldrin time- and dose-dependently inhibits depolarization-evoked $[Ca^{2+}]_i$, which likely affects (dopaminergic) neurotransmission. Furthermore, exposure to a binary mixture of dieldrin and lindane reveals additive effects on the inhibition of depolarization-evoked $[Ca^{2+}]_i$, whereas the lindane-induced increase in basal $[Ca^{2+}]_i$, is antagonized by dieldrin. Importantly, increasing the exposure duration results in a left-shift of the concentration-response curve and a LOEC

that is very close to environmentally relevant concentrations and already below the commonly accepted primary effect combined findings thus illustrate the need to widen current human risk assessment approaches by the inclusion of (low dose) chemical mixtures.

Acknowledgements

We are grateful to Aart de Groot, Gina van Kleef, and Kim Fornasari (Neurotoxicology Research Group) and Peter Nijssen (St. Elisabeth Hospital, Tilburg) for valuable discussions and expert technical assistance.

This work was funded by a grant from the Dutch "International Parkinson Fonds" (PAGES) and by the European Union-funded project ACROPOLIS [Grant Agreement KBBE-245163]. The authors declare they have no competing financial interests.

Chapter 6.1

In vitro exposure to dinitrophenolic herbicides induces dopaminergic neurodegeneration

Harm J Heusinkveld[1], Arie C van Vliet[1], Peter CG Nijssen[2], Remco HS Westerink[1]

[1] Neurotoxicology Research Group, Division of Toxicology, Institute for Risk Assessment Sciences, Faculty of Veterinary Medicine, Utrecht University, P.O. Box 80.177, NL-3508 TD Utrecht, The Netherlands.
[2] Department of Neurology, St. Elisabeth Hospital, P.O. Box 90151, NL-5000 LC Tilburg, The Netherlands.

Short Title: Dopaminergic degeneration by herbicides

Submitted for publication

Abstract

Recent research in a group of Parkinson's patients in an agricultural area of the Netherlands identified exposure to dinitrophenolic herbicides as common denominator. Dinitrophenolic compounds have a long history of use in agriculture and industry. Although agricultural workers experienced high exposure levels during the spraying season, long term effects of dinitrophenol exposure on human health are (still) largely unknown.

In this paper we describe the effects of two dinitrophenolic herbicides (DNOC and dinoseb) on parameters of dopaminergic neurodegeneration *in vitro*. Cell viability, mitochondrial activity, oxidative stress and caspase activation were assessed using fluorescence-based bioassays (CFDA, alamar Blue, H_2-DCFDA and Ac-DEVD-AMC, respectively), whereas changes in intracellular $[Ca^{2+}]_i$ were assessed using single-cell fluorescence microscopy with Fura-2AM. The results demonstrate that exposure to both DNOC and dinoseb is linked to modest cytotoxicity without overt oxidative stress as well as calcium release from the endoplasmic reticulum and activation of caspase-mediated apoptotic pathways. In subsequent experiments, immunofluorescent labelling with specific antibodies was used to determine changes in intracellular α-synuclein levels, demonstrating that both DNOC and dinoseb increase levels of intracellular α-synuclein. The combined results indicate that exposure to DNOC and dinoseb activates pathways implicated in Parkinson's disease and we therefore hypothesize that exposure to these dinitrophenolic herbicides can contribute to dopaminergic neurodegeneration.

Keywords

Dinitrophenolic herbicides; *in vitro* neurotoxicology; Endoplasmic Reticulum; single cell Fura-2 Ca^{2+}-imaging; Caspase-mediated apoptosis, α-Synuclein

Introduction

The dinitrophenolic compounds 4,6-dinitro-o-cresol (DNOC; CAS No. 534-52-1; Table 1) and 2-(1-methylpropyl)-4,6-dinitrophenol (dinoseb; CAS No. 88-85-7; Table 1) are derivatives of 2,4-dinitrophenol (2,4-DNP; CAS No. 51-28-7). Dinitrophenolics have a long history of use in polymer industry and in the manufacture of dyes and explosives. Human exposure to DNOC and dinoseb is mainly occupational due to the use as defoliating agents in potato culture, as herbicide targeting grass and broadleaf weeds and as insecticide in grape production (Whitacre and Ware 2004). These compounds are easily absorbed via various routes of exposure due to their lipophilicity (DNOC log K_{ow}: 2.56; dinoseb log K_{ow}: 3.56; Parker, *et al.* 1951). Despite a ban on the use of DNOC and dinoseb as pesticide in Europe in the late 1990's, both compounds have been found consistently in the environment (see e.g. Duyzer 2003, Quaghebeur, *et al.* 2004, Schummer, *et al.* 2009), which is at least partly due to their continuing use in (plastic) industry and their slow environmental degradation (Schummer, *et al.* 2009).

Table 1. Molecular structure and chemico-physical properties of DNOC and dinoseb.

	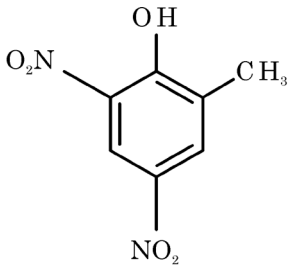	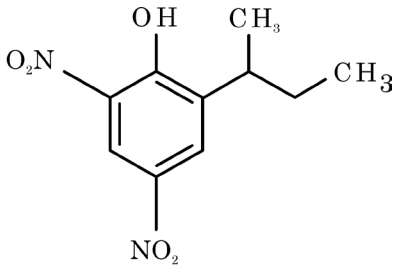
Chemical name:	2-Methyl-4,6-Dinitrophenol (DNOC)	2-(1-Methylpropyl)-4,6-Dinitrophenol (Dinoseb)
CAS number:	534-52-1	88-85-7
Mol. weight (g/mol):	198.1	240.2
Log K_{OW}:	2.56	3.56

Dinitrophenolic herbicides are powerful toxicants in plants, animals and humans with high acute toxicity, e.g. mammalian LD_{50} dinoseb: oral = 37, dermal = 200 mg/kg body weight (Puls 1988). Toxicity is thought to be related primarily to uncoupling of mitochondrial phosphorylation (uncoupling in mouse-brain mitochondrial preparation EC_{100}: DNOC 20 µM, dinoseb 0.5 µM; (Ilivicky and Casida 1969), leading to increased oxidative metabolism and depletion of cellular ATP, resulting in cell and tissue damage (Ilivicky and Casida 1969, Palmeira, *et al.* 1994). In patients with symptoms of acute poisoning, blood levels of DNOC and dinoseb are

typically over 200 μM. Blood levels up to 200 μM, as observed in applicators during the spraying season, typically occur symptom-less (Harvey, *et al.* 1951, van Noort, *et al.* 1960). The main reason for the build-up of such high internal dose in applicators is the (relatively) long half-life in humans (calculated $T_{1/2}$: 5-14 days), resulting in accumulation upon repeated exposure during the spraying season (Harvey, *et al.* 1951). *In vivo* experiments indicated that dinitrophenolic compounds cross biological membranes, such as the blood-brain and the placental barrier (Gibson and Rao 1973). However, data on human sub-lethal toxicity and long-term effects of (sub-chronic) exposure to dinitrophenolics are virtually absent.

Chronic exposure to environmental pollutants, in particular pesticides, has been linked to neurodegeneration and the development of Parkinson's disease (PD) in several epidemiologic studies (see e.g.Elbaz, *et al.* 2009, van der Mark, *et al.* 2011). PD is the most prevalent human neurodegenerative disorder after Alzheimer's disease, with a prevalence of more than 1% in people older than 65 years that is increasing with age (de Lau and Breteler 2006). Though mechanisms underlying pesticide-induced (dopaminergic) neurodegeneration are largely unknown, disturbance of mitochondrial phosphorylation, changes in the intracellular calcium concentration ($[Ca^{2+}]_i$), endoplasmic reticulum (ER) stress and increased production of reactive oxygen species (ROS) are recognized as inducers of tissue damage in dopaminergic brain areas (Bartels and Leenders 2009, Bezprozvanny 2009, Mattson 2007). Intracellular protein misfolding and aggregation contributes to the development of cytoplasmic inclusions, such as α-synuclein-containing Lewy bodies that are a common pathophysiological hallmark of PD (Marques and Outeiro 2012, Witt 2012).

The recent identification of a cluster of PD patients in a remote rural area in the Netherlands, both occupationally and non-occupationally involved in agriculture, pointed to pesticide exposure as common denominator (unpublished results). Interestingly, several of these patients reported (occupational) exposure to DNOC. Since dinitrophenolic herbicides are known to uncouple oxidative phosphorylation (Castilho, *et al.* 1997, Ilivicky and Casida 1969), the aim of the present study was to investigate the potential of DNOC and dinoseb to induce dopaminergic neurodegeneration *in vitro* and to reveal the mechanisms that could be underlying the development of PD in occupationally exposed agriculture workers.

Materials & Methods

Chemicals

Fura-2-AM, 5-carboxyfluorescein diacetate, acetoxymethyl ester (CFDA-AM) and 2,7-dichlorodihydrofluorescein diacetate (H_2-DCFDA) were obtained from Molecular Probes (Invitrogen, Breda, The Netherlands); DNOC and dinoseb were obtained Pestanal® grade, 99.8% purity (Riedel de Haën, Seelze, Germany); all other chemicals were obtained from Sigma (Zwijndrecht, The Netherlands), unless otherwise noted. Saline solutions, containing (in mM) 125 NaCl, 5.5 KCl, 2 $CaCl_2$, 0.8 $MgCl_2$, 10 HEPES, 24 glucose and 36.5 sucrose (pH 7.3), were prepared with de-ionized water (Milli-Q®; resistivity >18 MΩ•cm). Stock solutions of 2 mM ionomycin in DMSO were kept at 20°C. Stock solutions of 0.1-100 mM DNOC and dinoseb (Pestanal® grade, 99.8% purity, Riedel de Haën, Seelze, Germany) were prepared in DMSO and diluted in saline to obtain the desired concentrations just prior to the experiments (all solutions used in experiments, including control experiments, contained 0.1% DMSO).

Cell Culture

Experiments were performed in rat dopaminergic pheochromocytoma PC12 cells (Greene and Tischler 1976). This cell line has been characterized extensively for the study on parameters of intracellular calcium homeostasis and dopaminergic neurotransmission (Shafer and Atchison 1991, Westerink, *et al.* 2000) and provides therefore a suitable cell model to study pesticide-induced changes in calcium homeostasis and dopaminergic degeneration.

PC12 cells were grown for 10 passages in RPMI 1640 (Invitrogen, Breda, The Netherlands) supplemented with 5% fetal calf serum and 10% horse serum (ICN Biomedicals, Zoetermeer, The Netherlands) in a humidified incubator at 37°C and 5% CO_2 as described previously (Heusinkveld and Westerink 2012). For Ca^{2+} imaging experiments, cells were subcultured in poly-L-lysine coated glass-bottom dishes (MatTek, Ashland, MA, USA) as described previously (Heusinkveld and Westerink 2012). For cell viability and caspase experiments cells were sub-cultured in poly-L-lysine coated 24-wells plates (Greiner Bio-one, Solingen, Germany) at a density of $5x10^5$ cells/well. For experiments assessing oxidative stress (ROS), cells were seeded in poly-L-lysine coated 48-wells plates at a density of $2.5x10^5$ cells/well.

Absorbance spectra dinitrophenolics

To assess potential interference of DNOC and dinoseb with the excitation and emission wavelengths used in different fluorescence assays, absorbance spectra (300-600 nm) of increasing concentrations (0.1-100 μM) of DNOC and dinoseb have been measured spectrophotometrically (Infinite M200 microplate; Tecan Trading AG, Männedorf, Switzerland).

Mitochondrial activity and cell viability assay

The effects of DNOC and dinoseb on mitochondrial activity and cell viability were measured using a combined alamar Blue/CFDA-AM (aB/CFDA) assay as described earlier (Heusinkveld, *et al.* 2013), which is used to assess respectively mitochondrial activity and membrane integrity. Briefly, following exposure for 24 or 48h in phenol red- and serum-free medium, cells were incubated for 30 min with 12,5 µM and 4 µM CFDA-AM. Resorufin was measured spectrophotometrically at 540/590 nm (Infinite M200 microplate; Tecan Trading AG, Männedorf, Switzerland), whereas hydrolysed CFDA was measured spectrophotometrically at 493/541 nm.

ROS measurement using H_2-DCFDA

The involvement of oxidative stress in the observed reduction in cell viability was investigated using the fluorescent dye H_2-DCFDA as described earlier (Heusinkveld, *et al.* 2013). Briefly, cells were loaded with 1.5 µM H_2-DCFDA for 30 min at 37°C. Following exposure for up to 24 h to 0.1, 1, 10 or 100 µM DNOC or dinoseb, fluorescence was measured spectrophotometrically at 488/520 nm (Infinite M200 microplate; Tecan Trading AG, Männedorf, Switzerland). Rotenone (100 µM) was included as positive control for oxidative stress (Radad, *et al.* 2006).

Caspase activation assay

To investigate the role of apoptosis in the DNOC and dinoseb-induced reduction in cell viability, the effect of DNOC and dinoseb exposure (24 and 48h) on activation of the effector caspase-3 was determined using a fluorescent caspase-3 substrate (Ac-DEVD-AMC) according to the manufacturer's protocol. Fluorescence of cleaved caspase substrate was assessed spectrophotometrically at 360/460 nm (Infinite M200 microplate; Tecan Trading AG, Männedorf, Switzerland). Staurosporine (1 µM, 6h exposure) was included as a positive control. Fluorescence data was corrected for cell number using a fluorescamine-based assay (Udenfriend, *et al.* 1972) to quantify the protein content of the sample.

Intracellular Ca^{2+} imaging

Changes in cytosolic $[Ca^{2+}]_i$ upon exposure to DNOC (1-100 µM) and dinoseb (0.3-100 µM) were measured on a single-cell level using fluorescence microscopy in PC12 cells loaded with the Ca^{2+}-sensitive fluorescent ratio dye Fura-2 AM as described previously (Heusinkveld and Westerink 2012). Involvement of intracellularcalcium stores in effects on basal $[Ca^{2+}]_i$ was assessed using pharmacological manipulation with thapsigargin (1 µM; to empty the ER; see also: Dingemans, *et al.* 2010).

Immunofluorescence staining

To assess the effect of exposure to DNOC (1-100 µM) and dinoseb (0.3-30 µM) on intracellular α-synuclein aggregation, α-synuclein was labelled using specific fluorescent antibodies for subsequent analysis using confocal laser-scanning microscopy. Exposure concentrations were chosen based on the observed effects in calcium imaging, including for both compounds a concentration with no, intermediate and maximal Ca^{2+} influx observed. Briefly, cells were exposed for 24h or 48h and subsequently fixed (4% para-formaldehyde) and permeabilized (0.1% saponin). A-specific binding was blocked using bovine serum albumin (BSA). α-Synuclein was labelled using a polyclonal sheep-anti rat antibody (ab6162; 1:200; Abcam, Cambridge, UK). For fluorescent detection, a fluorochrome-conjugated secondary antibody was used (Alexa488 donkey-anti-sheep; 1:200; Invitrogen, Breda, The Netherlands). Immunostained coverslips were visualized using confocal laser-scanning microscopy (Leica DMI4000 equipped with TCS SPE-II), full preparation Z-stack images (0.5 µm) were analysed using LAS AF Lite software (version 2.6.0).

Data-analysis and statistics

Data on mitochondrial activity, cell viability and ROS production is presented as mean % ± standard error of the mean (SEM) of ≥ 3 independent experiments (N) with ≥ 4 wells (*n*) per experiment compared to (time-matched) controls. Data from single-cell fluorescence microscopy is presented as mean % increase of $[Ca^{2+}]_i$ over baseline (± SEM) from the number of individual cells (*n*) indicated, obtained from 4-9 independent experiments (N) (Heusinkveld and Westerink 2011). Data on intracellular α-synuclein levels from confocal images is quantified using ImageJ software v1.47C (Wayne Rasband, National Institutes of Health, USA) and presented as % α-synuclein compared to control. Data on caspase activation is presented as % increase in fluorescence (± SEM) compared to the time-matched control, corrected for protein level (≥ 3 independent experiments (N) with ≥ 4 wells (*n*) per experiment). Statistical analyses were performed using GraphPad Prism v6.04 (GraphPad Software, San Diego, California, USA). Continuous data were compared using One-way ANOVA with post-hoc Bonferroni test where applicable. A p-value ≤0.05 is considered statistically significant.

Results

Absorbance spectra dinitrophenolic herbicides

As high concentrations of DNOC or dinoseb results in an intense yellow colouration of the media and saline solutions, we investigated whether the presence of DNOC and dinoseb in the medium interfered with the yield in the different fluorescent assays. The results from the absorbance spectra demonstrate that increasing concentrations of DNOC and dinoseb (>10 µM) quench the wavelengths used in fluorescent calcium imaging (Fura-2: 340 and 380 nm) differently (for spectra see: Supporting Information). This is in line with recent findings of Hutanu and co-workers (Hutanu, *et al.* 2013), who demonstrated quenching of fluorescence by various dinitrophenolic compounds. As this could lead to misinterpretation of $[Ca^{2+}]_i$ data through an artefact in the calculation of F340/F380 ratios, results from the fluorescent calcium imaging are presented for concentrations ≤ 30 µM. The other assays, using (single) wavelengths >480 nm, are not subject to absorbance-induced artefacts. In those assays therefore, concentrations up to 100 µM are presented.

Effects of dinitrophenolic herbicides on cell viability and ROS production

To investigate the effects of DNOC and dinoseb on mitochondrial activity, cell viability and ROS production, dopaminergic PC12 cells were exposed to different concentrations DNOC and dinoseb (0.1-100 µM) for up to 24h (Fig 1A-B). The results from the alamar Blue assay demonstrate that exposure to 10 µM DNOC for 24h induced a significant increase in mitochondrial activity amounting to 131 ± 8% (N = 4; $p \leq 0.001$; Fig. 1A1). However, upon exposure to 100 µM DNOC mitochondrial activity decreased to 89 ± 5% (N = 4; $p \leq 0.001$; Fig. 1A1), indicative for cell death at this high concentration. This is confirmed by the results from the CFDA assay that demonstrate a concentration-dependent decrease of the fraction intact cells following 24h exposure to 10 or 100 µM DNOC, which reduced membrane integrity to 84 ± 5% (N = 3, $p \leq 0.001$; Fig 1A2) and 72 ± 2% (N = 3, $p \leq 0.001$; Fig 1A2), respectively.

Exposure for 24h to dinoseb already increased mitochondrial activity at 0.1 and 1 µM (Fig 1A1), amounting to 114 ± 10% (N = 4; $p \leq 0.01$) and 127 ± 4% (N = 4; $p < 0.01$), respectively. Upon exposure to 10 or 100 µM dinoseb, a decrease in mitochondrial activity was observed, amounting to respectively 89 ± 6% (N = 4; Fig 1A1) and 70 ± 7% (N = 4; $p \leq 0.001$; Fig 1A), indicative for cell death at these higher concentrations. In line with these findings, the results from the CFDA assay demonstrate that 24h exposure to 10 µM dinoseb reduced membrane integrity to 80 ± 3% (N = 3; $p < 0.001$; Fig. 1A2). Membrane integrity decreased further to 70 ± 7% (N = 3; $p < 0.001$; Fig. 1A2) upon exposure to 100 µM dinoseb.

Since increased ROS production is a well-known cause for decreased cell viability (Franco, *et al.* 2009), effects of exposure to DNOC and dinoseb for up to

24h on ROS production were assessed in PC12 cells loaded with the fluorescent H_2-DCFDA dye. The results demonstrate that exposure to DNOC (10-100 μM) did not increase ROS production compared to controls, whereas exposure to dinoseb produces a small increase in ROS production compared to control although only at the highest concentration dinoseb tested (100 μM) and only after 24h exposure (132 ± 7%; $p \leq 0.001$; N = 3; Fig 1B).

The combined results demonstrate that both DNOC and dinoseb concentration-dependently alter mitochondrial activity and cell viability in dopaminergic PC12 cells and that these effects appear not related to increased production of ROS.

Dinitrophenolic herbicides activate caspase-mediated apoptosis

Since the effects of DNOC and dinoseb on cell viability are apparently not related to production of ROS, we assessed whether exposure to these dinitrophenolic compounds induced caspase-3 activity following 24 (Fig. 1C) and 48h (see: Supplemental data Fig S2) exposure using the fluorescent caspase-3 substrate (Ac-DEVD-AMC). Staurosporine exposure (1 μM, 6h exposure) served as positive control and increased caspase-3 activity to 478 ± 93% (N = 9; $p<0.001$; Fig. 1C). The results indicate a significantly increased caspase-3 activity following 24h exposure to DNOC (100 μM) and dinoseb (10 μM) amounting to 190 ± 31% (N = 8; $p<0.001$; Fig. 1C) and 316 ± 87% (N = 3; $p<0.001$; Fig 1C), respectively. No further increase was observed upon exposure to 100 μM (358 ± 51% (N = 7; $p<0.001$; Fig 1C). Interestingly, increasing the exposure duration to 48h lowered the LOEC for both DNOC and dinoseb to 10 and 1 μM, respectively (see: Supplemental data Fig S2).

These data indicate that exposure to DNOC and dinoseb at low micromolar concentrations increased caspase-3 activity, which may underlie the observed effects on cell viability.

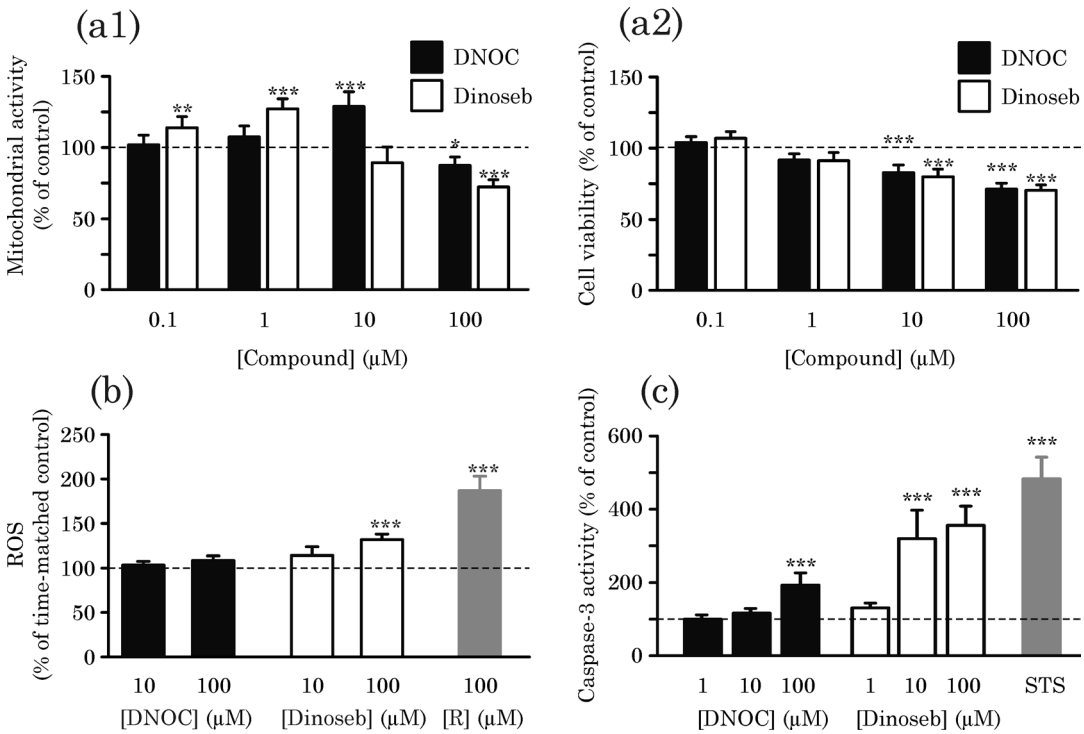

Fig. 1. DNOC (black bars) and dinoseb (white bars) concentration-dependently change parameters of cell viability, oxidative stress and apoptosis in PC12 cells upon exposure for 24h. A1 Bargraph displaying the DNOC and dinoseb-induced upregulation of mitochondrial activity (≥10 µM and ≥0.1 µM respectively). A2 Bargraph displaying the DNOC and dinoseb-induced decrease in membrane integrity (both ≥10 µM). Difference from control: ** $p \leq 0.01$, *** $p \leq 0.001$. B Bargraph displaying the results from the H_2-DCFDA oxidative stress assay in PC12 cells following 24h exposure to 10 or 100 µM DNOC or dinoseb. Only exposure to dinoseb (100 µM) is related to a modest increase in oxidative stress. Rotenone (R; 100 µM) was included as positive control. Difference from control: *** $p \leq 0.001$. C DNOC and dinoseb concentration-dependently induce caspase-3 activity. Bars display average data (± SEM) from ≥ 3 independent experiments. Staurosporine (STS; 1 µM, 6h) was included as positive control. Difference from control (dashed line) *** $p \leq 0.001$.

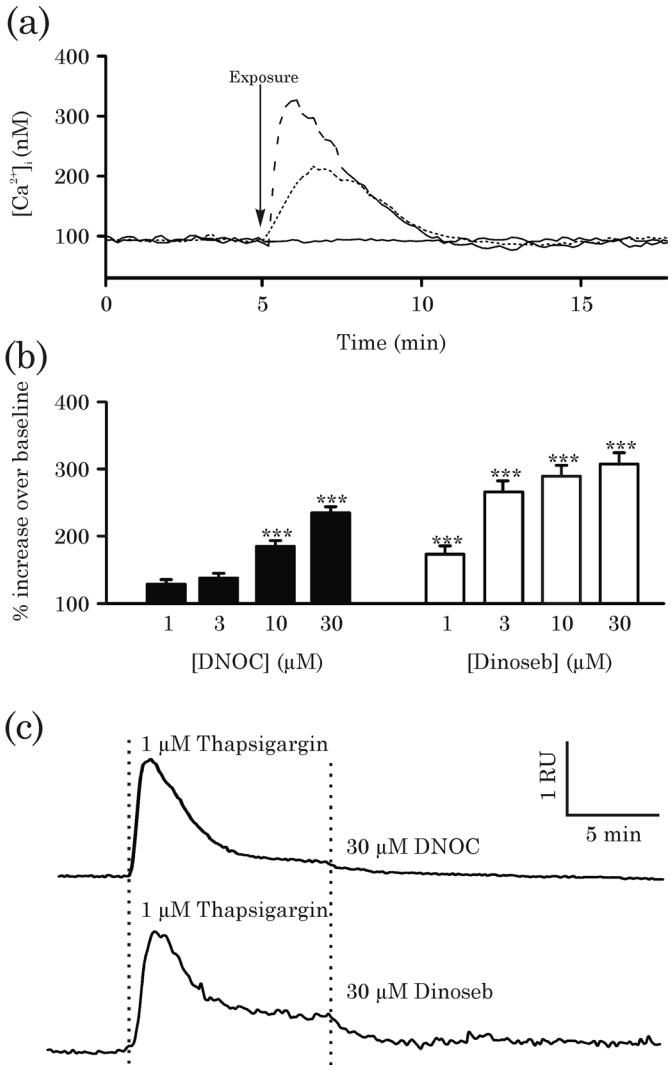

Fig. 2. Both DNOC and dinoseb concentration-dependently increase basal $[Ca^{2+}]_i$. A Example traces of basal $[Ca^{2+}]_i$ upon exposure to DMSO (solid line) 30 μM DNOC (dotted line) and 30 μM dinoseb (dashed line). B Bargraph displaying the concentration-response curve of DNOC and dinoseb. Bars display average data (± SEM) from at least 28 - 80 individual cells (4 - 9 experiments per concentration). C Example traces of basal $[Ca^{2+}]_i$ upon exposure to DNOC (30 μM) or dinoseb (30 μM) following thapsigargin (1 μM) pre-treatment under Ca^{2+}-free conditions. It can be seen that thapsigargin pretreatment completely abolishes the DNOC and dinoseb-induced increase in $[Ca^{2+}]_i$. Difference from control *** $p \leq 0.001$).

Dinitrophenolic herbicides disturb $[Ca^{2+}]_i$ via store-mediated release of Ca^{2+}

Since activation of caspase-mediated apoptotic pathways is calcium-dependent (Orrenius, *et al.* 2011), we investigated whether the effects of DNOC and dinoseb on activation of caspase-mediated apoptosis and cell viability are caused by disruption of Ca^{2+} homeostasis. We therefore measured $[Ca^{2+}]_i$ using single-cell fluorescence microscopy in Fura-2-loaded PC12 cells. In control cells (n = 85), basal $[Ca^{2+}]_i$ was low (97 ± 2 nM) with only minor fluctuations, whereas depolarization with high-K^+-containing saline evoked a strong transient increase in $[Ca^{2+}]_i$ amounting up to 2.0 ± 0.1 µM (n = 85).

Cells acutely (20 min) exposed to DNOC or dinoseb for up to 100 µM did not show changes in depolarization-evoked $[Ca^{2+}]_i$ (data not shown).

However, both DNOC and dinoseb induced an increase in basal $[Ca^{2+}]_i$ (Fig. 2A). Exposure of cells to 1 or 3 µM DNOC did not result in a significant increase in basal $[Ca^{2+}]_i$ compared to control cells. However, cells exposed to 10 µM DNOC induced a significant transient increase of basal $[Ca^{2+}]_i$ with an amplitude amounting to 157 ± 7% (n = 79, $p \leq 0.001$; Fig 2B). This increase was larger following exposure to 30 µM DNOC (199 ± 7%, n = 108; $p \leq 0.001$; Fig 2B).

Similarly, cells exposed to 0.3 µM dinoseb did not show a significant alteration of the basal $[Ca^{2+}]_i$ (data not shown). However, cells exposed to 1 µM dinoseb showed a significant transient increase of basal $[Ca^{2+}]_i$ with an amplitude amounting to 175 ± 11% (n = 62; $p \leq 0.001$; Fig 2B). This increase was larger following exposure to 3 µM dinoseb (277 ± 15%, n = 62, $p \leq 0.001$; Fig 2B) and apparently already maximal as exposure to 10 or 30 µM did not result in a further increase of basal $[Ca^{2+}]_i$ (287 ± 16%, n = 57 and 316 ± 17%, n = 67 respectively; Fig 2B).

Additional experiments were performed to identify the origin of the observed increase in $[Ca^{2+}]_i$. The increase in $[Ca^{2+}]_i$ is still observed when cells were exposed to DNOC or dinoseb under Ca^{2+}-free conditions, thus indicating that the increase originates from intracellular organelles. To assess whether Ca^{2+} release from the endoplasmic reticulum (ER) plays a role, the ER was emptied under Ca^{2+}-free conditions using 1 µM thapsigargin and cells were subsequently challenged with DNOC or dinoseb. As the thapsigargin treatment abolished both DNOC and dinoseb-induced increases in $[Ca^{2+}]_i$, the results demonstrate that the increase in $[Ca^{2+}]_i$ originates from the ER (Fig 2C).

Dinitrophenolic herbicides induce α-synuclein aggregation

ER-related changes in $[Ca^{2+}]_i$ and caspase-activation are linked to neuro degeneration (Mattson 2012, Nath, *et al.* 2011). A clear hallmark of dopaminergic degeneration is an increase in α-synuclein and eventually the occurrence of α-synuclein-containing cytoplasmic aggregates (Breydo, *et al.* 2012). We therefore investigated α-synuclein expression in cells exposed to DNOC (1-100 µM) and dinoseb (0.3-30 µM). Cells were exposed for 24 or 48h and subsequently intracellular

α-synuclein was labelled using specific antibodies. Confocal microscopy images of cells exposed to the solvent control (DMSO; Fig. 3A1-2) show a weak α-synuclein stain. Quantification of the α-synuclein fluorescence revealed no significant increase in intracellular α-synuclein upon 24h exposure (data not shown). However, cells exposed to DNOC (Fig 3B1-2) and dinoseb (Fig 3C1-2) for 48h revealed a more intense α-synuclein stain and the presence of small intracellular α-synuclein aggregates. Quantification of the α-synuclein fluorescence revealed a concentration-dependent increase in intracellular α-synuclein upon 48h exposure to DNOC (LOEC: 1 μM) and dinoseb (LOEC: 0.3 μM), amounting to a maximum of 203 ± 5% (100 μM; n = 10, $p \leq 0.001$; Fig 3D) and 183 ± 5% (30 μM; n = 28, $p \leq 0.001$; Fig 3D), respectively.

These results thus demonstrate that exposure to DNOC or dinoseb induced an increase in the intracellular level of an important protein marker associated with Parkinsonian dopaminergic neurodegeneration.

Figure 3. Exposure of PC12 to DNOC and dinoseb for 48h dose-dependently increases intracellular α-synuclein levels. a-c. Example 1-stack confocal fluorescence micrographs showing α-synuclein immunostaining (green) and DAPI nuclear stain (blue) upon exposure to DMSO (a1, detail: a2), 100 μM DNOC (b1, detail: b2) and 30 μM dinoseb (c1, detail: c2). d. Bars display quantified fluorescence data from 10 - 52 individual cells stained on at least 2 independent coverslips. Difference from control: *** $p \leq 0.001$.

Fig.3. (*next page*) Exposure of PC12 to DNOC and dinoseb for 48h dose-dependently increases intracellular α-synuclein levels. a-c. Example 1-stack confocal fluorescence micrographs showing α-synuclein immunostaining (green) and DAPI nuclear stain (blue) upon exposure to DMSO (a1, detail: a2), 100 μM DNOC (b1, detail: b2) and 30 μM dinoseb (c1, detail: c2). d. Bars display quantified fluorescence data from 10 - 52 individual cells stained on at least 2 independent coverslips. Difference from control: *** $p \leq 0.001$.

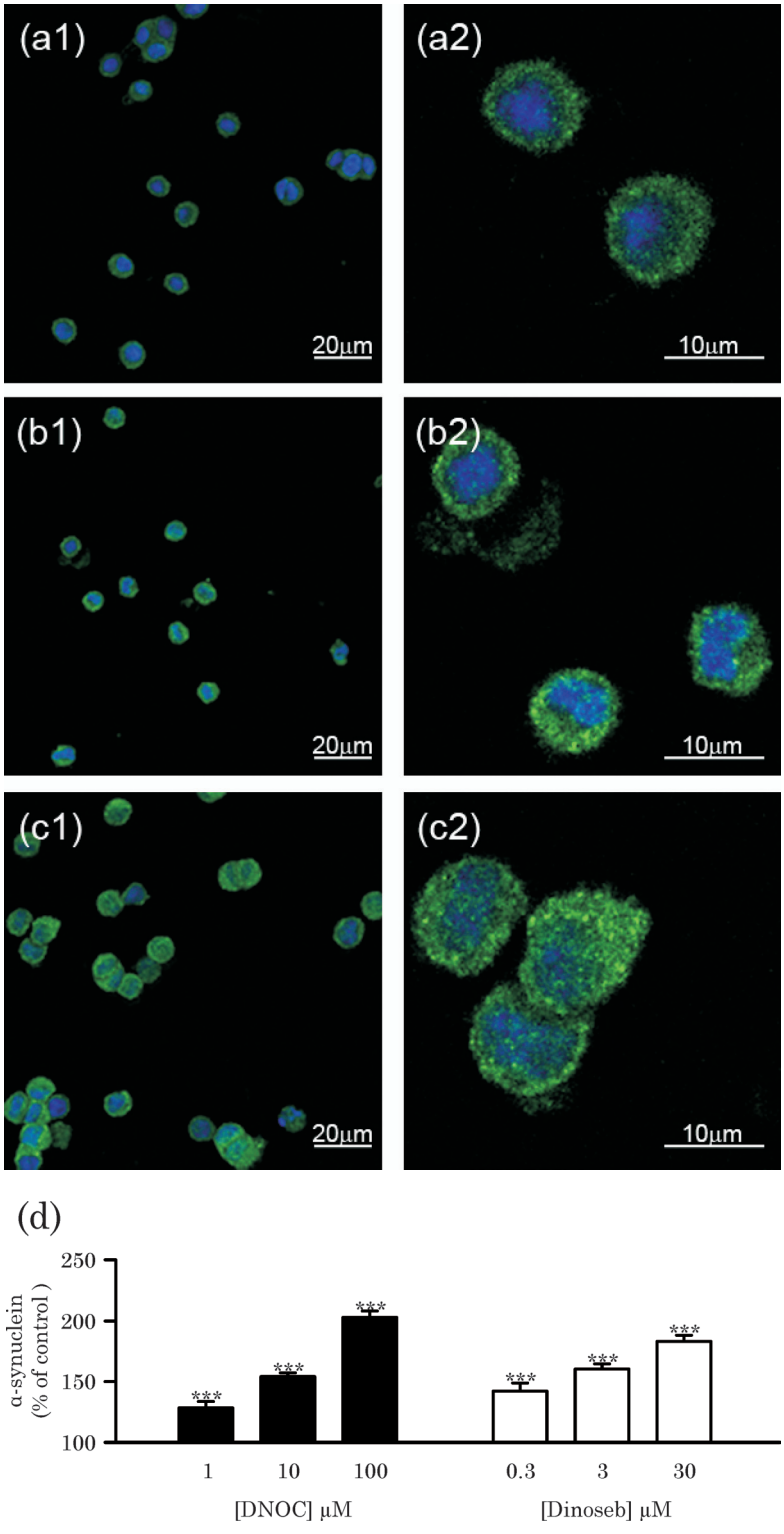
(a1)
20µm
(a2)
10µm
(b1)
20µm
(b2)
10µm
(c1)
20µm
(c2)
10µm
(d)
α-synuclein (% of control)
250
200
150
100
***
***
***
***
***
***
1
10
100
0.3
3
30
[DNOC] µM
[Dinoseb] µM

Discussion

The present results demonstrate that the dinitrophenolic herbicides DNOC and dinoseb induce an up-regulation of mitochondrial activity (Fig 1A1), activation of caspase-mediated apoptosis (Fig. 1C; LOEC DNOC 24h: 100 µM; LOEC dinoseb 24h: 10 µM) and a mild reduction in cell viability (Fig. 1A2) in dopaminergic PC12 cells. This is likely related to the observed acute and transient increase in basal $[Ca^{2+}]_i$ (LOEC DNOC: 10 µM; LOEC dinoseb: 1 µM), which originates from the ER (Fig. 2). In addition, cells surviving exposure to DNOC (≥1 µM) or dinoseb (≥0.3 µM) display an increase in intracellular α-synuclein levels (Fig. 3). Since the observed increase in ROS production is limited to the highest concentration of dinoseb tested (Fig. 1B) at which cytotoxicity is already evident (Fig 1A2), the increase in oxidative stress appears not be a causal factor for the observed effects on cell viability in PC12 cells.

Dinitrophenolic herbicides are primarily known to function as mitochondrial uncouplers via their protonophoric properties disturbing the proton gradient across the mitochondrial membrane (Ilivicky and Casida 1969, Judah 1951). This leads to an increase in mitochondrial activity to restore the proton gradient and upon a sufficiently high level of exposure this will result in a concentration-dependent deficiency in ATP production related to cell damage. It is therefore likely that uncoupling of oxidative phosphorylation is to some extent reflected in the increase in mitochondrial activity observed upon exposure to DNOC and dinoseb (Fig 1A1). Mitochondrial uncoupling occurs at exposures of the same order of magnitude as the observed effect concentrations for Ca^{2+} release (minimum uncoupling concentration in mouse-brain mitochondrial preparation DNOC 20 µM, dinoseb 0.5 µM; Ilivicky and Casida 1969). As ER-mediated apoptotic cascades will ultimately also involve mitochondria (for review see: Circu and Aw 2012), it remains to be determined what the effect of the compound-induced uncoupling is on the observed activation of apoptotic pathways. Nevertheless, the results from the single-cell fluorescence microscopy experiments demonstrate that $[Ca^{2+}]_i$ increases instantly due to release of Ca^{2+} from the ER upon exposure to DNOC or dinoseb. Ca^{2+} release from intracellular stores and from the ER in particular is well known for its ability to induce caspase-mediated apoptotic cascades (Orrenius, *et al.* 2011). Yet, cytotoxicity after 24h exposure is limited and no significant further decrease in cell viability occurs when exposure is prolonged from 24 to 48h (data not shown). However, upon 48h exposure to DNOC and dinoseb a left shift in caspase activation is observed revealing a lowering of the LOEC with one order of magnitude (Supporting Information Fig. S2; LOEC DNOC 48h: 10 µM; LOEC dinoseb 48h: 1 µM), which may be related to continued mitochondrial uncoupling or bioaccumulation of the dinitrophenolic herbicides.

The observed reduction in caspase activity in cells exposed for 48h to 100 µM DNOC as well as 10 and 100 µM dinoseb compared to 24h exposure (compare Fig 1C and Fig S2) is likely due to degradation of caspase following completion of apoptosis. Furthermore, the occurrence of calcium-related ER stress, is linked to changes in intracellular α-synuclein levels ultimately leading to formation of protein aggregates (Jiang, *et al.* 2010, Marques and Outeiro 2012, Mattson 2012). In line with this, the results from the immune-staining for α-synuclein reveal an increase in intracellular α-synuclein levels following 48h exposure to DNOC and dinoseb (Fig 3A-C). Remarkably, the increase in α-synuclein is not observed after 24h exposure but occur only after 48h exposure. However, this increase is observed already at exposure levels below the observed effect concentration for increases in basal $[Ca^{2+}]_i$. This is probably related to the fact that both mitochondria and the ER are targeted and that terminal intracellular changes, such as accumulation of α-synuclein, develop slowly as a function of continuing disturbance of function of both organelles. Also, despite the high level of detail, temporal and spatial resolution in the applied fluorescence microscopy may not be sufficient to determine small and fast oscillations in $[Ca^{2+}]_i$ or highly localized Ca^{2+} waves related to store-mediated signaling pathways (Eilers, *et al.* 1995).

In humans, a study with healthy volunteers given 5 -7 daily oral dosages of 75 mg (0.92 - 1.27 mg/kg) revealed that DNOC blood concentrations up to 100 µM occur without symptoms of acute poisoning, whereas severe symptoms of acute poisoning will develop at (blood) concentrations above 200 µM (Harvey, *et al.* 1951).

According to animal studies, DNOC and dinoseb spread quickly through all tissues in the animal, and easily pass biological membranes such as the blood-brain (Parker, *et al.* 1951) and placental barrier (Gibson and Rao 1973, Parker, *et al.* 1951). Detection of high concentrations of DNOC in cerebrospinal fluid of human poisoning victims indicate that the same is true in humans (Bidstrup and Payne 1951, Jiang Jiukun, *et al.* 2011). A single subcutaneous dose of 1.5 mg (corr. with approx 3 - 4 mg/kg) in rats resulted in a blood DNOC concentration of 100 µg/ml serum (approx. 270 µM whole blood) and brain concentration of 4 µg/g w.w. (corresponding with approx. 20 µM) without being lethal (Gibson and Rao 1973). Although animal studies have shown that systemic clearance of DNOC is rapid in rodents, cats and dogs without signs of accumulation of DNOC in the body ($T_{1/2}$: 24 - 72h; Parker, *et al.* 1951), in humans, DNOC appears remarkably persistent. Harvey and co-workers (Harvey, *et al.* 1951) demonstrated that in healthy human volunteers after 5 daily doses of 75 mg DNOC (0.92 - 1.27 mg/kg; peak blood concentration of ~100 µM), the compound was still measurable in reasonable amounts (1 - 1.5 µg/g blood ≈ 5 - 8 µM; calculated using average physiological values) after 40 days. This is confirmed by a study from the Netherlands, demonstrating that upon chronic exposure (agricultural workers;

1 month with daily exposure) blood DNOC levels rose to 11 - 88 µg/ml serum (corresponding with 30 - 240 µM; calculated using average physiological values), depending on the level of personal protection (van Noort, *et al.* 1960). Despite differences in clearance between species, the lethal blood concentration DNOC was in all cases ~125 µg/ml (corresponding with a concentration of ~630 µM; calculated using average physiological parameters). Human data on dinoseb exposure and blood levels is not available. However, based on the similarities in the use pattern and the physicochemical properties with a higher lipophilicity of dinoseb compared to DNOC, it can be anticipated that internal dose levels of dinoseb are at least equal, but likely even higher.

In conclusion, we demonstrated that *in vitro* exposure of dopaminergic cells to both DNOC and dinoseb results in ER-stress, which is followed by activation of apoptotic pathways and loss of cell viability as well as up-regulation of α-synuclein in surviving cells. Exposure of dopaminergic cells to concentrations of dinitrophenolic herbicides that are relevant to the human situation can thus lead to activation of pathways that are considered as part of the pathophysiological cascade ultimately leading to human Parkinson's disease. Although these findings need to be confirmed in animals or even human tissue, we hypothesize that historical exposure to dinitrophenolic herbicides may have contributed to the development of Parkinsonian neurodegeneration in agricultural workers.

Supplementary Data description

The supplementary data provided presents absorbance spectra for dinitrophenolic herbicides as well as data on caspase activation following prolonged (48h) exposure to the test compounds.

Acknowledgements/Disclaimers

We are grateful to Rob Bleumink, Marianne Bol, Aart de Groot and Gina van Kleef for expert technical assistance. This work was funded by a grant from the Dutch "International Parkinson Fonds" (PAGES), by the European Union-funded project ACROPOLIS (Grant Agreement KBBE-245163) and by the Faculty of Veterinary Medicine (Utrecht University). The authors declare they have no competing financial interests.

Supplementary Data

Absorbance spectra dinitrophenolic herbicides

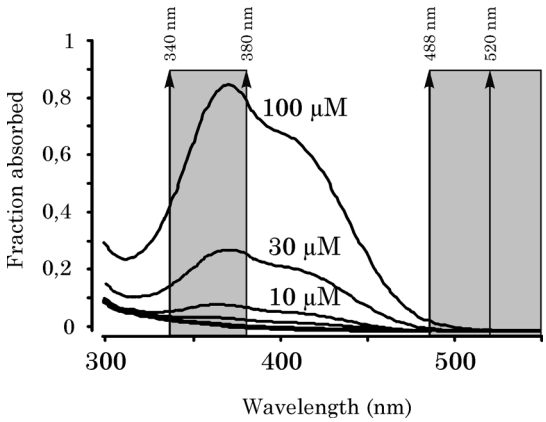

Fig. 1: Absorbance spectra for different concentrations DNOC. It can be seen that absorption could affect the results at the excitation wavelengths of Fura-2 (340 & 380 nm; fluorescent Ca^{2+} assay), whereas excitation wavelengths used with other assays (>488 nm) appear unbiased.

Dinitrophenolic herbicides activate caspase-mediated apoptosis

To assess whether the observed Ca^{2+} release from the ER is related to activation of caspase-mediated apoptotic pathways (Orrenius, *et al.* 2011), induction of Caspase-3 activity was measured after 48h. Staurosporine exposure (1 µM, 6h exposure) served as positive control, amounting to 478 ± 278% (N = 9; $p<0.001$). The results indicate significantly increased caspase-3 activity after 48h exposure to DNOC (10 µM) and dinoseb (1 µM) amounting to 142 ± 8% (N = 3; $p<0.001$; Fig. S2) and 149 ± 11% (N = 3; $p<0.001$; Fig 4), respectively.

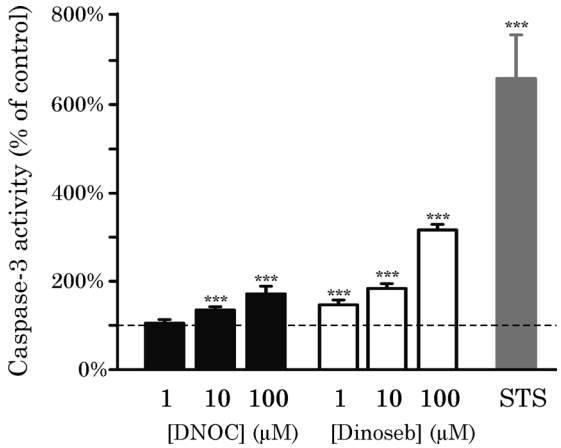

Fig. 2: DNOC and dinoseb concentration-dependently induce caspase-3 activity after 48h of exposure. Bars display average data (± SEM) from ≥ 3 independent experiments. Staurosporine (STS; 1 µM, 6h) was included as positive control. Difference from control (dashed line) *** $p\leq0.001$.

Chapter 6.2

Differential modulation of human $GABA_A$ receptors by dinitrophenolic herbicides

Harm J Heusinkveld[1], Regina GDM van Kleef[1], Peter CG Nijssen[2]
Remco HS Westerink[1]

[1] Neurotoxicology Research Group, Division of Toxicology, Institute for Risk Assessment Sciences (IRAS), Faculty of Veterinary Medicine, Utrecht University, P.O. Box 80.177, NL-3508 TD Utrecht, The Netherlands.
[2] Department of Neurology, St. Elisabeth Hospital, P.O. Box 90151, NL-5000 LC Tilburg, The Netherlands.

Submitted for publication

Abstract

Dinitrophenolic compounds have a long history of use in agriculture and industry. Additionally, some of these compounds have been used as weight loss drugs and are still readily available via the internet. Repeated exposure to dinitrophenolic compounds results in high internal levels due to their long half-life in humans. No signs of poisoning are observed with serum levels up to 200 μM, whereas serum levels ~600 μM are lethal. Upon acute poisoning, central nervous system effects such as anxiety, hyperpyrexia and lethargy may occur, though prolonged exposure can result in peripheral neuropathy. The clinical signs are usually ascribed to the primary mode of toxicity of dinitrophenolic compounds, i.e. uncoupling of mitochondrial phosphorylation, but more specific neurotoxic effects on the (central) nervous system are likely to be involved.

GABA is the main inhibitory neurotransmitter in the adult mammalian brain and is essential for a myriad of processes, including learning and memory, motor coordination, and thermoregulation. Considering the importance of GABA in the mammalian brain, we investigated the effect of four different dinitrophenolic herbicides as single compound and as binary mixtures on GABA-mediated ion currents using two-electrode voltage clamp in Xenopus Laevis oocytes expressing the human α1β2γ2 $GABA_A$ receptor. The results demonstrate that dinitrophenolic herbicides differentially affect GABA-evoked ion currents, likely via binding with varying potency to modulatory binding sites on the $GABA_A$ receptor. Moreover, the results from exposure to different binary mixtures demonstrate that the inhibitory effects at the $GABA_A$ receptor are not additive. Collectively, the results provide a novel mode of action that may be implicated in the observed neurological and neuro-psychological effects observed upon acute poisoning with dinitrophenolic herbicides.

Key words

Mixture toxicology, Postsynaptic human α1β2γ2 $GABA_A$ receptor, DNOC, dinoseb, DNP, dinoterb.

Introduction

DNOC (4,6-Dinitro-o-cresol; CAS No. 534-52-1), dinoseb (2-(1-methylpropyl)-4,6-dinitrophenol; CAS No. 88-85-7) and dinoterb (2-tert-butyl-4,6-dinitrophenol; 1420-07-1) are derivatives of 2,4-Dinitrophenol (2,4-Dinitrophenol, DNP; CAS No. 51-28-7) (Table 1). DNOC, dinoseb and dinoterb have until recently been used as broad-spectrum herbicides and insecticides (Gupta 2007), whereas DNP and DNOC also have a long history of use in the manufacture of explosives, dyes and polymers. Moreover, the continued use of dinitrophenolics in dye and polymer industry gives rise to environmental (Capel, *et al.* 1988, Pelfréne 2000, Schummer, *et al.* 2009) and occupational (accidental) exposure (Jiang Jiukun, *et al.* 2011). Additionally, DNP has a (continuing) history of use as an effective, though highly dangerous, weight-loss drug in bodybuilding (Colman 2007, Grundlingh, *et al.* 2011). Despite the danger, DNP is still readily available via the internet (Siegmueller and Narasimhaiah 2010).

In contrast to many other species, humans do not readily excrete dinitrophenolic compounds (calculated $T_{1/2}$: 5 - 14 days; Harvey, *et al.* 1951), which has resulted in high internal concentrations (high micromolar serum levels) in pesticide applicators that were repeatedly exposed during the spraying season (Heuts 1993, van Noort, *et al.* 1960). The neurological and neuropsychological symptoms of acute poisoning with dinitrophenolic herbicides, such as anxiety, lethargy, hyperpyrexia and peripheral neuropathy, are attributed to uncoupling of mitochondrial phosphorylation (mouse liver mitochondria EC_{100} 1 - 50 µM; Ilivicky and Casida 1969, Leftwich, *et al.* 1982, Tewari, *et al.* 2009). However, as these symptoms are clearly related to central nervous system (CNS) function, the aim of the present study was to study the effects of DNP, DNOC, dinoseb and dinoterb on human $GABA_A$ receptors, which are the major inhibitory neurotransmitter receptors in the human nervous system.

The GABA-ergic system is of critical importance in neurodevelopment and GABA functions as principal inhibitory input in the adult CNS in many processes, including memory and learning, motor functioning and body core-temperature control (Clapham 2012, Möhler 2007). The most common subunit composition of the pentameric $GABA_A$ receptor in the adult human CNS is α1ß2γ2. This receptor contains two specific binding sites (bridging α en ß subunits) for its natural agonist GABA. Upon binding of GABA to the receptor, the ion-channel opens resulting in a Cl^- current across the membrane that causes a hyperpolarization of the membrane (Möhler 2007). Besides the GABA binding sites, several other modulatory binding sites exist such as the ethanol-, benzodiazepine- and barbiturate binding sites, which upon binding result in either a potentiation or an inhibition of the GABA-evoked Cl^- current (for review see: Möhler 2007). Considering the

Table 1. Chemical Physical properties of 2,4-DNP, DNOC, dinoterb and dinoseb

	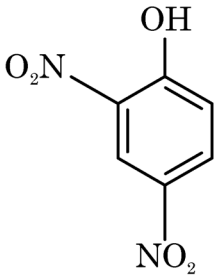	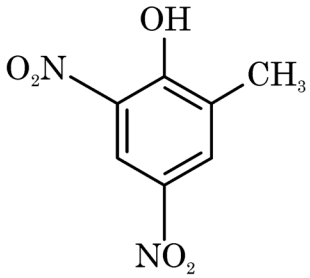
Chemical name:	2,4-Dinitrophenol (2,4-DNP, DNP)	2-Methyl-4,6-Dinitrophenol (DNOC)
CAS number:	51-28-5	534-52-1
Mol. weight (g/mol):	184.1	198.1
Log K_{OW}:	1.67	2.56

	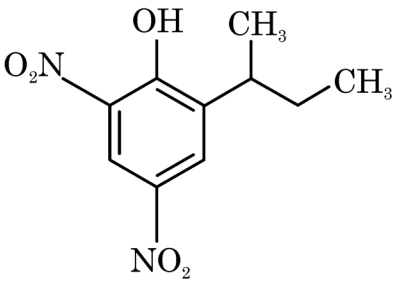	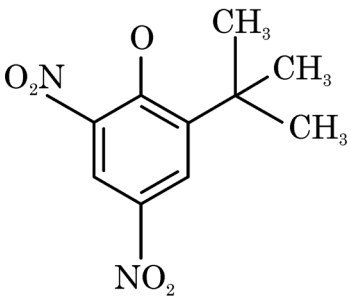
Chemical name:	2-(1-Methylpropyl)-4,6-Dinitrophenol (Dinoseb)	2-tert-butyl-4,6-Dinitrophenol (Dinoterb)
CAS number:	88-85-7	1420-07-1
Mol. weight (g/mol):	240.2	240.2
Log K_{OW}:	3.56	3.64

relevance of GABA-ergic neurotransmission for CNS function, studying the effect of chemical-induced receptor modulation is of particular relevance and will contribute to a more complete human risk assessment of dinitrophenolic compounds.

Materials and Methods

Animals

Xenopus Laevis oocytes were used to study the effects of dinitrophenolic herbicideson $GABA_A$-R function. Upon injection of oocytes with complementary DNA (cDNA), cDNA is efficiently translated into protein and neurophysiological studies have demonstrated that the expressed proteins are functional and transported to their physiological location (Brown 2004). This widely used model thus enables direct measurement of receptor function, rendering the *X. Laevis* oocyte the most appropriate model for this research.

Adult female *X. Laevis* frogs (provided by Dr. Wim Scheenen, Radboud University, Nijmegen, The Netherlands) were kept in standard aquaria (0.5 m x 0.4 m x 1m; 1 - 10/aquarium) with copper-free water (pH 6.5, 21 - 23°C) and a 12 h light/dark cycle.

Animals were fed earthworms three times a week (Hagens, Nijkerkerveen, The Netherlands). All procedures have been described previously (Antunes Fernandes, *et al.* 2010, Hondebrink, *et al.* 2013) and were conducted in accordance with Dutch law and approved by the Ethical Committee for Animal Experiments of Utrecht University.

Chemicals

All chemicals, unless otherwise noted, were obtained from Sigma-Aldrich (Zwijndrecht, The Netherlands). 2,4-dinitrophenol, DNOC, dinoseb and dinoterb (Pestanal® analytical grade) were dissolved in DMSO and stored at 4°C.

Expression of α1β2γ2 $GABA_A$ receptors in Xenopus Laevis oocytes

Adult female *Xenopus laevis* were anesthetized by submersion in 0.1% MS-222, and ovarian lobes were removed surgically. To de-folliculate, oocytes were incubated for 90 min (RT) with collagenase type I (1.5 mg/ml; Ca^{2+}-free Barth's solution).

cDNA coding for the human α1, ß2, and γ2 subunits of human $GABA_A$ receptors (Origene Rockville, MD) was dissolved in distilled water (1:1:1 molar ratio) and injected(23 nl/oocyte, ~1 ng of each subunit) into the nuclei of oocytes (stage V / VI) using a Nanoject Automatic Oocyte Injector (Drummond, Broomall, PA). Sham-injected oocytes were injected with 23 nl distilled water, i.e., without cDNA. Following injection with cDNA or distilled water, oocytes were incubated at 21°C in modified Barth's solution containing (in mM) 88 NaCl, 1 KCl, 2.4 $NaHCO_3$ 0.3 $Ca(NO_3)_2$, 0.41 $CaCl_2$, 0.82 $MgSO_4$, 15 HEPES, and 10 µg/ml neomycin (pH 7.6 with NaOH).

Electrophysiological recordings

Electrophysiological experiments were performed on oocytes after 4 - 6 days of incubation to ensure translation of injected cDNA and functional expression of α1β2γ2 $GABA_A$ receptors in the membrane. Ion currents associated with $GABA_A$ receptor activity were measured with the two-electrode voltage-clamp technique using a Gene Clamp 500B amplifier (Axon Instruments, Union City, CA) with high-voltage output stage as described previously (Antunes Fernandes, *et al.* 2010, Hondebrink, *et al.* 2013). Recording microelectrodes (0.5 - 2.5 MΩ) were filled with KCl (3 M). Oocytes, placed in a custom-built Teflon oocyte recording chamber, were voltage-clamped at -60 mV and continuously superfused (~30 ml/min) with saline. Membrane currents were low-pass filtered (8-pole Bessel; 3 dB at 0.3 kHz), digitized (12 bits; 1024 samples per record), and stored on disk for computer analysis. Aliquots of freshly thawed stock solutions of GABA in distilled water and dinitrophenolic herbicides in DMSO were added to the saline immediately before the experiments. Oocytes were exposed by switching the perfusate from saline to test compound and/or GABA-containing saline using a servomotor-operated valve (Hamilton Bonaduz AG, Bonaduz, Switzerland). A washout period of 2 - 5 min between each application was introduced, allowing receptors to recover from desensitization. For specific experiments, $GABA_A$ receptor-expressing oocytes were exposed to binary mixtures of dinitrophenolic herbicides. To minimize the influence of adsorption of compounds to the perfusion system the superfusion system was equipped with PTFE tubes (polytetrafluoroethylene; 4 x 6 mm, Rubber, Hilversum, The Netherlands) and glass reservoirs.

Data analysis and statistics

Inhibition or potentiation of GABA-evoked currents by dinitrophenolic herbicides was compared to the control current evoked by the application of 10 µM (~EC_{50}) or 1 mM (EC_{100}) GABA. The percentage of compound-induced alteration of the GABA-evoked ion current was calculated from the quotient of the amplitude of the GABA-drug co-application response (during 20 s) and the amplitude of the control part of the response (see Fig. 1 for example). Data represent mean ± SEM of n oocytes of at least two independent batches. Statistical analyses were performed using GraphPad Prism v6 (GraphPad Software, San Diego, California, USA). Continuous data were compared using One-way ANOVA with post-hoc Bonferroni test where applicable. A p-value ≤0.05 is considered statistically significant.

Results

Agonistic effects of dinitrophenolic herbicides on the α1β2γ2L GABA$_A$ receptor

To assess whether dinitrophenolic herbicides are agonists of the GABA receptor, responsive GABA$_A$-R-expressing oocytes were exposed to saline containing single dinitrophenolic herbicides without co-exposure to GABA. Exposure to DNP or DNOC did not result in measurable effects on the membrane current. However, the results demonstrate that dinoseb as well as dinoterb at 100 µM induce a small but reversible membrane current (Fig. 1B). As a similar effect was observed in experiments with non-injected oocytes (not shown), it was concluded that this current was not related to the presence of GABA$_A$ receptors, but to a compound-induced effect on the membrane itself. We therefore conclude that the observed effect on the membrane of dinoseb and dinoterb at these high concentrations is a non-specific effect and not related to an agonistic function on the GABA$_A$ receptor.

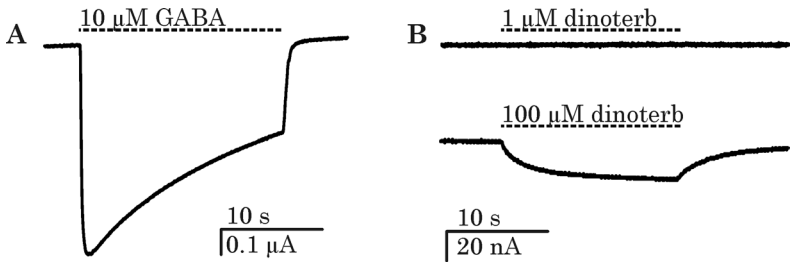

Fig. 1 Examples of electrophysiological recordings. (A) Example recording of the GABA-evoked current upon stimulation with 10 µM GABA. (B) Example recordings of the change in membrane current upon exposure to dinoterb alone. It can be observed that exposure to 100 µM dinoterb evokes a small, reversible membrane current, whereas exposure to 1 µM dinoterb does not induce a membrane current.

Effects of dinitrophenolic herbicides on α1β2γ2L GABA$_A$ receptor-induced ion current

To assess whether dinitrophenolic herbicides affect GABA$_A$ receptor-mediated ion currents, responsive GABA$_A$-R-expressing oocytes were exposed to a combination of 10 μM (EC_{50}, low receptor occupancy) GABA and one of the four test compounds. The results demonstrate that DNP, DNOC, dinoseb and dinoterb concentration-dependently affect the GABA-evoked response current (Fig. 2 & Table 2). There is a clear difference in potency visible with DNP being the least and dinoseb being the most potent test compound. DNP and DNOC both inhibit the GABA-evoked current (10 μM GABA) with a maximal inhibition at 100 μM of 10 ± 1% (n = 8; p<0.001; Fig. 2A) and 16 ± 1% (n = 10; p<0.001; Fig. 2B), respectively (both LOEC 10 μM). Dinoterb is also inhibiting the GABA-evoked current, but more potent with a maximum inhibition at 100 μM of 68 ± 4% (n = 10; LOEC 10 μM; Fig. 2D). In contrast, dinoseb induces a potentiation at concentrations ≤10 μM (maximum potentiation at 10 μM: 45 ± 8%, n = 10, LOEC 10 μM; Fig. 2C), whereas exposure to 100 μM results in a fast potentiation immediately followed by an inhibition of the GABA-mediated current (maximal potentiation: 35 ± 5%, n = 7; maximal inhibition: 29 ± 2%, n = 7; Fig. 2C & Table 2).

To assess whether dinitrophenolic herbicides exert the same differential effects with full GABA$_A$-R occupancy, GABA$_A$-R-expressing oocytes were exposed to dinitrophenolic herbicides in the presence of 1 mM GABA (EC_{100}). No overt differences were observed between the results from co-exposure of oocytes to test compounds with 10 μM or 1 mM GABA (Table 2A). Therefore, we conclude that dinitrophenolic herbicides do not bind to the GABA binding site on the GABA$_A$-R, but interact with modulatory binding sites.

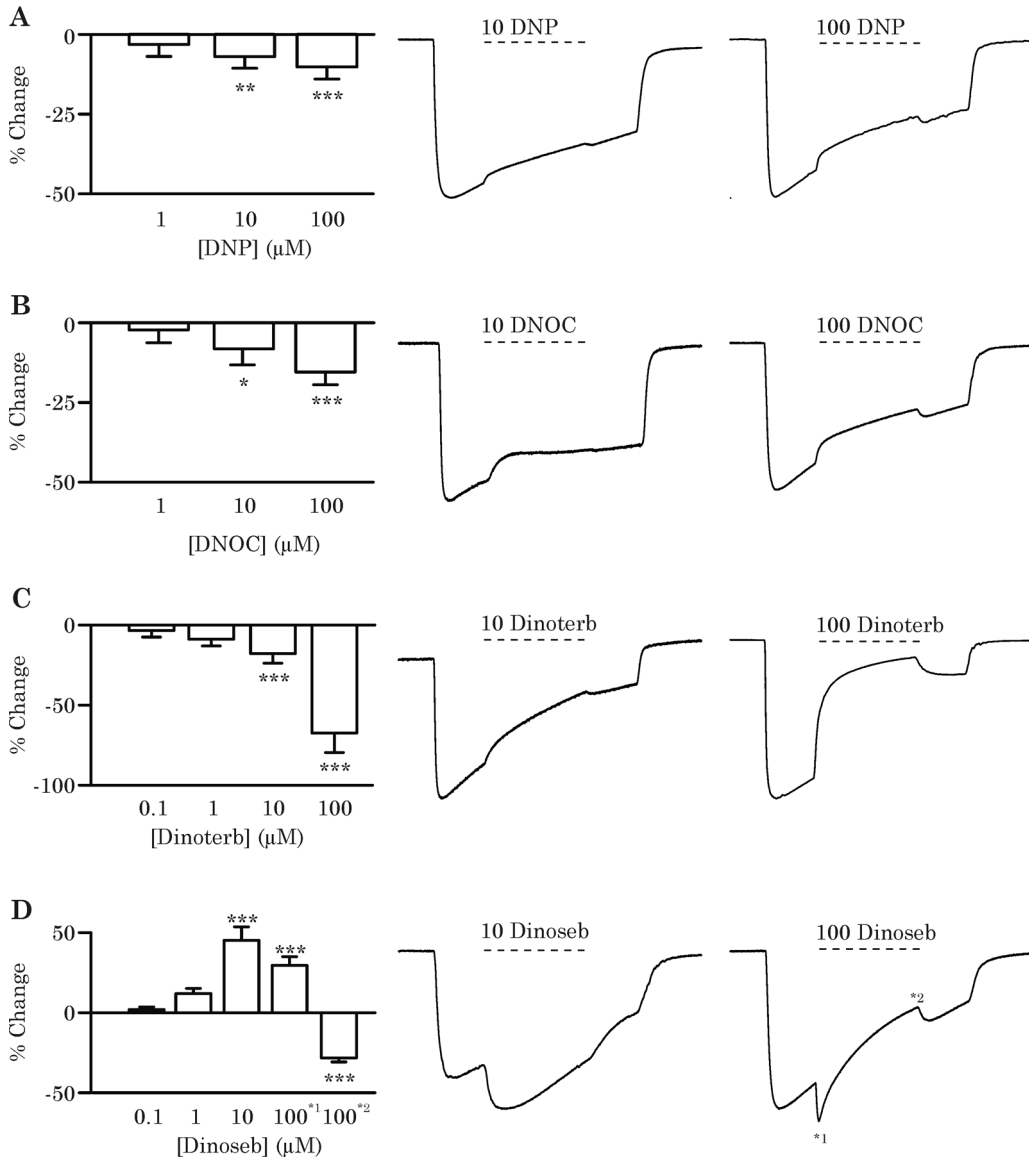

Fig. 2 Inhibitory and potentiating effects of dinitrophenolic herbicides on GABA-evoked ion currents. Bargraphs displaying the concentration-response curve of the inhibitory effect of DNP (A), DNOC (B), dinoterb (C) and dinoseb (D) on the GABA-evoked ion current with example traces (10 & 100 µM). (D) *1 and *2: point used to calculate the values given for exposure to 100 µM dinoseb. Inhibition and potentiation are expressed as percentage of the GABA-evoked response at EC_{50}. Bars represent mean ± SEM of 6-14 oocytes; * $p \leq 0.05$; ** $p \leq 0.01$; *** $p \leq 0.001$.

Effects of binary mixtures of herbicides on α1β2γ2L GABA$_A$ receptor-induced ion current.

Humans are exposed to a complex mixture of chemicals, including mixtures of herbicides. Often, the default assumption in the risk assessment of mixtures with similar mode of action is that the combined effect of a mixture can be predicted assuming additivity. To assess whether additivity applies upon exposure to a mixture of dinitrophenolic herbicides, four different binary mixtures were tested for their effect on the GABA-evoked current ([GABA]: 10 μM). Two low-concentration mixtures consisting of two inhibiting compounds (DNP or DNOC with dinoterb) and two high-concentration mixtures consisting of either two inhibiting compounds (DNOC and dinoterb) or two compounds with an apparent opposite mechanism of action (dinoseb and dinoterb).

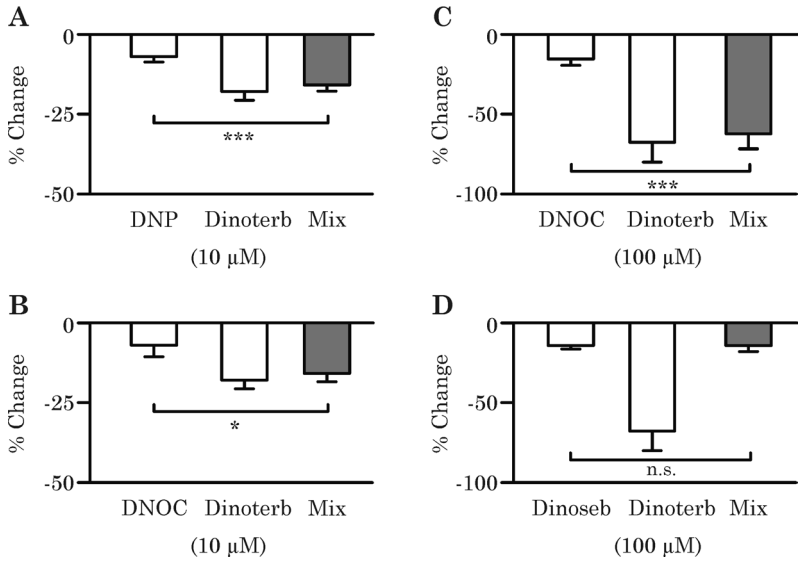

Fig. 3 Effects of different binary mixtures of dinitrophenolic herbicides on the GABA-evoked ion current. Bargraphs displaying the effects of equimolar, low-dose (10 μM), binary mixtures of DNP (A) and DNOC (B) with dinoterb as well as high-dose (100 μM) mixtures of DNOC (C) and dinoseb (D) with dinoterb on GABA-evoked ion current. Inhibition is expressed as percentage of the GABA-evoked response at EC_{50}. Bars represent mean ± SEM of 7-10 oocytes; * $p \leq 0.05$; *** $p \leq 0.001$.

The results from experiments assessing the combined effects of 10 µM DNP (-7 ± 1%, *n* = 7) with 10 µM dinoterb (-18 ± 2%, *n* = 8) demonstrate that the combined inhibition is comparable to dinoterb alone (-16 ± 1%, *n* = 8; Fig. 3A & Table 2B). Also, a binary mixture of 10 µM DNOC (-8 ± 2%, *n* = 7) with 10 µM dinoterb (-18 ± 2%, *n* = 8) induced a combined inhibition that was comparable to dinoterb alone (-16 ± 3%, *n* = 7; Fig. 3B & Table 2B). To test whether this lack of additivity was also observed for high-dose mixtures, a binary mixture of 100 µM DNOC (-16 ± 1%, *n* = 10) with 100 µM dinoterb (-68 ± 4%, *n* = 10) was tested. The results demonstrated that also at high concentrations, the observed inhibition did not exceed the inhibition induced by dinoterb alone (-60 ± 4%, *n* = 7; Fig. 3C & Table 2B). Interestingly, a mixture of 100 µM dinoseb (-29 ± 2%, *n* = 7) with 100 µM dinoterb (-68 ± 4%, *n* = 10) induced an inhibition that was comparable to the dinoseb-induced inhibition (-29 ± 4%, *n* = 7; Fig. 3D & Table 2B).

The combined results thus indicate that upon exposure to a mixture of dinitrophenolic herbicides, additivity does not apply as the compounds appear to antagonize each other's effect.

Discussion

In this study, we investigated the effects of four different dinitrophenolic congeners as single compounds and as binary mixtures on the human postsynaptic inhibitory $GABA_A$ receptor. The results demonstrate that all four compounds concentration-dependently modulate GABA-mediated currents with a similar LOEC (10 µM; Fig 2 & Table 2A), but with a different maximal effect. DNP, DNOC and dinoterb concentration-dependently inhibit the GABA-mediated current. In contrast, dinoseb potentiates the GABA mediated current at concentrations ≤10 µM, whereas a biphasic response, starting with a potentiation immediately followed by an inhibition, is observed at 100 µM (Fig. 2C).

None of the compounds displayed direct effects on the $GABA_A$ receptor in the absence of GABA, indicating that the compounds do not act as GABA-receptor agonist. Moreover, the inhibitory effects of dinitrophenolic herbicides on currents evoked by 10 µM GABA (~EC_{50}) do not differ from effects on ion currents evoked by 1 mM GABA (~EC_{100}). These results indicate that dinitrophenolic herbicides do not bind to one of the GABA binding sites, but likely bind to one of the modulatory binding sites on the $GABA_A$ receptor.

These modulatory binding sites are a target for a variety of compounds such as ethanol, benzodiazepines and barbiturates (D'Hulst, *et al.* 2009). The biphasic response observed upon exposure to a high concentration dinoseb (Fig. 2C) is an interesting finding in this respect, suggesting that dinoseb may bind to at least two different modulatory binding sites depending on the concentration. Also, the observation that dinoseb and dinoterb at concentrations ≤10 µM, despite their

minor molecular differences, have opposite effects on the GABA-evoked current indicates that both may bind to a different modulatory site. However, it has been demonstrated from research on benzodiazepine binding sites on the $GABA_A$ receptor that the same binding sites can give rise to both positive- and negative allosteric modulation resulting in for example anxiogenic or anxiolytic effects, respectively (D'Hulst, *et al.* 2009, Johnston 1996). We therefore consider the benzodiazepine binding sites a likely candidate for binding of dinitrophenolic herbicides, though the lack of truly specific inhibitors of the different modulating sites renders exact identification of the dinitrophenolic binding sites challenging.

The results from the experiments with binary mixtures of dinitrophenolic compounds (Fig. 3 & Table 2B) indicate that, despite an apparently shared mode of action, additivity does not apply. Since the effects of one of the mixture components seems to dominate the effect observed upon co-exposure, antagonism appears to play a role. This probably relates to differences in affinity for the receptor binding site. This is an important observation for risk assessment as this clearly proves that, even in case of mixtures of compounds with an apparent identical mode of action, the default assumption of additivity is not necessarily correct. This implies that in some cases detailed information about the mode of action as well as actual data on mixture effects is needed before a reliable risk assessment can be made.

GABA is the main inhibitory neurotransmitter system in the adult central nervous system. Among the CNS processes regulated by GABA, core body temperature is regulated by a complex neural feedback mechanism operating primarily through the hypothalamus. In the hypothalamus, GABA also constitutes the main inhibitory neurotransmitter (for review see: Clapham 2012). It has been demonstrated that local (hypothalamic) injection of the $GABA_A$-receptor antagonist bicucullin increased core-temperature (Amir 1990). The authors demonstrated that this effect could be antagonized by co-injection with the $GABA_A$ receptor agonist muscimol, which indicates that GABA-mediated inhibitory action is essential for maintenance of core-body temperature. Although uncoupling of mitochondrial phosphorylation is reportedly the main cause for the observed hyperpyrexia in case of poisoning with dinitrophenolic herbicides, it is not unlikely that core body-temperature can become deregulated by modulatory action of dinitrophenolic herbicides on GABA-ergic neurotransmission. Considering that the $GABA_A$-R is also involved in regulation of emotions and that (negative) modulation of the $GABA_A$-R is linked to anxiety and panic behavior (Sanders and Shekhar 1995), neuro-psychological symptoms of poisoning with dinitrophenolic herbicides could also be explained by modulation of GABA-ergic neurotransmission.

From monitoring studies, volunteer studies and case-reports on poisonings it is known that blood concentrations in humans occupationally or accidentally exposed can reach concentrations >200 μM without acute symptoms of poisoning, where-

as serum concentrations >600 µM are linked to symptoms of severe poisoning (Estuardo, *et al.* 2006, Harvey, *et al.* 1951, Parker, *et al.* 1951, van Noort, *et al.* 1960). In contrast to rodents, kinetics of dinitrophenolic compounds in the human body appear relatively slow ($T_{1/2}$ rodents: 24 - 72h vs. $T_{1/2}$ humans: 7 - 14 days; Harvey, *et al.* 1951, Parker, *et al.* 1951). Consequently, accumulation of dinitrophenolic compounds occurs upon repeated exposure. Although human brain concentrations are unknown, it can be anticipated from kinetic studies in animals (Parker, *et al.* 1951) and the lipophilic nature of these compounds (Table 1) that high brain concentrations may occur.

The reported primary mode of action of dinitrophenolic herbicides, i.e. uncoupling of mitochondrial phosphorylation (mouse liver mitochondrial preparation EC_{100} 1 - 50 µM; Ilivicky and Casida 1969), is until now held responsible for the observed toxicity *in vivo*. Disturbance of GABA-ergic neurotransmission therefore provides a novel mode of action of dinitrophenolic herbicides that may be implicated in the observed deregulation of thermo control as well as in the observed neuropsychological effects that occur upon poisoning with dinitrophenolic herbicides.

In addition, a change in function of the $GABA_A$-R and the GABA-ergic inhibitory circuitry in the basal ganglia is implicated in the pathophysiology of dopaminergic neurodegeneration (Blandini, *et al.* 2000, Luchetti, *et al.* 2011). Interestingly, compounds linked to the pathophysiology of PD or parkinsonism *in vitro* as well as *in vivo,* such as manganese and the organochlorine insecticides lindane and dieldrin, are well known for their inhibiting effect on the GABA-mediated currents (Fitsanakis, *et al.* 2006, Vale, *et al.* 2003). Notably, also the dopaminergic toxicant MPP^+ is reportedly an inhibitor of GABA-mediated neurotransmission (Wu, *et al.* 2002). In this respect it is interesting that both DNOC and dinoseb have recently been linked to *in vitro* dopaminergic neurodegeneration (Chapter 6.1). Altogether this implies a relationship between chemicals disturbing GABA-ergic neurotransmission and the occurrence of dopaminergic neurodegeneration. Whether this relationship is coincidental or causative remains to be determined.

In conclusion, our data reveals a novel mode of action for dinitrophenolic herbicides that potentially contributes to the observed effects of human poisoning with these dinitrophenolic compounds.

Funding Information

This work was funded by a grant from the Dutch "International Parkinson Fonds" (PAGES), by the European Union-funded project ACROPOLIS (Grant Agreement KBBE-245163) and by the Faculty of Veterinary Medicine (Utrecht University). The authors declare they have no competing financial interests.

Acknowledgements

We are grateful to Aart de Groot for expert technical assistance.

Chapter 7

Azole fungicides disturb intracellular Ca^{2+} in an additive manner in dopaminergic PC12 cells

Harm J Heusinkveld[1], Jeffrey Molendijk[1], Martin van den Berg[1], Remco HS Westerink[1]

[1] Neurotoxicology Research Group, Division of Toxicology, Institute for Risk Assessment Sciences (IRAS), Faculty of Veterinary Medicine, Utrecht University, P.O. Box 80.177, NL-3508 TD Utrecht, The Netherlands.

In vitro neurotoxicity of conazole fungicides

Toxicological Sciences **134**, 374 – 381 (2013)

Abstract

Humans are exposed to complex mixtures of pesticides and other compounds, mainly via food. Azole fungicides are broad spectrum antifungal compounds used in agriculture and in human and veterinary medicine. The mechanism of antifungal action relies on inhibition of CYP51, resulting in inhibition of fungal cell growth. Known adverse health effects of azole fungicides are mainly linked to CYP inhibition. Additionally, azole fungicide–induced neurotoxicity has been reported, though the underlying mechanism(s) are largely unknown. We therefore investigated the effects of a group of six azole fungicides (imazalil, flusilazole, fluconazole, tebuconazole, triadimefon, and cyproconazole) on cell viability using a combined alamar Blue/CFDA-AM assay and on oxidative stress using a H_2-DCFDA fluorescent assay. As calcium plays a pivotal role in neuronal survival and functioning, effects of these six azole fungicides and binary and quaternary mixtures of azole fungicides on the intracellular calcium concentration ($[Ca^{2+}]_i$) were investigated using single-cell fluorescence microscopy in dopaminergic PC12 cells loaded with the calcium-sensitive fluorescent dye Fura-2. Only modest changes in cell viability and ROS production were observed. However, five out of six azole fungicides induced a nonspecific inhibition of voltage-gated calcium channels (VGCCs), though with varying potency. Experiments using binary IC_{20} and quaternary IC_{10} mixtures indicated that the inhibitory effects on VGCCs are additive. The combined findings demonstrate modulation of intracellular Ca^{2+} via inhibition of VGCCs as a novel mode of action of azole fungicides. Furthermore, mixtures of azole fungicides display additivity, illustrating the need to take mixture effects into account in human risk assessment.

Key Words

In vitro neurotoxicology; Fura-2 Ca^{2+}-imaging; calcium homeostasis; voltage-gated calcium channels; dose addition; triazole/imidazole fungicides

Introduction

Azole fungicides constitute around 40 broad-spectrum fungicides that contain at least one triazole or imidazole moiety in their structure and are used for agricultural, horticultural, and pharmaceutical applications. The primary antifungal mechanism of action of these fungicides relies on inhibition of CYP51 (lanosterol 14 alpha-demethylase), a key enzyme for sterol biosynthesis in fungi (for review, see Zarn, *et al.* 2003). Inhibition of this enzyme leads to a depletion of ergosterol, a vital ingredient of the fungal cell wall, resulting in growth inhibition and death of fungi. Besides inhibition of CYP51, which is also present in humans, azole fungicides are known to exert a range of adverse health effects in mammals, including disturbance of mammalian steroidogenesis, induction of craniofacial malformations, and birth defects (Crofton 1996, Giavini and Menegola 2010, Menegola, *et al.* 2005, Zarn, *et al.* 2003). Adverse effects of azole fungicides on mammalian (sex-specific) steroidogenesis are mainly linked to disruption of cholesterol synthesis (Zarn, *et al.* 2003) or interaction with CYP 17/19 (Roelofs, *et al.* 2013, Sanderson, *et al.* 2002), whereas the mechanisms underlying other side effects are largely unknown.

A limited number of azole fungicides is known to exert neurotoxic effects *in vitro* and *in vivo*, including effects on uptake and release of monoamines in rat synaptosomes and neurobehavioral effects (Crofton 1996, Moser, *et al.* 2001). Calcium plays a pivotal role in many inter- and intraneuronal processes, including (dopaminergic) neurotransmission (for review, see Westerink 2006), gene transcription (Carrasco and Hidalgo 2006), neurodegeneration (Mattson 2012), and neurodevelopment (Pravettoni, *et al.* 2000). Neuronal cells, therefore, rely heavily on strict regulation of their intracellular calcium concentration ($[Ca^{2+}]_i$). For this reason, we investigated the effect of acute exposure to six selected azole fungicides on basal and depolarization-evoked intracellular calcium levels in PC12 cells, which are a widely used and extensively characterized model for mature dopaminergic neurons (Westerink and Ewing 2008).

The selection of azole fungicides consisted of fungicides used as veterinary (imazalil) or human (fluconazole) pharmaceutical or as agricultural fungicide (triadimefon, flusilazole, tebuconazole, and cyproconazole) (Table 1). For humans, exposure to fungicides is primarily via food and occupational routes (for review, see: Oates and Cohen 2011). Though current risk assessment approaches are predominantly based on individual azole fungicides, human exposure to these chemicals occurs predominantly to a complex mixture. We, therefore, included several binary mixtures and a quaternary mixture of fungicides to more closely resemble the human exposure situation in a qualitative way and to reveal whether additivity applies.

Table 1 Molecular structures and chemical-physical properties of the six selected azole fungicides

	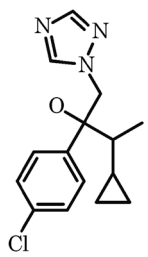	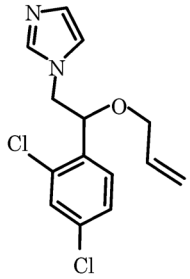	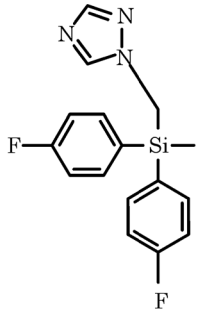	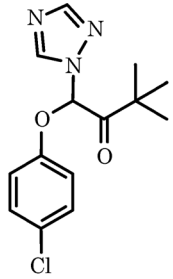	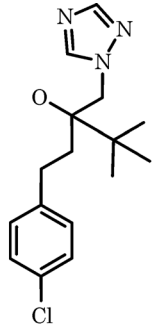	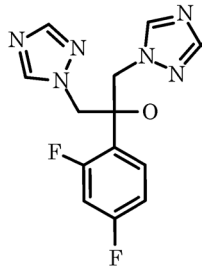
Name	Cyproconazole	Imazalil	Flusilazole	Triadimefon	Tebuconazole	Fluconazole
CAS no.	94361-06-5	35554-44-0	85509-19-9	43121-43-3	107534-96-3	86386-73-4
MW (g/mol)	292	297	315	294	308	306
Log K_{ow}	2.90	3.82	3.87	2.77	3.7	0.25

Chemicals

Fura-2-AM, CFDA-AM, and 2,7-dichlorodihydrofluorescein diacetate (H_2-DCFDA) were obtained from Molecular Probes (Invitrogen, Breda, The Netherlands); all other chemicals were obtained from Sigma- Aldrich (Zwijndrecht, The Netherlands), unless otherwise noted. Flusilazole, triadimefon, imazalil, tebuconazole, and cyproconazole were of 99.8% purity (Pestanal grade, Riedel de Haen, Seelze, Germany). Fluconazole was obtained with ≥ 98% HPLC purity grade from Sigma-Aldrich. Saline solutions, containing (in mM) 125 NaCl, 5.5 KCl, 2 $CaCl_2$, 0.8 $MgCl_2$, 10 HEPES, 24 glucose, and 36.5 sucrose (pH 7.3), were prepared with deionized water (Milli-Q®; resistivity >18 MΩ•cm). Stock solutions of 2 mM ionomycin in dimethyl sulfoxide (DMSO) were kept at −20°C. Stock solutions of 0.1–100 mM fungicide were prepared in DMSO and diluted in saline to obtain the desired concentrations just prior to the experiments (all solutions used in experiments, including control experiments, contained 0.1% DMSO).

Cell culture

Rat dopaminergic pheochromocytoma (PC12 cells; Greene and Tischler 1976) were grown for 10 passages in RPMI 1640 (Invitrogen) supplemented with 5% fetal calf serum and 10% horse serum (ICN Biomedicals, Zoetermeer, The Netherlands) in a humidified incubator at 37°C and 5% CO_2 as described previously (Dingemans, *et al.* 2009, Heusinkveld and Westerink 2012). For Ca^{2+} imaging experiments, cells were subcultured in poly-L-lysinecoated glass-bottom dishes (MatTek, Ashland, MA) as described previously (Dingemans, *et al.* 2009, Heusinkveld and Westerink 2012). For cell viability experiments, cells were subcultured in poly-L-lysine-coated 24-well plates (Greiner Bio-one, Solingen, Germany) at a density of 5×10^5 cells/well. For experiments assessing the production of reactive oxygen species (ROS), which is indicative for oxidative stress, cells were seeded in poly-L-lysine-coated 48-well plates at a density of 2.5×10^5 cells/well.

Cell viability assay

To assess the effects of the compounds on cell viability, a combined alamar Blue/CFDA-AM (aB/CFDA) assay was used (protocol adapted from Bopp and Lettieri 2007) to determine respectively mitochondrial activity and membrane integrity. Cells were exposed in serum- and phenol red-free medium to concentrations up to 100 µM for up to 24 h. Mitochondrial activity of the cells was recorded as a measure of cell viability with the aB assay, which is based on the ability of the cells to reduce resazurin to resorufin. In the same experiment, membrane integrity was assessed indirectly using a CFDA-AM assay, which is based on nonspecific cytoplasmic-esterase activity. Briefly, cells were incubated for 30 min with 12.5 µM aB and 4 µM CFDA-AM. Resorufin was measured spectrophotometrically at 540/590 nm (Infinite M200 microplate; Tecan Trading AG, Mannedorf, Switzerland), whereas

hydrolyzed CFDA was measured spectrophotometrically at 493/541 nm.

Measurement of ROS production using H_2-DCFDA

The involvement of oxidative stress in the observed reduction in cell viability was investigated using the fluorescent dye H2-DCFDA as described previously (Heusinkveld, *et al.* 2010). Briefly, cells were loaded with 1.5 µM H_2-DCFDA for 30 min at 37°C. Subsequently, cells were exposed for up to 24 h to 0.1 – 100 µM compound, and fluorescence was measured spectrophotometrically at 488/520 nm (Infinite M200 microplate; Tecan Trading AG). Rotenone (100 µM) was included as positive control for oxidative stress (Radad, *et al.* 2006).

Ca^{2+} imaging microscopy

Changes in the $[Ca^{2+}]_i$were measured on a single-cell level using the Ca^{2+}-sensitive fluorescent ratio dye Fura-2 AM as described previously (Hendriks, *et al.* 2012, Heusinkveld and Westerink 2012). Briefly, cells were loaded with 5 µM Fura-2 AM (Molecular Probes; Invitrogen) for 20 min at room temperature, followed by 15 min de-esterification. After deesterification, the cells were placed on the stage of an Axiovert 35M inverted microscope (Zeiss, Gottingen, Germany) equipped with a TILL Photonics Polychrome IV (TILL Photonics GmBH, Grafelfing, Germany). Fluorescence, evoked by 340 and 380 nm excitation wavelengths (F340 and F380), was collected every 6 s at 510 nm with an Image SensiCam digital camera (TILL Photonics GmBH). After 5-min baseline recording, cells were depolarized by high K^+-containing saline (100mM K^+) for 18 s. Following a 10-min recovery period, cells were exposed for 20 min (Fig. 3A) to DMSO (0.1%), methylhistamine (1 or 10 µM), a single fungicide (0.1 – 100 µM), or a mixture of equipotent concentrations of azole fungicides. Subsequently, cells were depolarized a second time to evaluate effects of fungicide exposure on depolarization-evoked Ca^{2+} influx. Minimum and maximum ratios (R_{min} and R_{max}) were determined at the end of the recording by addition of ionomycin (5 µM) and EDTA (17 mM).

In a separate set of experiments, exposure to azole fungicides prior to the second depolarization was reduced from 20 min to 12 s to assess whether lipophilicity, and thus intracellular accumulation, plays a role. Changes in the F340/F380 ratio (R), reflecting changes in $[Ca^{2+}]_i$, were further analyzed using custom-made MS-Excel macros calculating F340/F380 ratios and applying a correction for background fluorescence. Free cytosolic $[Ca^{2+}]_i$ was calculated using Grynkiewicz's equation

$$[Ca^{2+}]_i = Kd^* \times (R - R_{min})/(R_{max} - R)$$

where Kd* is the dissociation constant of Fura-2 determined in the experimental set-up (Deitmer and Schild 2000). The mean basal $[Ca^{2+}]_i$ during exposure was determined to quantify effects on basal $[Ca^{2+}]_i$. The maximum amplitude of $[Ca^{2+}]_i$

observed during depolarization was used to investigate possible effects on the depolarization-evoked increase of $[Ca^{2+}]_i$ (Hendriks, *et al.* 2012, Heusinkveld and Westerink 2011).

Data analysis and statistics

Cell viability data are presented as % viability ± SD compared with control from at least three independent experiments consisting of four replicates per experiment. Data on production of ROS are presented as % increase in ROS ± SD compared with time-matched controls from three independent experiments consisting of four replicates per experiment. Data from fluorescence microscopy are presented as mean $[Ca^{2+}]_i$ ± SD from the number of cells (*n*) indicated, obtained from 3 – 9 independent experiments (N). Treatment ratio (TR; see also Fig. 3A) represents the second depolarization- evoked increase in $[Ca^{2+}]_i$ in treated cells as a percentage of the response to the first depolarization, expressed relative to the TR in control cells. Statistical analyses were performed using GraphPad Prism v6.01 (GraphPad Software, San Diego, California). Continuous data were compared using oneway ANOVA with post hoc Bonferroni test where applicable. Concentration response curves for inhibition of depolarization-evoked Ca^{2+} influx were measured at concentrations of 0.1 – 100 µM with intermediate concentrations where needed. Concentration-response curves were fit using a nonlinear sigmoidal fit using GraphPad Prism v6.01. Calculated IC_{10} and IC_{20} concentrations are presented ± 95% confidence interval of the effect size. A p-value ≤ 0.05 is considered statistically significant. MDL ISIS/Draw version 2.5 was used to draw chemical structures.

Results

Effects of Azole Fungicides on Cell Viability

To exclude that effects on calcium homeostasis are confounded by cytotoxicity, cell viability was assessed using a combined alamar Blue/CFDA-AM assay. PC12 cells were exposed to different concentrations of azole fungicides (0.1 – 100µM) for 24 h. The results from the alamar Blue assay demonstrate that exposure to 0.1 or 1 µM imazalil does not result in an increase in mitochondrial activity (112 ± 5%: N = 3; 120 ± 10%: N = 3; Fig. 1A), whereas exposure to 10 or 100 µM does induce an increase in mitochondrial activity (179 ± 21%, N = 3, $p \leq 0.001$; 183 ± 36%, N = 3, $p \leq 0.001$; Fig. 1A) suggestive for oxidative stress. At these concentrations, none of the other tested fungicides induces a change in mitochondrial activity (results not shown).

The results from the CFDA-AM demonstrate that exposure to 0.1, 1, or 10 µM imazalil does not induce a significant change in membrane integrity (97 ± 5%, N = 3; 95 ± 3%, N = 3; 96 ± 3%, N = 3; Fig. 1B), whereas exposure to 100 µM decreases membrane integrity to 74 ± 12% (N = 3; $p \leq 0.001$; Fig. 1B). None of the other compounds induces a change in membrane integrity (results not shown).

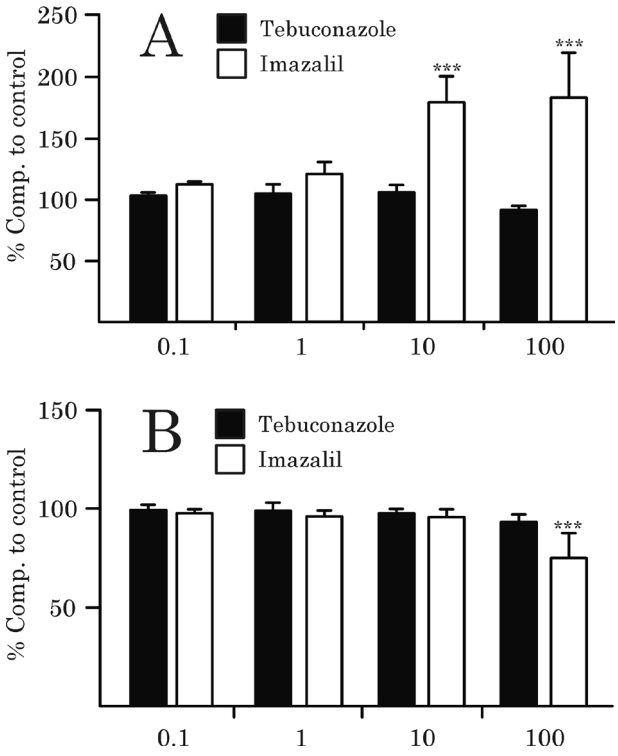

Fig. 1. Bar graphs displaying results from (A) the alamar Blue and (B) CFDA assays upon exposure to imazalil and tebuconazole for 24 h. (A) Imazalil induces an increase in mitochondrial activity, whereas tebuconazole does not change mitochondrial activity upon 24-h exposure. (B) Imazalil induces a decrease in membrane integrity upon exposure to 100µM, whereas tebuconazole does not affect membrane integrity upon 24-h exposure. Bars display average data ± SD of three independent experiments. Significance compared with control; ***$p < 0.001$.

Overall, none of the compounds induces overt toxicity after 24 h exposure except for imazalil, which induces an increase in mitochondrial activity (≥ 10 µM) and a decrease in membrane integrity (100 µM) indicative for a decrease in cell viability (Fig. 1).

Because oxidative stress is often considered a precursor of cell damage, production of ROS was assessed using the cumulative fluorescent dye H_2-DCFDA in PC12 cells exposed to different concentrations of fungicides (0.1 – 100 µM) for up to 24 h. The results demonstrate that exposure to tebuconazole, cyproconazole, triadimefon, and fluconazole does not increase ROS production, whereas exposure to flusilazole and imazalil induces ROS production, though only upon exposure to 100 µM (130 ± 4% and 166 ± 4%, respectively; N = 4; $p \leq 0.001$; Fig. 2).

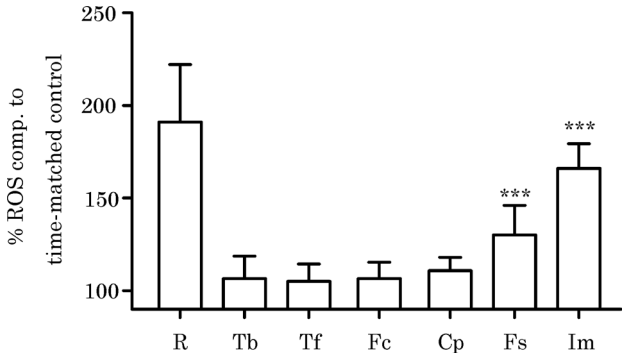

Fig. 2. Bar graph displaying results from the H_2-DCFDA assay assessing oxidative stress in PC12 cells after 24 h exposure to 100 µM of the different azole fungicides (Tb, tebuconazole; Tf, triadimefon; Fc, fluconazole; Cp, cyproconazole; Fs, flusilazole; Im, imazalil). Exposure to flusilazole and imazalil induces an increase in oxidative stress. Rotenone (R; 100 µM) was included as positive control. Bars display average data ± SD of four independent experiments. Difference from control: ***p<0.001.

Effects of Azole Fungicides on $[Ca^{2+}]_i$

Basal $[Ca^{2+}]_i$ in PC12 cells is typically low (≈100 nM; Fig. 3A) with only minor fluctuations. Upon depolarization with 100 mM K^+, $[Ca^{2+}]_i$ displays a strong, transient increase (2.0 ± 0.7 µM; n = 80; K1: Fig. 3A) that decreases to near basal $[Ca^{2+}]_i$ within minutes. During a subsequent 20 min exposure to DMSO-containing saline (1 µl/ml), basal calcium levels remain low. Similarly, 20 min exposure to flusilazole, tebuconazole, fluconazole, cyproconazole, and triadimefon (0.1 – 100 µM) does not affect basal $[Ca^{2+}]_i$ (results not shown). However, compared with DMSO, exposure to 100 µM imazalil induced a significant increase in basal $[[Ca^{2+}]_i$ amounting to 316 ± 49 nM (n = 47; $p \leq 0.001$; data not shown), whereas lower concentrations (0.1 – 30 µM) did not induce a change in basal $[Ca^{2+}]_i$.

When control cells are challenged with a second depolarization following 20 min exposure to DMSO, $[Ca^{2+}]_i$ increases to 1.9 ± 0.8 µM (n = 80; K2: Fig. 3A), (TR: 95 ± 1%; n = 98; Fig. 3A; set at 100% for controls). Cells exposed to fluconazole (0.1 – 100µM) for 20 min have a TR that is not different from control cells (Fig. 3B). However, in cells exposed for 20 min to flusilazole, imazalil, tebuconazole, cyproconazole, and triadimefon, the TR is concentration-dependently reduced (Fig. 3B; Table 2), demonstrating that these fungicides inhibit VGCC-mediated Ca^{2+} influx with clearly different potencies. To assess whether lipophilicity, and thus accumulation in the cell or membrane, plays a role in the observed effects on VGCCs, cells were exposed for 12 s instead of 20 min to 30µM cyproconazole. The results reveal a comparable effect of cyproconazole on VGCC-mediated Ca^{2+} influx (TR_{12s}: 79 ± 15%, n = 43 vs. TR_{20min}: 83 ± 17%, n = 55; data not shown).

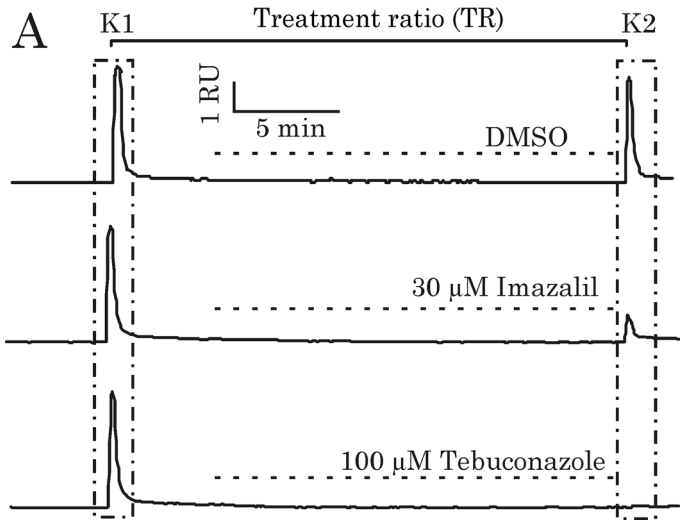

Fig. 3. Azole fungicides concentration-dependently inhibit depolarization-evoked $[Ca^{2+}]_i$ in PC12 cells. (A) Example traces of cytosolic $[Ca^{2+}]_i$ illustrating the inhibition of the second depolarization-evoked increase in $[Ca^{2+}]_i$ (K2) in PC12 cells exposed to DMSO (Control; upper trace), imazalil (30 µM; middle trace), and tebuconazole (100 µM; lower trace).

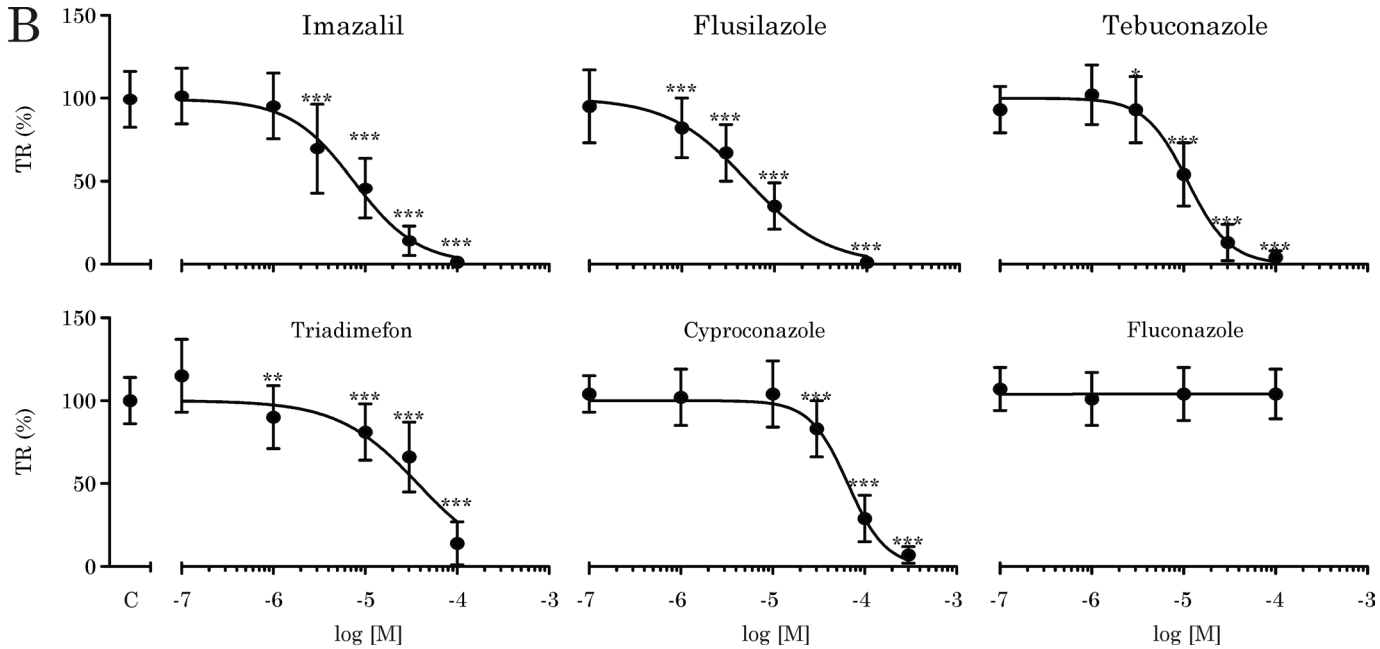

Fig. 3. Azole fungicides concentration-dependently inhibit depolarization-evoked $[Ca^{2+}]_i$ in PC12 cells. (B) Concentration-response curves of all six azole fungicides on the TR. Data points display average data (± SD) from at least 28 – 80 individual cells (four to nine experiments per concentration). Difference from control (C): *$p \leq 0.05$; **$p \leq 0.01$; ***$p \leq 0.001$.

As human exposure is in general to complex mixtures of pesticides, a number of mixture experiments were performed. To discriminate between additivity, antagonism, and synergism, mixtures were composed based on (calculated) IC_{10} and IC_{20} concentrations. Mixtures were composed of either two compounds (imazalil and flusilazole; tebuconazole and cyproconazole) at their relative IC_{20} concentrations or of these four compounds at their relative IC_{10} concentrations. The results from the mixture experiments of IC_{20} concentrations imazalil (2.5 µM; IC_{20} ± 3.5%; Table 2) and flusilazole (1.3 µM; IC_{20} ± 3.1%; Table 2) display additive inhibition of depolarization-evoked $[Ca^{2+}]_i$, amounting to 34 ± 13% (n = 40; Fig. 4B). Exposure to the calculated IC_{20} concentrations of cyproconazole (32.7 µM; IC_{20} ± 5.6%; Table 2) and tebuconazole (5.2 µM; IC_{20} ± 3.9%; Table 2) also displays additive inhibition of depolarization-evoked $[Ca^{2+}]_i$, amounting to 41 ± 14% (n = 55; Fig. 4B).

Table 2 NOEL concentrations and (calculated) inhibitory concentrations of azole fungicides on depolarization-evoked $[Ca^{2+}]_i$ (µM)

	NOEL	IC_{10} (µM)	IC_{20} (µM)	IC_{50} (µM)
Flusilazole	0.1	0.6	1.3	5.1
Imazalil	1	1.3	2.5	7.5
Tebuconazole	1	3.4	5	11.0
Triadimefon	1	4	9.4	37.2
Cyproconazole	10	23	32	65.0
Fluconazole	100	>100	>100	>100

To assess whether additivity applies for more complex mixtures at IC_{10} levels (a nonsignificant decrease in TR), mixture experiments were performed with the calculated IC_{10} concentrations of four fungicides (imazalil: 1.3 µM ± 2.7%; flusilazole: 0.6 µM ± 2.5%; tebuconazole: 3.4 µM ± 3.0%; cyproconazole: 23 µM ± 4.3%; Table 2). Inhibition of depolarization-evoked $[Ca^{2+}]_i$ upon exposure to this IC_{10} mixture amounted to 45 ± 15% (n = 46; Fig. 4B), again indicating that dose addition applies.

A recognized pathway of inhibition of VGCCs is via activation of neuronal histamine H_3 receptors (H_3R) leading to cAMP-dependent downregulation of VGCCs and as a result inhibition of depolarization-evoked Ca^{2+} influx and neurotransmission (Ferrada, *et al.* 2008, Threlfell, *et al.* 2004). To assess whether binding of azole fungicides to the H_3R could have caused the observed reduction in the depolarization-evoked $[Ca^{2+}]_i$ cells, we investigated the presence of functional H_3Rs in PC12 cells by 20 min incubation with the natural agonist methylhistamine prior to evoking depolarization. No effect was observed on the degree of calcium influx in histamine-exposed cells compared with the solvent control, indicating that our PC12 cells do not contain functional H_3Rs. We, therefore, conclude that fungicide-based activation of H_3Rs plays no role in the observed inhibition of VGCCs.

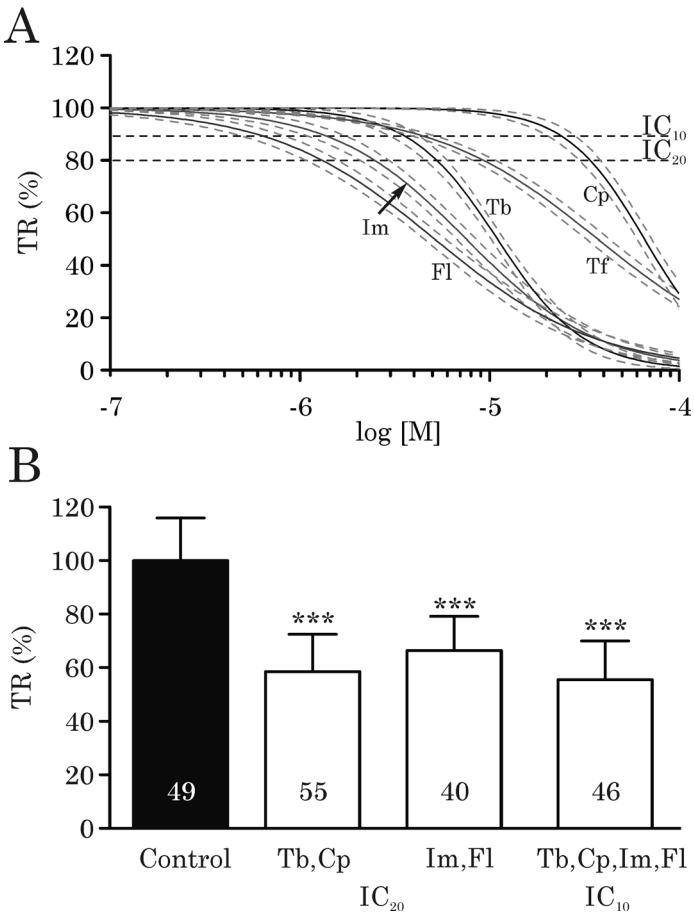

Fig. 4. Benchmark dose approach for mixture composition. (A) Fitted concentration-response curves for flusilazole (Fl), imazalil (Im), tebuconazole (Tb), triadimefon (Tf), and cyproconazole (Cp). Dashed lines alongside the curves represent the 95% confidence interval of the fitted curves. (B) Bargraph displays that the binary combinations of (near) IC_{20} and the quaternary combination of (near) IC_{10} exert an additive inhibition of TR. Bars display average data (± SD) from the number of cells indicated in the bars (≥four experiments per concentration). Difference from control: ***$p \leq 0.001$.

Discussion

The present results demonstrate that the azole fungicides imazalil, flusilazole, triadimefon, tebuconazole, and cyproconazole concentration-dependently inhibit depolarization-evoked calcium influx. Fluconazole does not induce an inhibition of depolarization-evoked calcium influx with exposures up to 100 µM. Though PC12 cells contain multiple subtypes of VGCCs, including L-, N-, and P/Q-type VGCCs (Dingemans, *et al.* 2009, Heusinkveld, *et al.* 2010, Dingemans, *et al.* 2009, Heusinkveld and Westerink 2012), all five compounds induce a (near) complete inhibition at the highest concentrations, indicative of a nonspecific inhibition of VGCCs. IC_{50} values (Table 2) range from 5 µM (flusilazole) to 65 µM (cyproconazole), revealing a one order of magnitude difference in potency. Exposure of cells to binary IC_{20} or quaternary IC_{10} mixtures provides clear indications for additivity with respect to inhibition of depolarization-evoked calcium influx.

The results from the cytotoxicity assays indicate that imazalil (≥ 10 µM, 24 h) is linked to an increase in mitochondrial activity (aB assay), which is only at the highest concentration (> 10 µM) related to a minor loss of viability (CFDA-AM assay). The results of the oxidative stress assay indicate only an increase in oxidative stress for exposure to imazalil and flusilazole (100 µM). None of the other four fungicides induced an effect on oxidative stress. Although the observed increase in basal $[Ca^{2+}]_i$ upon exposure to 100 µM imazalil could be related to acute cell stress, we conclude that the observed effects on depolarization-evoked calcium influx are not related to acute cytotoxicity or the occurrence of excess oxidative stress. Furthermore, it is unlikely that interactions with (steroidogenic) CYP enzymes or formation of (reactive) metabolites plays a role in the observed effects as (our) PC12 cells have poor metabolic capacity and cytochrome activity. In addition, the duration of calcium imaging experiments appears too short for considerable formation of metabolites rendering an effect of metabolites unlikely. However, in the *in vivo* situation, interaction with (steroidogenic) CYP enzymes is likely to play a role as (*in vitro*) effect concentrations for interaction of azole fungicides with (steroidogenic) CYP enzymes are in the same range (see Roelofs, *et al.* 2013, Sergent, *et al.* 2009).

In a study on neurobehavioral effects of a range of azole compounds, it has been reported that a strict structure-activity relationship is apparent for neurobehavioral effects caused by triadimefon and triadimenol (Crofton 1996). This appears also the case for inhibition of VGCCs because five out of six fungicides induce comparable effects, whereas one (fluconazole) displays no effect at all. Considering the chemical-physical properties of the group of azole fungicides used, there are some noticeable differences. First, fluconazole contains two triazole moieties, whereas the other fungicides contain only one, pointing toward the single triazole or imidazole moiety as effective group. The presence of two triazole moieties could cause

steric hindrance in binding of the molecules to receptors or channels. Second and more likely, the log K_{ow} value of fluconazole (0.25) indicates a low lipophilicity, whereas the other fungicides are more lipophilic (Table 1). In this data set, lipophilicity of the test compounds appears inversely correlated to the potency (IC_{50}) of VGCC inhibition because a higher lipophilicity appears related to a higher potency. This indicates that the target of azole fungicides could be located in the lipid membrane or even intracellularly. However, results from experiments with short exposure (12 s exposure; data not shown) demonstrate that effects develop immediately upon exposure, suggesting that azole fungicides act on an extracellular target such as the VGCC itself or a receptor-activated pathway that results in a specific inhibition of VGCCs. Activation of the neuronal histamine H_3 receptor (H_3R) is linked to inhibition of VGCCs via G-protein-coupled pathways acting on cAMP. As a result, H_3R activation causes negative regulation of striatal dopaminergic and serotonergic neurotransmission (Ferrada, *et al.* 2008, Threlfell, *et al.* 2004). Considering the structure analogy between azole fungicides and the natural H_3R agonist (R)-(-)-α-methyl-histamine, we hypothesized that binding of azole fungicides to the H_3R could underlie the observed inhibition of VGCCs. However, experiments with the natural agonist revealed that these receptors are not functional in PC12 cells, and therefore, another mechanism must be involved. Consequently, it cannot be excluded that binding to the H_3R plays a role in the *in vivo* situation.

Maintenance of intracellular calcium homeostasis is pivotal for proper development and functioning of the nervous system. Identification of inhibition of VGCCs as a novel mode of action for azole fungicides is therefore of importance. Notably, inhibition of VGCCs is a well-known common feature of several man-made (persistent) chemicals, such as brominated flame retardants (Dingemans, *et al.* 2010, Hendriks, *et al.* 2012), organochlorine insecticides (Heusinkveld and Westerink 2012), and PCBs (Langeveld, *et al.* 2012) and thus appears a common denominator for various groups of structurally different environmental contaminants and pesticides in risk assessment (Westerink 2013). In that way, it can be expected that a complex mixture of compounds - all below their individual effects levels - may evoke adverse effects because additivity may apply.

Human exposure data or data on pharmacokinetics of single azole fungicides are largely lacking. In addition, data on human exposure to mixtures of azole fungicides are limited to data on technical mixtures of fungicides applied in agriculture, residue levels in food, and (limited) data on animal-based kinetics. According to a recently published study on pesticide residue levels on food in France, residue levels of among others imazalil, tebuconazole, and cyproconazole are often > 10 µg/kg (Nougadère, *et al.* 2012), indicating that human exposure to (mixtures of) azole fungicides is very likely. An animal-based PBPK study in rats on triadimefon in-

dicated that upon single exposure (50 mg/kg, *i.v.*) a rapid increase in triadimefon throughout the body, including the brain, with tissue concentrations peaking between 10 and 100 µM (Crowell, *et al.* 2011). Using the PBPK modelling, the authors calculated a human equivalent dose to the rat NOAEL for neurotoxicity of 0.86 mg/ kg/day, which is only 25-fold higher than the human oral reference dose (RfD; 0.034 mg/kg/day; Crowell, *et al.* 2011). This indicates that current safety margins may not be sufficient, in particular, when additivity applies because exposure to multiple no effect concentrations may thus result in adverse effects (Kortenkamp 2008).

In conclusion, azole fungicides inhibit depolarization-evoked calcium influx via a-specific inhibition of VGCC, which likely reduces (dopaminergic) neurotransmission. Furthermore, exposure to complex mixtures reveals additive inhibition of VGCC-mediated calcium influx. The combined findings thus illustrate the need for inclusion of (complex) mixtures and the use of common assessment groups based on neurotoxicological endpoints in human risk assessment studies.

Funding

European Union-funded project ACROPOLIS (KBBE-245163); Faculty of Veterinary Medicine, Utrecht University. The authors declare that they have no competing financial interests.

Acknowledgments

We are grateful to Aart de Groot and Gina van Kleef for expert technical assistance.

Chapter 8

Comparison of *in vitro* cell models for assessment of pesticide-induced dopaminergic neurodegeneration

Harm J Heusinkveld[1], Remco HS Westerink[1]

[1] Neurotoxicology Research Group, Division of Toxicology, Institute for Risk Assessment Sciences (IRAS), Faculty of Veterinary Medicine, Utrecht University, P.O. Box 80.177, NL-3508 TD Utrecht, The Netherlands.

Submitted for publication

Summary

Current biomedical and (neuro)toxicity research on (neuro)degenerative diseases relies strongly on animal models. For both ethical and technical reasons this use of laboratory animals is often undesirable. Current *in vitro* research largely relies on tumor derived- or immortalized cell lines. However, the suitability of cell lines for studying neurodegeneration is determined by their intrinsic properties. We therefore characterized PC12, SH-SY5Y, MES23.5 and N27 cells with respect to the presence of functional membrane ion channels and receptors as well as for the effects of five different pesticides on cytotoxicity, oxidative stress and parameters of intracellular calcium homeostasis using a combined aB/CFDA assay, a H_2-DCFDA assay and single cell fluorescent (Fura-2) calcium imaging, respectively. Our results demonstrate considerable differences in intrinsic properties and pesticide-induced effects between the cell lines, indicating that care should be taken when interpreting (neuro)toxicity data as the chosen cell model may greatly influence the outcome.

Introduction

Current (neuro)toxicity and biomedical research on human (degenerative) diseases of the nervous system relies strongly on animal models, mainly rodents. According to the 2010 EU report on the annual laboratory animal use (SEC2010/1107) biomedical- and toxicological research involved nearly 2.5 million animals. These animal experiments are not only ethically debated but also expensive, time-consuming and unsuitable for high-throughput testing. *In vitro* approaches, in contrast, provide a fast and relatively cheap way of testing chemicals for their (neuro) toxic properties without the need for the use of laboratory animals.

Available *in vitro* techniques to study pathways of neurodegeneration rely mainly on the study of chemical-induced effects in a wide array of (tumour-derived) cell lines, either from rodent or human origin. Such *in vitro* studies using cell lines allow for in-detail, single-cell studies dissecting (human relevant) molecular pathways. Therefore, toxicological research on potential neurodegenerative properties of compounds could focus on *in vitro* strategies using one or more cell lines from the wide array of cell lines available.

Among the available cell lines, various cell models are reported to have dopaminergic properties and should thus be suitable for *in vitro* studies on dopaminergic neurodegeneration. Whether a cell line is suitable for answering a particular research question relies largely on its intrinsic (functional) properties. However, the choice for a particular cell line is often based on the availability and experience in a specific laboratory or institute, rather than on intrinsic properties of a particular cell line. Moreover, many cell lines are poorly characterized with respect to intrinsic properties, such as presence of membrane receptors and ion channels. As the presence of neurotransmitter receptors and ion channels in many cases determines toxicity, the use of inappropriate models may lead to an erroneous estimation of (neuro)toxicity. We therefore chose to characterize four cell lines (rat PC12, human SH-SY5Y, mouse/rat hybrid MES23.5 and rat N27 cells) using techniques widely used for *in vitro* neurodegeneration research and to compare their response to a number of known neurotoxic pesticides.

Rat pheochromocytoma cells (PC12; Greene and Tischler 1976) are a widely used model in neurotoxicology and an extensively characterized model for neurosecretion (Westerink and Ewing 2008). As these cells originate from an adrenal tumour, they provide a neuronal model from non-CNS origin. However, PC12 cells display several characteristics of mature dopaminergic neurons such as synthesis, storage and vesicular release of dopamine (DA) as well as the presence of different types of voltage-gated calcium- and sodium channels (Shafer and Atchison 1991, Westerink and Ewing 2008). Therefore, the PC12 cell has proven a suitable model for the functional study of neurotoxicity of compounds *in vitro* (Dingemans, *et al.* 2010, Heusinkveld, *et al.* 2013).

The SH-SY5Y cell line (Biedler, *et al.* 1973) is a well-studied neuroblastoma cell line from human origin and a widely used model to study chemical-induced neurotoxicity. The cells express tyrosine hydroxylase (TH), DAT and VMAT and synthesize DA and noradrenaline. Although SH-SY5Y cells reportedly release noradrenaline, there are no reports demonstrating vesicular release (i.e., exocytosis). As the cells express proteins implicated in both Alzheimer's disease (tau; Song and Ehrich 1998) and beta-amyloid; Huang, *et al.* 2011) and Parkinson's disease (α-synuclein; Choong and Say 2011), these cells are often used to study pathways of neurodegeneration.

The more recent MES23.5 cell line, developed by Crawford and co-workers in the early 1990's (Crawford 1992), is a product of somatic fusion of rat embryonic mesencephalon cells and the murine N18TG2 neuroblastoma-glioma cell line. The resulting hybrid cell line displays characteristics of mesencephalic dopaminergic neurons, such as expression of N-type VGCCs, DAT and TH as well as DA synthesis. As the cells also express α-synuclein, these cells are of interest for the study of (parkinsonian) dopaminergic neurodegeneration.

The N27 cell line is an immortalized rat mesencephalic dopaminergic cell line (Prasad, *et al.* 1994) used to study *in vitro* (parkinsonian) dopaminergic neurodegeneration (see e.g. Latchoumycandane, *et al.* 2011). N27 cells are derived from TH-positive fetal rat mesencephalic neurons and reportedly express DAT (Adams, *et al.* 1996).

As pesticides are implicated in dopaminergic neurodegeneration and the pathophysiology of PD both *in vivo* and *in vitro,* a reference set of five neurotoxic pesticides was composed consisting of rotenone, lindane, dieldrin, imazalil and dinoseb. Rotenone provides a well-known model compound for PD both *in vivo* and *in vitro* (see e.g. Greenamyre, *et al.* 2010). The organochlorine insecticides lindane and dieldrin are implicated in human PD and linked to *in vitro* neurotoxicity (Corrigan, *et al.* 2000, Heusinkveld and Westerink 2012). Furthermore, the azole fungicide imazalil was recently linked to disturbance of the intracellular calcium homeostasis (Heusinkveld, *et al.* 2013), whereas the dinitrophenolic herbicide dinoseb is linked to activation of pathways implicated in dopaminergic neurodegeneration *in vitro* (see: this thesis chapter 6.1).

As cell death and oxidative stress are clearly implicated in neurodegeneration (Goodwin, *et al.* 2013), we compared the (dopaminergic) cell lines with respect to effects on cell viability and production of reactive oxygen species (ROS) upon exposure to the reference set of five pesticides. In addition, Ca^{2+} plays a pivotal role in (dopaminergic) cells in neuronal function, development and survival (Gleichmann and Mattson 2011). Therefore, we also characterized the four cell lines with regards to functional parameters, such as the presence of functional neurotransmitter receptors and ion channels, as well as effects of the reference pesticides on basal- and depolarization-evoked changes in the intracellular Ca^{2+} concentration ($[Ca^{2+}]_i$)

Materials & Methods

Chemicals

Fura-2-AM, CFDA-AM and 2,7-dichlorodihydrofluorescein diacetate (H_2-DCF-DA) were obtained from Molecular Probes (Invitrogen, Breda, The Netherlands). Unless otherwise noted, all other chemicals were obtained from Sigma (Zwijndrecht, The Netherlands). The pesticides used as reference compounds (lindane, dieldrin, imazalil, dinoseb and rotenone) were obtained Pestanal® grade, 99.8% purity (Riedel de Haën, Seelze, Germany). Saline solutions, containing (in mM) 125 NaCl, 5.5 KCl, 2 $CaCl_2$, 0.8 $MgCl_2$, 10 HEPES, 24 glucose and 36.5 sucrose (pH 7.3), were prepared with de-ionized water (Milli-Q®; resistivity >18 MΩ•cm). Stock solutions of 2 mM ionomycin in DMSO were kept at 20°C. Stock solutions of 0.1-100 mM pesticide were prepared in DMSO and diluted in saline to obtain the desired concentrations just prior to the experiments (all solutions used in experiments, including control experiments, contained 0.1% DMSO).

Cell Culture

PC12 cells (Greene and Tischler 1976) were grown in RPMI 1640 (Invitrogen, Breda, The Netherlands) supplemented with 5% fetal calf serum (FCS) and 10% horse serum (HS; ICN Biomedicals, Zoetermeer, The Netherlands). MES23.5 hybridoma cells (kindly provided by Dr. S. Appel (Methodist Neurological Institute, Houston TX, USA)) were grown in DMEM (Invitrogen, Breda, The Netherlands) supplemented with 10% FCS, 2% HEPES and Satos supplements (Crawford 1992). Human SH-SY5Y cells (kindly provided by Dr. R. van Kesteren (VUmc, Amsterdam, The Netherlands)) were grown in 50/50 DMEM/F-12 medium (Invitrogen, Breda, The Netherlands) supplemented with 15% FCS. Rat N27 cells (kindly provided by Dr. JM Fuentes (Univ. de Extremadura, Caceres, Spain)) were cultured in RPMI 1640 supplemented with FCS (10%). All cells were grown for no more than 10 passages in a humidified incubator at 37°C and 5% CO_2. For cell viability experiments, cells were sub-cultured in poly-L-lysine coated 24-wells plates (Greiner Bio-one, Solingen, Germany) at a (near confluency) density of $5x10^5$ (PC12) or $2x10^5$ cells/well (MES23.5, SH-SY5Y and N27). For experiments assessing production of ROS, cells were sub-cultured in (poly-L-lysine coated) 48-wells plates (Greiner Bio-one, Solingen, Germany) at a (near confluency) density of $2.5x10^5$ (PC12) or $5x10^4$ (MES23.5, SH-SY5Y and N27) cells/well. For Ca^{2+} imaging experiments, cells were sub-cultured in poly-L-lysine coated glass-bottom dishes (MatTek, Ashland, MA) at a density of $1\text{-}1.5x10^6$ cells/dish.

Cell viability assays

Mitochondrial activity and membrane integrity were assessed as measures of cell viability using a combined alamar Blue (aB; resazurin-based) / CFDA-AM assay (non-specific cytoplasmic esterase activity; protocol adapted from Bopp and Lettieri 2007) as described previously (Heusinkveld, *et al.* 2013). Briefly, cells were exposed in serum- and phenol red-free medium to the reference pesticides (0.1 - 100 µM) for up to 24 hr. Mitochondrial activity of the cells was recorded with the aB assay. In the same experiment, membrane integrity was assessed using a CFDA-AM assay. Cells were incubated for 30-60 min with 12.5 µM aB and 4 µM CFDA-AM. Resorufin was measured spectrophotometrically at 540/590 nm, whereas hydrolysed CFDA was measured spectrophotometrically at 493/541 nm (Infinite M200 microplate; Tecan Trading AG, Männedorf, Switzerland).

Production of ROS

Basal production of reactive oxygen species and pesticide-induced oxidative stress were investigated using the fluorescent dye H_2-DCFDA as described previously (Heusinkveld, *et al.* 2013). Briefly, cells were loaded with 1.5 µM H_2-DCFDA for 30 min at 37°C. Subsequently, cells were exposed for up to 24 h to 0.1 - 100 µM of the reference pesticides and fluorescence was measured spectrophotometrically at 488/520 nm (Infinite M200 microplate; Tecan Trading AG, Männedorf, Switzerland).

Ca^{2+} imaging

Changes in $[Ca^{2+}]_i$ were measured on a single-cell level using the Ca^{2+}-sensitive fluorescent ratio dye Fura-2 AM as described previously (Heusinkveld and Westerink 2012, Heusinkveld, *et al.* 2013). Briefly, cells were loaded with 5 µM Fura-2 AM (Molecular Probes; Invitrogen, Breda, The Netherlands) for 20 min at room temperature, followed by 15 min de-esterification. After de-esterification, the cells were placed on the stage of an Axiovert 35M inverted microscope (Zeiss, Göttingen, Germany) equipped with a TILL Photonics Polychrome IV (TILL Photonics GmBH, Gräfelfing, Germany) under continuous superfusion. Fluorescence, evoked by 340 and 380 nm excitation wavelengths (F340 and F380), was collected every 6 s at 510 nm with an Image SensiCam digital camera (TILL Photonics GmBH).

To characterize the presence of neurotransmitter receptors and ion channels, cells were exposed to K^+ (100 mM), serotonin (5-HT; 100 µM) acetylcholine (ACh; 100 µM), glutamate (100 µM) or ATP (100 µM) following a 5 min baseline recording.

To test pesticide-induced effects on basal and depolarization-evoked $[Ca^{2+}]_i$, cells were depolarized by high-K^+ containing saline (100 mM K^+) for 18 s after a 5 min baseline recording. Following a 10 min recovery period, cells were exposed to DMSO (0.1 %), or one of the reference compounds for 20 min to evaluate the effects on basal $[Ca^{2+}]_i$. Subsequently, cells were depolarized for a second time to evaluate

effects of exposure on depolarization-evoked Ca^{2+}-influx. This is calculated as the treatment ratio (TR; %) between the first and second depolarization-evoked $[Ca^{2+}]_i$ peak values.

Data-analysis and statistics

Cell viability data is presented as % viability ± standard error of the mean (SEM) compared to control from at least three independent experiments consisting of at least three replicates per experiment. Data on production of ROS is presented as % increase in ROS ± SEM compared to time-matched controls from three independent experiments consisting of four replicates per experiment. A relevant effect size in cell viability and ROS experiments, indicated as lowest observed effect concentration (LOEC), is defined as the concentration that induces a ≥20% change in the parameter assessed.

Data from single-cell fluorescence microscopy is presented as F340/F380 ratio (R), reflecting changes in $[Ca^{2+}]_i$. and analysed using custom-made MS-Excel macros applying a correction for background fluorescence (Heusinkveld, *et al.* 2013). The data presented is based on average data from 15 – 63 individual cells (*n*) in 3 - 6 independent experiments (N).

Statistical analyses were performed using GraphPad Prism v6.01 (GraphPad Software, San Diego, California, USA). Concentration-response curves were fit in experiments assessing cell viability and ROS production using a nonlinear sigmoidal or bell-shaped curve-fit when applicable.

Results

Mitochondrial activity and membrane integrity

To assess differences between cellular responses to pesticide-exposure (0.1 - 100 µM; 24h), mitochondrial activity and membrane integrity were assessed using a combined alamar Blue (aB) and CFDA assay.

In PC12 cells, no change in mitochondrial activity or membrane integrity is observed upon exposure to lindane. Exposure to dieldrin induces a minor increase in mitochondrial activity in PC12 cells upon exposure to 10 µM, whereas membrane integrity is unchanged. Upon exposure to imazalil a concentration-dependent increase in mitochondrial activity is observed (LOEC: 1µM; Fig. 1A). The maximum increase in mitochondrial activity is paralleled by a decrease in membrane integrity (LOEC 100 µM, Fig. 2A). Exposure to dinoseb induced a bi-phasic change in mitochondrial activity starting with an increase (starting at 0.1 µM) followed by a decrease at higher concentrations (≥ 10 µM; Fig 1A). The decrease in mitochondrial activity is paralleled by a decrease in membrane integrity (LOEC: 10 µM; Fig. 2A). Likewise, rotenone induced a bi-phasic change in mitochondrial activity (LOEC: 0.1 µM; Fig. 1A) paralleled by a decrease in membrane integrity (LOEC: 1 µM; Fig.2A).

In SH-SY5Y cells, no change in mitochondrial activity or membrane integrity is observed upon exposure to lindane. Exposure to dieldrin and imazalil induced an increase in mitochondrial activity (both LOEC: 10 µM; Fig. 1B), whereas no change in membrane integrity was observed (Fig. 2B). In contrast, upon exposure to dinoseb a decrease in mitochondrial activity is observed (LOEC 100 µM; Fig. 1B), whereas membrane integrity was not changed (Fig. 2B). Also upon exposure to rotenone, a concentration-dependent decrease in mitochondrial activity was observed (LOEC: 1 µM; Fig. 1B), which is paralleled by a decrease in membrane integrity at 100 µM (Fig. 2B).

In MES23.5 cells exposure to lindane did not result in a change in mitochondrial activity. However, a small decrease in membrane integrity was observed at 100 µM. Exposure to dieldrin induced a bi-phasic change in mitochondrial activity starting with an increase (at 0.1 µM) followed by a decrease at higher concentrations (≥ 10 µM) (Fig. 1C). The decrease in mitochondrial activity is paralleled by a decrease in membrane integrity (LOEC: 10 µM; Fig. 2C). Exposure to imazalil induced a minor increase in mitochondrial activity upon exposure to 100 µM (Fig. 1C), paralleled by a decrease in membrane integrity (Fig 2C). Upon exposure to dinoseb a decrease in both mitochondrial activity and membrane integrity is observed (LOEC 100 µM and 10 µM resp.; Fig. 1C & 2C resp.). Also upon exposure to rotenone, a concentration-dependent decrease in mitochondrial activity was observed (LOEC: 1 µM ; Fig. 1C), paralleled by a decrease in membrane integrity (LOEC: 1 µM ; Fig. 2C).

In N27 cells, exposure to lindane did not change mitochondrial activity or membrane integrity. Exposure to dieldrin induced a bi-phasic change in mitochondrial

activity starting with an increase (at 0.1 μM) followed by a decrease at higher concentrations (≥ 10 μM), without changes in membrane integrity. Upon exposure to imazalil a concentration-dependent increase in mitochondrial activity was observed (LOEC: 10 μM; Fig. 1D), which was paralleled by a decrease in membrane integrity, but only at highest concentration (LOEC 100 μM; Fig. 2D). Exposure to dinoseb induced a bi-phasic change in mitochondrial activity starting with an increase (at 0.1 μM) followed by a decrease at higher concentrations (≥ 10 μM) (Fig. 1D). A change in membrane integrity upon exposure to dinoseb was only observed at the highest concentration (100 μM; Fig. 2D). Likewise, rotenone induced a bi-phasic change in mitochondrial activity starting with an increase (at 0.1 μM) followed by a decrease at higher concentrations (≥ 1 μM) (Fig. 1D), paralleled by a concentration-dependent decrease in membrane integrity (LOEC: 1 μM; Fig. 2D).

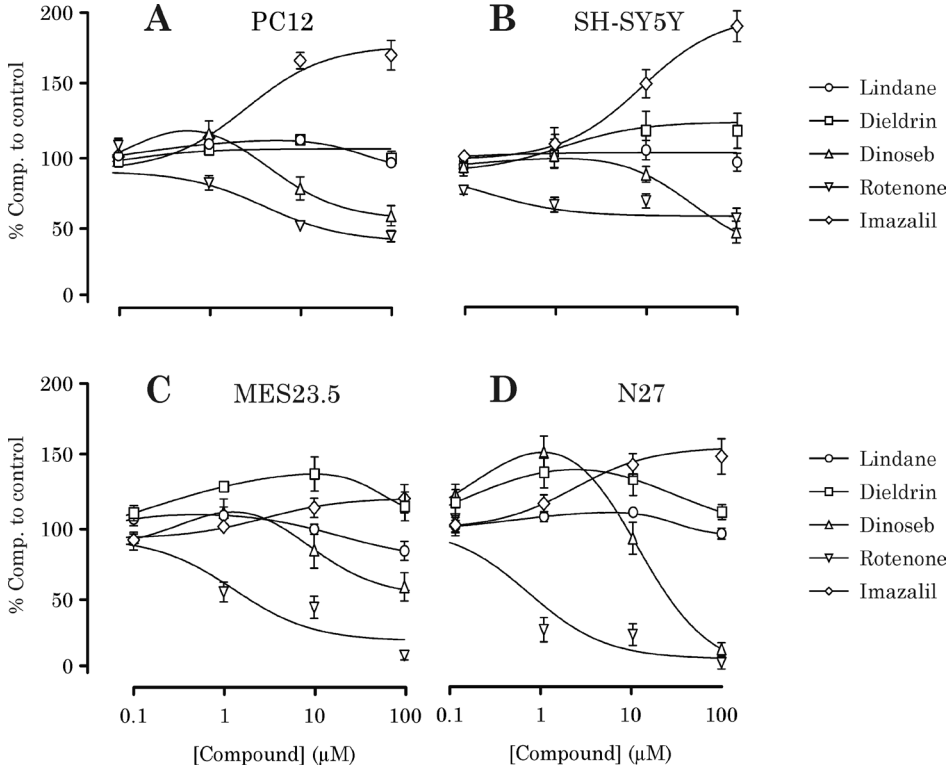

Figure 1. Differential effects of selected pesticides on mitochondrial activity as a measure of cell viability in PC12 (A), SH-SY5Y (B), MES23.5 (C) and N27 (D) cells following 24h of exposure to lindane (●), dieldrin (□), dinoseb (Δ), rotenone (▼), imazalil ( ). Several different concentration-dependent changes in mitochondrial activity can be observed in the various cell lines upon exposure to selected pesticides. Data points in the concentration-response curves represent the average percentage mitochondrial activity (±SEM; ≥3 independent experiments) compared to control

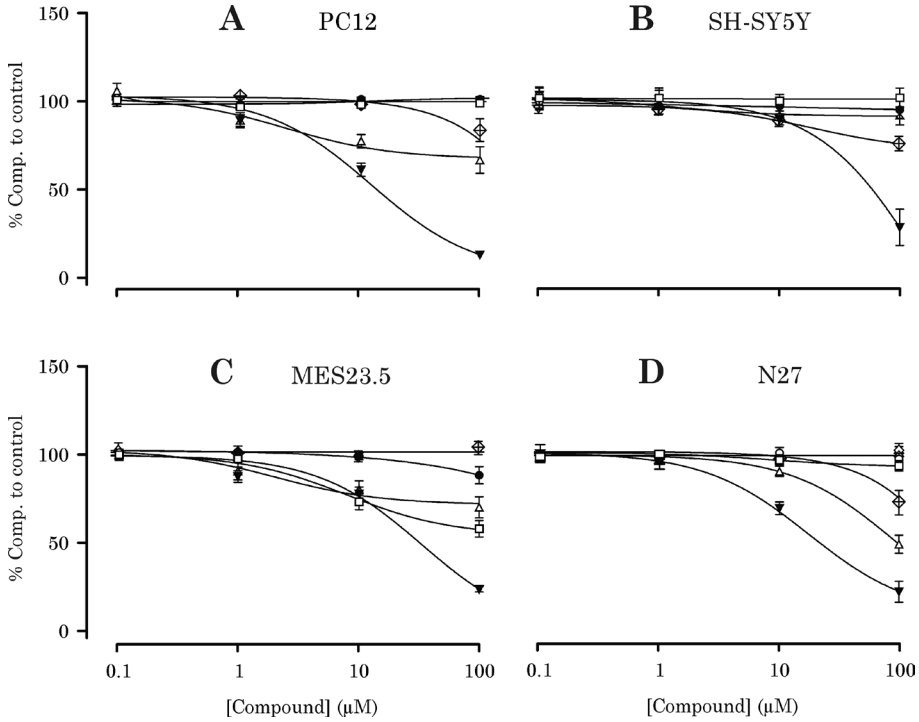

Figure 2. Differential on membrane integrity as a measure of cell viability in PC12 (A), SH-SY5Y (B), MES23.5 (C) and N27 (D) cells following 24h of exposure to lindane (●), dieldrin (□), dinoseb (Δ), rotenone (▼), imazalil ( ). It can be observed that the effects induced by particular pesticides differ between the cell lines assessed. Data points in the concentration-response curves represent the average percentage cell viability (±SEM; ≥3 independent experiments) compared to control.

ROS production

Increased production of reactive oxygen species and oxidative stress are clearly implicated in pathways of dopaminergic neurodegeneration (Goodwin, *et al.* 2013). As cell lines may differ in their coping with oxidative stress and thus in their sensitivity for oxidative insults, the production of reactive oxygen species upon exposure to a concentration range (0.1 - 100 µM) of the reference pesticides for 24h was assessed in the different cell lines.

In PC12 cells, exposure to lindane or dieldrin did not result in an increase in ROS production. However, an increase in ROS production was observed upon exposure to imazalil (LOEC: 100 µM; Fig. 3A), dinoseb (LOEC: 100 µM; Fig. 3A) and rotenone (LOEC: 10 µM; Fig. 3A). In SH-SY5Y cells, exposure to lindane, dieldrin and imazalil did not change ROS production. However, rotenone as well as dinoseb induced ROS production (both LOEC: 10 µM; Fig. 3B).

In MES23.5 cells, lindane, dieldrin and imazalil did not change ROS production, whereas both rotenone and dinoseb induced ROS production (both LOEC: 10 µM; Fig. 3C). In line with the results in both SH-SY5Y and MES23.5 cells, lindane, dieldrin and imazalil did not change ROS production in N27 cells, whereas exposure to rotenone and dinoseb induced an increase in ROS production (both LOEC 10 µM) (Fig. 3D).

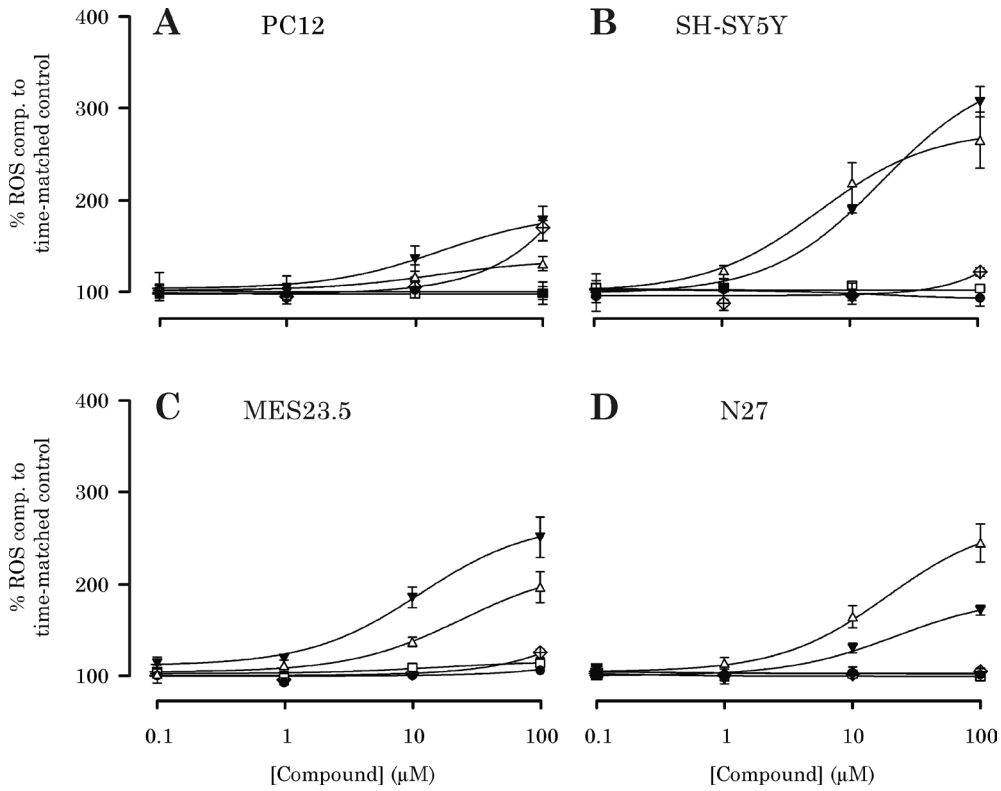

Figure 3. Differential changes in ROS production in PC12 (A), SH-SY5Y (B), MES23.5 (C) and N27 (D) cells following 24h of exposure to lindane (●), dieldrin (□), dinoseb (Δ), rotenone (▼), imazalil ( ). The data points in the concentration-response curves represent average percentage ROS production (±SEM; from ≥3 individual experiments) compared to time-matched control.

Characterization of neurotransmitter receptors and ion channels

To characterize the different cell lines with respect to the presence of (Ca^{2+}-permeable) receptors and ion channels, cell lines were stimulated with different stimuli and $[Ca^{2+}]_i$ was monitored using single-cell fluorescence microscopy.

The results demonstrate that PC12 displayed an increase in $[Ca^{2+}]_i$ upon depolarization with 100 mM K^+ (Fig. 4) indicative of the presence of VGCCs. Also, PC12 cells displayed an increase in $[Ca^{2+}]_i$ upon stimulation with 100 µM ACh and 100 µM ATP (Fig. 4), indicative of the presence of Ca^{2+}-permeable nicotinic ACh receptors (nACh-R) and P2 purinergic receptors, respectively. No increase in $[Ca^{2+}]_i$ was observed upon stimulation with serotonin (5-HT; 100 µM) or glutamate (100 µM) (Fig. 4).

SH-SY5Y cells also displayed an increase in $[Ca^{2+}]_i$ upon depolarization with K+ and ACh (Fig. 4), whereas they did not respond to stimulation with ATP, 5-HT or glutamate (Fig. 4).

Likewise, MES23.5 cells displayed an increase in $[Ca^{2+}]_i$ upon depolarization with K^+ and stimulation with ACh, but also upon stimulation with ATP and 5-HT. No change in $[Ca^{2+}]_i$ was observed upon stimulation with glutamate.

N27 cells did not respond to K^+-induced depolarization or to stimulation with ACh, 5-HT or glutamate (Fig. 4). However, N27 cells displayed an increase in $[Ca^{2+}]_i$ upon stimulation with ATP (Fig. 4).

The observation that none of these cell lines responded to stimulation with 100 µM glutamate either in the presence or absence of K^+ to remove the potential Mg^{2+} block, indicates the absence of functional ionotropic glutamate receptors in these cell lines (Fig. 4).

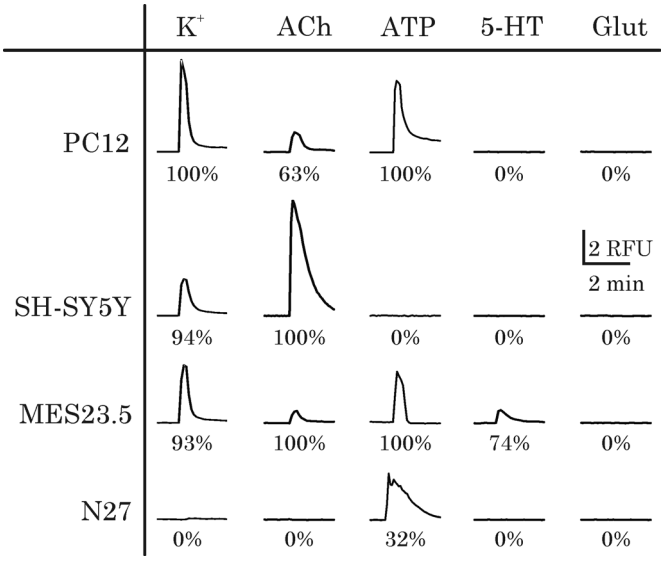

Figure 4 Average traces of the increase in $[Ca^{2+}]_i$ observed in the cell lines upon exposure to different stimuli. Percentages indicated below the traces represent the fraction of cells that responded to the particular stimulus (3-6 independent experiments; 15 – 63 individual cells).

Pesticide-induced changes in basal Ca^{2+}

The concentrations of the pesticides applied were chosen based on pilot experiments or previous results in which they were proven effective in PC12 cells without overt acute cytotoxicity (Heusinkveld and Westerink 2012, Heusinkveld, *et al.* 2010, Heusinkveld, *et al.* 2013).

In PC12 cells, exposure to 100 µM lindane resulted in an increase in basal $[Ca^{2+}]_i$. Also, exposure to 30 µM dinoseb induced an increase in basal [Ca2+]i (Fig 5). 10 µM dieldrin, 10 µM rotenone or 30 µM imazalil did not induce a change in basal $[Ca^{2+}]_i$ (Fig. 5). In contrast, exposure to 100 µM lindane did not induce a change in basal $[Ca^{2+}]_i$ in SH-SY5Y cells, whereas exposure to 30 µM dinoseb induced a bi-phasic increase in basal $[Ca^{2+}]_i$ with a fast transient increase followed by a sustained elevated level of $[Ca^{2+}]_i$ (Fig. 5). Exposure to 10 µM dieldrin, 10 µM rotenone or 30 µM imazalil did not change basal $[Ca^{2+}]_i$ in SH-SY5Y cells.

Also in MES23.5 cells, no effect of exposure to lindane on basal $[Ca^{2+}]_i$ was observed, whereas exposure to 30 µM dinoseb induced a transient increase in basal $[Ca^{2+}]_i$ (Fig. 5). No effect was observed upon exposure to 10 µM dieldrin, 10 µM rotenone or 30 µM imazalil.

Similarly, in N27 cells, no effect of exposure to 100 µM lindane was observed, whereas exposure to 30 µM dinoseb induced a transient increase in basal $[Ca^{2+}]_i$ (Fig. 5). No effect was observed upon exposure to 10 µM dieldrin, 10 µM rotenone or 30 µM imazalil.

Pesticide-induced changes in depolarization-evoked Ca^{2+}

In PC12 cells, depolarization with 100mM K^+ resulted in a fast, transient increase in $[Ca^{2+}]_i$ due to opening of VGCCs that rapidly recovered to near-baseline values. Repeated depolarization in control cells resulted in a treatment ratio (TR) of ~90%. Exposure to 100 µM lindane induced a decrease in depolarization-evoked $[Ca^{2+}]_i$ (Fig. 5). Upon exposure to 30 µM dinoseb, no change in depolarization-evoked [Ca2+]i was observed, whereas 10 µM dieldrin, 10 µM rotenone and 30 µM imazalil inhibited the depolarization-evoked $[Ca^{2+}]_i$ (Fig. 5).

SH-SY5Y cells also displayed a fast and transient increase in $[Ca^{2+}]_i$ upon depolarization, whereas repeated depolarization resulted in a TR of ~65%. In line with the effect observed in PC12 cells, exposure to lindane resulted in an inhibition of depolarization-evoked $[Ca^{2+}]_i$ (Fig. 5). Similarly, dinoseb, dieldrin, rotenone, and imazalil also inhibited VGCC opening upon depolarization (Fig. 5).

MES23.5 cells also displayed a fast and transient increase in $[Ca^{2+}]_i$ upon depolarization, with a TR of ~90% upon repeated depolarization. In line with the other cell lines, lindane inhibited the depolarization-evoked Ca^{2+}-influx in MES23.5 cells (Fig. 5). However, upon exposure to dinoseb in MES23.5 cells an increase in depolarization-evoked Ca^{2+}-influx was observed (Fig. 5).

In line with the results obtained in PC12 and SH-SY5Y cells, exposure to dieldrin, rotenone and imazalil resulted in an inhibition of depolarization-evoked Ca^{2+}-influx (Fig. 5).

As the characterization experiments (Fig. 4) revealed the absence of functional VGCCs in N27 cells, effects on depolarization-evoked Ca^{2+}-influx could not be tested in N27 cells.

Figure 5 (next page) Differential effects of pesticides on basal and depolarization-evoked $[Ca^{2+}]_i$. A Example traces of cytosolic $[Ca^{2+}]_i$ of individual PC12 cells, illustrating the inhibition of the second depolarization-evoked increase in $[Ca^{2+}]_i$ (K2) during exposure to DMSO (upper trace, control), 10 μM rotenone (middle trace) and 100 μM lindane (lower trace). B Summary table of effects of the five reference pesticides on basal and depolarization-evoked $[Ca^{2+}]_i$ in the different cell lines. ↑ Indicates an increase in $[Ca^{2+}]_i$ (≥25%), whereas ↓ indicates a decrease (↓: decrease ≤50%; ↓↓: decrease ≤75%; ↓↓↓: decrease >75%), = indicates that no changes were observed. (T) indicates a transient increase in basal $[Ca^{2+}]_i$, whereas (S) indicates a sustained increase in $[Ca^{2+}]_i$.

A

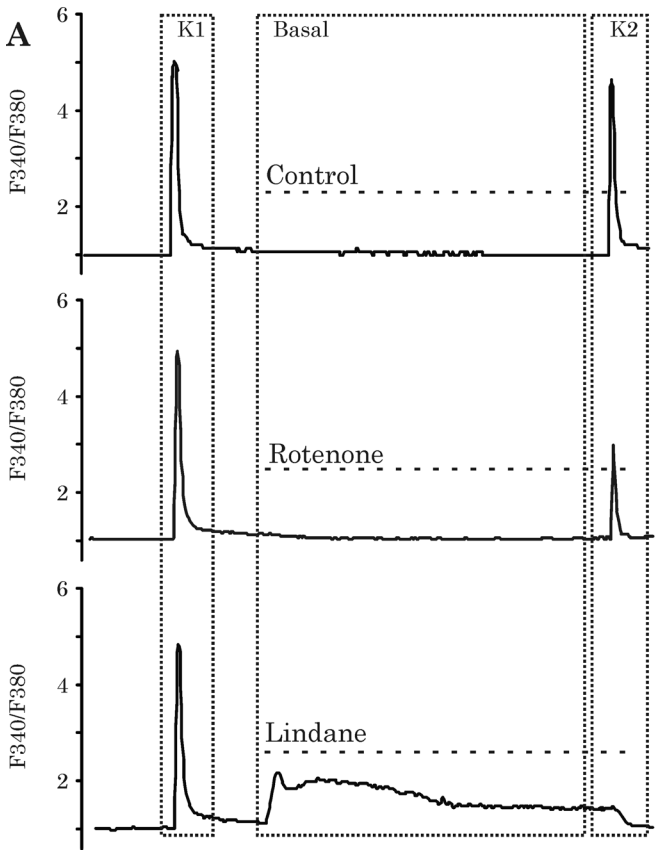

B

Cell line	Compound	Basal $[Ca^{2+}]_i$	K^+-evoked $[Ca^{2+}]_i$ (K2)
PC12	Lindane	↑(S)	↓↓↓
	Dinoseb	↑(T)	=
	Dieldrin	=	↓↓↓
	Rotenone	=	↓↓
	Imazalil	=	↓↓↓
SH-SY5Y	Lindane	=	↓↓
	Dinoseb	↑(S)	↓↓
	Dieldrin	=	↓↓↓
	Rotenone	=	↓↓
	Imazalil	=	↓↓
MES23.5	Lindane	=	↓
	Dinoseb	↑(T)	↑
	Dieldrin	=	↓↓↓
	Rotenone	=	↓↓
	Imazalil	=	↓↓↓
N27	Lindane	=	n.a.
	Dinoseb	↑(T)	n.a.
	Dieldrin	=	n.a.
	Rotenone	=	n.a.
	Imazalil	=	n.a.

Discussion

In this study we compared 4 different neuronal cell lines with respect to functional characteristics and toxicity of five neurotoxic pesticides. The results clearly indicate that the observed effects of a compound depend on the cell line used and are thus likely related to intrinsic properties of the cell line, such as the expression of ion channels and receptors.

The results from the experiments assessing mitochondrial activity and membrane integrity demonstrate clear differences in sensitivity between cell lines. This is illustrated by the observation of increased mitochondrial activity upon exposure to the organochlorine insecticide dieldrin in MES23.5 and N27 cells (LOEC: 0.1 μM for both cell lines), whereas this effect is less in SH-SY5Y cells (LOEC: 10 μM) and largely absent in PC12 cells. In addition, exposure to dieldrin only induced a change in membrane integrity in MES23.5, whereas in other cell lines membrane integrity was not changed. Likewise, exposure to lindane did not change mitochondrial activity in either of the cell lines, whereas only in MES23.5 cells a decrease in membrane integrity was observed upon exposure to 100 μM.

The results from the experiments assessing ROS production also indicate differences among the cell lines, although less pronounced. This is illustrated by the observation that imazalil-induced ROS is limited to PC12 cells only, whereas rotenone and dinoseb induce ROS production in all cell lines, though with small differences in effect concentration. In contrast, lindane and dieldrin do not induce ROS production in either of the cell lines.

All in all, the conclusion can be drawn that these cell lines display considerable differences in sensitivity towards toxicity of the reference set of pesticides. Remarkably, SH-SY5Y cells appear relatively insensitive in the cytotoxicity assay, while these cells display the largest relative increase in ROS production (Fig 3). Interestingly, the MES23.5 cells display a specific sensitivity towards effects on membrane integrity and cell death related to lindane and dieldrin exposure.

Calcium plays a pivotal role in many inter- and intraneuronal processes, including gene transcription (Carrasco and Hidalgo 2006), neurotransmission (Westerink 2006), neurodegeneration (Mattson 2012) and neurodevelopment (Pravettoni, *et al.* 2000). The observation that PC12, MES23.5 and SH-SY5Y cells respond to high-K^+-induced depolarization and thus express VGCCs is in line with other research (Reuveny and Narahashi 1991, Schneider, *et al.* 1995, Shafer and Atchison 1991). However, the types of VGCCs expressed differ among the cell lines as PC12 cells contain L-, N- and P/Q-type VGCCs (Dingemans, *et al.* 2009, Heusinkveld, *et al.* 2010), whereas SH-SY5Y cells are reported to contain L- and N-type VGCCs (Reuveny and Narahashi 1991) and MES23.5 cells reportedly contain predominantly N-type VGCCs (Schneider, *et al.* 1995). As N27 cells do not respond to high-

K^+ induced depolarization, we conclude that N27 do not express functional VGCCs. The absence of reports in literature describing the presence of functional VGCCs in N27 cells appears to confirm our observation.

Considering the responses of the cell lines to the stimuli applied (Fig. 3B), considerable differences in channel/receptor expression exist between the cell lines with MES23.5 cells being the most- and N27 cells the least versatile. Importantly, no response to glutamate was observed in either of the cell lines. This indicates that neither of these cell lines can be used to study effects of compounds on glutamate-mediated (excito-) toxicity. Consequently, the study of this important pathway of neurotoxicity requires other (primary) cell models. This illustrates the importance of characterization of cell lines as the presence or absence of a toxic response clearly can depend on the presence of receptors of (ion) channels. It is known that the observed increase in basal $[Ca^{2+}]_i$ in PC12 cells upon exposure to lindane is related to a lindane-induced depolarization of the membrane causing opening of ω-conotoxin sensitive high-voltage activated VGCCs (N- and P/Q-type) (Heusinkveld, *et al.* 2010). Therefore, the absence of a lindane-induced effect in SH-SY5Y and MES23.5 cells on basal $[Ca^{2+}]_i$ can be explained by the absence of responsible VGCCs, a difference in resting membrane potential, or both. As MES23.5 and SH-SY5Y cells are reported to contain N-type VGCCs, the latter argument is more likely. In PC12 cells, exposure to 30 μM lindane was demonstrated to induce a membrane depolarization of 32 ± 7 mV (Heusinkveld, *et al.* 2010). This is apparently enough to reach the activation potential (V_a; Catterall, *et al.* 2005) of the N- and P/Q-type VGCCs and to cause a Ca^{2+}-influx. As MES23.5 and SH-SY5Y contain N-type VGCCs, but also have a slightly more negative membrane potential (see: Colom, *et al.* 1998 & Åkerman, *et al.* 1984) the V_a is possibly not reached in these cells explaining the absence of lindane-induced Ca^{2+} influx.

The intercellular differences in VGCC composition and intracellular Ca^{2+} handling are also reflected in the observation that repeated high K^+-induced depolarization in control PC12 and MES23.5 cells results in a TR of ~90%, whereas in control SH-SY5Y cells a TR of ~65% is detected. Also, the differences observed in the depolarization-induced increase in $[Ca^{2+}]_i$ upon exposure to dinoseb (MES23.5: increase; PC12: no effect) are likely explained by differences in intracellular Ca^{2+} handling. The observed decrease observed in SH-SY5Y cells is most likely related to inhibition of VGCCs due to the sustained increase in $[Ca^{2+}]_i$.

All *in vitro* models provide their advantages and disadvantages. The functional properties of PC12 cells may render these cells the model of choice for the study of chemical-induced effects on Ca^{2+}-homeostasis and vesicular neurotransmission. However, as important VGCCs are also present in MES23.5 and SH-SY5Y cells, effects on VGCC-subtypes can be assessed in these cell lines as well. In conclusion, care should be taken when interpreting toxicity data as the intrinsic properties of a cell line may strongly influence the outcome. Therefore, it seems justified to state that the research question should determine which model is the most appropriate.

Science may be described as the art of
systematic oversimplification

Karl Popper

Chapter 9

Discussion, risk assessment and conclusion

Chapter 9.1 – Summary and general discussion

This thesis aimed at identifying pathways of toxicity that may link pesticide exposure to neuronal dysfunction and neurodegeneration. The foregoing chapters described the effects of a selection of compounds from three different classes of pesticides on parameters of (dopaminergic) neurotoxicity *in vitro*.

Considering the pivotal role of calcium in many processes, including degeneration in neuronal cells, calcium is a sensible endpoint of choice (Bezprozvanny 2009, Chan, *et al.* 2009). Default measurements of the intracellular calcium homeostasis are microscopy-based single cell approaches, which are slow and labour-intensive but sensitive and with high spatial and temporal resolution. As many existing high-throughput assays, such as those for cell viability and oxidative stress, do not assess specific (functional) neurotoxicological endpoints, attempts have been to made to measure intracellular calcium in a high-throughput manner. In chapter 4 we demonstrated that the high-throughput approach of intracellular calcium is nevertheless related to many pitfalls rendering high-throughput measurements of intracellular calcium hardly interpretable.

In chapter 5 we therefore used single-cell fluorescent Ca^{2+}-imaging to demonstrate that lindane has dual effects on the intracellular calcium homeostasis and vesicular dopamine release (chapter 5.1; Table 1). In addition to the well-known inhibitory effects on the GABA receptor (Vale, *et al.* 2003), we demonstrated that lindane causes a depolarization of the membrane, thereby evoking an increase in basal Ca^{2+} that is linked to dopamine release. Also, lindane causes a (non-specific) inhibition of VGCCs resulting in inhibition of depolarization-evoked Ca^{2+} influx and dopamine release. Dieldrin has comparable inhibitory effects on VGCCs (chapter 5.2), though with a two-order of magnitude higher potency (Table 1). In contrast to lindane, the effect of dieldrin on depolarization-evoked Ca^{2+} influx depends on (intracellular) accumulation since it increases over time. Also, we demonstrated that mixtures of lindane and dieldrin have additive effects on the inhibition of depolarization-evoked Ca^{2+}-influx. However, dieldrin inhibits the lindane-induced increase in basal Ca^{2+}, though dieldrin itself does not change basal $[Ca^{2+}]_i$.

These findings are of importance because both the organochlorine insecticides lindane and dieldrin are linked to PD and are detected in considerable amounts in the brain of PD patients (Corrigan, *et al.* 1996, Corrigan, *et al.* 2000). Notably in this respect, dieldrin and lindane are still abundant in the environment and food chain (Sonne 2010, Roche, *et al.* 2008), despite the ban on these compounds.

In chapter 6.1, we described *in vitro* experiments demonstrating functional deficits that are potentially linked to neurodegeneration in cells exposed to dinitro-

phenolic herbicides. Both DNOC and dinoseb caused endoplasmic reticulum (ER) stress as demonstrated by the release of Ca^{2+} from the ER upon acute exposure (Table 1). This acute effect is linked to an increase in apoptosis (caspase-3 activity) and moderate cytotoxicity in the absence of overt oxidative stress. Importantly, following exposure to DNOC and dinoseb we observed an increase in α-synuclein, a marker of parkinsonian degeneration in dopaminergic neurons. In addition to *in vitro* dopaminergic neurotoxicity, dinitrophenolic herbicides are also demonstrated to affect GABA-ergic neurotransmission by modulation of GABA-evoked membrane currents (chapter 6.2; Table 1). This is of interest because other compounds implicated in the aetiology of PD, such as lindane, dieldrin and MPP^+, are also known to interfere with GABA-ergic neurotransmission (Vale, *et al.* 2003, Wu, *et al.* 2002).

Nowadays, pesticidal use of lindane and dieldrin, as well as the use of dinitrophenolic compounds as herbicides, has been phased-out. Current human exposure is therefore mainly limited to food-borne exposure as a consequence of the persistence of lindane and dieldrin and occupational exposure to dinitrophenolic compounds due to the continuing use in e.g. plastic industry.

Azole fungicides on the contrary, are currently widely used in agriculture in both pre- and post-harvest applications as well as in human and veterinary medicine. In the Netherlands, fungicides comprise over fifty percent of the total amount of pesticides used (Source: De Snoo and Vijver; Bestrijdingsmiddelenatlas v2.0). Pesticidal residues of members of this group of compounds are detected regularly on food products (up to 10 µg/kg fresh product; see e.g. Blasco, *et al.* 2006, Nougadère, *et al.* 2012). Therefore, this class of compounds also comprises a part of our day-to-day chemical exposure. Upon exposure in our cell model, azole fungicides induced limited cytotoxicity and limited oxidative stress, though 5 out of 6 induced an inhibition of VGCCs (chapter 7; Table 1). Subsequent experiments with binary and quaternary mixtures of azole fungicides indicated that additivity applies for the observed effects on VGCC inhibition.

The majority of the research presented in this thesis has been performed in a model of mature dopaminergic neurons; PC12 cells. However, this cell model is often criticized for its non-human and adrenal, and hence non-neuronal, origin. Nevertheless, its characteristics render the PC12 cell a suitable model for the study of dopaminergic neurotoxicity (Shafer and Atchison 1991, Westerink and Ewing 2008). As other cell models are available, we compared three alternative (dopaminergic) cell models (human SH-SY5Y, hybrid MES23.5 and rat N27) to the PC12 cell for their functional properties (receptors and channels; calcium homeostasis). In addition, we compared the effect of five neurotoxic reference pesticides (lindane, dieldrin, rotenone, imazalil and dinoseb) on cell viability and oxidative stress in these different cell lines (chapter 8). The results demonstrate that the properties of the four investigated cell lines differ considerably with respect to ion-

channel and neurotransmitter receptor expression. Moreover, the effects induced by the selected reference pesticides on cell viability and oxidative stress differed among the cell lines. This likely relates to differences in intrinsic properties that underlie differences in vulnerability for toxic insults.

As insecticides are aimed at attacking the insects' nervous system, these compounds are neurotoxic by nature. Therefore, there is a considerable body of knowledge regarding the neurotoxicity of several classes of insecticides, such as organochlorine insecticides (see e.g. Bloomquist, *et al.* 2002, Kaushik and Kaushik 2007). The main body of knowledge about neurotoxicity of pesticides comprises information about the primary mode-of-action of insecticides (e.g. GABA-R inhibition induced by organochlorines). However, less is known about the effects of these compounds on other important neurotoxic endpoints, such as intracellular calcium homeostasis and effects on processes involved in neurodegeneration. Furthermore, the amount of available knowledge is considerably less for classes of compounds that are not primarily directed at a process or target relevant for humans, such as e.g. herbicides and fungicides.

The neurotoxic effects reported in chapters 5-7 clearly indicate that pesticides can have differential neurotoxic effects on dopaminergic neurotransmission and cellular health, beyond the well-known primary mode-of-action. However, the exact relationship between the observed effects and dopaminergic neurodegeneration as observed in PD and parkinsonisms remains elusive.

Dopaminergic neurotransmission in the basal ganglia is a complex system that involves several different pathways, brain areas and cell types (Obeso, *et al.* 2008, Rice, *et al.* 2011, Roeper 2013). PD becomes clinically manifest when at least 50% of the dopaminergic neurons in the nigrostriatal pathway (Fig 2, chapter 1) is lost (Braak, *et al.* 2003, Lees, *et al.* 2009). Epidemiological studies demonstrated that environmental factors, including exposure to pesticides, are implicated in the aetiology of PD. This has been underlined by observations of specific degeneration of dopaminergic midbrain neurons upon exposure to compounds such as MPTP and rotenone. Yet, why dopaminergic neurons in the substantia nigra (SN) are selectively vulnerable for degeneration is still puzzling scientists. Hypotheses addressing this question are either directed at intrinsic properties of the dopaminergic neurons in the SN_{pc} (cell-autonomous) or at characteristics and interactions within the structures and brain areas involved (non-cell autonomous).

Cell and non-cell autonomous pathways in PD

Early theories on particular vulnerability of dopaminergic neurons in SN_{pc} focussed on a high oxidative burden in dopaminergic cells in general as a result of DA handling and oxidation of cytosolic DA. Additionally, mitochondrial dysfunction has been indicated as an important pathway in the pathophysiology of PD. However, it is debatable whether the high oxidative burden and mitochondrial

function are causative factors since these are not specific for dopaminergic neurons in SN_{pc}.

Consequently, SN_{pc} dopaminergic neurons must have distinctive (functional) properties that, upon disturbance or malfunction, lead to selective degeneration of the SN_{pc} and the development of idiopathic PD. One of the things that distinguishes dopaminergic neurons in the SN_{pc} from other dopaminergic neurons in the CNS and the basal ganglia is a constant level of spontaneous activity; pacemaking (Guzman, *et al.* 2009, Imtiaz 2012). Dopaminergic neurons in the SN_{pc} generate action potentials on a rhythmic basis, thereby providing a constant dopaminergic input from the SN to the striatum. This process is held responsible for the maintenance of DA levels in the striatum and basal ganglia (Imtiaz 2012) and in that sense for the fine-tuning of neurotransmission. Pacemaking activity in the SN_{pc} involves a particular subtype of the dihydropyridine-sensitive high-voltage activated (HVA) Cav 1.3 (L-type) VGCCs (Chan, *et al.* 2007, Guzman, *et al.* 2009, Putzier, *et al.* 2009). In contrast, dopaminergic neurons in the neighbouring VTA depend largely on sodium channels for pacemaking activity (Chan, *et al.* 2007, Imtiaz 2012). Moreover, influx of Ca^{2+} through Cav 1.3 VGCCs increases DA metabolism leading to elevated cytosolic DA concentrations and created mitochondrial oxidative stress that was specific for SN_{pc} neurons (Mosharov, *et al.* 2009). Notably, other brain areas that experience cell loss parallel to the SN_{pc} in PD such as the locus coeruleus and the hypothalamus (Braak, *et al.* 2003) are also autonomous Ca^{2+}-dependent pacemakers (for review see: Surmeier, *et al.* 2011). The Ca^{2+}-dependence of autonomous pacemaking thus provides a plausible explanation for the specific vulnerability of dopaminergic neurons in the SN_{pc}.

Dopaminergic neurotransmission in the basal ganglia is regulated by a network that primarily consists of excitatory input from glutamatergic neurons and inhibitory input from GABA-ergic neurons. Unbalance in excitatory- and inhibitory input in the neuronal network of the basal ganglia is implicated in PD (Dexter and Jenner 2013). Importantly, chemical dopaminergic degeneration can be prevented by inhibition of glutamate receptors (Turski, *et al.* 1991), suggesting the involvement of excitotoxicity caused by glutamatergic over-excitation in the pathophysiology of PD (Dexter and Jenner 2013). However, excitotoxicity is considered merely a consequence of the degenerative process that is responsible for the disease progression (Blandini, *et al.* 2000). Notably, inhibitory input from GABA-ergic neurons is responsible for negative regulation of glutamatergic stimulation from the sub thalamic nucleus (STN). It is therefore likely that chemical interference with GABA-ergic neurotransmission, as observed for lindane and dieldrin (Vale, *et al.* 2003), MPP^+ (Wu, *et al.* 2002) and dinitrophenolic herbicides (this thesis chapter 6.2), can change the negative feedback thereby leading to glutamatergic overstimulation and excitotoxicity.

PD is often referred to as proteinopathy because of the distinctive role of proteins and protein depositions in its pathophysiology. PD is characterized by intracellular protein-rich inclusions, called Lewy-bodies, that consist mainly of α-synuclein (see e.g. Breydo, *et al.* 2012). It is known that ER-stress is related to misfolding of proteins, including α-synuclein, whereas excess oxidative stress and mitochondrial dysfunction is related to hampered protein degradation resulting in fibrilisation and aggregation of proteins in the cytoplasm (Goodwin, *et al.* 2013, Nath, *et al.* 2011). This is a dangerous process as pathogenic α-synuclein, which can be transferred from one cell to another in a prion-like manner (Dunning, *et al.* 2012, Yasuda, *et al.* 2013), is related to a change in intracellular DA handling, increased mitochondrial and ER-stress and cell death (Goodwin, *et al.* 2013, Wilkaniec, *et al.* 2013). A local change in α-synuclein production, as observed *in vitro* with dinitrophenolic herbicides (this thesis chapter 6.1), may thus result in the onset of a cascade that results in spreading of pathogenic proteins through the brain.

It has been demonstrated extensively *in vitro* as well as *in vivo* in animals and humans that neurodegenerative disorders (including PD) are associated with activation of glia and astrocytes resulting in inflammation (Purisai, *et al.* 2007, Tansey and Goldberg 2010, Taylor, *et al.* 2013). The notion that the immune system is involved in the aetiology of PD is underlined by the observation that non-aspirin NSAIDs are neuroprotective (Gagne and Power 2010). Additionally, peripheral inflammation is observed to influence neurodegeneration-associated brain inflammation (Hernández-Romero, *et al.* 2012). However, it remains to be determined whether central and peripheral inflammation are the cause or consequence of the degenerative process in the brain.

Considering the wide array of above mentioned factors, the dopaminergic system of the basal ganglia is best described by a delicately balanced complex system with special features that render the SN_{pc} dopaminergic neurons more vulnerable than others. The role of environmental factors, including pesticides, in idiopathic PD is therefore probably best explained by a multi-hit model in which no single factor or compound is causative but a complex interplay between exposure to environmental factors, individual genetic susceptibility, and specific vulnerability of the dopaminergic pathways in the basal ganglia determines the disease process.

The role of pesticides in PD

As stated before, it is known from epidemiology that pesticide exposure is related to an increased risk for the development of PD. The discovery of MPTP and rotenone causing PD *in vivo* illustrates that chemicals can be responsible for the specific degeneration of the brain areas implicated in PD. However, as the likelihood of exposure to MPTP and rotenone is very low for the general population and both compounds are linked to acute development of PD, the role of pesticides in slowly developing idiopathic PD remains elusive.

As demonstrated in the research presented in chapters 5 - 7, different classes of pesticides can exert neurotoxic effects beyond their primary mode of action. These neurotoxic effects are related to critical parts of the functional machinery that is also present in the basal ganglia and appears related to the specific vulnerability of neurons in this brain area. This includes effects on Ca^{2+}-homeostasis and DA handling as well as, but also regulatory (GABA-ergic) signalling at non-cytotoxic concentrations. Many factors that determine the vulnerability of SN_{pc} neurons appear related to functional properties. Assessment of pesticide-induced effects on functional parameters will therefore most likely be more predictive for the involvementof a particular pesticide in neurodegeneration than measurements indicating changes in e.g. cell viability. Nevertheless, the latter approach represents a large part of the *in vitro* evidence for pesticide-induced PD (see e.g. Kanthasamy, *et al.* 2008, Sharma, *et al.* 2010).

As explained in the foregoing paragraphs, numerous pathways determine the vulnerability of SN_{pc} neurons for degeneration with varying likelihood of involvement in pesticide-related PD. Therefore, thorough analysis of the pathways in the pathophysiology of neurodegeneration and PD is required to identify key processes that, upon chemical disturbance, can induce a cascade that leads to neuronal dysfunction and ultimately degeneration. Confirmatory *in vivo* research should then focus on examination of local and focal parameters of neurodegeneration following low-dose and long-term pesticide exposure in healthy wild-type animals. Although these animals may not readily develop clinical signs of PD, small changes on functional properties and protein levels will then have to indicate whether exposure to a certain pesticide is linked to neurodegeneration.

With the knowledge gained about chemical-induced effects on truly predictive *in vitro* parameters of neurodegeneration, it may be possible to identify structure-activity relationships or functional molecular groups can be identified. This may not only improve risk assessment efforts, but may ultimately lead to the development of pesticides that are less neurotoxic for humans.

Chapter 9.2 – Human risk assessment

Whether or not exposure to a certain pesticide poses a risk to the human population depends on the likelihood and degree of internal exposure, which is largely determined by the route of exposure and the fate (e.g. metabolism) of the compound upon exposure. The most likely exposure scenario for the general population is oral exposure through ingestion of food that contains pesticide residues (Oates and Cohen 2011). This comprises exposure to pesticides that are currently in use in food- and feed production (e.g. azole fungicides) as well as persistent compounds (e.g. lindane, dieldrin) that have accumulated in the food chain. In case of occupational exposure to pesticides in for instance agricultural and greenhouse workers and operators on spraying machines, also dermal and inhalational exposure are important (see e.g. Ramwell, *et al.* 2005).

Exposure of the brain to a pesticides is largely depending its physicochemical properties that determine the ADME (Absorption, Distribution, Metabolism and Excretion) characteristics and thus the pesticide concentration in the systemic circulation and the brain. It is important to have information on these characteristics as some pesticides (e.g. azole fungicides) are known to interfere with metabolism, which may influence the circulating pesticide concentration.

Brain exposure is also determined by the ability of a pesticide to cross the blood-brain barrier (BBB). The BBB separates the brain from the rest of the body protecting it against a plethora of compounds, including proteins and infectious agents. However, lipophilic compounds, including many pesticides (e.g. dieldrin), may passively diffuse through the BBB or be actively transported over the BBB by means of for instance the neutral amino acid transporter (e.g. paraquat) (Shimizu, *et al.* 2001).

Due to their persistence and bioaccumulation in the food chain, the organochlorine insecticides lindane and dieldrin are still detectable in human blood at picomolar to nanomolar levels (Table 2). Notably, increased serum levels of dieldrin have been related to the risk for PD (Weisskopf, *et al.* 2010). Furthermore, compared to controls or patients with Alzheimer's disease, increased levels of lindane and dieldrin (up to ~1 µg/g l.w.) have been detected in brain tissue of PD patients (Corrigan, *et al.* 2000, Fleming, *et al.* 1994).

Average serum levels of dieldrin and lindane in developed countries (see e.g. Koppen, *et al.* 2002, Thomas, *et al.* 2006, Xu, *et al.* 2010; Table 2) indicate that a margin of safety exists between the concentrations at which neurotoxic effects are observed *in vitro* (Table 1) and actual exposure. However, the lipophilicity renders it questionable whether serum levels truly represent internal exposure and exposure of the brain in particular. This was already underlined by a pharmacokinetic study from the 1970s with dieldrin (Walsh and Fink 1972) in which the authors

demonstrated comparable uptake kinetics in adipose tissue and the brain, whereas dieldrin disappeared from the blood quickly. Therefore, dieldrin concentrations in the fatty tissue may be a more reliable representation of actual internal (brain) dieldrin exposure than serum concentrations. Consequently, the detection of dieldrin at concentration around 130 ng/g l.w. (corresponding to ~270 nM, calculated using average physiological values) in adipose tissue of Spanish children (Lopez-Espinosa, *et al.* 2008) is worrying. In particular because it has been demonstrated that perinatal exposure of rodents to organochlorine insecticides is related to persistent changes in dopaminergic neurotransmission (Richardson, *et al.* 2006) and the development of PD later in life (see e.g. Barlow, *et al.* 2007).

The available data on human internal exposure to dinitrophenolic herbicides is limited to DNOC but clearly indicates that internal exposure in agricultural workers has been high (Table 2). Considering the lipophilicity of the other dinitrophenolic herbicides (Table 1, chapter 3) it can be expected that comparable levels are reached upon exposure to other dinitrophenolic herbicides. Also, these compounds pass biological membranes with relative ease (Gibson and Rao 1973). Considering this, the *in vitro* effect concentrations on parameters of dopaminergic neurodegeneration and GABA-ergic neurotransmission appear to be comparable to exposure levels in humans (Table 1 & 2). In fact, even when considering that brain exposure may be limited to a fraction of the blood levels (Gibson and Rao 1973), there appears to have been a very small (if at all) margin of safety. Therefore, exposure to dinitrophenolic herbicides has likely resulted in exposure levels comparable to effect concentrations for the observed *in vitro* effects. Thus, exposure may be related to dopaminergic neurodegeneration observed in agricultural workers exposed to these compounds.

Human exposure data on azole fungicides is largely lacking, rendering proper risk assessment hardly doable. However, residue levels of imazalil, tebuconazole and cyproconazole on food products are often >10 µg/kg (Nougadère, *et al.* 2012). Therefore, human exposure to azole fungicides appears very likely, though it is unclear how residue levels of these pesticides relate to human internal exposure as this depends on numerous factors, including for example food processing before consumption.

An animal-based PBPK study with triadimefon indicated that upon exposure to triadimefon the compound is spread throughout the body, including the brain (Crowell, *et al.* 2011). Using the pharmacokinetic data obtained in this study, the authors extrapolated a human equivalent dose (HED) for the rat NOAEL for neurotoxicity. The calculated HED turned out to be only 25-fold higher than the human oral reference dose (RfD), indicating that current safety margins for environmental exposure to triadimefon may not be sufficient.

Additional concern arises from the observation that different pesticides and classes of pesticides can act on the same endpoint (e.g. inhibition of VGCC and GABA-ergic neurotransmission). We demonstrate additive effects on VGCC inhibition in mixtures of lindane and dieldrin (Heusinkveld and Westerink 2012) as well as mixtures of azole fungicides (Heusinkveld, *et al.* 2013). Considering the fact that they share the same target, it appears thus realistic that additivity may also apply for mixtures of these different classes of compounds.

Human risk assessment of pesticides so far is based on effects induced by single compounds after short-term or acute exposure to relatively high doses. However, people experience chronic low-doses exposure to a mixture of chemicals, among which many pesticides. According to the usual approach, exposure to such a complex mixture of chemicals will not pose a risk when all individual compounds are below their individual effect level. However, as is known from research on endocrine disrupting chemicals, unexpected effects may occur due to chemical interactions in the body (Kortenkamp 2008). Therefore, the biggest, and yet unanswered question is whether safety margins currently applied are providing enough safety to assure that even complex mixtures of compounds are not evoking adverse effects.

Table 1 . *In vitro* effect concentrations

	Compound	Target	Measure	Effect Conc. (µM)	Chapter
Organochlorine Insecticide	Lindane	basal $[Ca^{2+}]_i$	LOEC	10	
		VGCC	LOEC	3	5.1 & 5.2
			EC_{50}	1	
	Dieldrin	VGCC	LOEC	0.1*	5.2
			EC_{50}	0.13	
Azole Fungicide	Imazalil	VGCC	LOEC	3	7
			EC_{50}	7.5	
	Flusilazole	VGCC	LOEC	1	7
			EC_{50}	5.1	
	Tebuconazole	VGCC	LOEC	3	7
			EC_{50}	11	
	Triadimefon	VGCC	LOEC	1	7
			EC_{50}	37.2	
	Cyproconazole	VGCC	LOEC	30	7
			EC_{50}	65	
Dinitrophenol Herbicide	2,4-DNP	GABA-R	LOEC	10	6.2
	DNOC	GABA-R	LOEC	10	6.2
		basal $[Ca^{2+}]_i$	LOEC	10	6.1
		α-synuclein	LOEC	1	6.1
	Dinoseb	GABA-R	LOEC	10	6.2
		basal $[Ca^{2+}]_i$	LOEC	1	6.1
		α-synuclein	LOEC	0.3	6.1
	Dinoterb	GABA-R	LOEC	10	6.2

* Following 20 minutes exposure

Table 2. Human exposure data

Lindane

Population	tissue / medium	median / max	Value	unit	corresponding conc. (nM)	Reference
Adults (GB)	serum	median	16	ng/g l.w.	0.6	Thomas, *et al.* 2006
		95th percentile	110		4.2	
Adults (PT)	serum	mean	0.7	ng/ml serum	1.3	Cruz, *et al.* 2003
		max	7.5		14	
Young men (ES)	serum	median	1.2	ng/ml serum	2.2	Carreno, *et al.* 2007
		95th percentile	17.7		33	
Children (MX)	serum	median	2543	ng/g l.w.	97	Trejo-Acevedo, *et al.* 2009
		95th percentile	8186		360	
Women (ES)	cord blood	mean	3.9	ng/ml serum	7.5	Jimenez-Torres, *et al.* 2006
		95th percentile	108.6		210	
Women (ES)	serum	mean	1.3	ng/ml serum	2.4	Jimenez-Torres, *et al.* 2006
		95th percentile	4.4		8.3	
Adult women (ES)	serum	mean	1.5	ng/ml serum	2.9	Botella, *et al.* 2004
		95th percentile	12.8		24	
Adult women (BE)	serum	median	1.6	ng/g l.w.	0.06	Koppen, *et al.* 2002
		95th percentile	8.1		0.3	
Women (SK)	breast milk	median	15	ng/g l.w.	2.2	Prachar, *et al.* 1993
		max	106		15	
Women (RO)	breast milk	mean	161	ng/g l.w.	23	Dirtu, *et al.* 2006

Table 2. continued

Dieldrin

Population	tissue / medium	median / max	Value	unit	corresponding conc. (nM)	Reference
Adults (US)	serum	min	1.2	ng/g l.w.	0.04	Xu, et al. 2010
		max	670		20	
Women (ES)	serum	mean	4	ng/ml serum	6.1	Rivas, et al. 2007
		max	28		41	
Women (arctic CA)	serum (cord)	max	0.3	ng/ml serum	0.4	Butler Walker, et al. 2003
	serum (maternal)	max	1		1.4	
Women (IN)	blood (cord)	max	4.7	ng/ml	6.9	Mustafa, et al. 2010
	blood (maternal)	max	4.5		6.5	
Women (IN)	breast milk	median	20	ng/g l.w.	2.2	Subramanian, et al. 2007
		max	4500		490	
Children (ES)	adipose tissue	median	130	ng/g l.w.	270	Lopez-Espinosa, et al. 2007
		max	3440		7200	

DNOC

Population	tissue / medium	median / max	Value	unit	corresponding conc. (µM)	Reference
Healthy volunteers* (US)	blood	min	15	µg/g	76	Harvey, et al. 1951
		peak	48		240	
Agricultural workers (NL)	serum	min	11	µg/ml	31	van Noort, et al. 1960
		max	88		240	
Agricultural workers (NL)	blood	min	0.6	µg/g	3	Heuts 1993
		max	0.8		4	

* 1 mg/kg for 7 days

Chapter 9.3 – Conclusions and recommendations for future research

In conclusion, although epidemiological research provides evidence that pesticides play a role in idiopathic PD, the underlying mechanisms remain elusive. The research presented in this thesis adds to the body of evidence that pesticides from different classes and with varying chemical structures can induce neurotoxicity *in vitro*. In many cases, neurotoxicity is due to mechanisms that are unrelated to the primary pesticidal mode of action. The neurotoxic effects observed comprise effects on hallmarks of neurodegeneration (α-synuclein, apoptosis) as well as effects on parameters that presumably determine the enhanced sensitivity of SN_{pc} neurons (Ca^{2+} homeostasis and VGCC functioning, DA handling, etc.) towards insults from environmental factors, including pesticides *in vivo*.

The elucidation of the potential role of pesticides in PD aetiology requires detailed knowledge about key processes determining the onset and progression of the disease. However, this knowledge is still largely absent. As a result, it still remains to be determined which particular effects observed *in vitro* or *in vivo* are truly predictive for the development of PD in humans.

It is generally accepted that a long latency period exists between the first neurobiological changes and the occurrence of clinical symptoms in idiopathic PD (Schapira 2009). Nevertheless, the majority of the research conducted *in vitro* as well as *in vivo* is based on (relatively) short-term exposures to concentrations of compounds that are often much higher than is realistic for the human situation. Hence, it is debatable to what extent the effects observed at these levels of exposure and exposure paradigms are predictive for the role of a chemical in idiopathic PD. Accordingly, compounds such as MPTP that are related to fast development of PD *in vivo* may not be entirely explanatory for the role of pesticides and environmental factors in idiopathic PD. Likewise, research on the neurodegenerative properties of compounds in animals or cell lines bearing genetic defects as observed in familial PD, may at best be informative for the role of chemicals in familial PD but whether this approach identifies compounds that are related to idiopathic PD remains to be determined.

From the foregoing it is clear that more research is necessary. Research in neurodegeneration and neurodegenerative properties of chemicals including pesticides is for obvious reasons increasingly performed in *in vitro* systems. However, as demonstrated in chapter 4 and 8, techniques and models may suffer from shortcomings and pitfalls. Therefore, thorough characterization and verification of existing models as well as development of new models is required.

Ideally, a research model is as complete, complex and non-manipulated as possible. Cell- or animal models with e.g. induced overexpression of human α-synuclein or knock-out models can be valuable for assessment of the effect

of chemicals on specific processes. Nevertheless, as the genetic background of idiopathic PD is still diffuse, it can be debated whether these models provide relevant information with regards to the role of e.g. pesticides in the occurrence of idiopathic PD. It is therefore possibly more relevant to study the involvement of chemical exposure in relation to early pathological signs of PD in (healthy) wild-type animals or cell lines, than to investigate the effect of a chemical on an animal or cell line bearing a genetic defect that renders it more vulnerable.

Also, new and promising non-mammalian models such as *Caenorhabditis elegans*, need to be explored. However, what holds true for a cell line also holds for *C. elegans*; thorough characterization of its strengths (e.g. limited number of good visible neurons, integrated model system) and weaknesses (e.g. no BBB, different metabolism, different route of exposure) is required to make it a successful model.

Furthermore, the role of activation of the immune system in the CNS, has to be examined. There is increasing evidence that the immune system and inflammatory processes play a (key) role in the onset and/or progression of neurodegenerative diseases. However, it remains to be determined whether for instance astrogliosis following pesticide exposure is cause or consequence. Testing the involvement of the immune system requires co-cultures of neurons and astroglial cells with conditioned media to determine whether glial activation triggers changes in neuronal function or the other way around.

As the BBB has a key-protective role in the CNS, the role of BBB (mal-)function in neurodegenerative processes also needs to be taken into account. In general, *in vitro* models do not take into account the fact that a BBB may prevent or aggravate toxicity as it may repel or concentrate toxicants. Therefore, to be able to reliably extrapolate from *in vitro* to *in vivo* the role of the BBB should be known and taken into account.

A well-known route for chemicals to largely by-pass the BBB is via the olfactory nerve. This has already been demonstrated for transport of nanoparticles and metals via the olfactory nerve into the brain (Henriksson, *et al.* 1999, Lucchini, *et al.* 2012, Wu, *et al.* 2013). As the early stages in PD are characterized by a loss of olfaction (Braak, *et al.* 2003), it remains to be determined whether or not the first event in the process(es) leading to PD can be related to transport of chemicals via or degeneration of the olfactory route. Testing this hypothesis would require animal studies with single as well as repeated exposure via instillation in the nasal cavity. Subsequently, the brain has to be examined for presence of the compound and signs of degenerative pathologies. Agricultural workers experience inhalational and olfactory exposure in addition to dermal and oral exposure in their occupational situation. Therefore, when olfactory exposure can give rise to neurotoxicity or degeneration, it needs to be determined whether health protection by measures of occupational hygiene provides an adequate level of protection.

Detailed human exposure data is one of the requirements for reliable risk assessment. Although monitoring programs exist for a plethora of compounds, including many phased-out but persistent organic pollutants such as lindane and dieldrin, hardly any human exposure data is available for many pesticides that are currently in use (e.g. azole fungicides). More elaborate monitoring data on human exposure is thus needed to avoid inadequate assessment of the risk posed by particular compounds. In addition, as discussed in section 9.2, current risk assessment is based on individual compounds, rendering it elusive whether the current approach is granting enough margin of safety in case of complex mixtures. However, the lack of human exposure data and the absence of (software) tools to realistically estimate internal exposure and the according risk of a complex mixture, hamper reliable risk assessment of mixtures.

Taking everything into account, the immense jigsaw provided by the question whether pesticide exposure is related to neurodegeneration is still far from finalized. Finding the core-pieces that speed up finalization of the jigsaw will likely require innovative *in vitro* and *in vivo* testing strategies that identify truly predictive processes determining chemical-induced neurodegeneration. Nevertheless, the research presented in this thesis added some new pieces to the puzzle, demonstrating that several classes of pesticides can induce *in vitro* (dopaminergic) neuronal dysfunction that may lead to degeneration.

Chapter 10

Nederlandse Samenvatting

Inleiding

Sinds het begin van de landbouw gebruikt de mens middelen om plagen te bestrijden die de productie van gewassen in gevaar kunnen brengen. Deze stoffen, de zogeheten bestrijdingsmiddelen, omvatten zowel natuurlijke als gesynthetiseerde (niet-natuurlijke) chemische verbindingen. Het oudste gedocumenteerde voorbeeld van het gebruik van een stof als bestrijdingsmiddel stamt uit de tijd van Homerus (~1000 v Chr.) toen zwaveldamp werd gebruikt om plagen te bestrijden. Ook tegenwoordig is zwavel nog een veel gebruikt middel in de wijnbouw.

In de jaren 30 van de 20e eeuw is men begonnen met het synthetiseren van nieuwe bestrijdingsmiddelen ter vervanging van de voor mensen schadelijke middelen zoals arseen. Na WOII heeft de ontwikkeling van bestrijdingsmiddelen een grote vlucht genomen en is er een grote variëteit aan middelen ontwikkeld. Dat het gebruik van veel van deze middelen niet zonder gevaar is, is uit de geschiedenis wel gebleken. Vele verschillende middelen zijn bewezen gevaarlijk bij (kortstondige) hoge blootstelling en kunnen zelfs dodelijk zijn. Wat er echter gebeurt bij langdurige blootstelling aan lagere concentraties waar de mens geen acute klachten van ondervindt is grotendeels onbekend. Epidemiologisch onderzoek geeft in ieder geval aan dat verhoogde blootstelling aan bestrijdingsmiddelen een potentieel risico is voor het ontwikkelen van neurodegeneratieve ziekten, zoals de ziekte van Parkinson. Vooral werknemers in de agrarische sector die veel werken met bestrijdingsmiddelen blijken een verhoogd risico te lopen op het ontwikkelen van Parkinson.

Het doel van het onderzoek dat gebundeld is in dit proefschrift was dan ook om te zoeken naar effecten van bestrijdingsmiddelen die van belang zijn bij het ontstaan of de progressie van neurodegeneratieve ziekten. Hierbij is in het bijzonder gekeken naar cellulaire processen die van belang zijn bij de ziekte van Parkinson.

Context van het proefschrift

Bestrijdingsmiddelen zijn onderverdeeld in verschillende klassen afhankelijk van het organisme waar ze tegen zijn gericht, zoals insecticiden tegen insecten en herbiciden tegen planten. Ook al lijkt het een open deur, het is goed om je te realiseren dat alle bestrijdingsmiddelen per definitie giftig zijn voor (een specifieke groep) levende organismen, anders zouden ze nutteloos zijn. Een wijd verspreidde aanname is dat de schadelijkheid van een middel voor de mens afhangt van het primaire doel en werkingsmechanisme. Anders gezegd, een middel dat gericht is tegen een chemisch proces in een plant wordt over het algemeen beschouwd als minder gevaarlijk voor de mens dan een middel dat gericht is tegen het zenuwstelsel van een insect. Voornamelijk vanwege de overeenkomsten tussen het menselijke en het insecten zenuwstelsel en het grotendeels ontbreken van overeenkom-

sten tussen de mens en de plant. Wat hierin niet meegenomen wordt is dat het primaire effect van een middel niet per definitie het enige effect is dat een middel kan hebben. Dit blijkt wel uit het feit dat het voorkomen van de ziekte van Parkinson wordt geassocieerd met blootstelling aan pesticiden die primair gericht zijn tegen bv. plant-specifieke processen die niet relevant zijn voor de mens.

In het brein zijn vele verschillende typen cellen aanwezig, zoals zenuwcellen (neuronen) en cellen van het immuunsysteem. Deze cellen zijn verdeeld over verschillende hersengebieden. De verschillende celtypen communiceren door middel van chemische en elektrische signalen. In het geval van neurodegeneratieve ziekten, zoals de ziekte van Parkinson, sterven cellen af in een specifiek gedeelte van de hersenen; de basale ganglia. Dit gebied is betrokken bij het uitvoeren van motorische taken. Bewegingen worden gecoördineerd vanuit de hersenen en continu teruggekoppeld om te checken of een beweging wordt uitgevoerd zoals gepland. Indien dit niet het geval is, wordt de beweging bijgestuurd. Als dit systeem niet meer goed werkt, ontstaan de symptomen die karakteristiek zijn voor de ziekte van Parkinson, waaronder het beven of trillen van armen of benen, verstijving en problemen bij het plannen en uitvoeren van bewegingen. In het geval van de ziekte van Parkinson zijn met name de zenuwcellen aangedaan die gebruik maken van dopamine als signaalmolecuul. Daarom is in dit proefschrift gekeken naar de effecten van verschillende bestrijdingsmiddelen op factoren die van belang zijn voor het functioneren van deze zogenaamde dopaminerge zenuwcellen.

Overzicht van de hoofdstukken

In hoofdstuk 1 van dit proefschrift wordt de context van het onderzoek geschetst en het doel van het onderzoek uitgelegd. De hoofdstukken 2 en 3 geven respectievelijk een kort overzicht van wat waar in het proefschrift staat en een overzicht van de gebruikte methoden en technieken.

In hoofdstuk 4 wordt ingegaan op de toepassing van een nieuwe techniek die erop gericht is om in korte tijd het effect van veel stoffen op een belangrijk aspect van neuronale functie, intracellulair calcium, te kunnen meten. Calcium is namelijk een belangrijk molecuul in de cel en betrokken bij vele processen inclusief de energiehuishouding en communicatie (zowel in de cel als tussen cellen) maar ook het besluit over leven en dood van de cel. De gevestigde techniek om calcium signalen te kunnen meten (fluorescentie microscopie) is arbeidsintensief en relatief traag en daarom wordt gezocht naar technieken die deze metingen kunnen vereenvoudigen en versnellen. Op basis van het onderzoek dat in hoofdstuk 4 wordt gepresenteerd kan worden geconcludeerd dat met de nieuwe, snellere techniek nog geen bruikbare data kunnen worden verkregen. Parameters van de intracellulaire calciumhuishouding zijn in de rest van het onderzoek dan ook met de arbeidsintensieve maar wel betrouwbare fluorescente microscopie bepaald.

In de hoofdstukken 5 tot en met 7 wordt onderzoek beschreven naar de effecten van verschillende groepen bestrijdingsmiddelen op onder andere overleving van dopaminerge cellen, het optreden van schade door reactieve zuurstof en effecten op de intracellulaire calciumconcentratie.

De resultaten geven aan dat stoffen uit drie verschillende klassen bestrijdingsmiddelen allemaal een neurotoxisch effect laten zien dat los staat van hun primaire werkingsmechanisme. In hoofdstuk 5.1 en 5.2 zijn effecten beschreven van de organochloor verbindingen lindaan en dieldrin. Organochloor verbindingen behoren tot de insecticiden en zijn gericht tegen het zenuwstelsel van insecten. Behalve in de landbouw zijn bepaalde organochloor verbindingen ook gebruikt in anti-luis shampoo voor mens en dier. Uit de resultaten blijkt dat deze stoffen effect hebben op de calciumkanalen in de celmembraan die afgifte van onder anderen dopamine reguleren. Dit heeft tot gevolg dat dopamine vrijkomt op het moment dat de cel niet wordt gestimuleerd en de dopamine afgifte bij stimulatie van de cel wordt geblokkeerd. Kort door de bocht betekent dit dat er communicatie plaatsvindt als dat niet gewenst is en juist geen communicatie als dat wel de bedoeling is.

In hoofdstuk 6.1 en 6.2 zijn effecten beschreven van herbiciden die de chemische verbinding dinitrofenol als basis hebben. Deze middelen zijn in de geschiedenis onder andere gebruikt als middel om aardappelloof dood te spuiten voor de oogst en als bestrijdingsmiddel tegen onkruid. Van deze middelen wordt in de hoofdstukken 6.1 en 6.2 uitgelegd dat ze effect hebben op twee verschillende niveaus. Op het niveau van de dopaminerge cel zorgen ze voor het verstoren van de calciumbalans waardoor effecten optreden die ook gezien worden in het brein van mensen met de ziekte van Parkinson (hoofdstuk 6.1). Het is bekend dat werknemers in de agrarische sector die bijvoorbeeld als spuiter werkten voor een loonbedrijf blootgesteld zijn aan grote hoeveelheden dinitrofenol verbindingen. Op basis van de resultaten van dit onderzoek wordt dan ook de conclusie getrokken dat blootstelling aan deze middelen bijgedragen kan hebben aan het ontstaan van de ziekte van Parkinson.

Aan de andere kant verstoren deze stoffen direct de communicatie tussen de verschillende hersengebieden door aan te grijpen op één van de belangrijkste signaalstoffen in het menselijk brein: GABA (hoofdstuk 6.2). GABA is de neurotransmitter die in de netwerken van het brein zorgt voor de negatieve feedback, dus demping en beheersing van signalen. Verstoring van de input van GABA in het neuronale netwerk zorgt in extreme gevallen dan ook óf voor over-stimulatie en epilepsie (ontbreken van demping) óf voor het uitvallen van functies door het uitdoven van het systeem (overdreven demping van signalen).

Zowel de dinitrofenol herbiciden als de organochloor insecticiden zijn reeds lange(re) tijd uit de handel. Daardoor is de menselijke blootstelling aan deze stoffen beperkt tot datgeen wat er in het milieu aanwezig is. Dit is vooral van belang voor de organochloor-verbindingen vanwege accumulatie van deze stoffen.

De vraag is echter hoe het zit met de bestrijdingsmiddelen waar de mens tegenwoordig aan wordt blootgesteld. In ons dagelijks leven wordt de mens blootgesteld aan een mengsel van verschillende stoffen waaronder, vooral via onze voeding, veel verschillende soorten bestrijdingsmiddelen. Van veel van deze middelen is weinig tot niets bekend over mogelijke effecten op het zenuwstelsel en het brein. In hoofdstuk 7 zijn de resultaten beschreven van een studie naar de effecten van zes veel gebruikte middelen tegen schimmels op groente en fruit. Stoffen uit deze klasse worden fungiciden genoemd. Enkele van de middelen worden ook in de (dier-) geneeskunde toegepast tegen schimmelinfecties. Uit de resultaten blijkt dat vijf van de zes middelen in staat zijn om bij voldoende blootstelling calciumkanalen te blokkeren die nauw betrokken zijn bij het vrijgeven van dopamine. Daarmee kan dus de communicatie binnen neuronale netwerken gehinderd of zelfs volledig geblokkeerd worden.

Om te voorkomen dat mensen een onacceptabel risico lopen door het eten van voedsel waar bestrijdingsmiddelen op zitten wordt een risicoschatting gemaakt per stof. Daarmee wordt bepaald aan welke hoeveelheid van een middel een mens blootgesteld kan worden zonder dat hij risico loopt op gezondheidsschade. Echter, in ons dagelijks leven wordt een mens niet blootgesteld aan één bepaald middel maar vaak aan een cocktail van verschillende middelen. Om in te schatten wat de risico's zijn van een dergelijk mengsel is het van belang om te weten of middelen die samen voorkomen een gedeeld werkingsmechanisme hebben. Als dat het geval is kan het theoretisch zo zijn dat de gecombineerde blootstelling wél een risico oplevert terwijl dat niet zo is voor de individuele middelen omdat de effecten bij elkaar optellen. Experimenten met zowel de insecticiden als de verschillende fungiciden geven aan dat verstoring van de intracellulaire calcium huishouding een gedeeld effect is tussen verschillende klassen bestrijdingsmiddelen. Bovendien laten experimenten met de fungiciden zien dat de effecten op de calciumhuishouding bij blootstelling aan mengsels inderdaad opgeteld moeten worden voor een realistische effect schatting.

Al het hierboven beschreven onderzoek is uitgevoerd in een celtype dat een model is voor de dopaminerge neuronen in het menselijk brein. Of een cel hiervoor een goed model is hangt voornamelijk af van de eigenschappen die deze cel heeft zoals aanwezige receptoren maar ook of een cel in staat is om dopamine te maken én uit te scheiden. Het cel model dat is gebruikt, is vanwege zijn eigenschappen zeer geschikt voor dit type onderzoek, maar wordt vaak bekritiseerd omdat het een cel van een rat is die van oorsprong uit een bijniertumor komt. Daarom hebben we in hoofdstuk 8 dit cel model vergeleken met drie andere modellen die op papier dezelfde kwalificatie van een goed model voor een dopaminerg neuron hebben.

Wat blijkt is dat de cellen grote verschillen vertonen op het gebied van receptoren, maar ook in reactie op een testset van bestrijdingsmiddelen. Hieruit blijkt dat de keuze voor een specifiek model gestuurd moet worden door de onderzoeksvraag en de eigenschappen die een cel moet hebben om deze te beantwoorden.

Conclusie

De vraag wat blootstelling aan bestrijdingsmiddelen te maken heeft met het voorkomen van de ziekte van Parkinson is een gigantische puzzel. Om deze puzzel volledig te kunnen leggen ontbreken helaas nog vele stukjes, zowel wat betreft kennis over het ontstaan van neurodegeneratieve processen als de effecten van bestrijdingsmiddelen op het centraal zenuwstelsel. Daarnaast betekent de observatie dat mengsels van stoffen additief kunnen werken (en dus opgeteld moeten worden om het risico realistisch te kunnen schatten) dat de huidige benadering van risico analyse potentieel tekort schiet. Om een schatting te maken van de risico's gerelateerd aan mengsels van bestrijdingsmiddelen is echter uitgebreide informatie nodig over de menselijke blootstelling aan een bepaald mengsel. Deze informatie is in veel gevallen afwezig wat de schatting van risico's gerelateerd aan ernstig mengsels limiteert.

Met het in dit proefschrift beschreven onderzoek is weer een puzzelstukje aangedragen door te laten zien dat verstoring van de calciumhuishouding een gemeenschappelijk effect is van verschillende klassen bestrijdingsmiddelen. Gezien de vitale rol van een gereguleerde calciumhuishouding in leven en dood van (dopaminerge) neuronen bestaat er daarom een gerede kans dat verstoring van de calciumhuishouding door bestrijdingsmiddelen een rol speelt bij neurodegeneratieve processen.

Do not condemn the judgment of another
because it differs from your own.
You may both be wrong.

Attrib. to Tao Tze

References

1. Adams, F.S., Rosa, F.G., Kumar, S., Edwards-Prasad, J., Kentroti, S., Vernadakis, A., Freed, C., Prasad, K., 1996. Characterization and transplantation of two neuronal cell lines with dopaminergic properties. Neurochemical Research 21, 619-627.

2. Agorogiannis, E.I., Agorogiannis, G.I., Papadimitriou, A., Hadjigeorgiou, G.M., 2004. Protein misfolding in neurodegenerative diseases. Neuropathol. Appl. Neurobiol. 30, 215-224.

3. Åkerman, K.E.O., Scott, I.G., Andersson, L.C., 1984. Functional differentiation of a human ganglion cell derived neuroblastoma cell line SH-SY5Y induced by a phorbol ester (TPA). Neurochem. Int. 6, 77-80.

4. Amir, S., 1990. Activation of brown adipose tissue thermogenesis by chemical stimulation of the posterior hypothalamus. Brain Res. 534, 303-308.

5. Anand, M., Agrawal, A., Rehmani, B., Gupta, G., Rana, M., Seth, P., 1998. Role of GABA receptor complex in low dose lindane (HCH) induced neurotoxicity: neurobehavioural, neurochemical and electrophysiological studies. Drug Chem. Toxicol. 21, 35-46.

6. Antunes Fernandes, E.C., Hendriks, H.S., van Kleef, R.G.D.M., Reniers, A., Andersson, P.L., van den Berg, M., Westerink, R.H.S., 2010. Activation and Potentiation of Human $GABA_A$ Receptors by Non-Dioxin–Like PCBs Depends on Chlorination Pattern. Toxicological Sciences 118, 183-190.

7. Ascherio, A., Honglei, C., Weisskopf M.G., O'Reilly, E., McCullough M.L., Calle, E.E., Schwarzschild, M.A., Thun, M.J., 2006. Pesticide exposure and risk for Parkinson's disease. Ann. Neurol. 60, 197-203.

8. Barbeau, A., 1984. Manganese and extrapyrimidal disorders (a critical review and tribute to Dr. George C. Cotzias). Neurotoxicology 5, 13-35.

9. Barclay, J.W., Morgan, A., Burgoyne, R.D., 2005. Calcium-dependent regulation of exocytosis. Cell Calcium 38, 343-353.

10. Barlow, B.K., Cory-Slechta, D.A., Richfield, E.K., Thiruchelvam, M., 2007. The gestational environment and Parkinson's disease: Evidence for neurodevelopmental origins of a neurodegenerative disorder. Reproductive Toxicology 23, 457-470.

11. Bartels, A.L., Leenders, K.L., 2009. Parkinson's disease: The syndrome, the pathogenesis and pathophysiology. Cortex 45, 915-921.

12. Beacham, D.W., Blackmer, T., O' Grady, M., Hanson, G.T., 2010. Cell-Based Potassium Ion Channel Screening Using the FluxOR™ Assay. Journal of Biomolecular Screening 15, 441-446.

13. Berridge, M.J., Bootman, M.D., Roderick, H.L., 2003. Calcium signalling: dynamics, homeostasis and remodelling. Nat. Rev. Mol. Cell Biol. 4, 517-529.

14. Betarbet, R., Sherer, T.B., MacKenzie, G., Garcia-Osuna, M., Panov, A.V., Greenamyre, T.J., 2000. Chronic systemic pesticide exposure reproduces features of Parkinson's disease. Nat Neurosci 3, 1301-1306.

15. Bezard, E., Przedborski, S., 2011. A tale on animal models of Parkinson's disease. Movement Disorders 26, 993-1002.

16. Bezprozvanny, I., 2009. Calcium signaling and neurodegenerative diseases. Trends Mol. Med. 15, 89-100.

17. Bidstrup, P., Payne, D., 1951. Poisoning by Dinitro-ortho-cresol; report of eight fatal cases occurring in Great Britain. Br. Med. J., 16-19.

18. Biedler, J.L., Helson, L., Spengler, B.A., 1973. Morphology and Growth, Tumorigenicity, and Cytogenetics of Human Neuroblastoma Cells in Continuous Culture. Cancer Research 33, 2643-2652.

19. Blandini, F., Nappi, G., Tassorelli, C., Martignoni, E., 2000. Functional changes of the basal ganglia circuitry in Parkinson's disease. Prog. Neurobiol. 62, 63-88.

20. Blasco, C., Font, G., Picó, Y., 2006. Evaluation of 10 pesticide residues in oranges and tangerines from Valencia (Spain). Food Control 17, 841-846.

21. Bloomquist, J.R., 1993. Toxicology, mode of action and target site-mediated resistance to insecticides acting on chloride channels. Comp Biochem Physiol C 106, 301-314.

22. Bloomquist, J.R., Barlow, R.L., Gillette, J.S., Li, W., Kirby, M.L., 2002. Selective Effects of Insecticides on Nigrostriatal Dopaminergic Nerve Pathways. Neurotoxicology 23, 537-544.

23. Bopp, S.K., Lettieri, T., 2007. Comparison of four different colorimetric and fluoreometric cytotoxicity assay in a zebrafish liver cell line. BMC Pharmacology 8.

24. Botella, B., Crespo, J., Rivas, A., Cerrillo, I., Olea-Serrano, M., Olea, N., 2004. Exposure of women to organochlorine pesticides in Southern Spain. Environmental Research 96, 34-40.

25. Braak, H., Tredici, K.D., Rnb, U., de Vos, R.A.I., Jansen Steur, E.N.H., Braak, E., 2003. Staging of brain pathology related to sporadic Parkinson's disease. Neurobiology of Aging 24, 197-211.

26. Breydo, L., Wu, J.W., Uversky, V.N., 2012. α-Synuclein misfolding and Parkinson's disease. Biochimica et Biophysica Acta (BBA) - Molecular Basis of Disease 1822, 261-285.

27. Briz, V., Galofré, M., Suñol, C., 2010. Reduction of Glutamatergic Neurotransmission by Prolonged Exposure to Dieldrin Involves NMDA Receptor Internalization and Metabotropic Glutamate Receptor 5 Downregulation. Toxicological Sciences 113, 138-149.

28. Brooks, D.J., 2012. Parkinson's disease: Diagnosis. Parkinsonism Relat. Disord. 18, Supplement 1, S31-S33.

29. Brown, T.P., Rumsby, P.C., Capleton, A.C., Rushton, L., Levy, L.S., 2006. Pesticides and Parkinson's disease - is there a link? Environmental health perspectives 114, 156-164.

30. Brown, D.D., 2004. A Tribute to the Xenopus laevis Oocyte and Egg. Journal of Biological Chemistry 279, 45291-45299.

31. Budde, T., Meuth, S., Pape, H., 2002. Calcium-dependent inactivation of neuronal calcium channels. Nat. Rev. Neurosci. 3, 873-883.

32. Bywood, P.T., Johnson, S.M., 2003. Mitochondrial Complex Inhibitors Preferentially Damage Substantia Nigra Dopamine Neurons in Rat Brain Slices. Exp. Neurol. 179, 47-59.

33. Campoy, C., Jimenez, M., Olea-Serrano, M.F., Moreno Frias, M., Canabate, F., Olea, N., Bayes, R., Molina-Font, J.A., 2001. Analysis of organochlorine pesticides in human milk: preliminary results. Early Human Development 65, S183-S190.

34. Capel, P., Giger, W., Reichert, P., Wanner, O., 1988. Accidental input of pesticides into the Rhine River. Environ. Sci. Technol. 22, 992-997.

35. Carrasco, M.A., Hidalgo, C., 2006. Calcium microdomains and gene expression in neurons and skeletal muscle cells. Cell Calcium 40, 575-583.

36. Carreno, J., Rivas, A., Granada, A., Lopez-Espinosa, M., Mariscal, M., Olea, N., Olea-Serrano, F., 2007. Exposure of young men to organochlorine pesticides in Southern Spain. Environmental Research 103, 55-61.

37. Castilho, R.F., Vicente, J.A.F., Kowaltowski, A.J., Vercesi, A.E., 1997. 4,6-Dinitro-o-cresol uncouples oxidative phosphorylation and induces membrane permeability transition in rat liver mitochondria. Int. J. Biochem. Cell Biol. 29, 1005-1011.

38. Catterall, W.A., Few, A.P., 2008. Calcium Channel Regulation and Presynaptic Plasticity. Neuron 59, 882-901.

39. Catterall, W.A., Perez-Reyes, E., Snutch, T.P., Striessnig, J., 2005. International union of pharmacology. XLVIII. Nomenclature and structure-function relationships of voltage-gated calcium channels. Pharmacological reviews 57, 411-425.

40. Chan, C.S., Gertler, T.S., Surmeier, D.J., 2009. Calcium homeostasis, selective vulnerability and Parkinson's disease. Trends Neurosci. 32, 249-256.

41. Chan, C.S., Guzman, J.N., Ilijic, E., Mercer, J.N., Rick, C., Tkatch, T., Meredith, G.E., Surmeier, D.J., 2007. `Rejuvenation' protects neurons in mouse models of Parkinson's disease. Nature 447, 1081-1086.

42. Chinta, S., Rane, A., Poksay, K., Bredesen, D., Andersen,JK,Rao,RV, 2008. Coupling endoplasmic reticulum stress to cell death program in dopaminergic cells: effect of paraquat. Neuromolecular Med. 10, 333-342.

43. Choong, C., Say, Y., 2011. Neuroprotection of α-synuclein under acute and chronic rotenone and maneb treatment is abolished by its familial Parkinson's disease mutations A30P, A53T and E46K. Neurotoxicology 32, 857-863.

44. Cicchetti, F., Drouin-Ouellet, J., Gross, R.E., 2009. Environmental toxins and Parkinson's disease: what have we learned from pesticide-induced animal models? Trends Pharmacol. Sci. 30, 475-483.

45. Circu, M.L., Aw, T.Y., 2012. Glutathione and modulation of cell apoptosis. Biochimica et Biophysica Acta (BBA) - Molecular Cell Research 1823, 1767-1777.

46. Clapham, J.C., 2012. Central control of thermogenesis. Neuropharmacology 63, 111-123.

47. Colman, E., 2007. Dinitrophenol and obesity: An early twentieth-century regulatory dilemma. Regulatory Toxicology and Pharmacology 48, 115-117.

48. Colom, L.V., Diaz, M.E., Beers, D.R., Neely, A., Xie, W., Appel, S.H., 1998. Role of Potassium Channels in Amyloid-Induced Cell Death. J. Neurochem. 70, 1925-1934.

49. Corrigan, F., French, M., Murray, L., 1996. Organochlorine compounds in human brain. Human and Experimental Toxicology 15, 262-264.

50. Corrigan, F., Wienburg, C., Shore, R., Daniel, S., Mann, D., 2000. Organochlorine insecticides in substantia nigra in Parkinson's disease. J. Toxicol. Environ. Health A 59, 229-234.

51. Cory-Slechta, D.A., Thiruchelvam, M., Richfield, E.K., Barlow, B.K., Brooks, A.I., 2005. Developmental pesticide exposure and the Parkinson's disease phenotype. Birth Defects Research 73, 136-139.

52. Crawford, G.D., 1992. A novel N18TG2 X Mesencephalon cell hybrid expresses properties that suggest a dopaminergic cell line of substantia nigra origin. The Journal of Neuroscience 12, 3392-3398.

53. Cristofol, R.M., Rodriguez-Farre, E., 1994. Hippocampal noradrenaline release is modulated by [gamma]- and [delta]-hexachlorocyclohexane isomers: which mechanisms are involved? European Journal of Pharmacology 252, 305-312.

54. Criswell, K., Stuenkel, E., Loch-Caruso, R., 1994. Lindane increases intracellular calcium in rat myometrial smooth muscle cells through modulation of inositol 1,4,5-trisphosphate-sensitive stores. J. Pharmacol. Exp. Ther. 270, 1015-1024.

55. Crofton, K.M., 1996. A structure-activity relationship for the neurotoxicity of triazole fungicides. Toxicol. Lett. 84, 155-159.

56. Crowell, S.R., Henderson, W.M., Kenneke, J.F., Fisher, J.W., 2011. Development and application of a physiologically based pharmacokinetic model for triadimefon and its metabolite triadimenol in rats and humans. Toxicol. Lett. 205, 154-162.

57. D'Hulst, C., Atack, J.R., Kooy, R.F., 2009. The complexity of the $GABA_A$ receptor shapes unique pharmacological profiles. Drug Discov. Today 14, 866-875.

58. de Lau, L.M., Breteler, M.M., 2006. Epidemiology of Parkinson's disease. The Lancet Neurology 5, 525-535.

59. Deitmer, J., Schild, D., 2000. Calcium - Imaging, Protocolle Und Ergebnisse. in Ca^{2+} Und pH, Ionenmessungen in Zellen Und Geweben. Spektrum Akademischer Verleger, Heidelberg.

60. Denizot, F., Lang, R., 1986. Rapid colorimetric assay for cell growth and survival: Modifications to the tetrazolium dye procedure giving improved sensitivity and reliability. Journal of Immunological Methods 89, 271-277.

61. Dexter, D.T., Jenner, P., 2013. Parkinson disease: from pathology to molecular disease mechanisms. Free Radical Biology and Medicine 62, 132-144.

62. Di Virgilio, F., Steinberg, T.H., Silverstein, S.C., 1990. Inhibition of Fura-2 sequestration and secretion with organic anion transport blockers. Cell Calcium 11, 57-62.

63. Dingemans, M.M.L., Heusinkveld, H.J., Bergman, A., van den Berg, M., Westerink, R.H.S., 2010. Bromination Pattern of Hydroxylated Metabolites of BDE-47 Affects Their Potency to Release Calcium from Intracellular Stores in PC12 Cells. Environmental Health Perspectives 118, 519-525.

64. Dingemans, M.M.L., Heusinkveld, H.J., de Groot, A., Bergman, A., van den Berg, M., Westerink, R.H.S., 2009. Hexabromocyclododecane inhibits depolarization-induced increase in intracellular calcium levels and neurotransmitter release in PC12 cells. Toxicol. Sci. 107, 490-497.

65. Dirtu, A., Cernat, R., Dragan, D., Mocanu, R., van Grieken, R., Neels, H., Covaci, A., 2006. Organohalogenated pollutants in human serum from Iassy, Romania and their relation with age and gender. Environ. Int. 32, 797-803.

66. Drechsel, D.A., Patel, M., 2008. Role of reactive oxygen species in the neurotoxicity of environmental agents implicated in Parkinson's disease. Free Radical Biology and Medicine 44, 1873-1886.

67. Dunning, C.J.R., Reyes, J.F., Steiner, J.A., Brundin, P., 2012. Can Parkinson's disease pathology be propagated from one neuron to another? Prog. Neurobiol. 97, 205-219.

68. Duyzer, J., 2003. Pesticide concentrations in air and precipitation in the Netherlands. J. Environ. Monit. 5, 77N-80N.

69. Eilers, J., Schneggenburger, R., Konnerth, A., 1995. Patch clamp and calcium imaging in brain slices, in: Sakmann, B., Neher, E. (Eds.), , pp. 213-229.

70. Elbaz, A., Clavel, J., Rathouz, P.J., Moisan, F., Galanaud, J., Delemotte, B., Alpérovitch, A., Tzourio, C., 2009. Professional exposure to pesticides and Parkinson disease. Ann. Neurol. 66, 494-504.

71. Elbaz, A., Tranchant, C., 2007. Epidemiologic studies of environmental exposures in Parkinson's disease. J. Neurol. Sci. 262, 37-44.

72. Estuardo, M., McIntyre, I., Parker, D., Gary, R., Loga, B., 2006. Case report: Two deaths attributed to the use of 2,4-Dinitrophenol. J. Anal. Toxicol. 30, 219-222.

73. Fabbro, A., Skorinkin, A., Grandolfo, M., Nistri, A., Giniatullin, R., 2004. Quantal release of ATP from clusters of PC12 cells. The Journal of Physiology 560, 505-517.

74. Ferguson, C.A., Audesirk, G., 1995. Non-$GABA_A$-mediated effects of lindane on neurite development and intracellular free calcium ion concentration in cultured rat hippocampal neurons. Toxicology in Vitro 9, 95-97.

75. Ferrada, C., Ferré, S., Casadó, V., Cortés, A., Justinova, Z., Barnes, C., Canela, E.I., Goldberg, S.R., Leurs, R., Lluis, C., Franco, R., 2008. Interactions between histamine H_3 and dopamine D_2 receptors and the implications for striatal function. Neuropharmacology 55, 190-197.

76. Fitsanakis, V.A., Au, C., Erikson, K.M., Aschner, M., 2006. The effects of manganese on glutamate, dopamine and γ-aminobutyric acid regulation. Neurochem. Int. 48, 426-433.

77. Fleming, L., Mann, J., Bean, J., Briggle, T., Sanchez-Ramos, J., 1994. Parkinson's disease and brain levels of organochlorine pesticides. Ann. Neurol. 36, 100-103.

78. Forsby, A., Blaauboer, B., 2007. Integration of *in vitro* neurotoxicity data with biokinetic modelling for the estimation of *in vivo* neurotoxicity. Human and Experimental Toxicology 26, 333-338.

79. Franco, R., Sánchez-Olea, R., Reyes-Reyes, E.M., Panayiotidis, M.I., 2009. Environmental toxicity, oxidative stress and apoptosis: Ménage à Trois. Mutation Research/Genetic Toxicology and Environmental Mutagenesis 674, 3-22.

80. Freire, C., Koifman, S., 2012. Pesticide exposure and Parkinson's disease: Epidemiological evidence of association. Neurotoxicology.

81. Fromberg, A., Granby, K., Højgård, A., Fagt, S., Larsen, J.C., 2011. Estimation of dietary intake of PCB and organochlorine pesticides for children and adults. Food Chem. 125, 1179-1187.

82. Gagne, J.J., Power, M.C., 2010. Anti-inflammatory drugs and risk of Parkinson disease: A meta-analysis. Neurology 74, 995-1002.

83. Garcia, A.G., Garcia-De-Diego, A.M., Gandia, L., Borges, R., Garcia-Sancho, J., 2006. Calcium Signaling and Exocytosis in Adrenal Chromaffin Cells. Physiol. Rev. 86, 1093-1131.

84. Giavini, E., Menegola, E., 2010. Are azole fungicides a teratogenic risk for human conceptus? Toxicol. Lett. 198, 106-111.

85. Gibson, J.E., Rao, K.S., 1973. Disposition of 2-sec-butyl-4,6-dinitrophenol (dinoseb) in pregnant mice. Food Cosmet. Toxicol. 11, 45-52.

86. Gleichmann, M., Mattson, M.P., 2011. Neuronal calcium homeostasis and dysregulation. Antioxid Redox Signal. 14, 1261-1273.

87. Goodwin, J., Nath, S., Engelborghs, Y., Pountney, D.L., 2013. Raised calcium and oxidative stress cooperatively promote alpha-synuclein aggregate formation. Neurochem. Int. 62, 703-711.

88. Greenamyre, J.T., Cannon, J.R., Drolet, R., Mastroberardino, P., 2010. Lessons from the rotenone model of Parkinson's disease. Trends Pharmacol. Sci. 31, 141-142.

89. Greene, L., Tischler, A., 1976. Establishment of a noradrenergic clonal line of rat adrenal pheochromocytoma cells which respond to nerve growth factor. Proc. Natl. Acad. Sci. USA 73, 2424-2428.

90. Grundlingh, J., Dargan, P., El-Zanfaly, M., Wood, D., 2011. 2,4-Dinitrophenol (DNP): A weight loss agent with significant acute toxicity and risk of death. Journal of Medical Toxicology 7, 205-212.

91. Gupta, R.C., 2007. Veterinary Toxicology - Chapter 51. , 567-586.

92. Guzman, J.N., Sánchez-Padilla, J., Chan, C.S., Surmeier, D.J., 2009. Robust pacemaking in substantia nigra dopaminergic neurons. The Journal of Neuroscience 29, 11011-11019.

93. Hales, T.G., Tyndale, R.F., 1994. Few cell lines with $GABA_A$ mRNAs have functional receptors. J. Neurosci. 14, 5429-5436.

94. Harvey, D., Bidstrup, P., Bonnell, J., 1951. Poisoning by Dinitro-ortho-cresol; some observations on the effects of Dinitro-ortho-cresol administered by mouth to human volunteers. Br. Med. J., 13-16.

95. Hatcher, J.M., Delea, K.C., Richardson, J.R., Pennell, K.D., Miller, G.W., 2008. Disruption of dopamine transport by DDT and its metabolites. Neurotoxicology 29, 682-690.

96. Hawkinson, J., Shull, L., Joy, R., 1989. Effects of lindane on calcium fluxes in synaptosomes. Neurotoxicology 10, 29-39.

97. Hendriks, H.S., van Kleef, R.G.D.M., van den Berg, M., Westerink, R.H.S., 2012. Multiple novel modes of action involved in the *in vitro* neurotoxic effects of tetrabromobisphenol-A. Toxicological Sciences 128, 235-246.

98. Hernández-Romero, M.C., Delgado-Cortés, M.J., Sarmiento, M., de Pablos, R.M., Espinosa-Oliva, A.M., Argüelles, S., Bández, M.J., Villarán, R.F., Mauriño, R., Santiago, M., Venero, J.L., Herrera, A.J., Cano, J., Machado, A., 2012. Peripheral inflammation increases the deleterious effect of CNS inflammation on the nigrostriatal dopaminergic system. Neurotoxicology 33, 347-360.

99. Heusinkveld, H.J., Westerink, R.H.S., 2012. The organochlorine insecticides lindane, dieldrin and their binary mixture disturb calcium homeostasis in dopaminergic PC12 cells. Environ. Sci. Technol. 46, 1842-1848.

100. Heusinkveld, H.J., Molendijk, J., van den Berg, M., Westerink, R.H., 2013. Azole fungicides disturb intracellular Ca^{2+} in an additive manner in dopaminergic PC12 cells. Toxicological Sciences 134, 374-381.

101. Heusinkveld, H.J., Thomas, G.O., Lamot, I., van den Berg, M., Kroese, A.B.A., Westerink, R.H.S., 2010. Dual actions of lindane (γ-hexachlorocyclohexane) on calcium homeostasis and exocytosis in rat PC12 cells. Toxicol. Appl. Pharmacol. 248, 12-19. |

102. Heusinkveld, H.J., Westerink, R.H.S., 2011. Caveats and limitations of plate reader-based high-throughput kinetic measurements of intracellular calcium levels. Toxicol. Appl. Pharmacol. 255, 1-8.

103. Heuts, F., 1993. Biological Monitoring of DNOC in applicators after use as haulmkiller in seed potatoes. Unpublished report prepared for Elf Atochem Agri bv

104. Hoferkamp, L., Hermanson, M.H., Muir, D.C.G., 2010. Current use pesticides in Arctic media; 2000–2007. Sci. Total Environ. 408, 2985-2994.

105. Hondebrink, L., Meulenbelt, J., Meijer, M., van den Berg, M., Westerink, R.H.S., 2011. High concentrations of MDMA ('ecstasy') and its metabolite MDA inhibit calcium influx and depolarization-evoked vesicular dopamine release in PC12 cells. Neuropharmacology 61, 202-208.

106. Hondebrink, L., Tan, S., Hermans, E., van Kleef, R.G.D.M., Meulenbelt, J., Westerink, R.H.S., 2013. Additive inhibition of human α1β2γ2 $GABA_A$ receptors by mixtures of commonly used drugs of abuse. Neurotoxicology 35, 23-29.

107. Huang, H., Bihaqi, S.W., Cui, L., Zawia, N.H., 2011. *In vitro* Pb exposure disturbs the balance between Aß production and elimination: The role of AßPP and neprilysin. Neurotoxicology 32, 300-306.

108. Hudspeth, A., Corey, D., 1978. Controlled bending of high-resistance /glass microelectrodes. Am. J. Physiol. 234, C56-C57.

109. Hughes, A.J., Daniel, S.E., Kilford, L., Lees, A.J., 1992. Accuracy of clinical diagnosis of idiopathic Parkinson's disease: a clinico-pathological study of 100 cases. J Neurol Neurosurg Psychiatry 55, 181-184.

110. Hutanu, C.A., Zaharia, M., Pintilie, O., 2013. Quenching of tryptophan fluorescence in the presence of 2,4-DNP, 2,6-DNP, 2,4-DNA and DNOC and their mechanism of toxicity. Molecules 18, 2266-2280.

111. Ilivicky, J., Casida, J.E., 1969. Uncoupling action of 2,4-dinitrophenols, 2-trifluoromethylbenzimidazoles and certain other pesticide chemicals upon mitochondria from different sources and its relation to toxicity. Biochemical Pharmacology 18, 1389-1401.

112. Imtiaz, M., 2012. Calcium Oscillations and Pacemaking, in: Islam, M.S. (Ed.), Calcium Signaling. Springer Netherlands, pp. 511-520.

113. Jakubowski, W., Bartosz, G., 2000. 2,7-dichlorofluorescin oxidation and reactive oxygen species: what does it measure? Cell biology international 24, 757-760.

114. Jiang Jiukun, Yuan Zhihua, Huang Weidong, Wang Jiezan, 2011. 2,4-dinitrophenol poisoning caused by non-oral exposure. Toxicology and Industrial Health 27, 323-327.

115. Jiang, P., Gan, M., Ebrahim, A., Lin, W., Melrose, H., Yen, S., 2010. ER stress response plays an important role in aggregation of alpha-synuclein. Molecular Neurodegeneration 5, 56.

116. Jimenez-Torres, M., Campoy-Folgoso, C., Canabate-Reche, F., Rivas-Velasco, A., Cerrillo-Garcia, I., Mariscal-Arcas, M., Olea-Serrano, F., 2006. Organochlorine pesticides in serum and adipose tissue of pregnant women in Southern Spain giving birth by cesarean section. Sci. Total Environ. 372, 32-38.

117. Johnston, G.A.R., 1996. $GABA_A$ receptor pharmacology. Pharmacol. Ther. 69, 173-198.

118. Judah, J.D., 1951. The action of 2:4-dinitrophenol on oxidative phosphorylation. Biochem. J. 49, 271-285.

119. Kanthasamy, A.G., Anantharam, V., Zhang, D., Latchoumycandane, C., Jin, H., Kaul, S., Kanthasamy, A., 2006. A novel peptide inhibitor targeted to caspase-3 cleavage site of a proapoptotic kinase protein kinase C delta (PKC[delta]) protects against dopaminergic neuronal degeneration in Parkinson's disease models. Free Radical Biology and Medicine 41, 1578-1589.

120. Kanthasamy, A., Kitazawa, M., Yang, Y., Anantharam, V., Kanthasamy, A., 2008. Environmental neurotoxin dieldrin induces apoptosis via caspase-3-dependent proteolytic activation of protein kinase C delta (PKCdelta): Implications for neurodegeneration in Parkinson's disease. Molecular Brain 1, 12.

121. Kassack, M.U., Höfgen, B., Lehmann, J., Eckstein, N., Quillan, J.M., Sadée, W., 2002. Functional Screening of G Protein-Coupled Receptors by Measuring Intracellular Calcium with a Fluorescence Microplate Reader. Journal of Biomolecular Screening 7, 233-246.

122. Katzenschlager, R., Evans, A., Manson, A., Patsalos, P.N., Ratnaraj, N., Watt, H., Timmermann, L., Van der Giessen, R., Lees, A.J., 2004. Mucuna pruriens in Parkinson's disease: a double blind clinical and pharmacological study. Journal of Neurology, Neurosurgery & Psychiatry 75, 1672-1677.

123. Kaushik, P., Kaushik, G., 2007. An assessment of structure and toxicity correlation in organochlorine pesticides. J. Hazard. Mater. 143, 102-111.

124. Koppen, G., Covaci, A., Van Cleuvenbergen, R., Schepens, P., Winneke, G., Nelen, V., van Larebeke, N., Vlietinck, R., Schoeters, G., 2002. Persistent organochlorine pollutants in human serum of 50–65 years old women in the Flanders Environmental and Health Study (FLEHS). Part 1: concentrations and regional differences. Chemosphere 48, 811-825.

125. Kortenkamp, A., 2008. Low dose mixture effects of endocrine disrupters: implications for risk assessment and epidemiology. Int. J. Androl. 31, 233-240.

126. Kostyuk, P., Verkhratsky, A., 1994. Calcium stores in neurons and glia. Neuroscience 63, 381-404.

127. Langeveld, W.T., Meijer, M., Westerink, R.H.S., 2012. Differential effects of 20 non-dioxin-like PCBs on basal and depolarization-evoked intracellular calcium levels in PC12 cells. Toxicological Sciences 126, 487-496.

128. Langston, J., 1996. The etiology of Parkinson's disease with emphasis on the MPTP story. Neurology 47, S153-60.

129. Langston, J., Ballard, P., Tetrud, J., Irwin, I., 1983. Chronic Parkinsonism in humans due to a product of meperidine-analog synthesis. Science 219, 979-980.

130. Latchoumycandane, C., Anantharam, V., Kitazawa, M., Yang, Y., Kanthasamy, A., Kanthasamy, A.G., 2005. Protein kinase Cdelta is a key downstream mediator of manganese-induced apoptosis in dopaminergic neuronal cells. J. Pharmacol. Exp. Ther. 313, 46-55.

131. Latchoumycandane, C., Anantharam, V., Jin, H., Kanthasamy, A., Kanthasamy, A., 2011. Dopaminergic neurotoxicant 6-OHDA induces oxidative damage through proteolytic activation of PKCδ in cell culture and animal models of Parkinson's disease. Toxicol. Appl. Pharmacol. 256, 314-323.

132. Lee, Y., Park, K., Park, H., Kim, Y., Lee, K., Kim, S., Koh, S., 2009. Cilnidipine mediates a neuroprotective effect by scavenging free radicals and activating the phosphatidylinositol 3-kinase pathway. J. Neurochem. 111, 90-100.

133. Lees, A.J., Hardy, J., Revesz, T., 2009. Parkinson's disease. The Lancet 373, 2055-2066.

134. Leftwich, R., Floro, J., Neal, R., Wood, A., 1982. Dinitrophenol poisoning: a diagnosis to consider in undiagnosed fever. South. Med. J. 75, 182-189.

135. Li, Y., McMillan, A., Scholtz, I., 1996. Global HCH usage with 1ø x 1ø longitude/latitude resolution. Environ. Sci. Technol. 30, 3525-3533.

136. Liu, K., Southall, N., Titus, S.A., Inglese, J., Eskay, R.L., Shinn, P., Austin, C.P., Heilig, M.A., Zheng, W., 2010. A Multiplex Calcium Assay for Identification of GPCR Agonists and Antagonists. ASSAY and Drug Development Technologies 8, 362-374.

137. Lopez-Espinosa, M.J., Lopez-Navarrete, E., Rivas, A., Fernandez, M.F., Nogueras, M., Campoy, C., Olea-Serrano, F., Lardelli, P., Olea, N., 2008. Organochlorine pesticide exposure in children living in southern Spain. Environmental Research 106, 1-6.

138. Lövborg, H., Gullbo, J., larsson, R., 2005. Screening for apoptosis - classical and emerging techniques. Anti-Cancer Drugs 16, 593-599.

139. Lu, C., Lee, K., Chen, Y., Cheng, J., Yu, M., Chen, W., Jan, C., 2000. Lindane (gamma-hexachlorocyclohexane) induces internal Ca^{2+} release and capacitative Ca^{2+} entry in Madin-Darby canine kidney cells. Pharmacol. Toxicol. 87, 149-155.

140. Luchetti, S., Huitinga, I., Swaab, D.F., 2011. Neurosteroid and $GABA_A$ receptor alterations in Alzheimer's disease, Parkinson's disease and multiple sclerosis. Neuroscience 191, 6-21.

141. Luzardo, O.P., Mahtani, V., Troyano, J.M., Alvarez de la Rosa, M., Padilla-P,rez, A.I., Zumbado, M., Almeida, M., Burillo-Putze, G., Boada, C., Boada, L.D., 2009. Determinants of organochlorine levels detectable in the amniotic fluid of women from Tenerife Island (Canary Islands, Spain). Environmental Research 109, 607-613.

142. Magnani, E., Bettini, E., 2000. Resazurin detection of energy metabolism changes in serum-starved PC12 cells and of neuroprotective agent effect. Brain Research Protocols 5, 266-272.

143. Mao, H., Liu, B., 2008. Synergistic microglial reactive oxygen species generation induced by pesticides lindane and dieldrin. Neuroreport 27, 1317-1320.

144. Mariussen, E., Fonnum, F., 2006. Neurochemical Targets and Behavioral Effects of Organohalogen Compounds: An Update. Critical Reviews in Toxicology 36, 253-289.

145. Marques, O., Outeiro, T.F., 2012. Alpha-synuclein: from secretion to dysfunction and death. Cell Death Dis 3, e350.

146. Mattson, M.P., 2012. Parkinson's disease: don't mess with calcium. J Clin Invest 122, 1195-1198.

147. Mattson, M.P., 2007. Calcium and neurodegeneration. Aging Cell 6, 337-350.

148. McGeer, P.L., McGeer, E.G., 2004. Inflammation and neurodegeneration in Parkinson's disease. Parkinsonism Relat. Disord. 10, S3-S7.

149. Menegola, E., Broccia, M.L., Di Renzo, F., Massa, V., Giavini, E., 2005. Study on the common teratogenic pathway elicited by the fungicides triazole-derivatives. Toxicology in Vitro 19, 737-748.

150. Miller, R.J., 1991. The control of neuronal Ca2+ homeostasis. Prog. /Neurobiol. 37, 255-285.

151. Möhler, H., 2007. Molecular regulation of cognitive functions and developmental plasticity: impact of GABAA receptors. J. Neurochem. 102, 1-12.

152. Monteith, G.R., Bird, G.S.J., 2005. Techniques: High-throughput measurement of intracellular Ca^{2+} - back to basics. Trends Pharmacol. Sci. 26, 218-223.

153. Moser, V.C., Barone, S., Smialowicz, R.J., Harris, M.W., Davis, B.J., Overstreet, D., Mauney, M., Chapin, R.E., 2001. The effects of perinatal tebuconazole exposure on adult neurological, immunological, and reproductive function in rats. Toxicological Sciences 62, 339-352.

154. Mosharov, E.V., Larsen, K.E., Kanter, E., Phillips, K.A., Wilson, K., Schmitz, Y., Krantz, D.E., Kobayashi, K., Edwards, R.H., Sulzer, D., 2009. Interplay between cytosolic dopamine, calcium, and α-synuclein causes selective death of substantia nigra Neurons. neuron 62, 218-229.

155. Mostafalou, S., Abdollahi, M., 2013. Pesticides and human chronic diseases: Evidences, mechanisms, and perspectives. Toxicol. Appl. Pharmacol. 268, 157-177.

156. Mueller, J.F., Harden, F., Toms, L.M., Symons, R., Fürst, P., 2008. Persistent organochlorine pesticides in human milk samples from Australia. Chemosphere 70, 712-720.

157. Mundy, W.R., Freudenrich, T.M., Crofton, K.M., DeVito, M.J., 2004. Accumulation of PBDE-47 in Primary Cultures of Rat Neocortical Cells. Toxicol. Sci. 82, 164-169.

158. Mustafa, M., Pathak, R., Tripathi, A., Ahmed, R., Guleria, K., Banerjee, B., 2010. Maternal and cord blood levels of Aldrin and Dieldrin in Delhi population. Environmental Monitoring and Assessment 171, 633-638.

159. Nath, S., Goodwin, J., Engelborghs, Y., Pountney, D.L., 2011. Raised calcium promotes α-synuclein aggregate formation. Molecular and Cellular Neuroscience 46, 516-526.

160. Neve, K.A., Seamans, J.K., Trantham-Davidson, H., 2004. Dopamine receptor signalling. Journal of receptors and signal transduction 24, 165-205.

161. Nolan, K., Kamrath, J., Levitt, J., 2012. Lindane toxicity: a comprehensive review of the medical literature. Pediatr. Dermatol. 29, 141-146.

162. Nougadère, A., Sirot, V., Kadar, A., Fastier, A., Truchot, E., Vergnet, C., Hommet, F., Baylé, J., Gros, P., Leblanc, J., 2012. Total diet study on pesticide residues in France: Levels in food as consumed and chronic dietary risk to consumers. Environ. Int. 45, 135-150.

163. Oates, L., Cohen, M., 2011. Assessing Diet as a Modifiable Risk Factor for Pesticide Exposure. Int. J. Environ. Res. Public Health 8, 1792-1804.

164. Obeso, J.A., Rodríguez-Oroz, M.C., Benitez-Temino, B., Blesa, F.J., Guridi, J., Marin, C., Rodriguez, M., 2008. Functional organization of the basal ganglia: Therapeutic implications for Parkinson's disease. Movement Disorders 23, S548-S559.

165. Orrenius, S., Nicotera, P., Zhivotovsky, B., 2011. Cell Death Mechanisms and Their Implications in Toxicology. Toxicological Sciences 119, 3-19.

166. Otey, C.A., Boukhelifa, M., Maness, P., 2003. B35 neuroblastoma cells: an easily transfected, cultured model of central nervous system neurons. Methods Cell Biol. 71, 287-304.

167. Palmeira, C.M., Moreno, A.J., Madeira, V.M.C., 1994. Interactions of Herbicides 2,4-D and Dinoseb with Liver Mitochondrial Bioenergetics. Toxicol. Appl. Pharmacol. 127, 50-57.

168. Parker, V., Barnes, J., Denz, F., 1951. Some Observations on the Toxic Properties of 3:5-Dinitro-Ortho-Cresol. Brit. J. Industr. Med. 8, 226-235.

169. Parkinson, J., 2002. An essay on the shaking palsy. Neuropsychiatry Classics 14, 223-236.

170. Patterson, J.,Donald G., Wong, L., *et al.* 2009. Levels in the U.S. Population of those Persistent Organic Pollutants (2003-2004) Included in the Stockholm Convention or in other Long-Range Transboundary Air Pollution Agreements. Environ. Sci. Technol. 43, 1211-1218.

171. Pelfréne, A.F., 2000. Environmental Health Criteria 220 - Dinitro-ortho-cresol. , 105.

172. Pezzoli, G., Cereda, E., 2013. Exposure to pesticides or solvents and risk of Parkinson disease. Neurology 80, 2035-2041.

173. Prachar, V., Veningerov , M., Uhn k, J., 1993. Levels of polychlorinated biphenyls and some other organochlorine compounds in breast milk samples in Bratislava. Sci. Total Environ. 134, 237-242.

174. Prasad, K.N., Carvalho, E., Kentroti, S., Edwards-Prasad, J., Freed, C., Vernadakis, A., 1994. Establishment and characterization of immortalized clonal cell lines from fetal rat mesencephalic tissue. *In Vitro* Cellular and Developmental Biology - Animal 30 A, 596-603.

175. Pravettoni, E., Bacci, A., Coco, S., Forbicini, P., Matteoli, M., Verderio, C., 2000. Different localizations and functions of L-type and N-type calcium channels during development of hippocampal neurons. Dev. Biol. 227, 581-594.

176. Publicover, S., Duncan, C., 1979. The action of lindane in accelerating the spontaneous release of transmitter at the frog neuromuscular junction. Naunyn Schmiedebergs Arch. Pharmacol. 308, 179-82.

177. Puls, R., 1988. Dinoseb toxicity in dairy heifers. Can. Vet. J. 29, 847

178. Purisai, M.G., McCormack, A.L., Cumine, S., Li, J., Isla, M.Z., Di Monte, D.A., 2007. Microglial activation as a priming event leading to paraquat-induced dopaminergic cell degeneration. Neurobiol. Dis. 25, 392-400.

179. Putzier, I., Kullmann, P.H.M., Horn, J.P., Levitan, E.S., 2009. Cav1.3 channel voltage dependence, not Ca^{2+} selectivity, drives pacemaker activity and amplifies bursts in nigral dopamine neurons. The Journal of Neuroscience 29, 15414-15419.

180. Qin, Z., Szabo, G., Cafiso, D.S., 1995. Anesthetics reduce the magnitude of the membrane dipole potential. Measurements in lipid vesicles using voltage-sensitive spin probes. Biochemistry (N. Y.) 34, 5536-5543.

181. Quaghebeur, D., De Smet, B., De Wulf, E., Steurbaut, W., 2004. Pesticides in rainwater in Flanders, Belgium: results from the monitoring program 1997-2001. J. Environ. Monit. 6, 182-190.

182. Radad, K., Rausch, W.D., Gille, G., 2006. Rotenone induces cell death in primary dopaminergic culture by increasing ROS production and inhibiting mitochondrial respiration. Neurochemistry International 49, 379-386.

183. Rajput, A.H., Birdi, S., 1997. Epidemiology of Parkinson's disease. Parkinsonism Relat. Disord. 3, 4.

184. Ramwell, C.T., Johnson, P.D., Boxall, A.B.A., Rimmer, D.A., 2005. Pesticide residues on the external surfaces of field crop sprayers: occupational exposure. Annals of Occupational Hygiene 49, 345-350.

185. Ray, D.E., Fry, J.R., 2006. A reassessment of the neurotoxicity of pyrethroid insecticides. Pharmacol. Ther. 111, 174-193.

186. Raymond-Delpech, V., Matsuda, K., Sattelle, B.M., Rauh, J.J., Sattelle, D.B., 2005. Ion channels: molecular targets of neuroactive insecticides. 5, 119-133.

187. Repetto, G., del Peso, A., Zurita, J.L., 2008. Neutral red uptake assay for the estimation of cell viability/cytotoxicity. Nat. Protocols 3, 1125-1131.

188. Reuveny, E., Narahashi, T., 1991. Potent blocking action of lead on voltage-activated calcium channels in human neuroblastoma cells SH-SY5Y. Brain Res. 545, 312-314.

189. Rice, M.E., Patel, J.C., Cragg, S.J., 2011. Dopamine release in the basal ganglia. Neuroscience 198, 112-137.

190. Richardson, J.R., Caudle, W.M., Wang, M., Dean, E.D., Pennell, K.D., Miller, G.W., 2006. Developmental exposure to the pesticide dieldrin alters the dopamine system and increases neurotoxicity in an animal model of Parkinson's disease. FASEB J. 20, 1695-1697.

191. Rivas, A., Cerrillo, I., Granada, A., Mariscal-Arcas, M., Olea-Serrano, F., 2007. Pesticide exposure of two age groups of women and its relationship with their diet. Sci. Total Environ. 382, 14-21.

192. Roche, H., Vollaire, Y., Persic, A., Buet, A., Oliveira-Ribeiro, C., Coulet, E., Banas, D., Ramade, F., 2008. Organochlorines in the Vaccares Lagoon trophic web (Biosphere Reserve of Camargue, France). Environmental Pollution 157, 2493-2506.

193. Roe, M.W., Lemasters, J.J., Herman, B., 1990. Assessment of Fura-2 for measurements of cytosolic free calcium. Cell Calcium 11, 63-73.

194. Roelofs, M.J.E., Piersma, A.H., van den Berg, M., van Duursen, M.B.M., 2013. The relevance of chemical interactions with CYP17 enzyme activity: Assessment using a novel *in vitro* assay. Toxicol. Appl. Pharmacol. 268, 309-317.

195. Roeper, J., 2013. Dissecting the diversity of midbrain dopamine neurons. Trends Neurosci. 36, 336-342.

196. Rosa, R., Sanfeliu, C., Sunol, C., Pomés, A., Rodriguez-Farré, E., Schousboe, A., Frandsen, A., 1997. The mechanism for hexachlorocyclohexane-induced cytotoxicity and changes in intracellular Ca^{2+} homeostasis in cultured cerebellar granule neurons is different for the [gamma]- and [delta]-isomers. Toxicol. Appl. Pharmacol. 142, 31-39.

197. Ross, R.A., Biedler, J.L., 1985. Presence and regulation of tyrosinase activity in human neuroblastoma cell variants *in vitro*. Cancer Research 45, 1628-1632.

198. Sanders, S.K., Shekhar, A., 1995. Regulation of anxiety by $GABA_A$ receptors in the rat amygdala. Pharmacology Biochemistry and Behavior 52, 701-706.

199. Sanderson, J.T., Boerma, J., Lansbergen, G.W.A., van den Berg, M., 2002. Induction and inhibition of aromatase (CYP19) activity by various classes of pesticides in H295R human adrenocortical carcinoma cells. Toxicol. Appl. Pharmacol. 182, 44-54.

200. Schapira, A.H., Jenner, P., 2011. Etiology and pathogenesis of Parkinson's disease. Movement Disorders 26, 1049-1055.

201. Schneider, T., Perez-Reyes, E., Nyormoi, O., Wei, X., Crawford, G.D., Smith, R.G., Appel, S.H., Birnbaumer, L., 1995. Alpha-1 subunits of voltage gated Ca^{2+} channels in the mesencephalon × neuroblastoma hybrid cell line MES23.5. Neuroscience 68, 479-485.

202. Schoonen, W., Westerink, W.M., Horbach, G.J., 2009. High-throughput screening for analysis of *in vitro* toxicity. EXS 99, 452.

203. Schummer, C., Groff, C., Al Chami, J., Jaber, F., Millet, M., 2009. Analysis of phenols and nitrophenols in rainwater collected simultaneously on an urban and rural site in east of France. Sci. Total Environ. 407, 5637-5643.

204. Sergent, T., Dupont, I., Jassogne, C., Ribonnet, L., van der Heiden, E., Scippo, M., Muller, M., McAlister, D., Pussemier, L., Larondelle, Y., Schneider, Y., 2009. CYP1A1 induction and CYP3A4 inhibition by the fungicide imazalil in the human intestinal Caco-2 cells—Comparison with other conazole pesticides. Toxicol. Lett. 184, 159-168.

205. Shafer, T.J., Atchison, W.D., 1991. Transmitter, ion channel and receptor properties of pheochromocytoma (PC12) cells: a model for neurotoxicological studies. Neurotoxicology 12, 473-92.

206. Sharma, H., Zhang, P., Barber, D.S., Liu, B., 2010. Organochlorine pesticides dieldrin and lindane induce cooperative toxicity in dopaminergic neurons: role of oxidative stress. Neurotoxicology 31, 215-222.

207. Sherer, T.B., Betarbet, R., Kim, J., Greenamyre, J.T., 2003a. Selective microglial activation in the rat rotenone model of Parkinson's disease. Neurosci. Lett. 341, 87-90.

208. Sherer, T.B., Kim, J., Betarbet, R., Greenamyre, J.T., 2003b. Subcutaneous rotenone exposure causes highly selective dopaminergic degeneration and α-synuclein aggregation. Exp. Neurol. 179, 9-16.

209. Shimizu, K., Ohtaki, K., Matsubara, K., Aoyama, K., Uezono, T., Saito, O., Suno, M., Ogawa, K., Hayase, N., Kimura, K., Shiono, H., 2001. Carrier-mediated processes in blood-brain barrier penetration and neural uptake of paraquat. Brain Res. 906, 135-142.

210. Siegmueller, C., Narasimhaiah, R., 2010. 'Fatal 2,4-dinitrophenol poisoning... coming to a hospital near you'. Emerg Med J.

211. Silva, B., Breydo, L., Fink, A., Uversky, V., 2013. Agrochemicals, alpha-synuclein, and Parkinson's disease. Molecular Neurobiology 47(2), 598-612

212. Silvestroni, L., Fiorini, R., Palleschi, S., 1997. Partition of the organochlorine insecticide lindane into the human sperm surface induces membrane depolarization and Ca^{2+} influx. Biochem. J. 321, 691-698.

213. Singal, A., Thami, G., 2006. Lindane neurotoxicity in childhood. Am. J. Ther. 13, 277-280.

214. Sladek, J.R., 2012. Neural development, a risky period. Exp. Neurol. 237, 43-45.

215. Solomon, G.M., Weiss, P.M., 2002. Chemical contaminants in breast milk: time trends and regional variability. Environ.Health Perspect. 110, A339-A347.

216. Song, X., Ehrich, M., 1998. Alterations of cytoskeletal tau protein of SH-SY5Y human neuroblastoma cells after exposure to MPTP. Neurotoxicology 19, 73-81.

217. Sonne, C., 2010. Health effects from long-range transported contaminants in Arctic top predators: An integrated review based on studies of polar bears and relevant model species. Environ. Int. 36, 461-491.

218. Srivastava, A., Shivanandappa, T., 2010. Stereospecificity in the cytotoxic action of hexachlorocyclohexane isomers. Chem. Biol. Interact. 183, 34-39.

219. Starke-Peterkovic, T., Turner, N., Else, P.L., Clarke, R.J., 2005. Electric field strength of membrane lipids from vertebrate species: membrane lipid composition and Na^+-K^+-ATPase molecular activity. Am. J. Physiol. Regul. Integr. Comp. Physiol. 288, R663-670.

220. Stevens, D.A., 2012. Advances in systemic antifungal therapy. Clin. Dermatol. 30, 657-661.

221. Subramanian, A., Ohtake, M., Kunisue, T., Tanabe, S., 2007. High levels of organochlorines in mothers' milk from Chennai (Madras) city, India. Chemosphere 68, 928-939.

222. Surmeier, D.J., Guzman, J.N., Sanchez-Padilla, J., Schumacker, P.T., 2011. The role of calcium and mitochondrial oxidant stress in the loss of substantia nigra pars compacta dopaminergic neurons in Parkinson's disease. Neuroscience 198, 221-231.

223. Surmeier, D.J., Guzman, J.N., Sanchez-Padilla, J., 2010. Calcium, cellular aging, and selective neuronal vulnerability in Parkinson's disease. Cell Calcium 47, 175-182.

224. Tansey, M.G., Goldberg, M.S., 2010. Neuroinflammation in Parkinson's disease: Its role in neuronal death and implications for therapeutic intervention. Neurobiol. Dis. 37, 510-518.

225. Taylor, J.M., Main, B.S., Crack, P.J., 2013. Neuroinflammation and oxidative stress: Co-conspirators in the pathology of Parkinson's disease. Neurochem. Int. 62, 803-819.

Tewari, A., Ali, A., O'Donnell, A., Butt, M.S., 2009. Weight loss and 2,4-dinitrophenol poisoning. Br. J. Anaesth. 102, 566-567.

226. Thomas, G.O., Wilkinson, M., Hodson, S., Jones, K.C., 2006. Organohalogen chemicals in human blood from the United Kingdom. Environmental Pollution 141, 30-41.

227. Threlfell, S., Cragg, S.J., Kalló, I., Turi, G.F., Coen, C.W., Greenfield, S.A., 2004. Histamine H_3 Receptors Inhibit Serotonin Release in Substantia Nigra Pars Reticulata. The Journal of Neuroscience 24, 8704-8710.

228. Toescu, E.C., Verkhratsky, A., 2007. The importance of being subtle: small changes in calcium homeostasis control cognitive decline in normal aging. Aging Cell 6, 267-273.

229. Trejo-Acevedo, A., Diaz-Barriga, F., Carrizales, L., Dominguez, G., Costilla, R., Ize-Lema, I., Yarto-Ramirez, M., Gavilan-Garcia, A., Jesus Mejia-Saavedra, J., Perez-Maldonado, I.N., 2009. Exposure assessment of persistent organic pollutants and metals in Mexican children. Chemosphere 74, 974-980.

230. Turski, L., Bressler, K., Rettig, K.J., Loschmann, P.A., Wachtel, H., 1991. Protection of substantia nigra from MPP^+ neurotoxicity by N-methyl-D-aspartate antagonists. Nature 349, 414-418.

231. Udenfriend, S., Stein, S., Böhlen, P., Dairman, W., Leimgruber, W., Weigele, M., 1972. Fluorescamine: A Reagent for Assay of Amino Acids, Peptides, Proteins, and Primary Amines in the Picomole Range. Science 178, 871-872.

232. Vale, C., Fonfra, E., Bujons, J., Messeguer, A., Rodriguez-Farré, E., Sunol, C., 2003. The organochlorine pesticides [gamma]-hexachlorocyclohexane (lindane), [alpha]-endosulfan and dieldrin differentially interact with $GABA_A$ and glycine-gated chloride channels in primary cultures of cerebellar granule cells. Neuroscience 117, 397-403.

233. van der Mark, M., Brouwer, M., Kromhout, H., Nijssen, P., Huss, A., Vermeulen, R., 2011. Is pesticide use related to Parkinson disease? Some clues to heterogeneity in study results. Environ. Health Perspect. 120, 3.

234. van Noort, H., Mandema, E., Juul Christensen, E.K., Huizinga, T., 1960. 4,6-Dinitro-o-cresol poisoning caused by sprays. Nederlands Tijdschrift voor Geneeskunde 104, 676-84.

235. Venda, L.L., Cragg, S.J., Buchman, V.L., Wade-Martins, R., 2010. α-Synuclein and dopamine at the crossroads of Parkinson's disease. Trends Neurosci. 33, 559-568.

236. Walsh, G.M., Fink, G.B., 1972. Comparative toxicity and distribution of endrin and dieldrin after intravenous administration in mice, Toxicol. Appl. Pharmacol. 23, 408-416.

237. Weisskopf, M.G., Knekt, P., O'Reilly, E.J., Lyytinen, J., Reunanen, A., Laden, F., Altshul, L., Ascherio, A., 2010. Persistent organochlorine pesticides in serum and risk of Parkinson disease. Neurology 74, 1055-1061.

238. Westerink, R.H.S., 2013. Modulation of cell viability, oxidative stress, calcium homeostasis, and voltage- and ligand-gated ion channels as common mechanisms of action of (mixtures of) non-dioxin-like polychlorinated biphenyls and polybrominated diphenyl ethers. Environ Sci Pollut Res in press.

239. Westerink, R.H.S., 2006. Targeting exocytosis: Ins and outs of the modulation of quantal dopamine release. CNS and Neurological Disorders - Drug Targets 5, 57-77.

240. Westerink, R.H.S., 2004. Exocytosis: Using amperometry to study presynaptic mechanisms of neurotoxicity. Neurotoxicology 25, 461-470.

241. Westerink, R.H.S., de Groot, A., Vijverberg, H.P.M., 2000. Heterogeneity of catecholamine-containing vesicles in PC12 cells. Biochemical and Biophysical Research Communications 270, 625-630.

242. Westerink, R.H.S., Ewing, A.G., 2008. The PC12 cell as model for neurosecretion. Acta Physiol 192, 273-285.

243. Westerink, R.H.S., Vijverberg, H.P.M., 2002a. Ca^{2+}-independent vesicular catecholamine release in PC12 cells by nanomolar concentrations of Pb^{2+}. J. Neurochem. 80, 861-873.

244. Westerink, R.H.S., Vijverberg, H.P.M., 2002b. Vesicular catecholamine release from rat PC12 cells on acute and subchronic exposure to polychlorinated biphenyls. Toxicol. Appl. Pharmacol. 183, 153-159.

245. Westerink, R.H.S., Hondebrink, L., 2010. Are high-throughput measurements of intracellular calcium using plate-readers sufficiently accurate and reliable? Toxicol. Appl. Pharmacol. 249, 247-248.

246. Whitacre, D., Ware, G., 2004. The Pesticide Book 6th Edition. Meister-Pro Information Resources (Meister Media Worldwide), Willoughby, Ohio.

247. Wilkaniec, A., Strosznajder, J.B., Adamczyk, A., 2013. Toxicity of extracellular secreted alpha-synuclein: Its role in nitrosative stress and neurodegeneration. Neurochem. Int. 62, 776-783.

248. Witt, S., 2012. Molecular chaperones, alpha-synuclein, and neurodegeneration. Molecular Neurobiology, 1-9.

249. Wu, J., Chan, P., Schroeder, K.M., Ellsworth, K., Partridge, L.D.L., 2002. 1-Methyl-4-phenylpridinium (MPP^+)-induced functional run-down of $GABA_A$ receptor-mediated currents in acutely dissociated dopaminergic neurons. J. Neurochem. 83, 87-99.

250. Xu, X., Dailey, A.B., Talbott, E.O., Ilacqua, V.A., Kearney, G., Asal, N.R., 2010. Associations of serum concentrations of organochlorine pesticides with breast cancer and prostate cancer in U.S. adults. Environmental health perspectives 118, 60-66.

251. Yasuda, T., Nakata, Y., Mochizuki, H., 2013. α-Synuclein and Neuronal Cell Death. Molecular Neurobiology 47, 466-483.

252. Zarn, J.A., Brüschweiler, B.J., Schlatter, J.R., 2003. Azole fungicides affect mammalian steroidogenesis by inhibiting sterol 14 alpha-demethylase and aromatase. Environ Health Perspect 111, 255-261.

Dankwoord

Poeh keek eens naar zijn twee pootjes. Hij wist dat het ene zijn rechterpootje was en als je wist welke het rechter was, dan was het andere het linker. Maar hij kon nooit onthouden hoe je beginnen moest. "Ja…." zei hij langzaam.

De Tao van Poeh, Benjamin Hoff.

Het bovenstaande citaat geeft naadloos aan hoe ik me voel als ik begin te schrijven aan het dankwoord. In de ICE terugreizend van Düsseldorf naar Amersfoort zit ik terug te denken aan de afgelopen 5 jaar promoveren inclusief het voor en na-traject. Er komt een massa namen in mij op van mensen aan wie ik dank verschuldigd ben inclusief het knagende gevoel dat ik waarschijnlijk nog mensen ga vergeten. Hoe begin je dan een dankwoord… Ik denk dat ik maar een min of meer chronologische volgorde aanhoud door te beginnen bij het begin.

Het begon allemaal met een reis naar Dioxin in Oslo in 2006. Mam, ik ben jullie nog steeds dankbaar dat jullie het mogelijk maakten dat ik daar op eigen houtje heen ging. Twijfelend over welke richting te kiezen binnen de Tox en dus in welke richting af te studeren liep ik in Oslo Leo (vd Ven) tegen het lijf. Hij heeft mij, eenmaal terug in NL, doorgestuurd naar de NTX groep bij het IRAS om stage te kunnen lopen in de Neurotoxicologie. And all the rest is history, zoals dat in correct Nederlands heet. Het moge duidelijk zijn: Leo bedankt!

Na 6 maanden stage bij Milou en "wat verlenging" om het onderzoek af te ronden en om te zetten in een publicatie verliet ik begin April 2008 het IRAS om drie maanden later terug te komen als onderzoeksmedewerker voor minimaal twee jaar. Twee jaar later ben ik doorgeschoven naar ACROPOLIS, toen officieel als PhD candidate, omdat het zicht op verlenging bij het eerste project vertroebeld was en de mengsels van pesticiden binnen ACROPOLIS prima aansloten op de individuele pesticiden. De aansluiting was inderdaad goed, getuige dit proefschrift! Al deze tijd was er 1 iemand die dat alles mogelijk maakte: Remco. Co-promotor, begeleider, partner-in-crime of, om Martin te citeren, "lichtend pad"? Allemaal denk ik, many thanks for all!

Martin, dankjewel voor de verhelderende discussies en het vertrouwen dat je als promotor in mij en Remco gesteld hebt om deze klus te klaren!

Al die jaren waren er natuurlijk nog veel meer mensen die het lab-leven aangenaam maakten en ervoor zorgden dat het aantal dagen dat ik met tegenzin naar het IRAS ging tot een absoluut minimum beperkten. Natuurlijk Milou, eerst als stagebegeleidster en later collega, (Meneer) Aart voor de broodnodige "aarding"

links en rechts, Gina voor de praktische ondersteuning in het lab, de rest van de NTX roedel, Jakub, Laura, Hester, Marieke, Martje, en Elsa maar ook de studenten die de afgelopen jaren bij mij stage liepen, Arie, Jan, Kim, en Jeffrey.

Verder de studenten die niet bij mij stageliepen maar met wie het wel erg gezellig was. Veerle, thanks voor het meeblèren met het foute uur op de vroege ochtend in het lab! Ik zeg maar zo, voor gek verklaard worden is altijd fijner met z'n tweeën… Mijn kamergenoten in Nieuw Gildestein en het JDV: Laura, Hester H, Irene, Marieke, Martje, Hester P en Jessica. Karin en Anita voor het mede organiseren van de NVT AiO dagen die groter uitpakten dan ooit. Ingrid en Evelyn als hulp en bijstand in administratief-bange dagen :-).

Natuurlijk ook nog de mensen van de IRAS partycommittee met wie het goed uitjes en feesten organiseren was!

Leo nog een tweede keer dankjewel (ik heb begrepen dat je het verhaal inmiddels kent) voor het doorverwijzen van Maarke naar het IRAS, wat daarna gebeurde is bekend.

Buiten de mensen die het lableven aangenaam maakten waren er natuurlijk ook nog legio mensen, vrienden, bekenden en familie. Voor *al* deze mensen en voor *alle* mensen die ik nog niet genoemd heb maar er wel voor mij waren geldt: DANK dat jullie er waren in de afgelopen fijne jaren, ik hoop dat jullie er nog lang zijn, het ga jullie goed.

Lief, dank voor je (on)geduld, 2 promoverende mensen in 1 huis lijkt een onmogelijk iets maar blijkt toch mogelijk. Nog even volhouden, je bent er bijna!

Almost Last but zeker niet least wil ik dankjewel zeggen tegen de verantwoordelijke man voor het zeer geslaagde cover ontwerp: Bart. Last-minute erin gesprongen zei Bart "stuur maar op, ik bedenk wel wat". En zo geschiedde!

Voor het dankjewel zeggen tegen sommige mensen schiet taal tekort. Pap, mam, dankjewel dat jullie het mogelijk gemaakt hebben dat Jannes en ik geworden zijn wie we zijn en dat we geland zijn op onze plek met de bagage die we hebben.

Om af te sluiten natuurlijk nog un grand MERCI *millefois* voor mijn ongevleugelde maar niet minder bevlogen paranimfen, Jannes en Stas. Dank dat jullie met vaart en daadkracht hebben geholpen om dit alles mogelijk te maken!

Tot zover.

Curriculum Vitae

&

List of Publications

Curriculum Vitae

This book is the product of 5 years of PhD research by Harm J Heusinkveld (born Februari 19, 1982). The research was performed at the Neurotoxicology Research Group of the Institute for Risk Assessment Sciences (IRAS; Veterinary Faculty, Utrecht University) and supervised by Dr. Remco Westerink and Prof. Dr. Martin van den Berg. Harm's research focussed on unravelling the mechanisms via which pesticide exposure could be linked to the aetiology of neurodegeneration with special emphasis on Parkinson's disease. At the 12th biannual meeting of the International Neurotoxicology Association (Jerusalem, 2009) he was awarded the INA award for Student support.

Before starting his PhD research in 2008, Harm obtained his Bachelors degree in Biomedical Sciences and his Masters degree in Toxicology at the Radboud University of Nijmegen in 2003 and 2007 respectively. As part of his Masters training he did internships at the Dutch National Institute of Public Health and the Environment (RIVM) and the IRAS

Peer reviewed publications

Dingemans, M.M., Heusinkveld, H.J., de Groot, A., Bergman, Å., van den Berg, M. and Westerink, R.H.S. (2009). Hexabromocyclododecane inhibits depolarization-induced increase in intracellular calcium levels and neurotransmitter release in PC12 cells. Toxicological Sciences **107**(2), 490-497.

Dingemans, M. M. L., Heusinkveld, H.J., Bergman, A., van den Berg, M. and Westerink, R. H. S. (2010). Bromination pattern of hydroxylated metabolites of BDE-47 affects their potency to release calcium from intracellular stores in PC12 cells. Environmental Health Perspectives. **118**, 519-525.

Heusinkveld, H. J., Thomas, G. O., Lamot, I., van den Berg, M., Kroese, A. B. A. and Westerink, R. H. S. (2010). Dual actions of lindane (gamma-hexachlorocyclohexane) on calcium homeostasis and exocytosis in rat PC12 cells. Toxicol. Appl. Pharmacol. 248, 12-19.

Heusinkveld H.J. and Westerink R.H.S. (2011). Caveats and limitations of platereader-based high throughput kinetic measurements of intracellular calcium levels. Toxicol Appl Pharmacol. **255**(1):1-8

Heusinkveld H.J. and Westerink R.H.S. (2012). The organochlorine insecticides lindane, dieldrin and their binary mixture disturb calcium homeostasis in dopaminergic PC12 cells. Environmental Science & Technology **46**: 1842-1848

Heusinkveld H.J., Molendijk J., van den Berg M. and Westerink R.H.S. (2013) Azole fungicides disturb intracellular Ca^{2+} in an additive manner in dopaminergic PC12 cells. Toxicological Sciences **34**(2): 374-381

Heusinkveld, H.J., van Kleef, R.G.D.M., Nijssen, P.C.G. and Westerink R.H.S. Differential modulation of human $GABA_A$ receptors by dinitrophenolic herbicides. *Submitted.*

Heusinkveld, H.J., van Vliet, A.C., Nijssen, P.C.G. and Westerink R.H.S. *In vitro* exposure to dinitrophenolic herbicides induces dopaminergic neurodegeneration. *Submitted.*

Heusinkveld, H.J., and Westerink R.H.S. Comparison of *in vitro* cell models for assessment of pesticide-induced dopaminergic neurodegeneration. *Submitted.*

Aut numquam tentes,

aut perfice.

Ovidius - Ars Amatoria